

Copyright
By
Jamie Fiedelia Farris
2008

Behavior of Horizontally Curved Steel I-Girders During Construction

by

Jamie Fiedelia Farris, B.S.C.E

Thesis

Presented to the Faculty of the Graduate School of

The University of Texas at Austin

in Partial Fulfillment

of the Requirements

for the Degree of

Master of Science in Engineering

The University of Texas at Austin

December 2008

Behavior of Horizontally Curved Steel I-Girders During Construction

**APPROVED BY
SUPERVISING COMMITTEE:**

Todd A. Helwig, Supervisor

Karl H. Frank

Dedication

To Dad, Mom, Brad, Ryan, Stephanie, Shelby, Sean,
Mark, Susan, Lindsey, and the rest of my incredible family.

I appreciate all of your love and support.

Acknowledgements

I am extremely grateful to my employer, the Texas Department of Transportation (TxDOT), for giving me the opportunity to reach for a goal that I never dreamed possible. TxDOT sponsored this research project and through the “Master’s Program,” funded my educational pursuit and allowed me to remain a full time employee. I would like to thank Randy Cox, David Hohmann, Dacio Marin, and all of my colleagues at Bridge Division for their continuous support, guidance, and friendship.

This thesis would not have been possible without the wisdom and direction from the professors on my project: Dr. Todd Helwig, Dr. Karl Frank, Dr. Michael Engelhardt, and Dr. Eric Williamson. I would especially like to thank Dr. Helwig and Dr. Frank. Both contributed a great deal to the research project and this thesis, and I am grateful for their belief in me and all of the knowledge I have gained from their expertise. I would also like to express my gratitude to Jason Stith and Andrew Schuh for all of their encouragement and insight. From the moment I stepped onto the project, they welcomed me and made me feel part of the team.

The project field work would not have run as smoothly without the help of Joe Mace, who assisted in the coordination on behalf of the construction contractor of the instrumented bridge. I would also like to thank all of the graduate students who helped instrument the bridge and for the long hours that they put in. It was a pleasure working with such an enthusiastic and talented group of people.

I am grateful for the time that the TxDOT Bridge Division Construction and Maintenance Branch and Bill McEleney from the National Steel Bridge Alliance (NSBA) took to compile a contact list of steel bridge erection specialists in the United States. Part of this thesis would be nonexistent without the detailed responses from the contractors, engineers, and inspectors who participated in the survey. I wish to thank all of the survey participants for their time and great efforts on communicating their experience and knowledge.

I would like to thank Dr. Joseph Yura, who sparked my interest in research years

ago when he offered me an undergraduate research job, even though I was so young and inexperienced. One of my heroes, I will never forget the many office hours he spent explaining moment diagrams to me.

The friends I have made in graduate school have made my time here unforgettable. I appreciate their constant encouragement and friendship. Thank you also to my oldest and dearest friends who have always supported whatever I endeavor and who have never left my side, though many living several miles away.

All that I am - is because of God and my huge caring family, who have supported me throughout my entire life. I would have never made this journey without the foundation of love, encouragement, and unending faith from my mom and dad. They taught me at a young age about reaching for goals and working hard towards them. Finally and most importantly, I would like to thank my patient and loving husband, who is my best friend and the person I am lucky enough to adventure through this great life.

Jamie F. Farris

December 5, 2008

Behavior of Horizontally Curved Steel I-Girders During Construction

Jamie Fiedelia Farris, M.S.E.

The University of Texas at Austin, 2008

SUPERVISOR: Todd Helwig

Elevated direct connector bridges have become a frequent solution to moving traffic from one highway to the next at efficient operating levels, without disturbing the underlying roadways and businesses. Horizontally curved I-girders provide a means to build longer spans with complex roadway geometry. With the increasing use of curved I-girders, their behavior is of paramount concern during the critical construction stages of erection and concrete deck placement. Preferred practices for TxDOT steel bridges recommend girder proportions that are conservative with respect to the American Association of State Highway and Transportation Officials (AASHTO) minimum requirements; however the State of Texas also has a good record with respect to safety of the girders during erection and construction. Many of the TxDOT preferred practices are based upon past experience without research justification. An accurate evaluation of the construction sequence of curved steel I-girders requires in-depth knowledge about stability, phasing, support conditions, composite action, and concrete curing time and temperature. The nature of the curved geometry causes warping stresses in the members in addition to the bending stresses. The interaction between warping and bending stresses complicates the design and the erection process for curved bridges.

The critical construction stages of girder erection and concrete deck placement are discussed and evaluated in this thesis. Field studies were performed during the construction of a concrete bridge deck and the data captured from that investigation provide valuable information to validate finite element models. Field data during concrete placement are presented and discussed in this thesis. In addition, a parametric study for the lateral-torsional buckling of non-prismatic curved I-girders during lifting was also performed. The trends from the analysis results are evaluated and discussed. Finally, in order to capture actual curved I-girder erection situations, a questionnaire was developed and sent to erection construction contractors, inspectors, and engineers in Texas and around the United States. The responses from the questionnaire are presented in this thesis.

Table of Contents

CHAPTER 1 INTRODUCTION	1
1.1 Motivation	1
1.2 Scope of Study	3
1.3 Thesis Overview	5
CHAPTER 2 BACKGROUND STUDIES	7
2.1 Introduction.....	7
2.2 Background Studies	7
2.3 Previous Field Work	8
2.3.1 Early Field Tests	8
2.3.2 Recent Field Test	10
2.3.3 Girder Lifting Field Tests	11
2.4 Summary	16
CHAPTER 3 INSTRUMENTATION	17
3.1 Introduction.....	17
3.2 Bridge Instrumentation	17
3.2.1 Girder Description and Gage Locations	19
3.2.2 Cross Frame Description and Gage Locations.....	22
3.2.3 Data Acquisition System Configuration	23
3.3 Data Acquisition system	27
3.3.1 Datalogger.....	27
3.3.2 AM416 Multiplexer	29
3.3.3 Strain Gages	29
3.3.4 Wire Full Bridge Terminal Input Module.....	30

3.4	Steel Girder Vertical Deflection Reading Setup	31
3.4.1	Hilti PD 32 Laser Range Meter	33
3.4.2	Construction of Reference Ground Locations	34
3.5	Thermal Expansion Test Setup	36
3.6	Summary	38
CHAPTER 4 FIELD RESULTS FROM SH 130/US 71 SPAN 14 CONCRETE PLACEMENT		39
4.1	Introduction.....	39
4.2	SH 130/US 71 Direct Connector Concrete Placement	40
4.2.1	Unit 3: Spans 16 and 15	43
4.2.2	Unit 3: Span 14	45
4.3	Girders 3 and 4.....	46
4.3.1	Girder Data Reduction Technique	47
4.3.2	Girders 3 and 4 Results	50
4.3.3	Summary of Results for Girders 3 and 4	62
4.4	Cross Frames X1 and X2	66
4.4.1	Cross Frame Data Reduction Technique	67
4.4.2	Cross Frame Results	69
4.4.3	Summary of Cross Frame Results.....	74
4.5	Vertical Deflection Results	75
4.5.1	Mid Span Deflection Readings	75
4.5.2	Girders 3 and 4 Vertical Deflection Results	77
4.5.3	Girders 3 and 4 Vertical Deflection Summary	81
4.6	Horizontal Thermal Expansion Results	81
4.7	Summary	86

**CHAPTER 5 PARAMETRIC STUDY OF THE LATERAL-TORSIONAL BUCKLING
OF NON-PRISMATIC CURVED I-GIRDERS DURING LIFTING 88**

5.1 Introduction.....88

5.2 Background.....88

5.2.1 Lateral -Torsional Buckling.....88

5.2.2 Previous Work: Curved I-Girder Rotation During Lifting92

5.2.3 Previous Work: Prismatic Curved I-Girder Stability.....94

5.3 Study Description.....98

5.3.1 Non-Prismatic Girders99

5.3.2 Eigenvalue Analysis Approach.....99

5.3.3 Parameter Descriptions101

5.3.4 Constant Variables104

5.4 Parametric Study Results104

5.4.1 Non-Prismatic I-Girder, Symmetric Lift Locations.....104

5.4.2 Non-Prismatic I-Girder, Unsymmetric Lift Locations.....110

5.5 Accounting for the Effect of Lifting of Curved I-Girders118

5.5.1 Determining M_o for Non-Prismatic Curved I-Girders118

5.5.2 C_b Formulation for Non-Prismatic Curved I-Girders124

5.5.3 Critical Buckling Moment: Non-Prismatic Curved I-Girder During Lifting129

5.5.4 Checking for Stability129

5.5.5 Stability of Curved Girder Systems131

5.6 Summary.....132

**CHAPTER 6 ERECTION PRACTICES FOR LIFTING OF HORIZONTALLY
CURVED I-GIRDERS 133**

6.1 Introduction.....133

6.2 Question 1: Typical Lifting Scenario.....133

6.3 Question 2: Spreader Beams.....138

6.4	Question 3: Cranes.....	141
6.5	Question 4: Girder Tilt.....	142
6.6	Question 5: Determining Lifting Points.....	145
6.7	Question 6: Problems or Concerns	146
	6.7.1 Shoring.....	146
	6.7.2 Erection.....	147
	6.7.3 Tight Radius of Curvature	148
	6.7.4 Unbraced Length.....	148
6.8	Summary	148
	CHAPTER 7 CONCLUSIONS	151
7.1	Overview.....	151
7.2	Summary of Results.....	151
	7.2.1 Field Instrumentation	152
	7.2.2 Parametric Study.....	153
	7.2.3 Questionnaire	154
7.3	Future Work.....	155
	APPENDIX A CROSS FRAME X2 EXTRAPOLATION	157
	APPENDIX B SH 130/US 71 SPAN 14 VERTICAL DEFLECTION FIGURES	159
	APPENDIX C PARAMETRIC STUDY SUMMARY AND EXAMPLE CALCULATIONS	163
C.1	Parametric Study Summary	163
C.2	Example Calculations	181
	APPENDIX D CURVED I-GIRDER ERECTION QUESTIONNAIRE	188
	References.....	190
	Vita	193

List of Tables

Table 4.1 Girder 3 Flange Stress Change Summary.....	62
Table 4.2 Girder 3 Web Stress Change Summary	62
Table 4.3 Girder 4 Flange Stress Change Summary.....	64
Table 4.4 Girder 4 Web Stress Change Summary	64
Table 4.5 Cross Frame X2 Axial Force Summary.....	74
Table 4.6 Vertical Deflection Readings Along Girder 3	79
Table 4.7 Vertical Deflection Readings Along Girder 4	80
Table 4.8 Bridge 88, Unit 3 Girders 1 and 4 Lengths.....	84
Table 4.9 Summary of Thermal Movement on Unit 3.....	85
Table 5.1 Section Definitions	113
Table 5.2 Stability Check: Girder Cross Section Properties.....	130
Table 6.1 Single Girder Segment Reported Lengths	136
Table 6.2 Pre-spliced Girder Segment Reported Lengths	138
Table 6.3 Reported Spreader Beam Lengths	140
Table 6.4 Reported Typical Rotation Tolerances	144
Table 6.5 Topics of Question 6 Responses.....	146
Table A.1 Stress Change Comparison of X1-4 and X2-4.....	158
Table A.2 Stress Change Extrapolation of X2-4 Member.....	158

List of Figures

Figure 1.1 Early Stages of Curved I-Girder Bridge Construction	1
Figure 1.2 Girder Staged (a), Cross Frames Attached (b), Girder Erection (c).....	2
Figure 1.3 Single Crane I-Girder Erection.....	3
Figure 1.4 SH 130/US 71 Unit 3 Deck Placement.....	4
Figure 1.5 Instrumentation of SH 130/US 71 Bridge	5
Figure 2.1 Hirschfield Lift Test	12
Figure 2.2 Girder Elevations w/ Gage and Tilt Sensor Locations (Schuh, 2008)	13
Figure 2.3 MI-JACK Travelift Provided By Hirschfeld Steel.....	14
Figure 2.4 16C4 Rotation Changes for Support S1 (Schuh, 2008).....	15
Figure 2.5 16C4 Bending Stress Change at Section A for Support S1 (Schuh, 2008).....	15
Figure 3.1 Bridge Location (Google Maps 2008).....	17
Figure 3.2 Typical Roadway Cross Section.....	18
Figure 3.3 Unit 6 Framing Plan	19
Figure 3.4 Span 14 Plan View - Girder Designations.....	19
Figure 3.5 Girder 3 and 4 Gage Locations.....	21
Figure 3.6 X1 and X2 Elevation with Gage Locations.....	23
Figure 3.7 Wax protection on strain gage on bottom flange.....	24
Figure 3.8 Flange Strain gages protected by steel channel caps.....	24
Figure 3.9 Dataloggers and Multiplexers protected in steel boxes on erected girder.....	25
Figure 3.10 Spliced strain gage wire (Schuh, 2008).....	26
Figure 3.11 Instrumented Cross frames X1 and X2	27
Figure 3.12 CR5000 Datalogger and AM416 Multiplexer.....	28
Figure 3.13 Multiplexer setup schematic (Campbell, 1996).....	29
Figure 3.14 CEA-06-250UN-350/P2 Strain Gage.....	30
Figure 3.15 Completion Bridge Module (Campbell, 2007).....	31
Figure 3.16 Span 14 mid span deflection reading locations	32
Figure 3.17 Vertical Deflection Schematic.....	33

Figure 3.18 Hilti PD 32 Laser Range Meter	34
Figure 3.19 Hydro-Stone bucket and preparation.....	35
Figure 3.20 Pouring Hydro-Stone into hole.....	35
Figure 3.21 Wax Trace Box with ½" Grid.....	37
Figure 3.22 Wax pot and stylus test set up	38
Figure 4.1 Bridge 88 Unit 3 Concrete Deck Placement.....	41
Figure 4.2 Concrete Deck Placement at beginning of pour	42
Figure 4.3 Transverse Screed used in deck construction	43
Figure 4.4 Bridge 88 Unit 3 Concrete Deck Placement Timeline	44
Figure 4.5 Early Morning Temperature Comparison	47
Figure 4.6 Curved I Girder Flange Stress Distribution (Schuh 2008)	49
Figure 4.7 Bending and Warping Stress Isolation (Schuh 2008).....	49
Figure 4.8 Girder 3: Section A Top Flange Stress.....	52
Figure 4.9 Girder 3: Section A Bottom Flange Stress	52
Figure 4.10 Girder 3: Section B Bottom Flange Stress	53
Figure 4.11 Girder 3: Section C Top Flange Stress	53
Figure 4.12 Girder 3: Section C Quarter Depth Web Stress.....	54
Figure 4.13 Girder 3: Section C Mid Depth Web Stress	54
Figure 4.14 Girder 3: Section C Three Quarter Depth Web Stress	55
Figure 4.15 Girder 3: Section C Bottom Flange Stress	55
Figure 4.16 Girder 4: Section A Top Flange Stress.....	57
Figure 4.17 Girder 4: Section A Bottom Flange Stress	57
Figure 4.18 Girder 4: Section B Top Flange Stress	58
Figure 4.19 Girder 4: Section B Bottom Flange Stress	58
Figure 4.20 Girder 4: Section C Top Flange Stress	59
Figure 4.21 Girder 4: Section C Quarter Depth Web Stress.....	59
Figure 4.22 Girder 4: Section C Mid Depth Web Stress	60
Figure 4.23 Girder 4: Section C Three Quarter Depth Web Stress	60
Figure 4.24 Girder 4: Section C Bottom Flange Stress	61

Figure 4.25 Girder 3 Bending Stress Change at Section C.....	63
Figure 4.26 Girder 3 Warping Stress Change at Section C	63
Figure 4.27 Girder 4 Bending Stress Change at Section C.....	65
Figure 4.28 Girder 4 Warping Stress Change at Section C	65
Figure 4.29 Cross Frame with Equation Nomenclature.....	69
Figure 4.30 Cross Frame X1 and X2 member labels.....	70
Figure 4.31 Average Stress Change for X2	72
Figure 4.32 Cross Frame X1 Axial Force.....	73
Figure 4.33 Cross Frame X2 Axial Force.....	73
Figure 4.34 Vertical Deflection Readings at Mid Span 14.....	77
Figure 4.35 Vertical Deflection Reading Locations	78
Figure 4.36 Summary of Girder 3 Vertical Deflection Results	79
Figure 4.37 Summary of Girder 4 Vertical Deflection Results	80
Figure 4.38 Wax Trace Box for Measuring Bearing Movements	82
Figure 4.39 Wax Thermal Expansion Device Measurement.....	85
Figure 4.40 Wax Device attached to Bent 14	86
Figure 5.1 Lateral-Torsional Buckling of a Curved I-Girder during Lifting.....	89
Figure 5.2 Lift Apparatus Axis of Rotation (Schuh 2008)	93
Figure 5.3 Approximating the Axis of Rotation (Schuh 2008)	94
Figure 5.4 Prismatic Girder Lift Point Variable Definition (Schuh 2008)	96
Figure 5.5 Example Non-Prismatic Girder and Lifting Locations	100
Figure 5.6 Example Non-Prismatic Girder Moment Diagram.....	100
Figure 5.7 Parametric Study Parameter Nomenclature.....	102
Figure 5.8 Three Cross Section Girder Schematic.....	105
Figure 5.9 Effect of λ on Radius of Curvature.....	106
Figure 5.10 Three Cross Section L/d Study (Average λ vs. a/L).....	108
Figure 5.11 Three Cross Section b/d Study (Average λ vs. a/L)	110
Figure 5.12 Two Cross Section Girder Schematic.....	111
Figure 5.13 Plan View – Center of Gravity, Non-Prismatic Girder	112

Figure 5.14 λ vs. L_{Lift} (Section 1=Section 2 = 60')	114
Figure 5.15 λ vs. Average a/L (Section 1=Section 2 = 60')	114
Figure 5.16 λ vs. L_{Lift} (Section 1 = 40', Section 2 = 80')	115
Figure 5.17 λ vs. Average a/L (Section 1 = 40', Section 2 = 80')	116
Figure 5.18 λ vs. L_{Lift} (Section 1=80', Section 2 = 40')	117
Figure 5.19 λ vs. Average a/L (Section 1=40', Section 2 = 80')	117
Figure 5.20 Case Study Girder Schematic	120
Figure 5.21 Case 1: Cross Sectional Properties for Calculating M_o	121
Figure 5.22 Case 2: Unbraced Length (L_b) Comparison (C_b vs. a/L)	122
Figure 5.23 Case 2: Unbraced Length (L_b) Comparison (λ vs. a/L)	123
Figure 5.24 C_b vs. a/L for Given Radius of Curvatures (Symmetric Lift)	125
Figure 5.25 C_b vs. a/L for Given Radius of Curvatures (Un-Symmetric Lift)	126
Figure 5.26 C_b vs. a/L for Given Flange Width to Depth Ratios (Symmetric Lift)	126
Figure 5.27 C_b vs. a/L for Given Flange Width to Depth Ratios (Un-symmetric Lift)	127
Figure 5.28 C_b vs a/L for Given Span to Depth Ratios (Symmetric Lift)	127
Figure 5.29 C_b vs a/L for Given Span to Depth Ratios (Un-Symmetric Lift)	128
Figure 5.30 Stability Check: Girder Dimensions	130
Figure 6.1 Air Splice	134
Figure 6.2 Shore Tower Supporting Curved Girders	134
Figure 6.3 Shore Tower Beam Supporting I-Girders	135
Figure 6.4 Ground Spliced Curved I-Girders	137
Figure 6.5 Spreader Beam Connected to I-Girder	139
Figure 6.6 Crane Lifting Curved I-Girder	141
Figure 6.7 Effect of Eccentricity on Curved I-Girder Tilt (Schuh, 2008)	143
Figure 6.8 Girder Segment Ends Connected at Splice	144
Figure 6.9 Lifting Curved I-Girder Segment	145
Figure 7.1 Lift Point Location Variable Definition	154
Figure A.1 Cross Frame Member Labels	157
Figure B.1 Vertical Deflection – Span 16 Complete (3:45am)	159

Figure B.2 Vertical Deflection – $\frac{1}{4}$ Span 15 Complete (5:50am)	160
Figure B.3 Vertical Deflection – $\frac{1}{2}$ Span 15 Complete (6:25am)	160
Figure B.4 Vertical Deflection – $\frac{3}{4}$ Span 15 Complete (7:10am)	161
Figure B.5 Vertical Deflection – Span 15 Complete (8:00am)	161
Figure B.6 Vertical Deflection – $\frac{1}{2}$ Span 14 Complete (9:00am)	162
Figure B.7 Vertical Deflection – Span 14 Complete (11:20am)	162
Figure C.1 Girder Cross Section Nomenclature	163
Figure C.2 Two Cross Section Girder Schematic.....	164
Figure C.3 Three Cross Section Girder Schematic.....	165
Figure C.4 Prismatic Girder Schematic ($t_f = 1.25''$)	165
Figure C.5 Prismatic Girder Schematic ($t_f = 2.00''$)	166
Figure C.6 Singly Symmetric Girder Schematic	167
Figure C.7 Singly Symmetric Girder Schematic, Varying Flange Transition.....	168
Figure C.8 Study 4 Girder Schematic.....	172
Figure C.9 Study 6 Girder Schematic.....	174
Figure C.10 Two Cross Section Girder Schematic (60' - 60')	176
Figure C.11 Two Cross Section Girder Schematic (40' - 80')	177
Figure C.12 Two Cross Section Girder Schematic (80' - 40')	178

CHAPTER 1

Introduction

1.1 MOTIVATION

Horizontally curved steel I-girder highway bridges are used throughout Texas for long spans and complex roadway geometry. Unlike simply supported prestress concrete beams, curved steel girders are usually continuous over supports and spliced near inflection points. The group of steel I-girders that make up a curved bridge behave as one unit with cross-frame braces that connect the girders. The critical phases for stability of the steel girders often occur during girder erection and early stages of construction when the braces are not fully installed (Figure 1.1). Curved I-girders are subjected to various loading and support conditions throughout the different stages of construction. These critical early stages often dictate the proportions of the steel section and therefore have a significant impact on overall girder economy.



Figure 1.1 Early Stages of Curved I-Girder Bridge Construction

Preferred practices for TxDOT steel bridges recommend girder proportions that are conservative with respect to the American Association of State Highway and Transportation Officials (AASHTO) minimum requirements; however the State of Texas also has a good record with respect to safety of the girders during erection and construction. Many of the TxDOT preferred practices are based upon past experience without research justification. An accurate evaluation of the construction sequence of curved steel I-girders requires in-depth knowledge about stability, phasing, support conditions, composite action, and concrete curing time and temperature. The nature of the geometry causes torsion on the girders that can result in significant shear and warping stresses in the girder cross-sections that add to the bending stresses. The interaction between warping and bending stresses complicates the design and the erection process for curved bridges.



Figure 1.2 Girder Staged (a), Cross Frames Attached (b), Girder Erection (c)

The research presented in this thesis is part of a larger study investigating the behavior of horizontally curved girders during construction. The study is considering the behavior during early stages of construction when little or no bracing is provided as well as the behavior during placement of the concrete bridge deck. Research on the bridge behavior during early stages of construction will provide valuable insight into the accuracy of past practices and help formulate safe construction procedures during girder erection and construction.

1.2 SCOPE OF STUDY

The research for this thesis was funded by the Texas Department of Transportation for project 0-5574 which was entitled, *Curved Plate Girder Design for Safe and Economical Construction*. As mentioned in the previous section, the study focuses on the behavior during early stages of construction to assist in justifying some of TxDOT's curved steel I-girder design practices during erection and construction and proposing new design guidelines where necessary. Typically, bridge design engineers analyze the girder system using grid-analysis to predict how the girder system will behave once the bridge is fully constructed. The computer programs are generally unable to provide accurate analyses during the early construction stages of girder erection and slab construction. With increased material costs, many engineers are designing curved I-girders with flange widths at the extreme limits of the AASHTO requirements. The decreased flange widths increase the slenderness of the girder. Therefore, the lateral flexibility of slender girders lead to stability problems before the bridge is fully braced and the slab is constructed (Figure 1.3).



Figure 1.3 Single Crane I-Girder Erection

In this research project, TxDOT would like to target all phases of girder erection and deck placement. When using the AASHTO LRFD Specifications and grid analyses, the goal for this project is to provide a set of design guidelines that will result in safe yet

economically erected steel plate girders. The necessity of shore towers is also being considered in the study. The research methods include field monitoring of curved girders during erection (Figure 1.3) and slab construction (Figure 1.4), parametric finite element modeling studies, surveys of erectors to determine common erection practices, and the development of a PC-based finite element program. This thesis will focus on results from the field studies during construction of the concrete bridge deck as well as computational results from parametric finite element analysis on non-prismatic curved I-girders during lifting. Results from the survey of erectors on common erection practices, is also presented. The results from the field results will be used to compare to the PC-based finite element program created by another graduate student on the project. The information provides data for verification of the finite element models and guidance on design issues that bridge engineers face when designing curved steel plate I-girders.

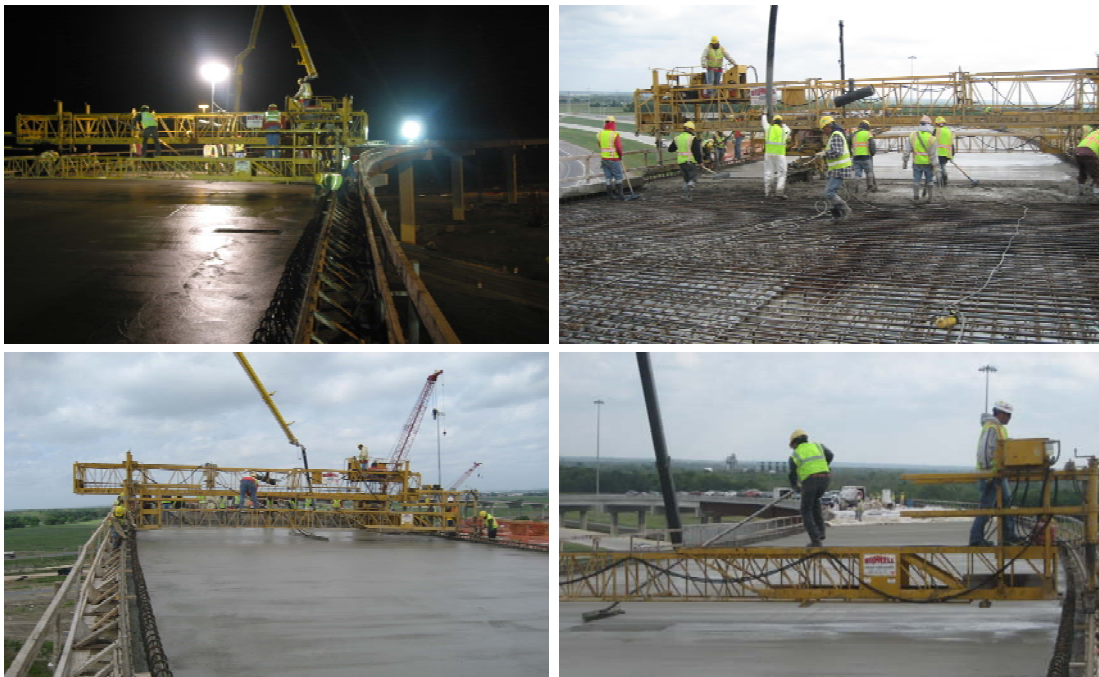


Figure 1.4 SH 130/US 71 Unit 3 Deck Placement

1.3 THESIS OVERVIEW

This thesis covers a range of topics dealing with the critical stages of horizontally curved I-girder construction. Following this Introduction chapter, a summary of previous curved I-girder research projects and field work pertaining to the behavior of curved I-girders during critical construction stages is presented in Chapter 2.

Chapter 3 provides a discussion of the instrumentation of a bridge on SH 130 located in Austin, Texas (Figure 1.5). The bridge was monitored to determine the behavior of two curved I-girders and two cross frames during the concrete slab placement stage of construction. Data from the field monitoring during construction of the concrete bridge deck is then presented and discussed in Chapter 4. The data includes strain gage data from the girders and the cross-frames as well as the vertical deflection readings. The thermal expansion of this bridge was also measured and reported.

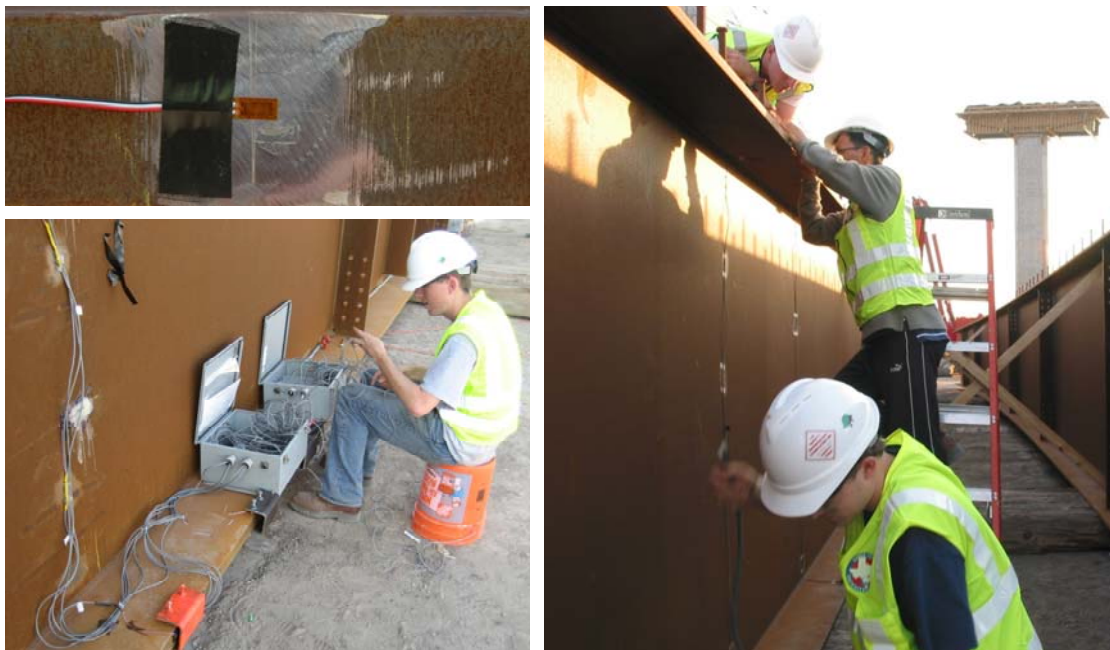


Figure 1.5 Instrumentation of SH 130/US 71 Bridge

Chapter 5 presents the results of a parametric study for the lateral-torsional buckling of non-prismatic curved I-girders during lifting. An elastic buckling analysis

was performed using the finite element program, ANSYS 11.0 (2007). Background information is introduced to explain the previous work related to the stability of lifting curved I-girders. A section on lateral-torsional buckling is also included to explain the behavior that a curved I-girder undergoes during lifting and erection.

Chapter 6 discusses the results of a questionnaire created to survey various curved steel I-girder erection contractors, inspectors, and engineers. The questionnaire centers around the common practices for lifting curved I-girders, including spreader beam length, number of cranes, lift points, shore towers, and length of girder segments lifted (Figure 1.3). The final chapter summarizes the results from this thesis as well as gives recommendations for future work.

CHAPTER 2

Background Studies

2.1 INTRODUCTION

There have been a number of previous research efforts that provide important background information for understanding the focus of this research. These efforts support the objectives of this research project as well as assist in helping the reader understand the procedures presented throughout this thesis. While some of the material outlined in this chapter includes summaries of previous curved I-girder projects, an overview of the work that was completed in the first phases of this current project are also outlined.

2.2 BACKGROUND STUDIES

This section will highlight some of his pertinent literature findings regarding curved I-girder behavior during lifting. The first examination into curved girders was performed in the 1840's in France by Barre De Saint Venant. Although there were several other studies following this, it wasn't until 1969 that organized research efforts into curved steel bridges began in the United States, through the Federal Highway Administration (FHWA). The FHWA Consortium of University Research Teams (CURT) project focused on laboratory scale model tests, along with theoretical work and analytical studies. The CURT project did not specifically study the behavior of curved steel I-girder erection, but it did examine the behavior before and after the bridge deck was placed (Brennan 1970). Following this project, the FHWA initiated the Curved Steel Bridge Research Project (CSBRP) in 1992. This project compiled all of the curved bridge research performed previously and addressed weaknesses of the earlier CURT research, specifically the absence of full-scale tests or field tests with realistic boundary conditions. The CSBRP produced a comprehensive document consisting of close to 900

references relating to all curved bridge research to date (Zureick et al. 1994). This project, which lasted over 10 years, became the basis for more recent work on curved bridges as well as AASHTO's publication on the topic, Guide Specifications for Horizontally Curved Steel Girder Highway Bridges 2003 (AASHTO 2003).

The first step on this current research study was to conduct an in-depth literature review on curved I-girder systems. The literature for the study was presented by Schuh (2008). Many of the projects and findings referenced in by Schuh are products of the CSBRP, both directly and indirectly. His review discusses areas of study pertaining to structural stability of curved I-girders, cross frame behavior in curved I-girder bridge systems, as well as effectiveness of analytical techniques. Schuh also investigated literature pertaining to the analysis of curved I-girders and field study evaluations. His conclusions state that there is a visible lack of full scale monitoring of curved I-girder bridges during early construction stages such as girder erection.

2.3 PREVIOUS FIELD WORK

Field testing is invaluable to understanding the true behavior and performance of curved I-girder bridges. However due to the difficulties associated with conducting research in field settings, documentation of field studies in the literature are relatively limited. Some of the difficulties in the field include getting access to the field site, installing instrumentation and data acquisition systems in the harsh field environment, as well as meeting the time demands of the contractor. To date, there have been relatively few measurements of actual stresses in curved I-girder systems (Galambos et al.). The following subsections provide an overview of some of the past studies on steel bridge girders in the field.

2.3.1 Early Field Tests

The results of one of the first field tests performed on a curved I-girder bridge were published by Beal and Kissane (1971a) in New York. The simple span bridge consisted of 4-girders spanning 123 feet with a 478 ft radius of curvature. The time

available for planning and testing the instrumentation was restricted due to the fact that the decision to test the structure was not made until after the contract for construction had been awarded. This short lead time led to deficiencies in the instrumentation. Dead load and static live load measurements were taken to determine the stress and deflection in the girders, which were then compared to theoretical values. The dead and live load behavior of the bridge was evaluated by monitoring the strains and deflections. Electrical resistance strain gages were used to capture the strain in the girders. Gage output was monitored with a manually operated BLH strain indicator and channel switching controls. Gages were located on the girders as well as the transverse diaphragms. Lead wires to the strain gages were not attached until after the girders were erected, to prevent the possibility of any damage during this phase of construction. Thus, there were no strains captured during the lifting of the curved I-girders. The behavior of the bridge was monitored during deck placement and during live load testing. The test results showed that most of the girder and diaphragm gages were damaged during the construction phase. The poor performance of the strain gages was also attributed to inadequate water proofing, the gage bonding cement, and the high humidity at the site. Despite the incomplete data, two conclusions were made from this test; the present design method was conservative with respect to in-plane bending stress and the total midspan measured deflections exceeded design camber values.

Five months after the first test was published, a second test was performed by Beal and Kissane (1971b). The simple span bridge, which consisted of four girders spanning 95' in length, was instrumented with 132 strain gages. The bridge had a relatively tight radius of curvature of 162' which was much smaller than the first bridge they had instrumented. Dead load and static live load measurements of stress, deflection, rotation, and shear were presented and compared with values from a planar grid analysis. Thermal expansion was also measured. Similar to the first test, they had problems with gages being damaged, but the number of failed gages was significantly less than the first instrumentation attempt. The conclusions of this test showed that the existing planar grid method, with appropriate member properties, was reliable in predicting deflection and

vertical bending stresses due to static loads. However, the planar grid model was incapable of predicting the lateral bending stresses in the flange and several of the flange gages measured significant values above the allowable stress. Further investigation into developing a method to account for these stresses was recommended.

Following the second test, Beal and Kissane (1972) published results from a third field test. The third structure evaluated was a symmetrical two span continuous curved I-girder bridge. The bridge consisted of 5 girders with symmetrical span lengths of 200.25' and a radius of curvature of 265.5'. Strains, deflections, and rotations were monitored with 160 gages, in one of the two spans of the structure. Similar to the first two tests, several gages were damaged, but the strains that were captured showed a significant difference between the inside and outside edge of the bottom flanges, which represents lateral flange bending. They also concluded through examination of the experimental stresses on the diaphragm, that they were distributing the load through these members under the dead load condition, but the actual mechanics of the load transfer were unclear, especially at the center pier. Furthermore, the conclusions of the third test were similar to the second and showed that lateral bending played a significant role in the stress distribution of the girder, which could not be determined from their planar grid analysis. Finally, their tests showed that the negative moment region of the bridge should control the bridge design because this region appeared to have the highest stresses.

2.3.2 Recent Field Test

More recent field tests on curved I-girder bridges were performed by Galambos et al. in 1996. The goal of this test was to monitor the behavior of a curved I-girder bridge during all phases of construction and compare the actual stresses in the bridge to a linear elastic analysis software model. The bridge chosen for this project was a two span continuous, four-girder bridge with a radius of curvature varying from 270' to 300'. Span ranges of this bridge, which was located in Minnesota, were 139' to 155'. The girder depths varied from 50" (inside girder) to 72" (outside girder). The bridge was instrumented with 60 vibrating wire strain gages on the girders as well as the cross

frames. To determine member stresses in the positive moment region, a total of 24 gages were placed near the midspan. The gages were attached to the girders and cross frames at the fabrication plant in order to obtain a set of baseline strain readings that corresponded to a state of zero stress. Field measurements were taken at all phases of construction, including erection and concrete deck placement. The bridge was also monitored after it was opened to traffic with several live load tests. Deflection readings were taken with a survey level. The field measured results were compared to computed results obtained from a computer program that employed the planar grid method that was specifically developed for the research study. The project yielded conclusions relating to the different phases of construction. The computational results for stresses and deflections generally matched qualitatively with measured results; however the quantitative agreement had mixed success. Throughout construction, the stresses were well below the yield stress. The measured data showed little correlation with the computer model during the first construction stage, especially in the cross frames, due to a low level of girder self weight stress and fairly large fit-up stresses. As construction progressed and after the concrete deck was placed, the measured data correlated better, as the fit-up stresses became more insignificant. Due to erratic effects of warping restraint and minor axis bending on the measured results, there was some difference between the measured and computed results. When composite action was assumed in the negative moment region (over the pier), the correlation between the measured and the computed results due to live loading improved considerably. There were no shear connectors in this region, therefore it was concluded that the composite action was due to friction and adhesion (Galambos et al 2000).

2.3.3 Girder Lifting Field Tests

Prior to the work done within the scope of this project, curved I-girders were instrumented to specifically monitor their behavior during lifting (Schuh, 2008). Schuh reported on the behavior of two separate field tests. The first test was conducted on a bridge located east of the Austin Bergstrom International Airport (ABIA) on SH 130 at US 71. The second test, which will be the test that this section focuses on, was

performed in San Angelo, Texas at the Hirschfeld Steel Company storage site. The tests provided valuable rotation and stress data for calibrating a finite element model. The researchers are aware of no other data including both rotation and stress during girder lifting. Figure 2.1 shows the rotation gage connection, instrumentation of one of the girders, and the lift tests that were performed.

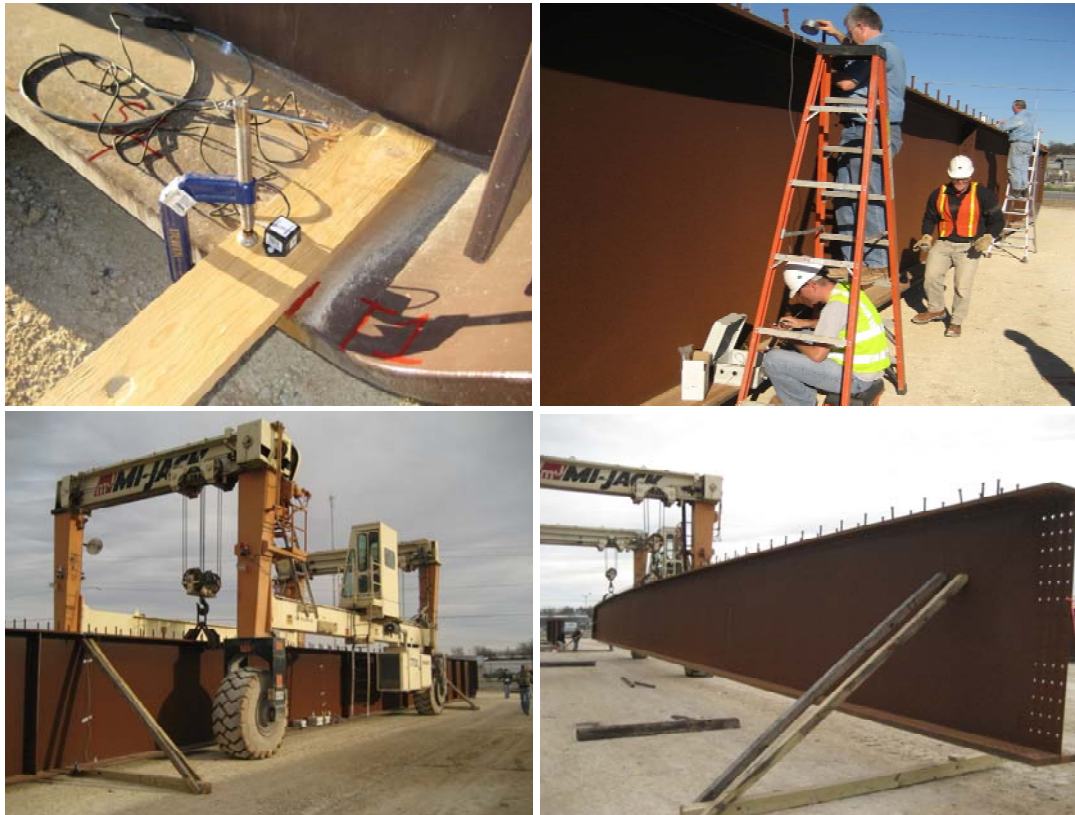


Figure 2.1 Hirschfield Lift Test

The Hirschfeld lift tests were undertaken to capture the stresses and rotations while lifting a girder with known support conditions. Two curved I-girder segments were instrumented with strain gages and tilt sensors. The first girder (164C) was 127'-4" long, with an 84" deep web plate and a radius of curvature of 1236'. The second girder (14C2) instrumented was 124'-1" long, with an 84" deep web plate and a radius of curvature of 1215'. Strain gages were installed at the mid-thickness of the four flange tips at three locations on both girders. Five tilt sensor locations were placed along each girder and

were intended to capture rotation changes at the ends, quarter points, and midspan of the girder. Figure 2.2 shows the elevation view and cross section depicting the locations of the strain gages and tilt sensors on the two girders.

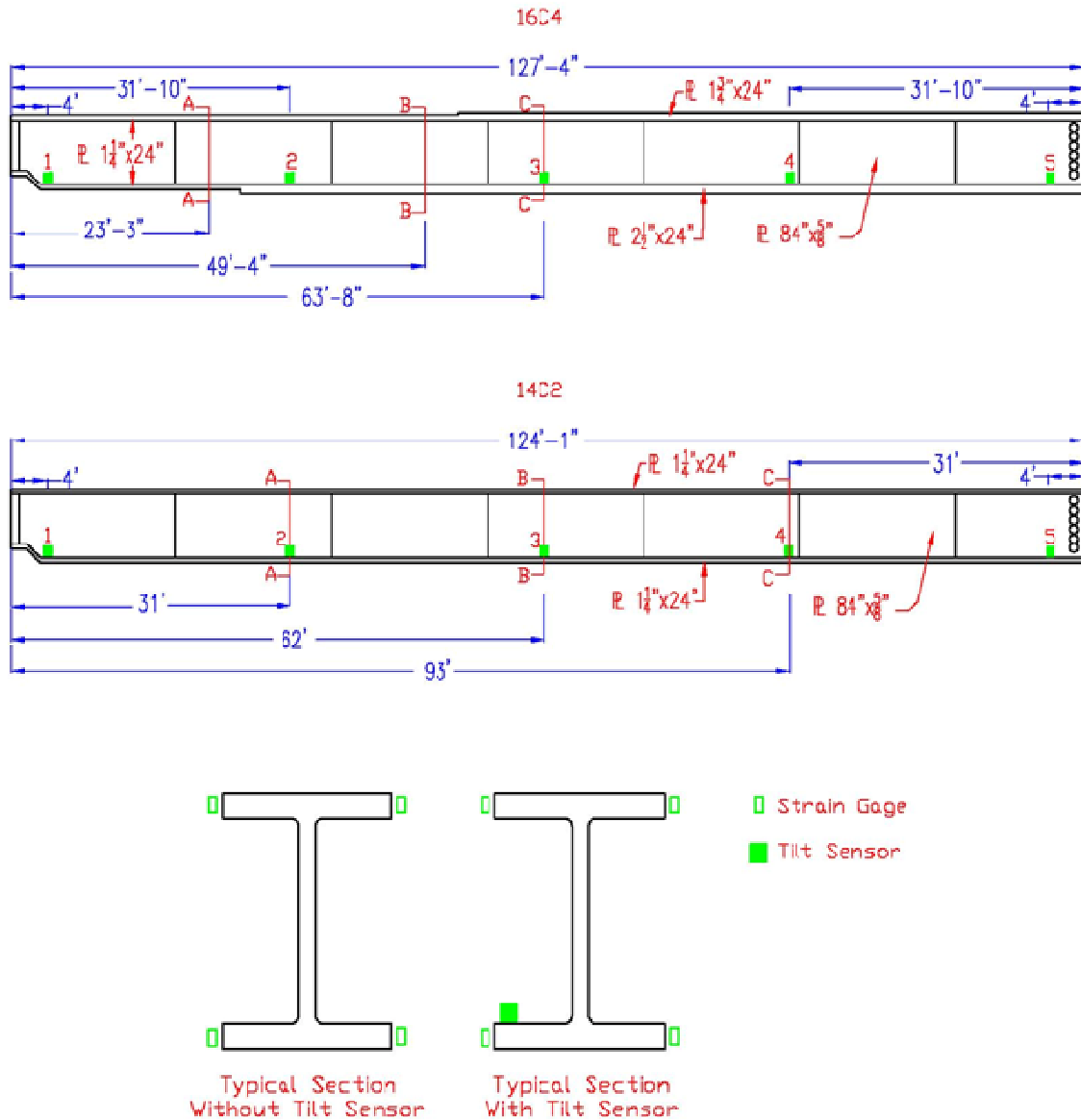


Figure 2.2 Girder Elevations w/ Gage and Tilt Sensor Locations (Schuh, 2008)

The supports used in the tests were identical and yielded a statically determinate structure. Two different girder support locations were tested. The first support location (S1) was located near the ends of the girder, while the second support location (S2) was closer to the lift points. The girders were lifted using a MI-JACK, as shown in Figure 2.3, with a lift clamp spacing of approximately 40 feet.



Figure 2.3 MI-JACK Travelift Provided By Hirschfeld Steel

During the lifts, milestone occurrences were recorded in order to correlate the lifting times with the data. The data that was collected and analyzed consisted of bending and warping stresses, as well as girder rotations. The following graphs are examples of the data captured by the Hirschfeld lift tests. Figure 2.4 plots the time history of the girder rotation for the first girder in the first support condition. Figure 2.5 plots the time history of the bending stress at Section A for the first girder in the first support condition.

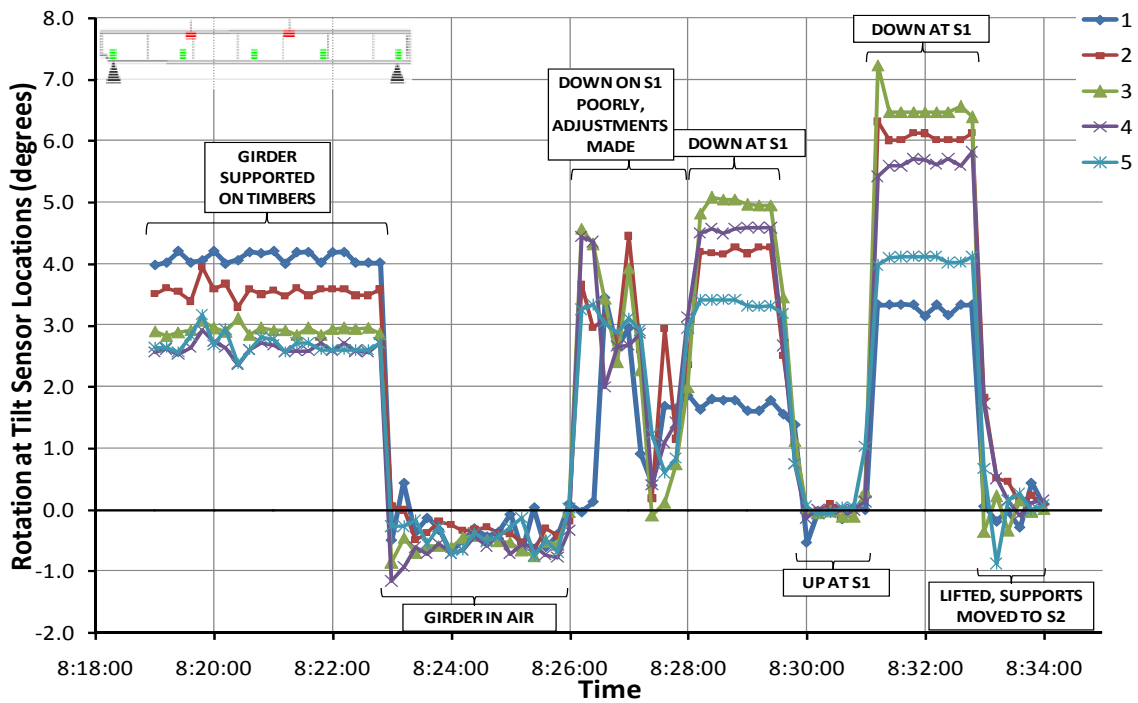


Figure 2.4 16C4 Rotation Changes for Support S1 (Schuh, 2008)

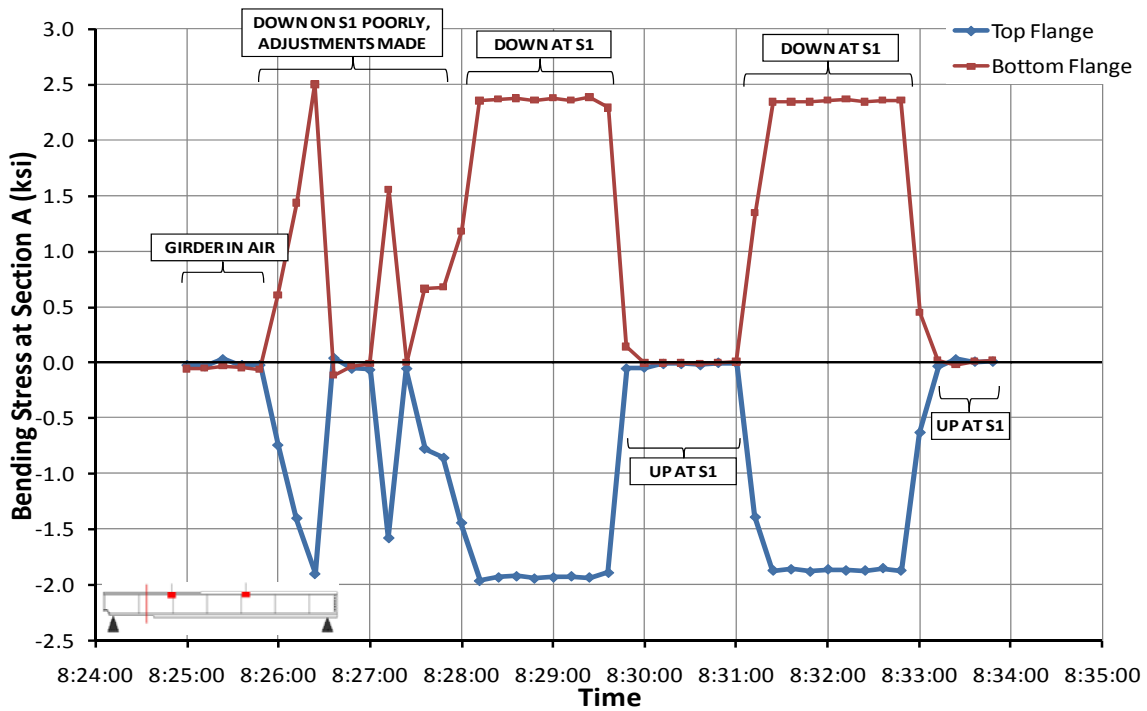


Figure 2.5 16C4 Bending Stress Change at Section A for Support S1 (Schuh, 2008)

The Hirschfeld test yielded conclusions related to the lifting of curved I-girders. Schuh found that rigid body rotation, which can create significant erection problems, is an important issue when lifting curved I-girders. This could lead to difficulty in placement and fit up following girder erection. The results showed that rigid body rotations of the girders while lifted can cause stress distributions in the girder flanges that are significantly different than predicted from the theory of warping torsion (Schuh, 2008). The data also showed that stresses induced by weak axis bending can also be caused by rotations during lifting.

2.4 SUMMARY

This chapter provided a summary of previous curved I-girder research projects and field work pertaining to the behavior of curved I-girders during erection and early stages of construction. An in-depth literature review for this research project was published previously (Schuh, 2008) and highlights work done regarding structural stability of curved I-girders, cross frame behavior in curved I-girder bridge systems, as well as effectiveness of analytical techniques. Previous field work performed on full scale curved I-girder bridges in the 1970's, 1990's and 2000's was also summarized. Furthermore, the review shows that there is very little monitoring of full scale curved I-girder bridges during construction stages such as girder lifting and concrete placement. Schuh detailed field studies and results that attempt to fill in the gap in the current research on I-girder lifting with the Hirschfeld lift tests. As a follow up to the data presented by Schuh, Chapter 3 and 4 of this thesis describe and report the results during the concrete deck pour of the bridge located near the airport in Austin, Texas. Results from these studies were used to validate finite element models to accurately predict the behavior of curved I-girder bridges during the critical stages of construction.

CHAPTER 3

Instrumentation

3.1 INTRODUCTION

This chapter summarizes the geometry and layout used to monitor the behavior of a steel girder unit during the concrete deck placement. A brief discussion about the instrumentation techniques and data collection procedures used to measure the behavior at various locations of the bridge is also given. The information was gathered to provide data for verification of the finite element models and guidance on design issues that bridge engineers face when designing curved steel plate I-girders.

3.2 BRIDGE INSTRUMENTATION

The field investigation was conducted on a bridge located east of the Austin Bergstrom Airport on SH 130 as indicated in Figure 3.1. Bridge 88 is a direct connector between east-bound US 71 to north-bound SH 130 and is comprised of 4 continuous horizontally curved steel girder units and 5 precast prestressed concrete beam units.

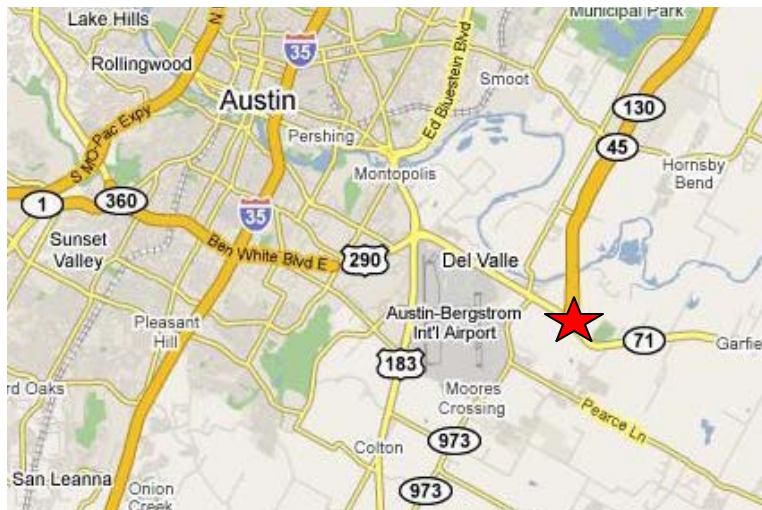


Figure 3.1 Bridge Location (Google Maps 2008)

The third steel unit, which contains Span 14, 15, and 16 on the engineering plans (Span F, G, and H on the shop drawings) was chosen for instrumentation and field monitoring. The three-span continuous girder system has spans of 185', 205', and 158.5' with a radius of curvature of 1206' at the base line. The basic cross-sectional layout is depicted in Figure 3.2. The center to center spacing between adjacent girders is 10.33'. Strain gages were placed on the girders labeled 3 and 4, which were located on the outside of the curved bridge. Two cross-frames that will be referred to as X1 and X2 were also instrumented. An illustration of the framing plan of the four-girder system is provided in Figure 3.3. The instrumented girder cross sections and braces were located in Span 14. The location of Girders 3 and 4 and cross frames X1 and X2 are highlighted in Figure 3.4.

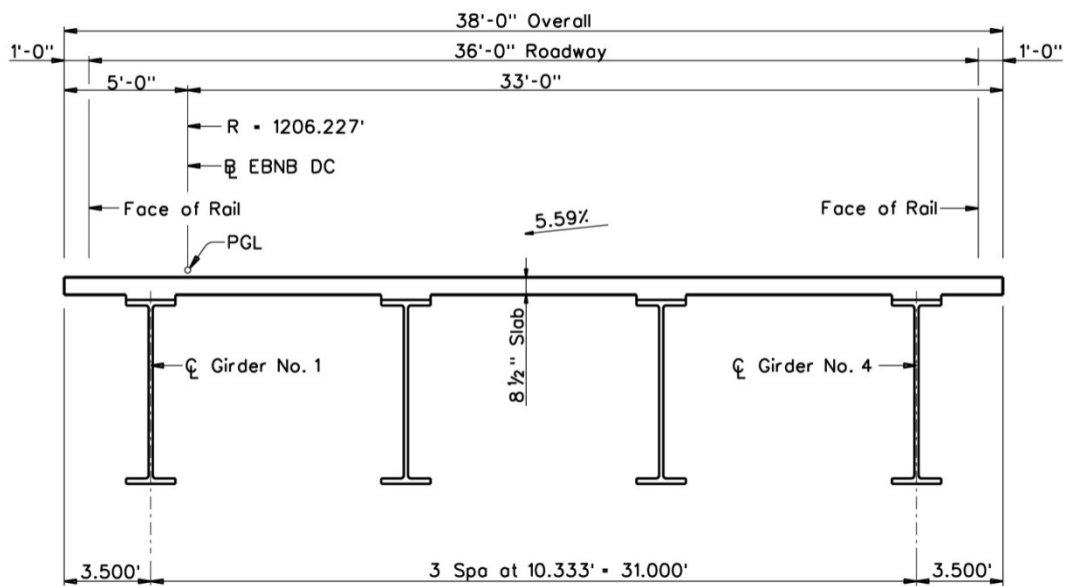


Figure 3.2 Typical Roadway Cross Section

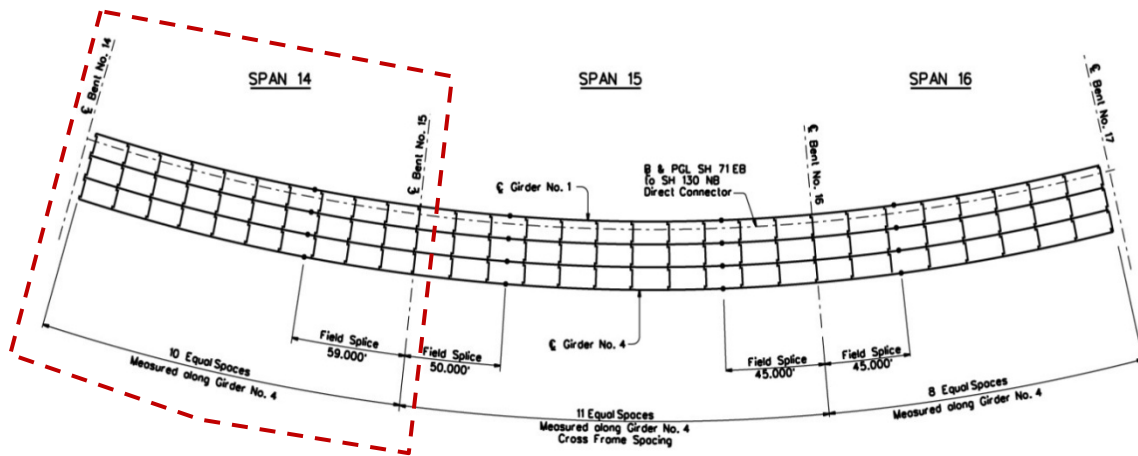


Figure 3.3 Unit 6 Framing Plan

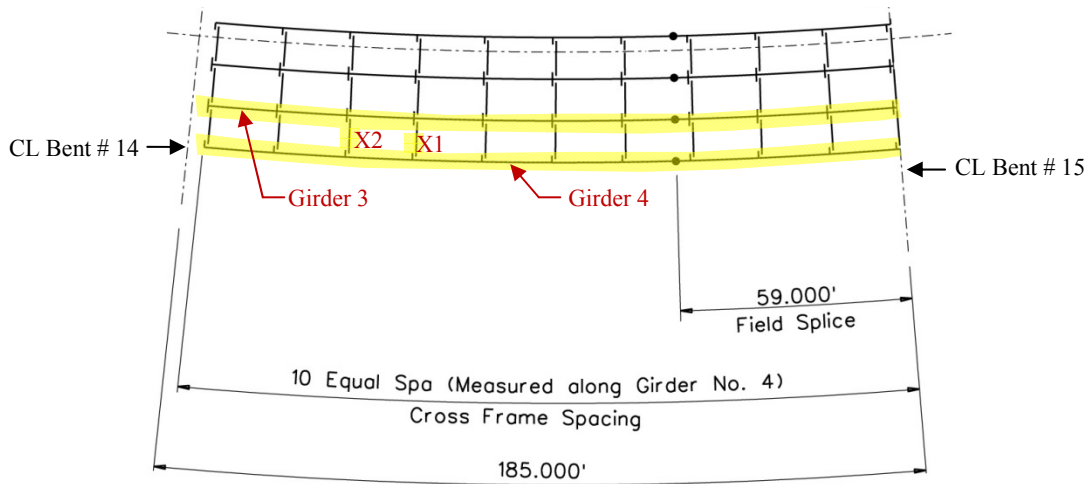


Figure 3.4 Span 14 Plan View - Girder Designations

3.2.1 Girder Description and Gage Locations

One of the main objectives of this research project is to monitor the behavior of the girders during critical construction stages. The locations of the strain gages were

placed at critical sections during the erection and concrete placement stages of construction. In a preceding thesis, *Behavior of Horizontal Curved Steel I-Girders During Lifting* (Schuh, 2008), the gage placement is extensively detailed. A summary of the instrumentation arrangement is provided in this section.

In Span 14, Girder 3 has a span of 184.61', with a radius of curvature of 1229.39' and like all the girders in this span, is dapped at the Bent No. 14 end. The girder has an 84" x $\frac{5}{8}$ " web plate with top and bottom flange plate sizes of 24" x 1 $\frac{1}{4}$ " at the location before the field splice and transitions to an 84" x $\frac{3}{4}$ " web plate after the field splice. The top and bottom flange plates increase to 24" x 2", 11.0' from the centerline of Bent No. 15. Gage locations on Girder 3 are designated on Figure 3.5.

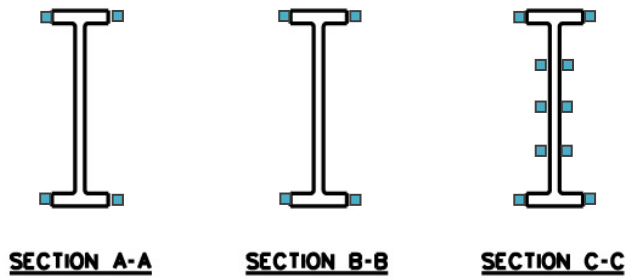
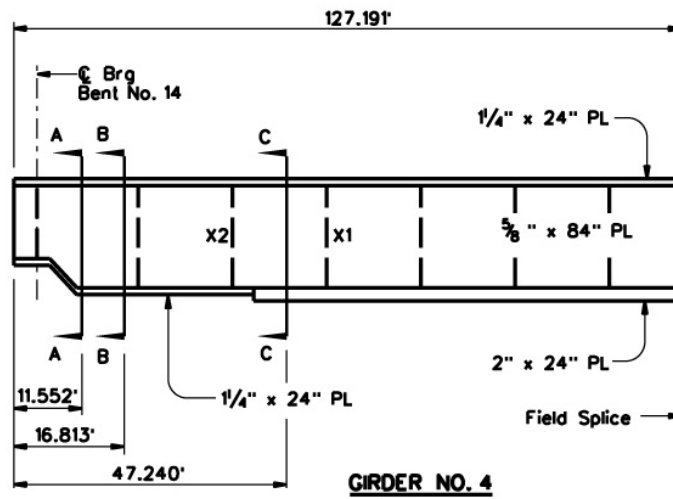
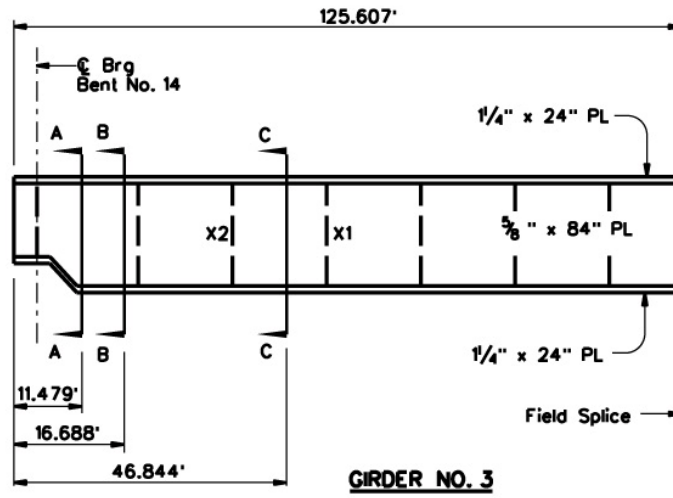


Figure 3.5 Girder 3 and 4 Gage Locations

Two gage locations at 11.48' and 16.69' from the end of Girder 3 near Bent 14 were chosen to collect data at Section A-A and B-B. Section C-C gages were used to collect data near the mid span of Girder 3 and in between the two instrumented cross frames, X1 and X2. The top and bottom flange tips were instrumented with strain gages at the mid flange thickness at Sections A-A and B-B as shown in Figure 3.5. Both sides of the top and bottom flanges were instrumented to observe the bending and warping stress behavior during data collection. At Section C-C, the top and bottom flange tips were instrumented as well as three locations on both sides of the web to monitor the bending stress throughout the cross section. The web gages in Section C-C were placed at 0.25, 0.50, and 0.75 of the web depth.

Girder 4, which is the fascia girder, is 186.29' with a radius of curvature of 1239.73' in Span 14. Similar to Girder 3, Girder 4 has an 84" x $\frac{5}{8}$ " web plate and transitions to an 84" x $\frac{3}{4}$ " web plate after the field splice. The top and bottom flange plates stay at a constant width of 24", but the thickness varies from 1 $\frac{1}{4}$ " to 3" as depicted in Figure 3.5. The gage locations on Girder 4 are the same as Girder 3 and are indicated in Figure 3.5.

3.2.2 Cross Frame Description and Gage Locations

The cross frames were comprised of four L5" x 5" x $\frac{1}{2}$ " angle sections. The two top and bottom horizontal struts have lengths of 8'-7" while the two diagonals are 9'-1" in length. The angles were instrumented with four strain gages that were positioned on both sides of the angle legs at a location 1" from the tip of the angle leg. Axial forces can be monitored in the braces and between Girders 3 and 4 during the concrete placement by tracking the strains in the gages; however the effects of angle bending must be accounted for using expressions developed by Fan (1999). Figure 3.6 provides a schematic of the cross frames and gage locations on the four members.

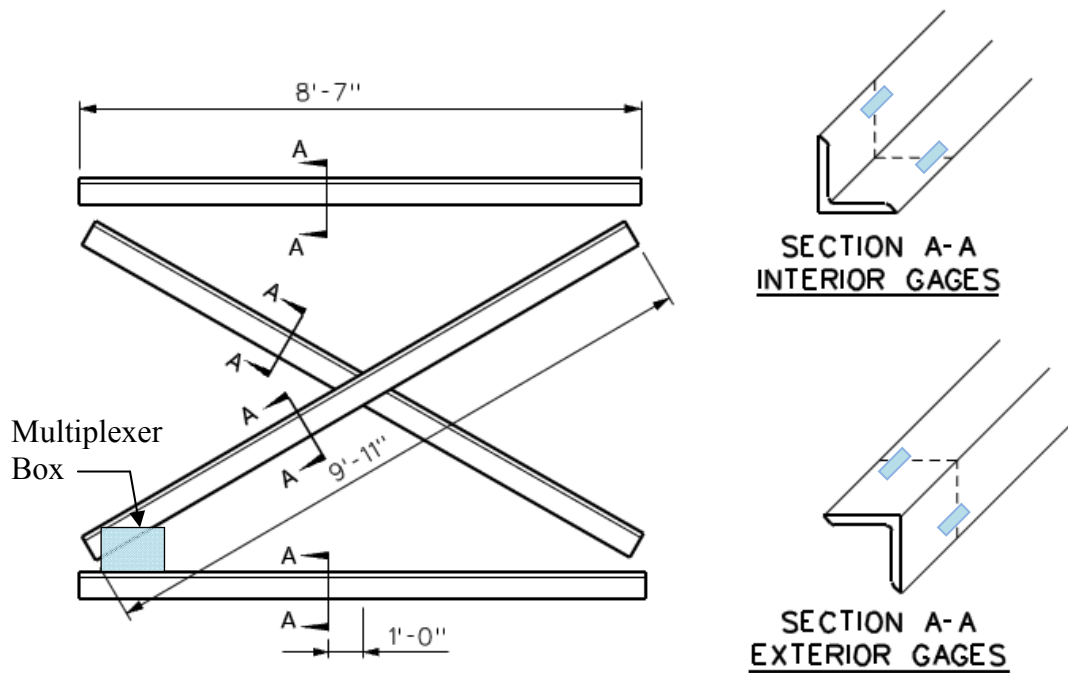


Figure 3.6 X1 and X2 Elevation with Gage Locations

3.2.3 Data Acquisition System Configuration

A total of 68 gages were used to examine the behavior of Span 14 of Bridge 88 during the concrete placement stage. The gages were installed while the girders were staged on the ground at the bridge site. As outlined in the previous section Girders 3 and 4 were each instrumented with 18 gages, while cross frames X1 and X2 were instrumented with 16 gages. Detailed steps were taken to ensure that the strain gage wires, multiplexers, and dataloggers were protected from the handling during the erection phase as well as from the environment. Figure 3.7 through Figure 3.9 depict some of the various protection methods that were used for the instrumentation in the field test. In-depth details of the protection measures were outlined by Schuh, 2008.

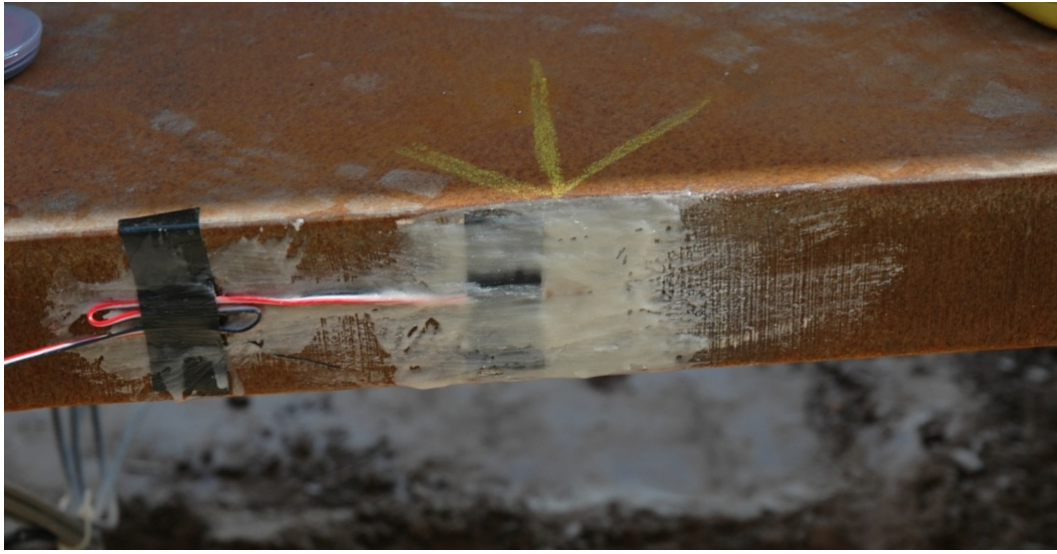


Figure 3.7 Wax protection on strain gage on bottom flange



Figure 3.8 Flange Strain gages protected by steel channel caps



Figure 3.9 Dataloggers and Multiplexers protected in steel boxes on erected girder

3.2.3.1 Girders

Girders 3 and 4 were instrumented on the ground at the job site prior to being erected onto the concrete bent caps. The same strain gages were used to collect data for the erection of the girders as well as the concrete deck placement.

To provide moisture protection to the electrical wiring of the gages, heat shrink wrap was placed on the spliced area and then wrapped with electrical tape. The wires leading the multiplexers and dataloggers were organized inside a flexible metal conduit shown in Figure 3.10. The conduit was used to redirect the wiring in complicated areas on the girders and braces.

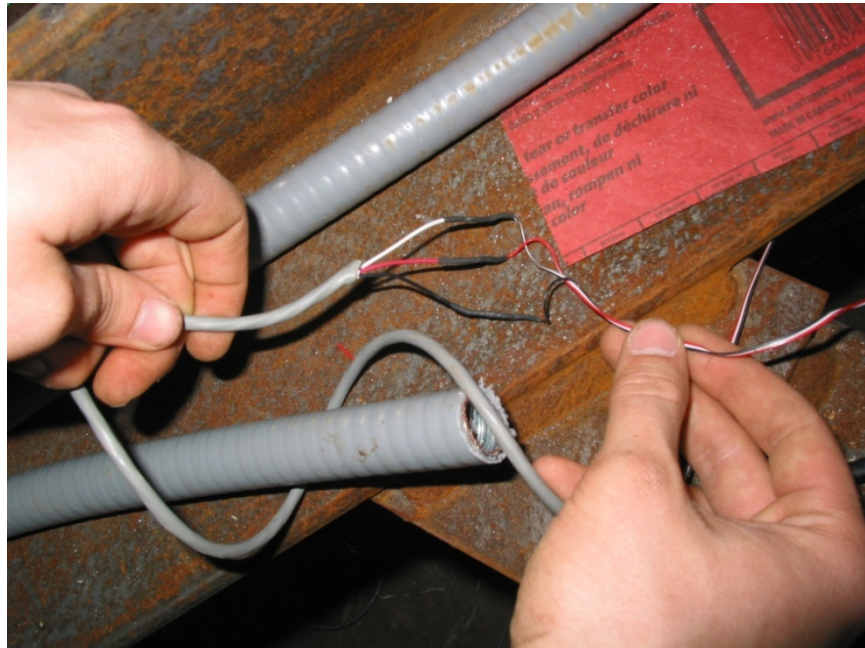


Figure 3.10 Spliced strain gage wire (Schuh, 2008)

The strain gages were attached to the flange tips and web plate using a two part adhesive. Prior to installing the gages, the steel area was ground smooth and the surface cleaned with acetone. The gages were then bonded to the steel sections using the two-part adhesive and then covered with a microcrystalline wax to protect the sensors from any moisture contamination that could occur in an outdoor field setting. After the layer of wax was applied, a second layer of silicone was applied. As a further precaution, the flange gages were protected by specially fabricated steel channels that were attached to the flanges with two bolts. The channel caps provided protection from inadvertent damage from construction activity. Figure 3.9 shows the protective steel channel attachment to the bottom flange.

3.2.3.2 Cross Frames

The cross frames were transported from the field to the Phil M. Ferguson Structural Engineering Laboratory to be instrumented. Figure 3.11 shows the cross

frames in laboratory after the instrumentation was installed. The measures for gage protection outlined in the previous section were used on the cross frame gages. Wooden blocks were attached on the outside cross frame strain gages with hose clamps to prevent damage to the gages during transport back to the field or when the cross frames were connected to the girder and erected.



Figure 3.11 Instrumented Cross frames X1 and X2

3.3 DATA ACQUISITION SYSTEM

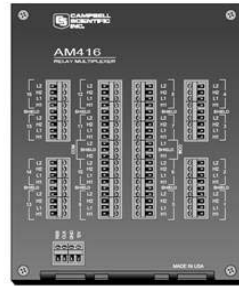
3.3.1 Datalogger

A CR5000 datalogger manufactured by Campbell Scientific, Inc was used to collect and store data from the bridge during the concrete placement stage. The CR5000

is suitable for this type of field application because of its resilience in outdoor environments as well as having a high level of accuracy. While being versatile and transportable, the CR5000 is capable of taking measurements up to 5,000 samples/second with a 16 bit resolution. The data logger, which is pictured in Figure 3.12, can record voltage measurements up to 5V.



CR5000 Datalogger



AM416 Relay Multiplexer

Figure 3.12 CR5000 Datalogger and AM416 Multiplexer

The CR5000 can be programmed directly with the key pad, but also has the ability to sync with a computer using the PC9000 software provided by Campbell Scientific. The software, which is included with the purchase of the CR5000, was used to manage the output from the data acquisition system. The software provides program generation and editing, retrieval of data files, and real time monitoring (Campbell Scientific, 2006). The CR5000 has the ability to connect to 40 single ended connections and 20 differential connections. The strain gages used in this project must connect to a differential connector, which allows up to 20 strain gages to connect to a single datalogger. The number of data channels was expanded in this study using the AM416 Multiplexers from Campbell Scientific. The gages are connected directly to the multiplexer which is connected to the datalogger.

3.3.2 AM416 Multiplexer

A multiplexer makes it possible for several input signals to share one output device. Up to 16 strain gages (16 differential channels) can be connected to the AM416 Multiplexer and up to 7 multiplexers can be connected to the datalogger. In addition to increasing the number of input sensors the data acquisition system can handle, multiplexers can be connected closer to the strain gages, reducing the amount of wire needed for instrumentation. Figure 3.13 depicts this scenario.

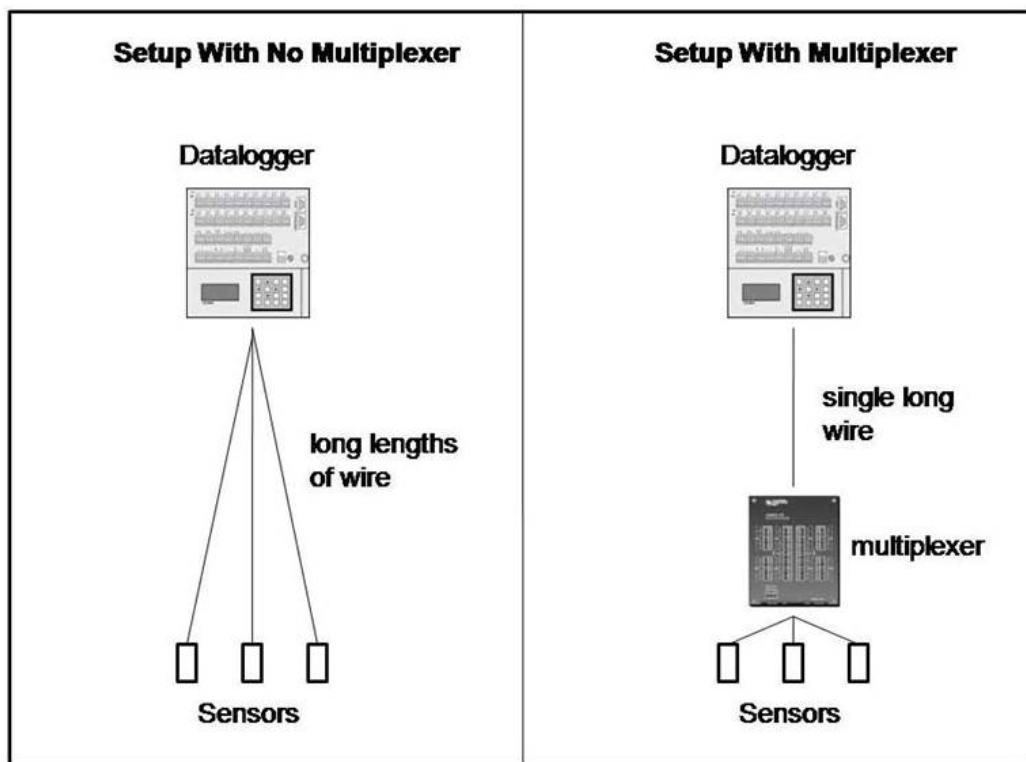


Figure 3.13 Multiplexer setup schematic (Campbell, 1996)

3.3.3 Strain Gages

To monitor the bending and warping stress behavior of the girders and axial forces in cross frames during the concrete placement construction phase, strain gages

were used to capture the change in strain using the electrical resistance. Strain is defined as the amount of deformation per unit length of an object when a stress is applied. A change in resistance is proportional to the strain that the sensor experiences (www.omega.com). The sensors used in this research project are resistive-type strain gages that consist of an insulating flexible backing supporting a metallic foil pattern. The method for calculating the bending and warping stress is discussed in detail in Chapter 4.

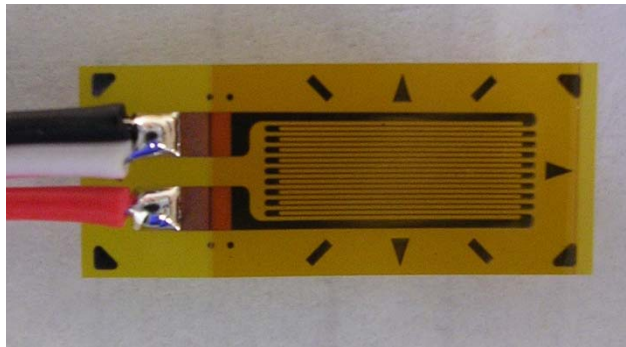


Figure 3.14 CEA-06-250UN-350/P2 Strain Gage

The foil strain gages that were used were Vishay Micromeasurements' model CEA-06-250UN-350/P2. The gages have 350 ohm resistance, a gage length of 0.250 in. and a strain range of $\pm 3\%$. Figure 3.14 shows the Vishay foil strain gage with covered lead wires. The preattached covered lead wires improved the ease of installation and avoided the need to insulate the wires with electrical tape, which saved time during field instrumentation (Schuh, 2008).

3.3.4 Wire Full Bridge Terminal Input Module

To complete the strain gage circuit, the 4WFB350 4 Wire Full Bridge Terminal Input Model from Campbell Scientific was used. Terminal input modules connect directly to the datalogger's input terminals to provide the bridge completion resistors and provide for a connection point for the three wires from the strain gage (Campbell, 2007). Foil gages are quarter-bridge circuits, whereas the datalogger must read full-bridge circuits. Therefore, in order for the datalogger to accurately extract data from the strain

gages, a completion bridge must be used. A completion bridge module is shown in Figure 3.15.



Figure 3.15 Completion Bridge Module (Campbell, 2007)

3.4 STEEL GIRDER VERTICAL DEFLECTION READING SETUP

Another aspect of the field instrumentation that is important to improve the understanding of the behavior of the steel bridges during construction is the measurement of the vertical deflections of the girders during placement of the concrete bridge deck. In order to monitor the actual deflections of the girders from the ground, a technique was developed and applied to SH 130/US 71 Director Connector, Span 14. Key locations on all four girders in Span 14 were identified on the underside of the bottom flange. These locations were at mid span of all four girders, with additional marks on Girders 3 and 4 at 1/8, 1/4 and 3/8 of Span 14. The locations were identified prior to the concrete deck placement using spray paint to make a circular mark of approximately 2 inch diameter as shown in Figure 3.16. Locations were also established on the ground to correlate with the marked locations on the girders. Some of the ground locations were positioned on the underlying roadway, while some of the locations were on uneven “right of way” areas beside the roadway. Prior to the deck construction, initial measurements were taken at the four locations mentioned previously on Girders 3 and 4 using a laser distance meter that is discussed in the following section. The initial reading establishes the distance between the ground and the girders prior to concrete placement. After the concrete is placed, the girders deflect causing the distance between the ground and the girders to

change as depicted in Figure 3.17. Therefore, follow up readings were taken at each location after concrete placement. The vertical deflection was calculated by subtracting the respective readings taken prior to concrete placement from those taken after the concrete placement. Figure 3.16 shows the marked locations for vertical deflection readings.



Figure 3.16 Span 14 mid span deflection reading locations

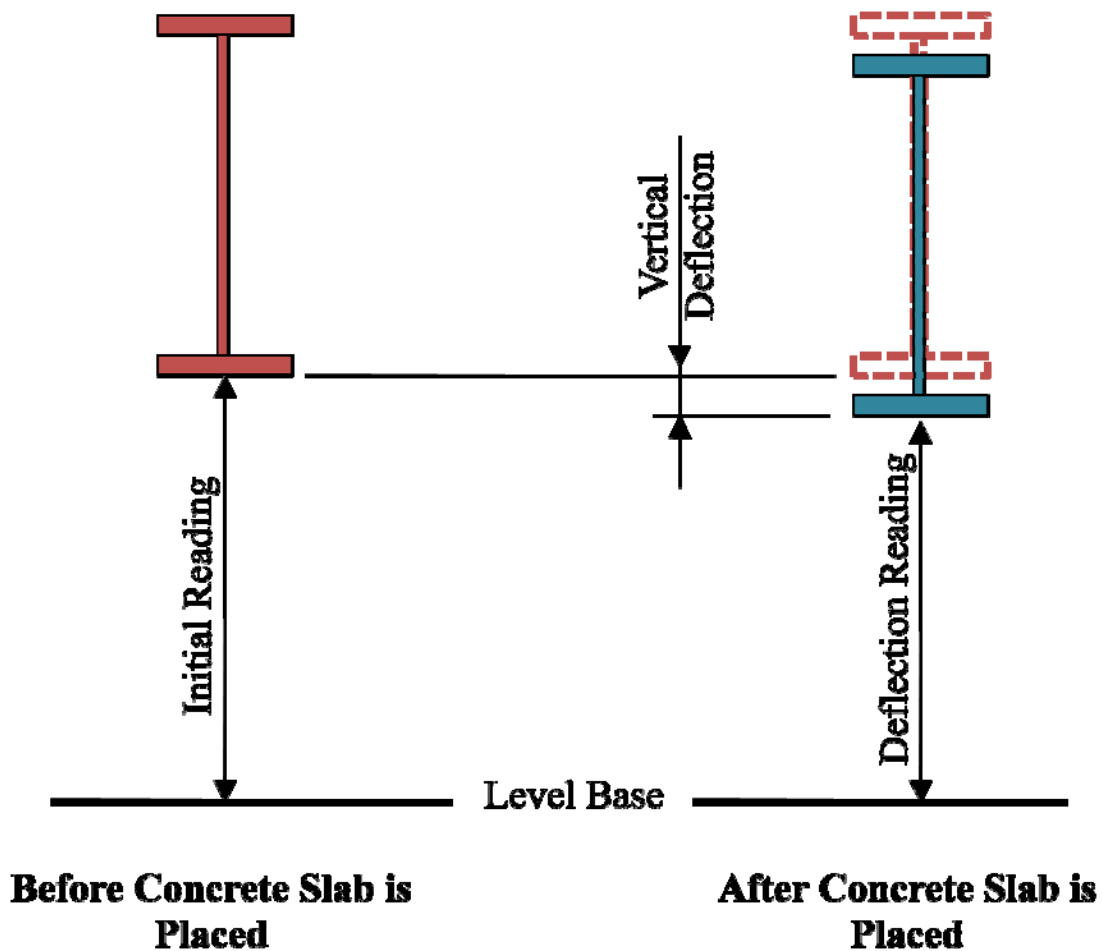


Figure 3.17 Vertical Deflection Schematic

3.4.1 Hilti PD 32 Laser Range Meter

At Span 14 of Bridge 88, the distance to the bottom of the girder to the ground ranges from 50' to 70'. With this magnitude of height, the Hilti PD 32 Laser Range Meter allowed relatively accurate measurements to be easily captured. The laser has a range from 2" to 600'. The readings are accurate to within 1/16". The laser is a visible 620-690 nm, class 2 laser. As shown in Figure 3.18, this versatile device is also portable, only weighing 0.48 lbs. To ensure accuracy of the readings, three readings were taken at

each location and the corresponding readings were averaged. In all cases, the readings did not vary by more than 1/16".



Figure 3.18 Hilti PD 32 Laser Range Meter

3.4.2 Construction of Reference Ground Locations

In order to get an accurate measurement reading, the laser range meter must rest on a level and isolated surface. In cases where the gage location was not over the roadway, a small hole was dug in the ground at the instrumentation site and lined with plastic. Hydro-Stone, which is a self-leveling gypsum cement, was used to create a level surface. Hydro-Stone has a high compressive strength and a relatively fast set-up time. Water was mixed with the Hydro-stone in a large bucket, and then poured into the previously dug hole. Figure 3.19 demonstrates the ease of mixing Hydro-Stone and Figure 3.20 shows the fluidity of the material as it is being poured into the established measurement location.



Figure 3.19 Hydro-Stone bucket and preparation



Figure 3.20 Pouring Hydro-Stone into hole

After the Hydro-Stone was poured into the holes and hardened, the laser meter was used to pin point the exact location of the marked girder above. Once this location was determined, a nail was driven into the Hydro-Stone. This allowed the laser to be put in the exact location to easily get accurate vertical measurement readings. The locations on the roadway were marked with a nail in the pavement.

3.5 THERMAL EXPANSION TEST SETUP

In addition to the girder behavior that was captured during concrete placement, the researchers also desired to obtain a measure of the thermal expansion and contraction of the Girders. The technique used to evaluate this involved a fabricated device from a previous study on the thermal performance of steel bridges (Grisham, 2005 And Chen 2008). The device consists of a stylus that is connected to the steel girder at the bearing location plates. The type of bearings on the bridge are the standard TxDOT steel girder bearing design (TxDOT Standard issued September 1998), consisting of steel plate resting on an elastomeric bearing pad. For the expansion end of a span the plate has slotted holes to accommodate the expected movement, whereas for the fixed end of the span, the plate has round holes. Dowels connect the bearings to the concrete bent cap to restrain global movements of the girders. The stylus rests in a plastic container filled with microcrystalline wax that is attached by an adhesive to the supporting pier cap or abutment. When the girder expands or contracts with temperature, the stylus leaves a trace in the wax medium and provides an indication of the magnitude and direction of the deformation relatively to the pier cap.

The movement at Bent 14, which is an expansion bent, was monitored. The bearing plate that is attached to the bent as well as the girder has longitudinal slotted holes, which allows the steel girder unit to expand and contract as the temperature changes. The stylus was attached to the bearing plate with a steel fabricated channel, which was clamped to the bearing plate with two bolts. The stylus, which was made out of a threaded rod, was attached to the channel with a small flat plate.

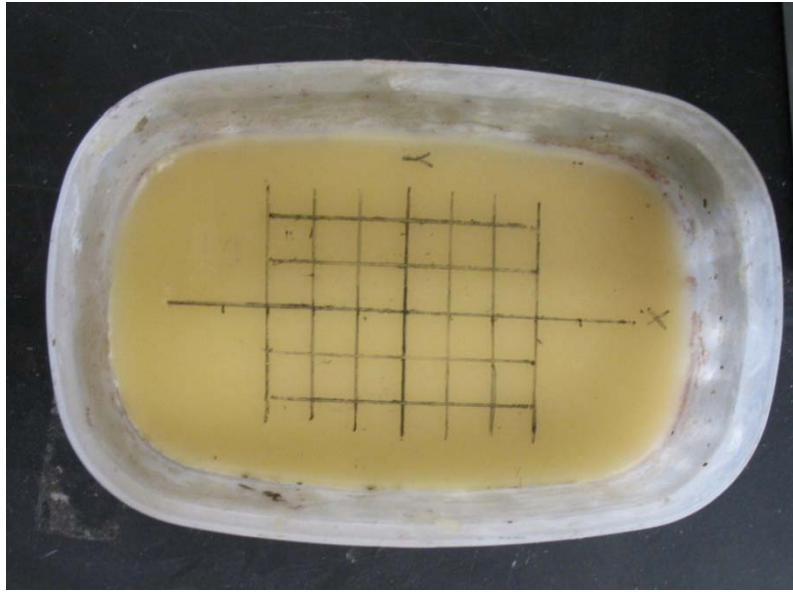


Figure 3.21 Wax Trace Box with ½" Grid

The location of the plastic container was determined and was connected to the bent cap with a fast setting adhesive. Microcrystalline wax is an ideal etching medium to record the longitudinal displacement since it has a melting temperature of 190°F, which is higher than any temperature that the bridge will experience but is also low enough to easily fabricate the trace boxes. The microcrystalline wax is easily poured and molded into the plastic container. A ½" by ½" grid, which is shown in Figure 3.21, was drawn on the wax to record any thermal movement, which was tangent to the girders, from the stylus. The origin of the grid as well as the transverse (Y) and longitudinal (X) directions were labeled on the grid. Figure 3.22 shows the test setup for this phase of the field monitoring.



Figure 3.22 Wax pot and stylus test set up

3.6 SUMMARY

This chapter provided a discussion of the instrumentation of Bridge 88 to monitor the behavior of curved plate steel girders and two cross frames during the concrete slab placement stage of construction. Discussion of the procedures and equipment involved were outlined. The data from the field monitoring were used to analyze bending and warping stresses of two girders, axial forces in two cross frames, vertical deflection, and thermal expansion. The data is discussed in the following chapter. This information will be used to validate the finite element models in the study.

CHAPTER 4

Field Results from SH 130/US 71 Span 14 Concrete Placement

4.1 INTRODUCTION

For many horizontally curved girders, the critical loading stage often occurs during the construction stage, prior to composite action with the concrete deck. The steel section must support the entire construction load during this phase. This chapter discusses the measurements and timeline during the concrete placement of Bridge 88, which is located east of the Austin Bergstrom International Airport (ABIA) on SH 130 at US 71. SH 130 is a large toll road containing many bridges. The bridges are numbered along SH 130 from North to South and the instrumented bridge is therefore named Bridge 88 through this naming convention. Most of the horizontally curved steel girder bridges that are constructed in Texas follow a traditional concrete pouring sequence that involves placing the positive dead load moment regions of the continuous unit first, followed by the negative dead load moment regions (area over the supports). Contrary to this common practice, the instrumented bridge was poured continuously from beginning to end. Concrete placement began at the North end of the bridge on Span 16 and proceeded along the length of the bridge to Spans 15 and 14. Recalling from the previous chapter, the instrumentation was placed in Span 14 which was the last region of concrete placement. The geometry and gage locations were discussed in the previous chapter. Following data collection, the data was reduced and processed. This chapter focuses on the presentation of the data including strain gage data from the girders and the cross-frames as well as the vertical deflection readings. In addition to strain gages, the bridge was instrumented with 16 tilt sensors to measure twist of the girders. Data from the tilt sensors during the concrete placement is reported by Fasl (2008). As outlined in the previous chapter, the thermal expansion of Unit 3 was also measured and will be reported

in this chapter along with comparisons to the theoretical value using American Association of State Highway Officials (AASHTO) equations.

4.2 SH 130/US 71 DIRECT CONNECTOR CONCRETE PLACEMENT

Concrete bridge deck construction involves more than a concrete truck and skilled workers. When designing a bridge, most engineers focus on the substructure and beams or girders. The reality is that the majority of the people who use the bridge will only notice and be concerned with the bridge deck. The deck is what the traveling public sees as they cross a bridge. Extra care is taken to ensure that the ride quality is smooth and above average. Because of the high volume of concrete and significant role that the bridge deck plays in the overall structure, the construction of the deck is an “event” that involves meticulous planning, coordination, and testing so that this stage of construction runs efficiently. Just scheduling the numerous concrete trucks to arrive at the site on time takes extreme planning in order to deliver hundreds of cubic yards of concrete to the bridge site. There are a number of critical aspects to consider in the planning of the concrete cast to ensure quality control of the finished deck. One key aspect is that the ready mix trucks will not be delayed by traffic or that the temperature during placement is not too high or too low so as to affect the hydration of the cement in the concrete. Because of the effects of traffic and hot weather, many deck casts are done during the nighttime hours when the temperature is cooler and traffic is much more predictable. The casting of the deck on the test bridge began at night and was completed in the morning. After the concrete truck arrives on site, the concrete is then poured into a pump truck that pumps the concrete up to the bridge deck. Figure 4.1 shows the pump that was used to place the concrete on the instrumented bridge.



Figure 4.1 Bridge 88 Unit 3 Concrete Deck Placement

As the concrete is pumped onto the deck and in between the deck reinforcing, a screed, as seen in Figure 4.2 and Figure 4.3, is positioned transversely on the bridge, vibrates and levels the freshly poured concrete. The picture in Figure 4.2 was taken at the start of the concrete pour at 1:30am. Transverse screeds are used because they permit the rapid placement of wide decks while reducing the amount of hand finishing. Supporting a rotating drum, auger, and pan drag, transverse screeds have a carriage system that is supported by screed rails on each side of the deck. The screed travels the length of the placement as the drums, augers, and pan drag move back and forth on the carriage. Additional vibrating of the concrete by construction workers, before the screed passes over, is also required. After the deck is finished and textured, a membrane curing compound is typically sprayed on the surface of the deck. The membrane curing

compound forms a thin film on the surface of the deck to prevent evaporation of moisture from the surface of the concrete that would adversely affect the hydration of the concrete.



Figure 4.2 Concrete Deck Placement at beginning of pour



Figure 4.3 Transverse Screed used in deck construction

4.2.1 Unit 3: Spans 16 and 15

The third steel unit of this bridge, which contains the instrumented girders and cross frames in Span 14, was scheduled for pouring the concrete deck on April 16, 2008. Deck placement on Unit 3 began at 1:30 am with Span 16 and finished Span 14 at 11:20 am. Public safety necessitated intermittent lane closures of the roadways below the bridge as concrete directly above the various lanes was placed. Because the instrumented sections were above the roadway, access to the instrumented sections was limited until the lanes were closed below those sections of the bridge. The timeline in Figure 4.4 gives a history of the deck placement and highlights the important milestones.

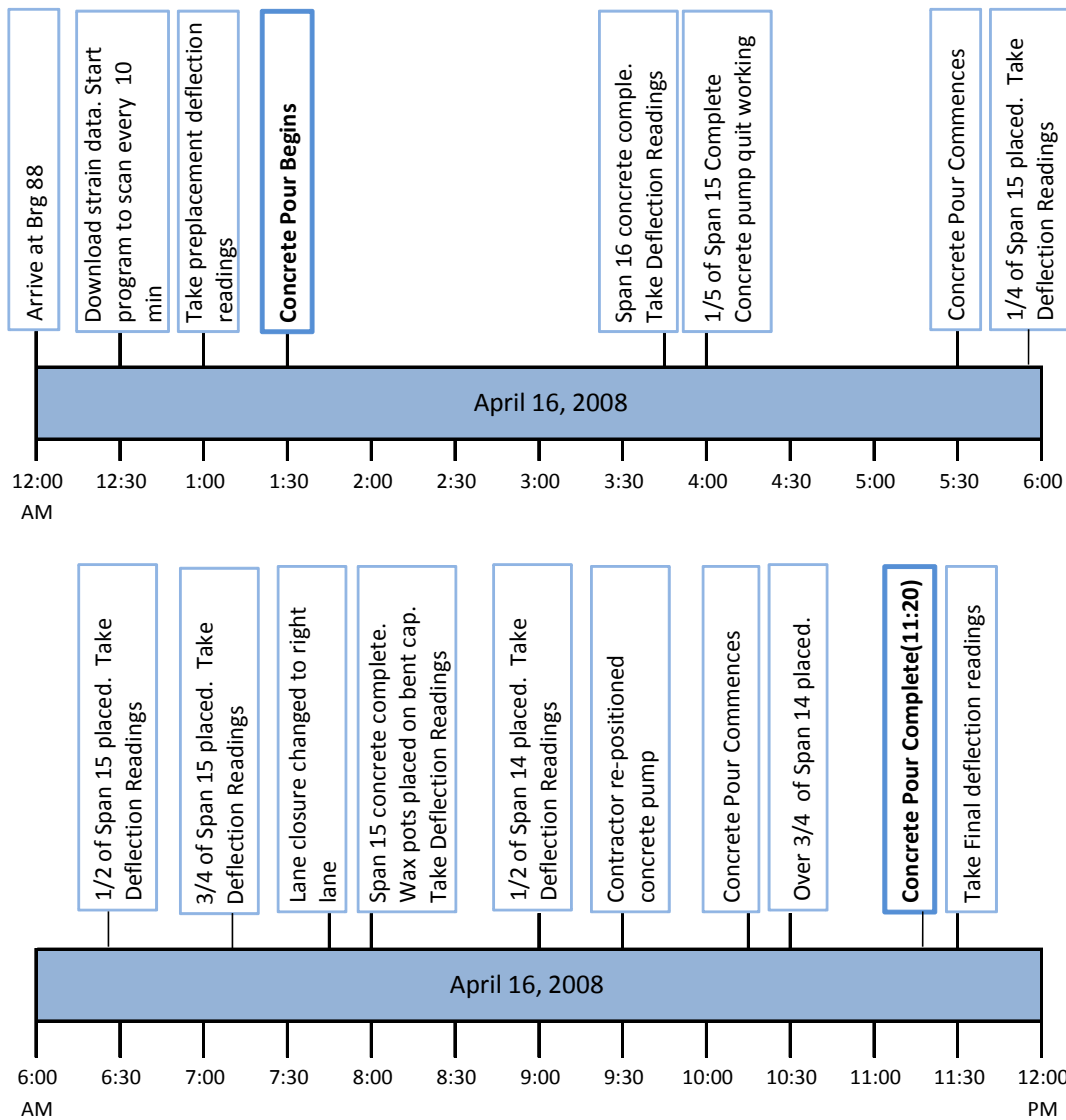


Figure 4.4 Bridge 88 Unit 3 Concrete Deck Placement Timeline

Upon arriving on the bridge construction site at 12:30 am, the previous strain data was downloaded and a new program was set to scan every 10 minutes. The information from the strain gages was captured in the datalogger, and downloaded to a laptop. There were two data loggers located on the bridge: one for the strain gages and one for the tilt sensors. The dataloggers, which were located on the flanges of the girders, were each connected to a booster cable to increase the signal to the lap top. Staged on top of the bridge (Span 14) near the overhang bracket, the use of the booster cable made

downloading the data to the laptop easy and accessible. The booster cable also saved time because it decreased the need for using a man-lift for downloading the data. The booster cable for the tilt sensors was cut before the researchers arrived on the construction site, therefore they were only able to get pre-pour and post-pour rotation data. At 1:00 am, initial vertical deflection readings were taken to provide baseline readings before the bridge deck was placed. Completion of the concrete placement on the first span (Span 16) was occurred at 3:45 am and deflection readings were taken at this time. After 1/5th of the second span (Span 15) was placed, the remote control on the concrete pump arm quit working. Work did not recommence until 5:30 am after a second backup pump truck was setup. During the concrete pour of Span 15, several deflection readings were taken as shown on the timeline in Figure 4.4. Before the third span (Span 14) was poured, the contractor closed the right lane of the underlying roadway, which is a requirement, so that there is no vehicular damage during concrete construction. This lane closure was helpful to the research crew because deflection readings could be taken easily and safely.

4.2.2 Unit 3: Span 14

At 8:00 am, the concrete placement for Span 15 was complete and the contractor began pouring Span 14. Vertical deflection readings were taken at this milestone and recorded. At 8:11 am, a man lift was used to install the wax containers to measure thermal expansion of Unit 3. Although it would have been preferable to have the wax trace boxes in place on the bridge for longer period of time, the researchers could not get access to the supports without traffic lane closures. At 9:00 am half of Span 14 was poured and deflection readings were taken. Throughout the entire concrete pour of Span 14, deflection readings were taken, as shown in Figure 4.4. Finally, at 11:20 am, with an total concrete quantity of approximately 660 yd³ for Unit 3, the last span (Span 14) was complete.

4.3 GIRDERS 3 AND 4

The following section summarizes the results of the change in bending and warping stress for the SH 130/US 71 Direct Connector during the casting of the concrete bridge deck of Unit 3. The entire construction stage was monitored and documented with photos. The graphs in this section represent the stress history before, during, and after the concrete pour. Each graph corresponds to the bending (blue dotted line) and warping stress (red line) at a specific location on the girder for a specific set of strain gages. Milestone events are highlighted on the graphs, to understand the behavior of the girder and relate it to a particular time during the concrete pour. The accurate assessment of strain changes due to construction activity necessitated the researchers to negate the effects of thermal gradients on the bridge. Thermal gradients can cause relatively large changes in the strain gage readings due to thermal constraints in the bridge as well as thermal drift in the gage readings. Despite the fact that the strain gages were compensated for thermal changes in steel, these gages will still drift slightly due to thermal changes. To minimize the impact of these thermal changes, the researchers typically determine change in strain due to construction activity by monitoring the gages in the early morning hours before and after the construction activity when the bridge is not exposed to solar radiation and the temperature of the bridge is uniform. By subtracting the strain in the early morning hours after completion of the activity from those before the construction, the change can be attributed purely to the construction event. The times that are selected are typically after midnight when the bridge temperature is uniform. Efforts are made to find nighttime temperatures before and after the construction that are relatively close. The ambient temperature at the beginning of the deck pour was 60.4°F at 1:30am. As shown in Figure 4.5, the temperature on April 19th at 2:30am is relatively close to the beginning deck pour temperature, at 60.9°F. Therefore, the strain values from April 19th at 2:30am were used to determine the overall change in stress for the construction of the concrete deck.

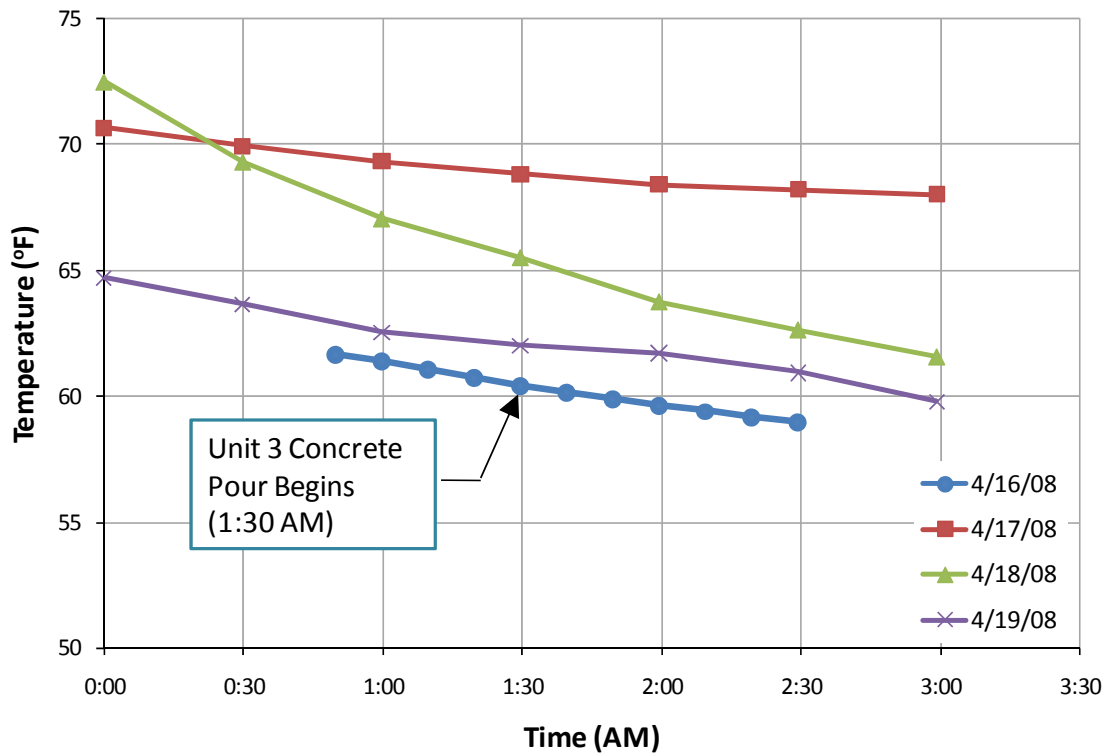


Figure 4.5 Early Morning Temperature Comparison

4.3.1 Girder Data Reduction Technique

As stated previously, two girders and two cross frames were instrumented with strain gages on the three-span curved steel girder unit. The strain from each gage was converted to stress (σ_L or σ_R) by multiplying by the modulus of elasticity for steel, which is 29,000 ksi. The purpose of measuring strain in the members was to isolate the bending and warping stresses. The bending and warping stresses will be used to validate finite element models as well as observe the behavior of the bridge during the concrete placement construction stage. This section describes how the bending and warping stresses were calculated from strains that were recorded during the concrete deck pour of Unit 3.

To understand the data reduction technique, the interaction between bending and warping stresses must be recognized. Considering the case of bending about one of the principle axes, the bending stresses vary linearly as a function of the distance from the

geometric centroid of the section with the maximum values at the top and bottom flanges. Since the width of the flange plates are not overly wide, effects of shear lag are minimal and, the bending stress is uniform across the width of the flange. Warping torsion on the cross section arise from restraints that cause lateral bending in the flange plates when the section twists. As a result, warping stresses typically result in a linear stress distribution across the width of the flange with tensile warping stresses on one side of the flange and compression on the other. Because the flanges are typically symmetric across the web of the girder, the magnitude of the tensile warping stress at the flange tip is equal to the compressive warping stress at the opposing flange tip. As shown in Figure 4.6, warping normal stresses act perpendicular to the surface of the cross-section and are constant across the thickness of an element of the cross-section but vary in magnitude along the length of the element. By superposition, the warping normal stresses add directly to the bending stresses already imparted on the member by vertical bending and act in the same direction.

Placing the strain gages on flange tips plays a key role in isolating the bending and warping stresses. These stresses are designated as σ_L and σ_R , which refers to the stress in the left flange tip and the right flange tip. For this field instrumentation set up, σ_L refers to the stress located on the girder flange tip that lies on the inside of the horizontal curve and σ_R correlates in this same manner to the flange tip on the outside of the curve. Figure 4.7 depicts the top flange of a girder under combined bending and torsion with two strain gages at the edges/tips of the flange. The figure also includes a plan view of the stresses that develop in the flange and are helpful in understanding the equations that were used to isolate the bending and warping components of the flange stresses. Equation 4.1 takes the average of σ_L and σ_R to compute the bending stress. Equation 4.2 divides the difference between σ_L and σ_R by 2 to compute the warping stress.

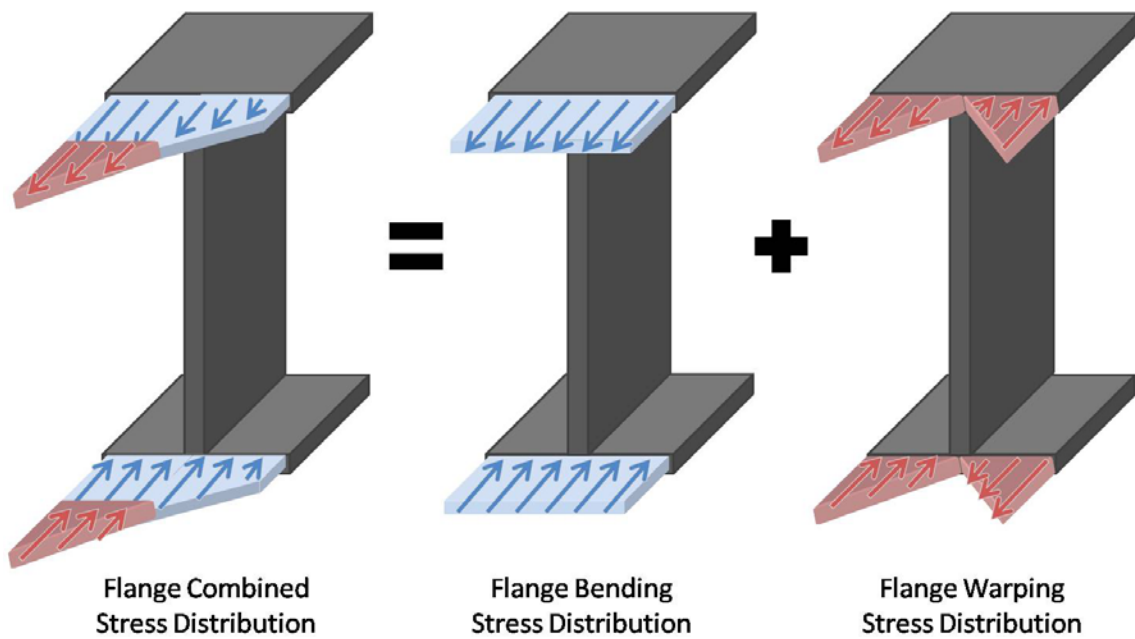


Figure 4.6 Curved I Girder Flange Stress Distribution (Schuh 2008)

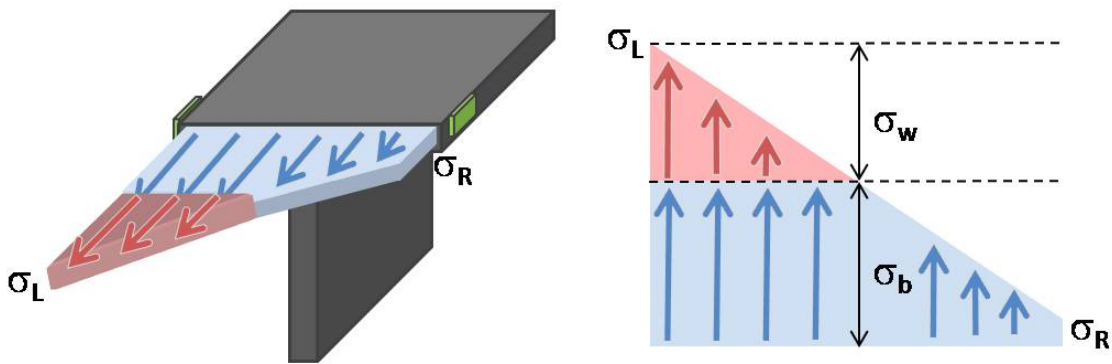


Figure 4.7 Bending and Warping Stress Isolation (Schuh 2008)

$$\sigma_{bending} = \frac{(\sigma_L + \sigma_R)}{2} \quad \text{Equation 4.1}$$

$$\sigma_{warping} = \frac{(\sigma_L - \sigma_R)}{2} \quad \text{Equation 4.2}$$

4.3.2 Girders 3 and 4 Results

The results for Section A on Girder 3, which is 11.48' from the end of the girder (near Bent 14), are reflected in Figure 4.8. All of the results are related to the stress in the girders before concrete was placed on Unit 3. The first significant bending stress change in the top flange, at Section A, occurred after half of Span 14 was poured and the bending stress changed to -1 ksi. Negative bending stress values indicate increasingly changes in compressive stress. At roughly 11:00 am, the gages for the top flange give values that are not typical. The reason for the changes in the gage readings may be due to a malfunction in the gage, but also may be due to temperature effects on the bridge. The temperature change may be a result of the warming of the bridge from the sun or may also be affected by the heat of hydration from the concrete deck. Figure 4.8 shows the progression of this and the time when the gage data became unusable.

The bending stress changes at the bottom flange at Section A correlates well with the data from the top flange at this location with gages on the top flange showing compressive strains and the bottom flange gages indicating tension. After the second span (Span 15) was poured at 8:00 am, there was a slight stress change in the bottom flange of -0.6 ksi. The corresponding change was 0.20 ksi after half of Span 14 was poured. After the concrete was placed up to the seventh cross frame in Span 14 at approximately 9:30 am, the bending stress change stayed at an average of 0.95 ksi until 10:15 am. This plateau in the stress occurred because the concrete construction was halted temporarily while the contractor repositioned the concrete pump. This trend can be seen on all of the figures in this report associated with the concrete pour. The total change in bending stress due to construction activity was 2.8 ksi. As shown in Figure 4.9, the change in warping stress had a small range, varying from -0.06 ksi to 0.03 ksi. The relatively small change in warping stress could be due to the close proximity of the gages to the support.

The second set of strain gages on Girder 3 was located 16.69' from the end of the girder near Bent 14, which is denoted by Section B-B. Due to a faulty strain gage on the

top left flange tip, only bending and warping stresses for the bottom flange can be reported. At 8:00 am, which is when Span 15 was finished, the bottom flange bending stress had a compressive stress change of -0.9 ksi. As Span 14 was poured, the bending stress change began to escalate to 0.4 ksi after the concrete was poured up to mid span. The total change in bending stress due to construction activity was 4.0 ksi. Similar to Section A, the Section B strain gages recorded minimal changes in warping stress.

Section C, which is 46.84' from the end of the girder near Bent 14, is the last set of gages monitoring the behavior on Girder 3. The top flange at Section C had a bending stress change of 1.9 ksi after Span 15 was poured. At this same time the top flange gages at Section A recorded a change in bending stress of 0.3 ksi, which is significantly lower than observed in Section C. At the time when the concrete was completed for Span 14, the change in bending stress for the top flange was -8.8 ksi. The total change in bending stress due to construction activity was -9.9 ksi. The top flange results correlate well with the predicted behavior of a continuously supported girder. The top flange at Section C is also where a significant change in warping stress appears. The overall warping stress, after the bridge temperature was normalized, was -1.2 ksi. This is noteworthy, considering that the strain gages at the other Sections recorded warping stress changes less than 0.1 ksi. The change in web bending stress at a quarter of the web depth mirrors the change in web bending stress at three quarters of the web depth, as shown in Figure 4.12 and Figure 4.14. This behavior matches what would be expected at this location. The top quarter section of the web reached a total bending stress of -3.1 ksi and the bottom quarter of the web reached 4.8 ksi. At the mid depth of the web there was minimal change in bending and plate bending stress. The highest values of the change in plate bending stress occurred at the top flange and the top quarter depth of the web. The following figures present the data obtained from the locations instrumented on Girder 3 during the placement of the concrete deck.

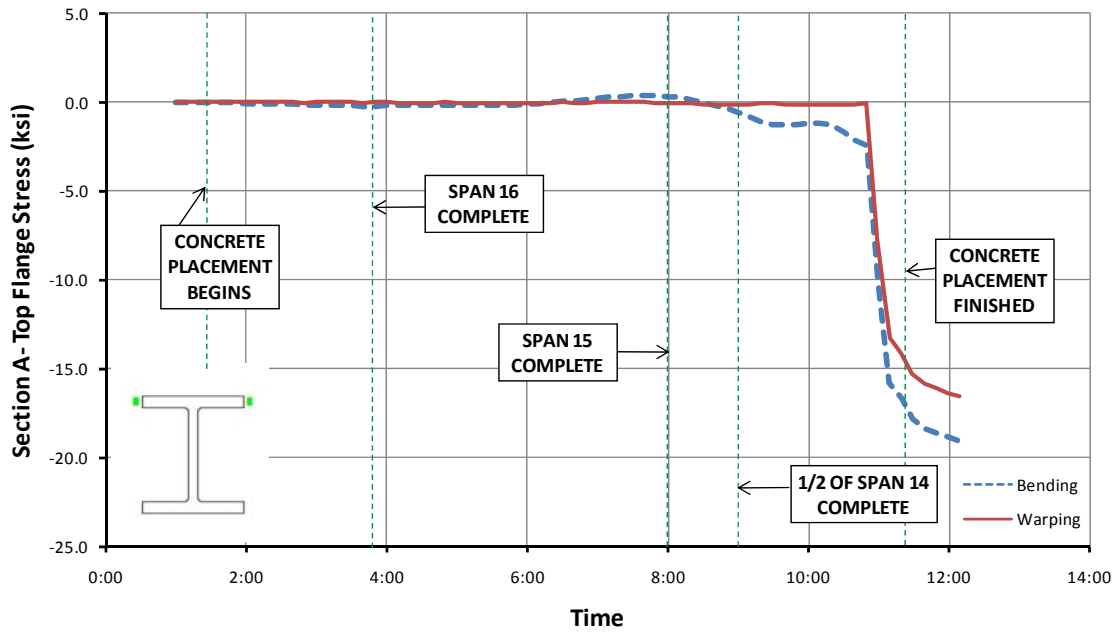


Figure 4.8 Girder 3: Section A Top Flange Stress

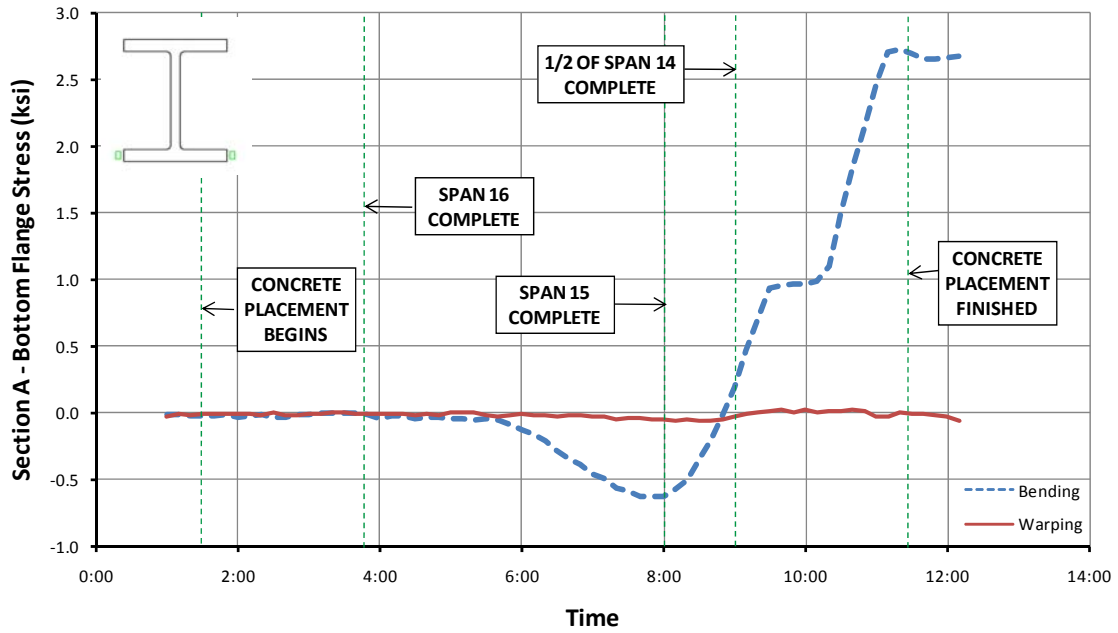


Figure 4.9 Girder 3: Section A Bottom Flange Stress

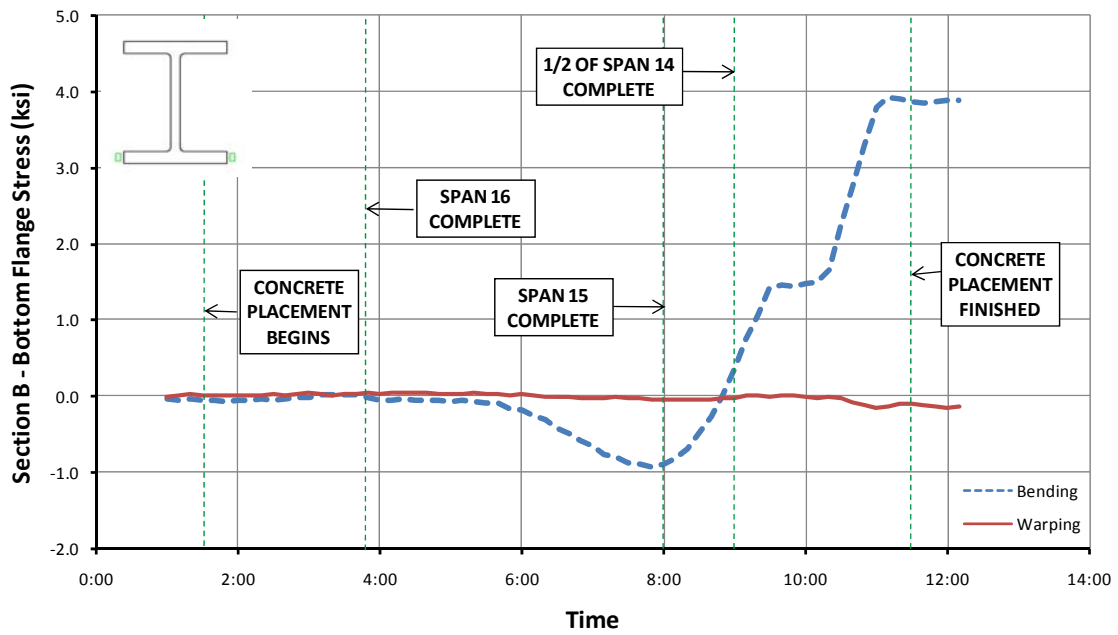


Figure 4.10 Girder 3: Section B Bottom Flange Stress

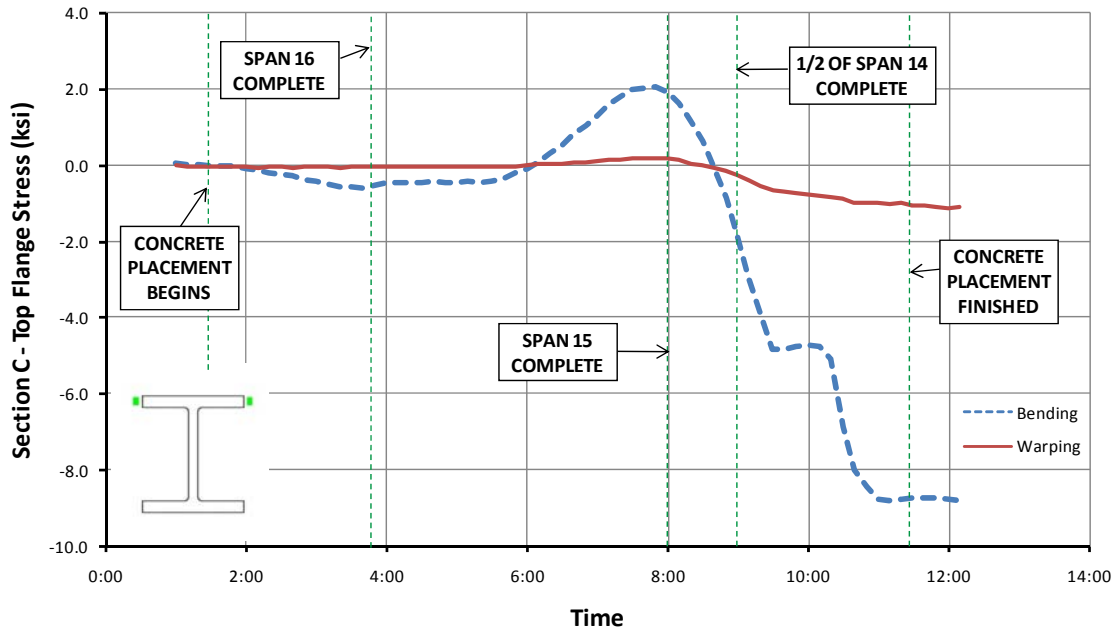


Figure 4.11 Girder 3: Section C Top Flange Stress

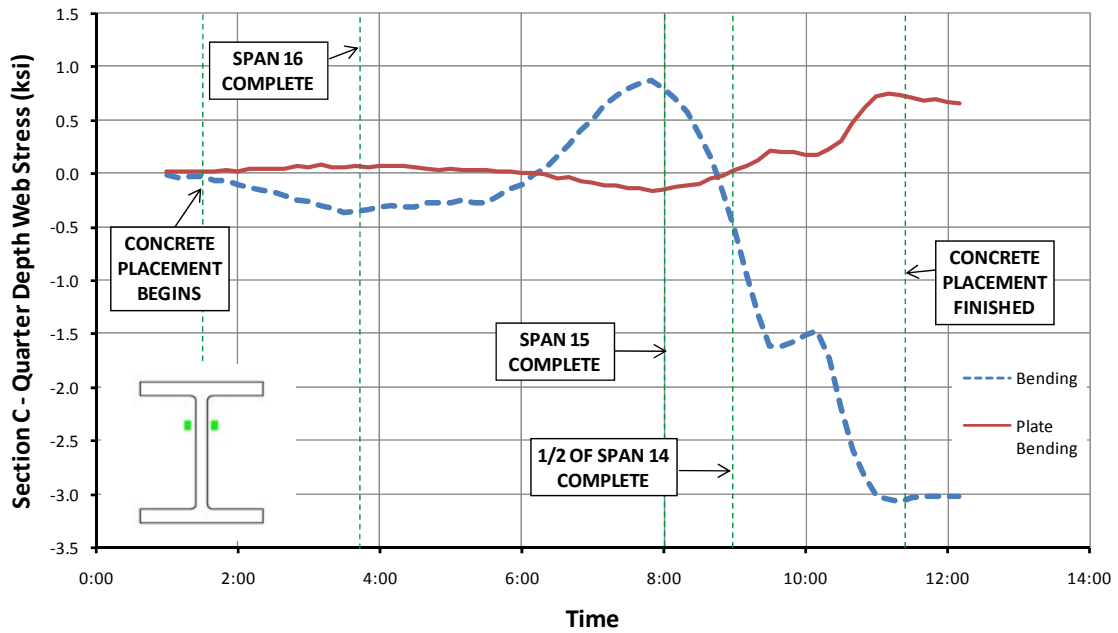


Figure 4.12 Girder 3: Section C Quarter Depth Web Stress

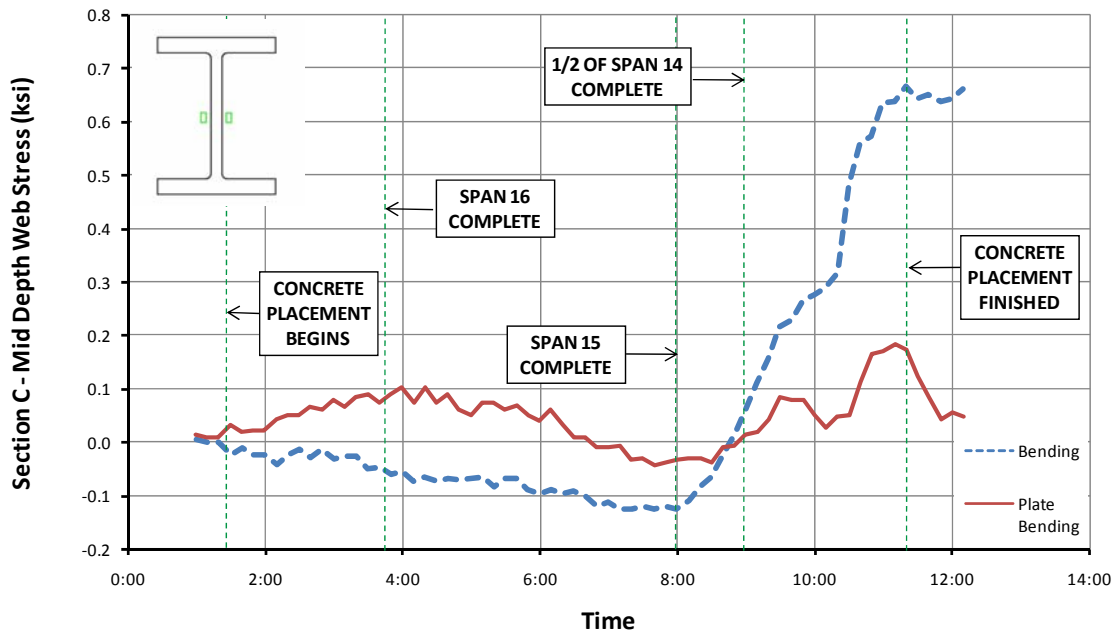


Figure 4.13 Girder 3: Section C Mid Depth Web Stress

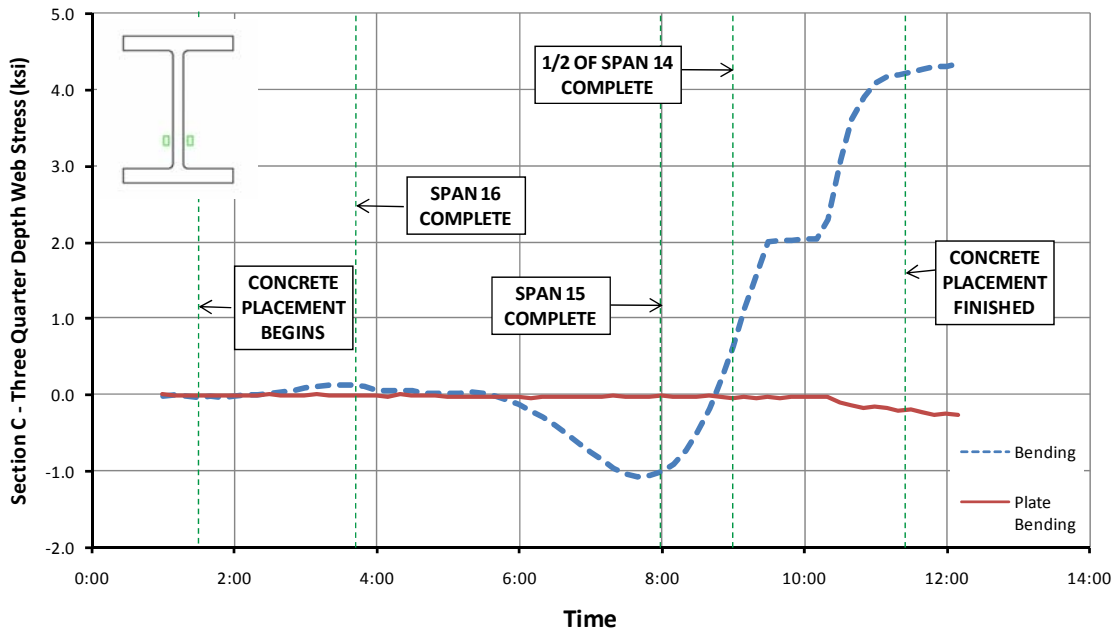


Figure 4.14 Girder 3: Section C Three Quarter Depth Web Stress

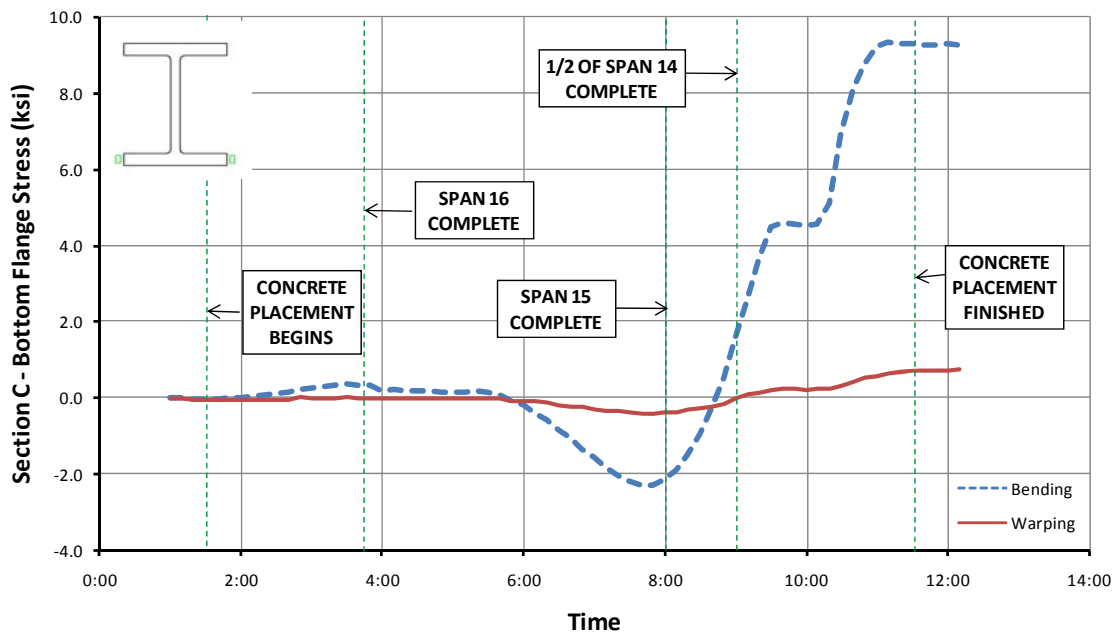


Figure 4.15 Girder 3: Section C Bottom Flange Stress

The strain gages for Girder 4 were placed in roughly the same places along the girder as on Girder 3. Section A, which is 11.55' from the end of the girder near Bent 14, was instrumented on the top and bottom flange tips. The graph of girder stresses versus time for the top flange on Girder 4 followed the expected trends, unlike the graph for Girder 3 at Section A. The reason for the poor performance of the gages at Girder 3 – Section A is not clear. The bottom flange at Section A of Girder 4 behaved nearly the same as the bottom flange on Girder 3 at the same section. Girder 3 had a total change in bending stress which ranged from -0.3 ksi to 2.8 ksi, while the range for Girder 4 was -0.4 ksi to 2.9 ksi. Figure 4.17 also shows the minimal change in warping stress that occurred at Section A of Girder 4.

Girder 4 at Section B, which is 16.81' from the end of the girder near Bent 14, was also instrumented on the top and bottom flange tips. The top flange had a change in bending stress of 1.0 ksi (tension) after Span 15 was completed and finished with a stress of -4.0 ksi (compression), as shown in Figure 4.18. The total change in bending stress due to construction activity was -4.7 ksi. The change in warping stress at the top flange reached -0.4 ksi, and then spiked back towards zero when the bridge temperature was normalized. The bottom flange at Section B had close to zero change in bending stress until 6:00 am, which is when about 20% of Span 15 had been poured. After the Span 15 concrete placement was completed the change in bending stress increased to -1.1 ksi in compression, then when Span 14 was completed the stress increased in the positive direction to 4.9 ksi. The total change in bending stress due to construction activity was 4.8 ksi. As before, the change in warping stress at this location was minimal.

The graphs for Section C on Girder 4 are similar to Girder 3, with slightly higher stress values. The top flange bending stress ranged from -11.1 ksi to 2.8 ksi, while the bottom flange stresses ranged from -2.3 ksi to 8.2 ksi. The bottom quarter of the web recorded the highest change in bending stress at Section C, with a value of 3.9 ksi. The following figures present the data obtained from the locations instrumented on Girder 4 during the placement of the concrete deck. The difference in web gages on each side is from plate bending due to initial imperfections and the curvature of the web.

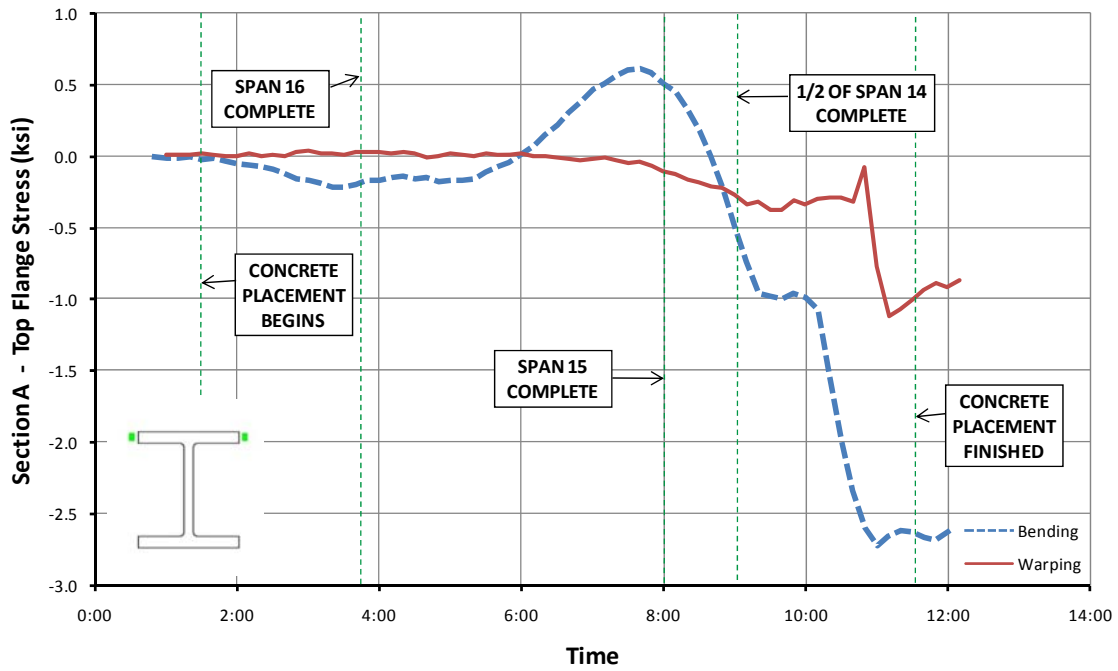


Figure 4.16 Girder 4: Section A Top Flange Stress

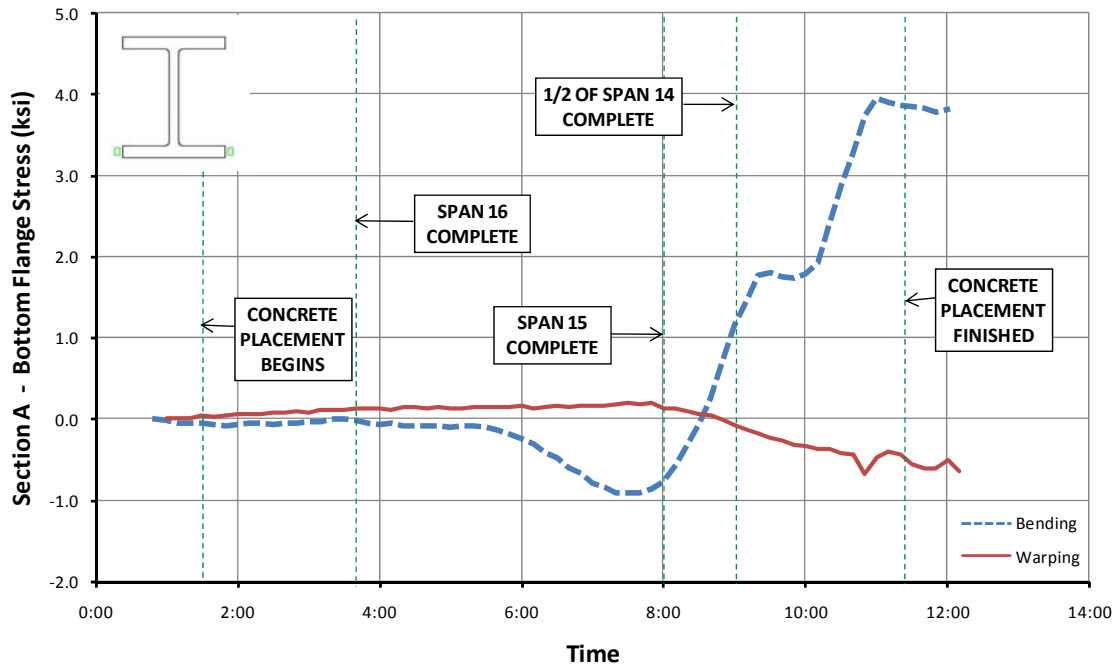


Figure 4.17 Girder 4: Section A Bottom Flange Stress

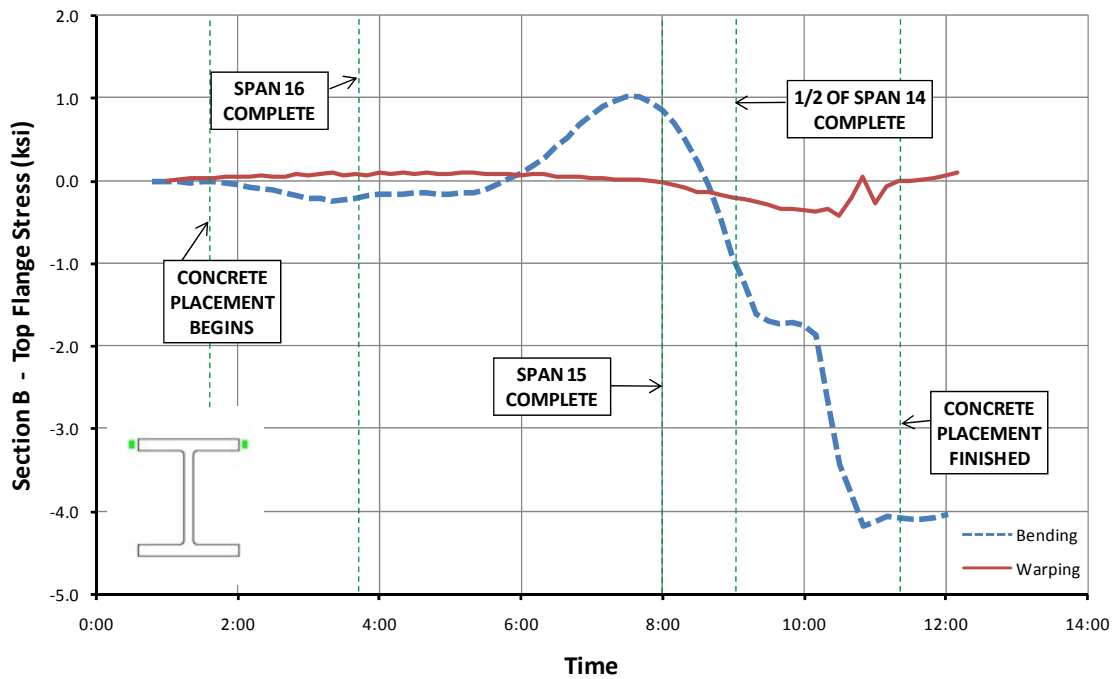


Figure 4.18 Girder 4: Section B Top Flange Stress

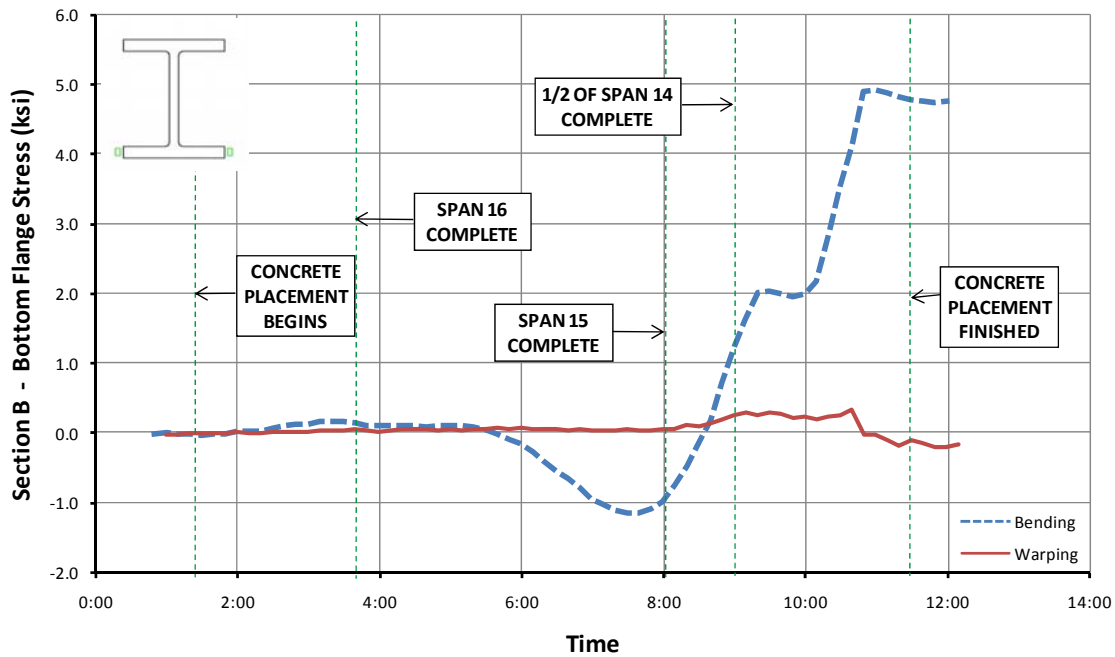


Figure 4.19 Girder 4: Section B Bottom Flange Stress

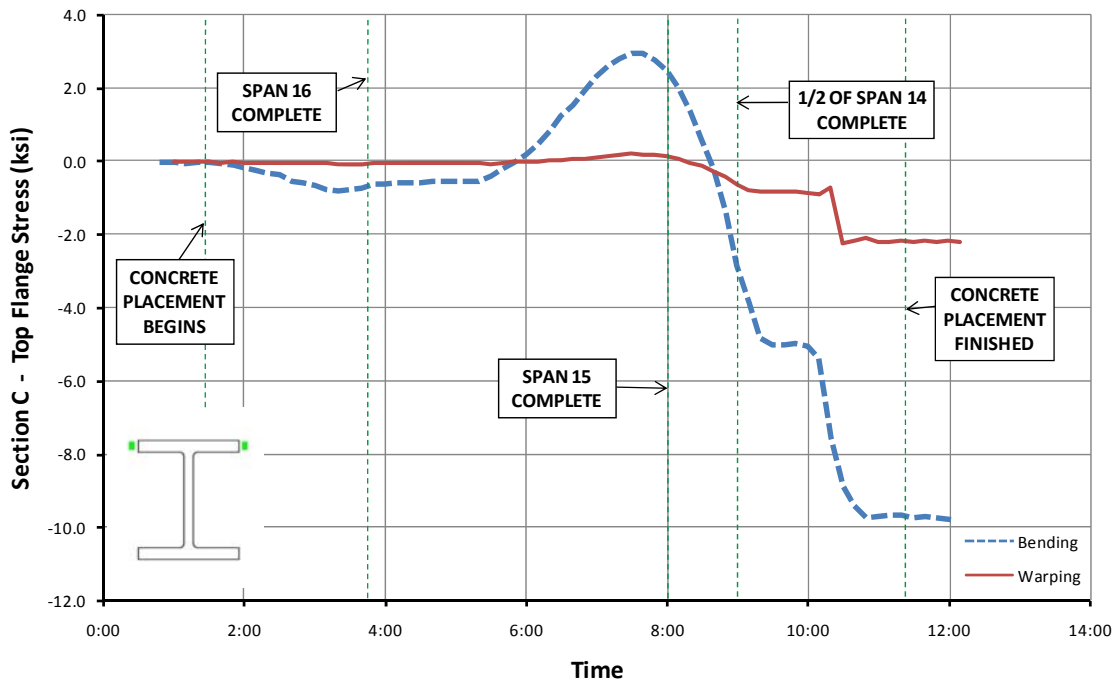


Figure 4.20 Girder 4: Section C Top Flange Stress

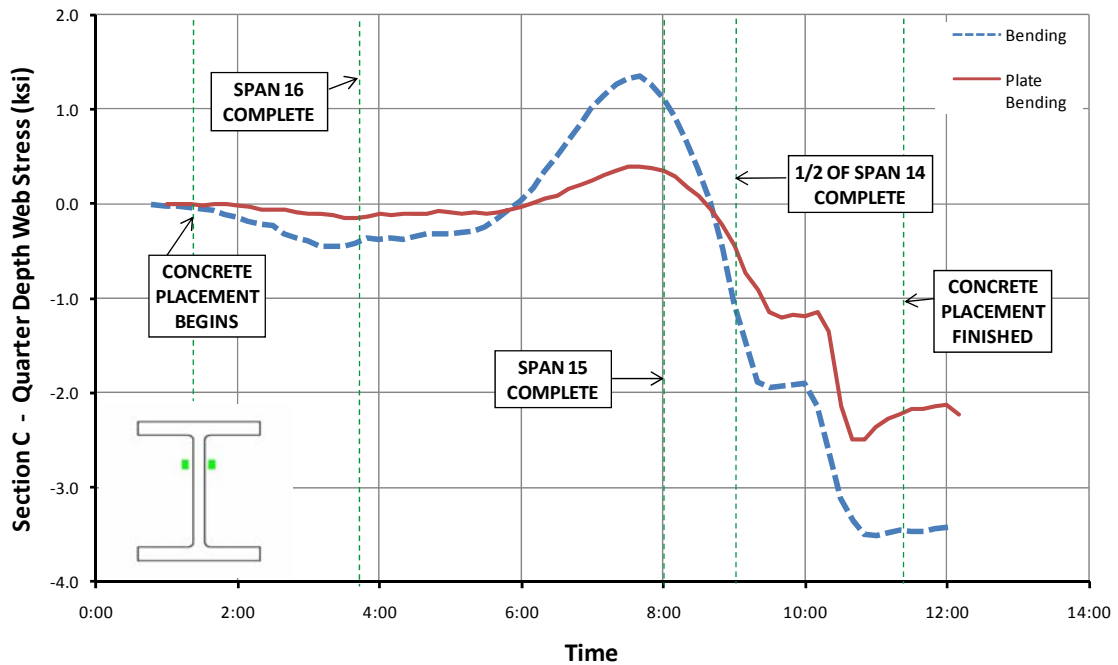


Figure 4.21 Girder 4: Section C Quarter Depth Web Stress

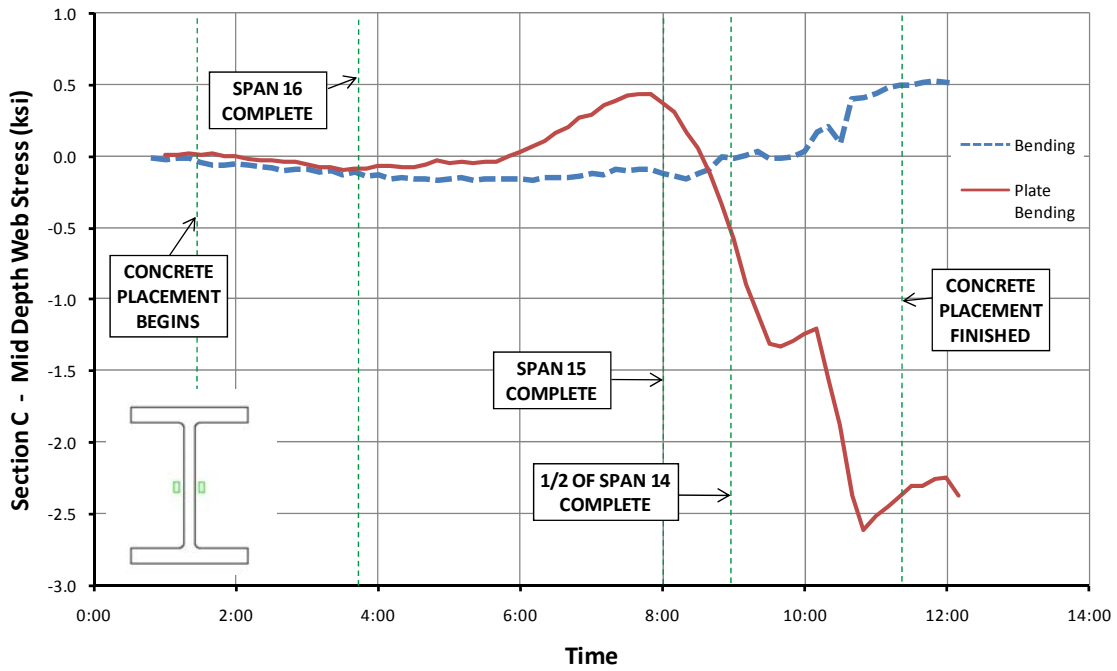


Figure 4.22 Girder 4: Section C Mid Depth Web Stress

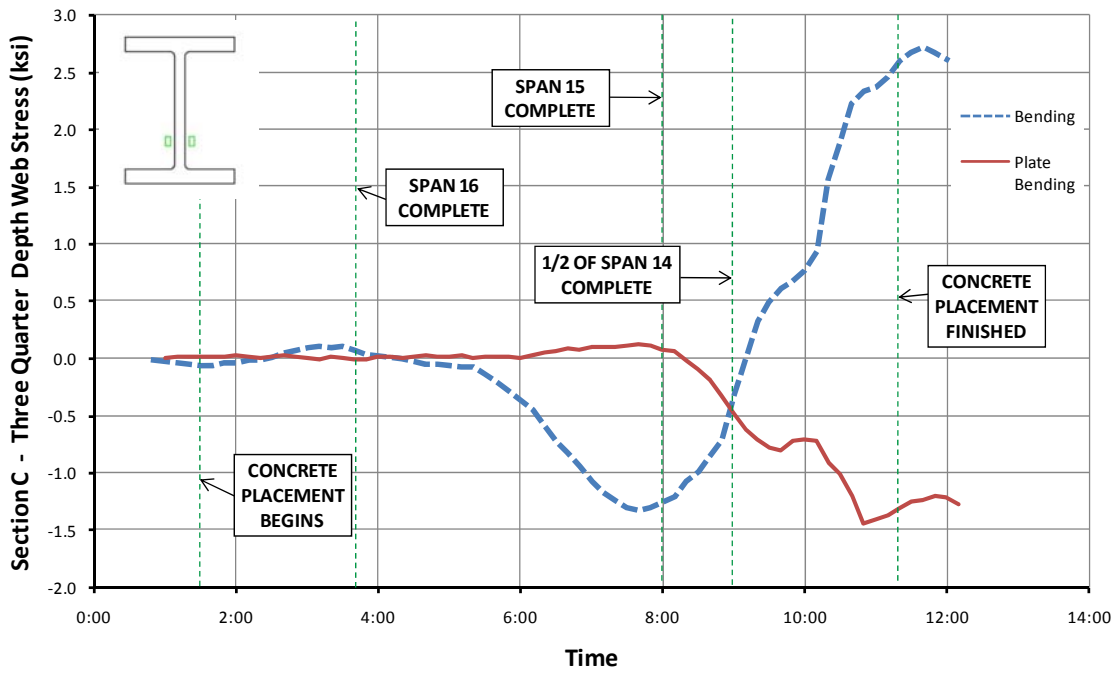


Figure 4.23 Girder 4: Section C Three Quarter Depth Web Stress

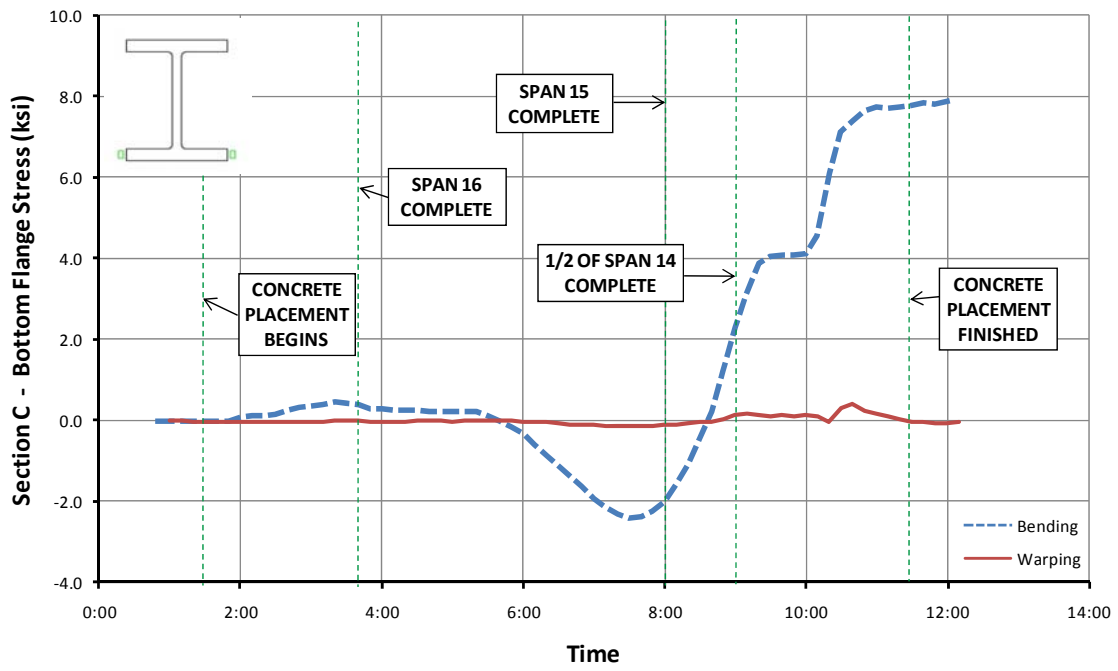


Figure 4.24 Girder 4: Section C Bottom Flange Stress

4.3.3 Summary of Results for Girders 3 and 4

			Girder 3 Stress Change During Concrete Pour (ksi)			
Location	Stress	Flange	1/2 Span 15 Poured (6:25 am)	Span 15 Pour Complete (8:00 am)	1/2 Span 14 Poured (9:00 am)	Span 14 Complete*
Section A	Bending	Top	0.034	0.333	-0.56	-4.276
		Bottom	-0.285	-0.626	0.193	2.823
	Warping	Top	-0.03	-0.057	-0.1666	-0.549
		Bottom	-0.023	-0.047	-0.024	-0.038
Section B	Bending	Top	N/A	N/A	N/A	N/A
		Bottom	-0.406	-0.888	0.365	3.973
	Warping	Top	N/A	N/A	N/A	N/A
		Bottom	-0.014	-0.037	-0.028	-0.159
Section C	Bending	Top	0.526	1.887	-1.897	-9.898
		Bottom	-0.825	-2.153	1.532	9.404
	Warping	Top	0.049	0.186	-0.242	-1.154
		Bottom	-0.171	-0.377	-0.020	0.934

* Represents total change in stress for construction activity.

Table 4.1 Girder 3 Flange Stress Change Summary

			Girder 3 Stress Change During Concrete Pour (ksi)			
Location	Stress	Web	1/2 Span 15 Poured (6:25 am)	Span 15 Pour Complete (8:00 am)	1/2 Span 14 Poured (9:00 am)	Span 14 Complete*
Section C	Bending	Top 1/4	0.155	0.799	-0.531	-3.138
	PL Bending	Top 1/4	-0.049	-0.143	0.041	0.552
	Bending	Mid	-0.092	-0.124	0.062	0.626
	PL Bending	Mid	0.008	-0.034	0.013	-0.150
	Bending	3/4 depth	-0.407	-1.010	0.640	4.756
	PL Bending	3/4 depth	-0.028	-0.014	-0.037	-0.470

* Represents total change in stress for construction activity.

Table 4.2 Girder 3 Web Stress Change Summary

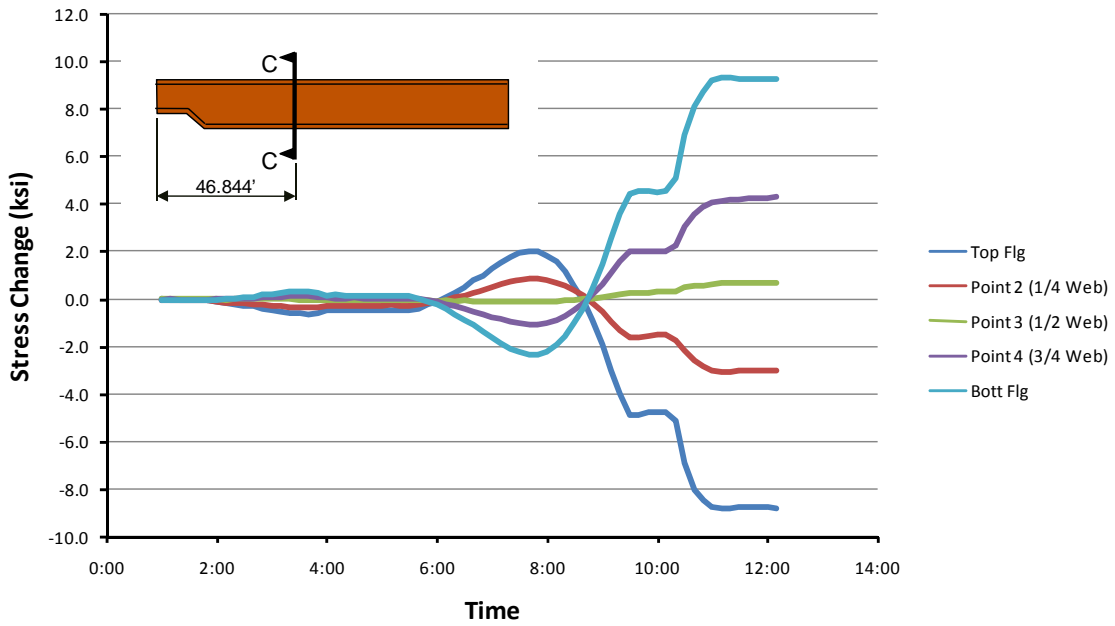


Figure 4.25 Girder 3 Bending Stress Change at Section C

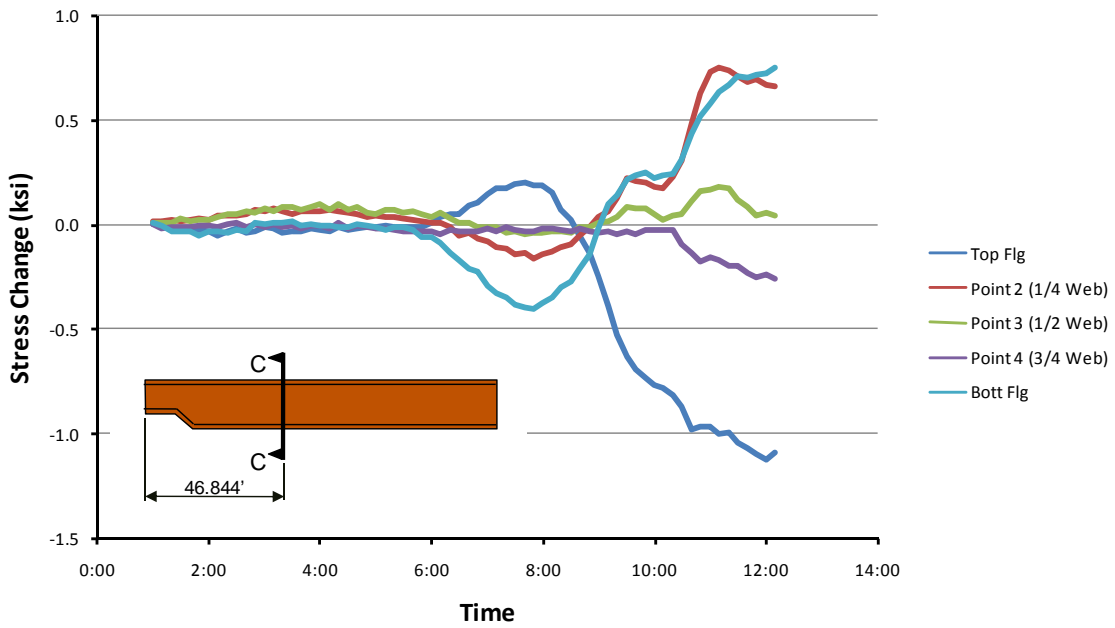


Figure 4.26 Girder 3 Warping Stress Change at Section C

			Girder 4 Stress Change During Concrete Pour (ksi)			
Location	Stress	Flange	1/2 Span 15 Poured (6:25 am)	Span 15 Pour Complete (8:00 am)	1/2 Span 14 Poured (9:00 am)	Span 14 Complete*
Section A	Bending	Top	0.156	0.586	-0.228	-3.394
		Bottom	-0.416	-0.855	0.734	2.926
	Warping	Top	-0.007	-0.100	-0.271	-0.910
		Bottom	0.161	0.142	-0.073	-0.068
Section B	Bending	Top	0.289	0.9504	-0.4722	-4.680
		Bottom	-0.410	-1.093	0.716	4.754
	Warping	Top	0.049	-0.018	-0.208	0.036
		Bottom	0.056	0.075	0.275	-0.398
Section C	Bending	Top	0.853	2.790	-1.418	-11.083
		Bottom	-0.891	-2.259	1.202	8.236
	Warping	Top	0.043	0.139	-0.631	-2.268
		Bottom	-0.083	-0.106	0.142	-0.267

* Represents total change in stress for construction activity.

Table 4.3 Girder 4 Flange Stress Change Summary

			Girder 3 Stress Change During Concrete Pour (ksi)			
Location	Stress	Web	1/2 Span 15 Poured (6:25 am)	Span 15 Pour Complete (8:00 am)	1/2 Span 14 Poured (9:00 am)	Span 14 Complete*
Section C	Bending	Top 1/4	0.334	1.259	-0.477	-3.206
	PL Bending	Top 1/4	0.095	0.355	-0.434	-1.813
	Bending	Mid	-0.147	-0.091	-0.003	0.585
	PL Bending	Mid	0.170	0.375	-0.574	-1.276
	Bending	3/4 depth	-0.579	-1.301	-0.707	3.921
	PL Bending	3/4 depth	0.067	0.074	-0.473	-0.313

* Represents total change in stress for construction activity.

Table 4.4 Girder 4 Web Stress Change Summary

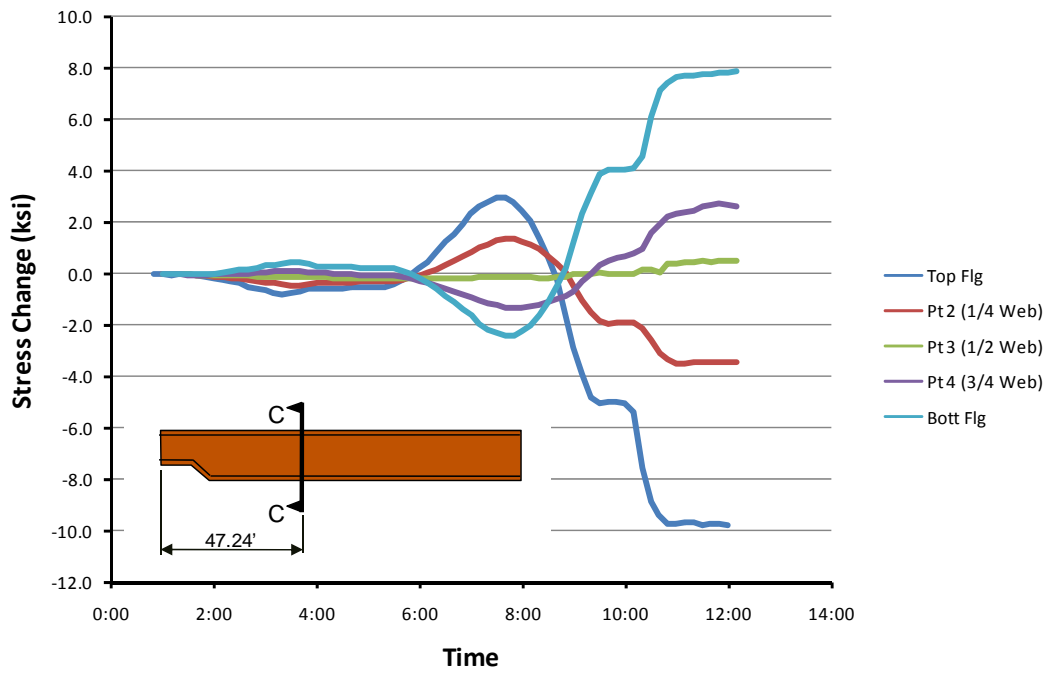


Figure 4.27 Girder 4 Bending Stress Change at Section C

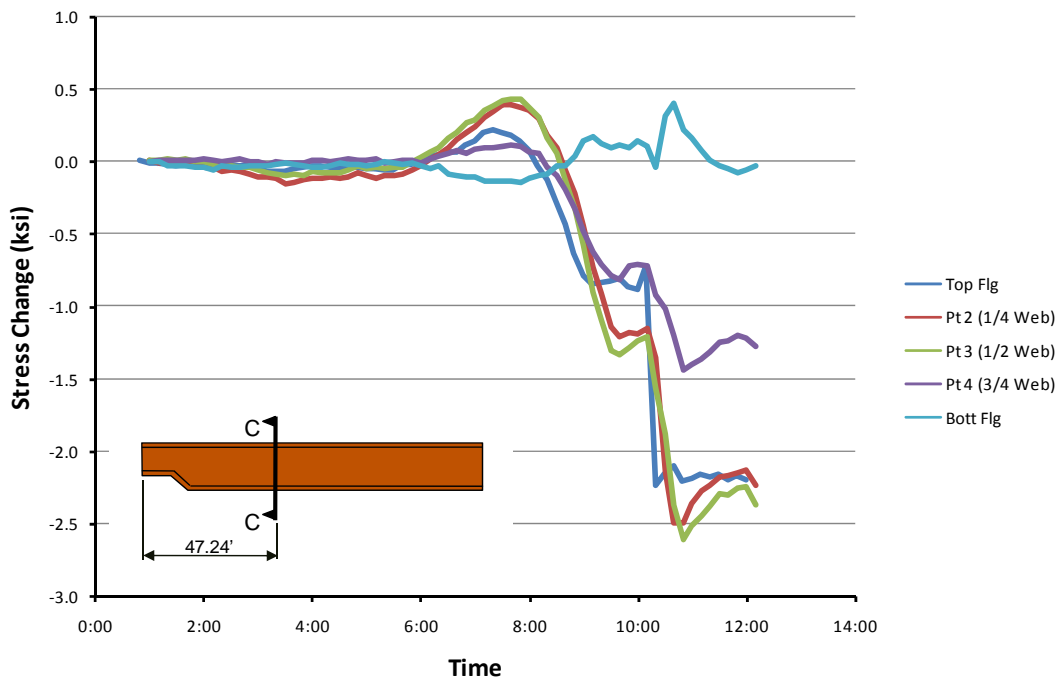


Figure 4.28 Girder 4 Warping Stress Change at Section C

Table 4.1 and Table 4.2 summarize the stress change at certain times during the concrete pour of Unit 3 for Girder 3. Similarly, Table 4.3 and Table 4.4 summarize the stress change for Girder 4. Negative bending stress denotes a compressive stress change, while a positive bending stress denotes a tensile stress change. For warping stress, negative values are associated with higher combined stresses being present on the exterior flange tip of the girder.

Overall, the recorded warping stress change during the concrete placement for Girder 3 was low. The maximum value of total warping stress change occurred at Section C, on the top flange, with a stress change of -1.2 ksi. The maximum total warping stress change in the web occurred in the top quarter depth of the web, at 0.55 ksi. The maximum total bending stress change in the flange area occurred at Section C in the top flange with a value of -9.9 ksi. Unlike the warping stress change in the web, the maximum bending stress change in the web occurred on the bottom quarter of the web, with a value of 4.8 ksi. As stated previously, the maximum values are given as the total stress change due to the construction activity.

Most of the stress changes for Girder 4 had higher values than Girder 3, but not significantly. The maximum value of warping stress change occurred at Section C, on the top flange, with a stress change of -2.3. This is roughly twice the amount of change in maximum warping stress as Girder 3, in the same location. The maximum total change in warping stress in Girder 4, in the web at Section C, was -1.8 ksi at the top quarter depth. The maximum change in total bending stress occurred in the top flange at Section C, with a value of -11.1 ksi. This is the maximum change in bending stress overall. The instrumented web recorded a maximum change in bending stress at the bottom quarter depth of the web (Section C), with a value of 3.9 ksi.

4.4 CROSS FRAMES X1 AND X2

To increase the torsional stiffness of the bridge and brace the girders before the concrete deck cures, cross frames are installed between each adjacent girder. As described in Chapter 3, the cross frames on the SH 130/US 71 Direct Connector are

comprised of four angles; two diagonals and two struts. The angles that make up the cross frames transmit axial forces from the vertical loads on the girders. This section discusses the cross frame results as well as the data reduction technique used to transform the strain data from the gages to axial forces. The axial forces will be used to validate finite element models of curved bridge systems.

4.4.1 Cross Frame Data Reduction Technique

This section will summarize the method used for determining the axial forces in the angles for this specific bridge. It will summarize previous methods and research by others (Fan, 2000) for determining the axial forces using the Regression Method.

The data reduction technique begins with assuming that the longitudinal stress induced by the axial forces and bending moments, is distributed linearly along the cross section. The stress distribution is expressed as

$$f = a + bx + cy \qquad \text{Equation 4.3}$$

where f is the longitudinal stress and a , b , and c are constants. The x and y correlate to the coordinate system of the cross-section. After a , b , and c are determined, axial forces can be derived using beam-column theory. In addition, if the origin of the coordinate system passes through the centroid of the cross-section, which is the case with the cross frame angle members instrumented, then the axial force in the member is calculated as

$$N = aA \qquad \text{Equation 4.4}$$

$N = \text{Calculated Axial Force}$

$A = \text{Cross sectional Area}$

The Regression Method was used to calculate the constants a , b , and c in Equation 4.3. A three-dimensional linear regression algorithm was used to approximate the stress distribution. The history and derivation of the Regression Method was not

researched in the scope of this project. This section will summarize the Regression method as a means of explaining the cross frame instrumentation data reduction technique. The basis for the method as well as the history behind the method was researched previously by Fan & Helwig et. al. 2000 at the University of Houston.

The Regression Method assumes that the strain gage i is located on a coordinate plane at a point (x_i, y_i) , with a stress reading of f_i . The constants b and c are calculated using this method from the following equations:

$$\begin{cases} l_{11}b + l_{12}c = l_{10} \\ l_{21}b + l_{22}c = l_{20} \end{cases} \quad \text{Equation 4.5}$$

$$l_{11} = \sum_{i=1}^n (x_i - \bar{x})^2 \quad \text{Equation 4.6}$$

$$l_{22} = \sum_{i=1}^n (y_i - \bar{y})^2 \quad \text{Equation 4.7}$$

$$l_{12} = l_{21} = \sum_{i=1}^n (x_i - \bar{x})(y_i - \bar{y}) \quad \text{Equation 4.8}$$

$$l_{10} = \sum_{i=1}^n (x_i - \bar{x})(f_i - \bar{f}) \quad \text{Equation 4.9}$$

$$l_{20} = \sum_{i=1}^n (y_i - \bar{y})(f_i - \bar{f}) \quad \text{Equation 4.10}$$

$$\bar{x} = \frac{1}{n} \sum_{i=1}^n x_i \quad \text{Equation 4.11}$$

$$\bar{y} = \frac{1}{n} \sum_{i=1}^n y_i \quad \text{Equation 4.12}$$

$$\bar{f} = \frac{1}{n} \sum_{i=1}^n f_i \quad \text{Equation 4.13}$$

The above equations can be used to solve for the constants b and c . After rearranging Equation 4.3, a can be solved for as follows

$$a = \bar{f} - b\bar{x} - c\bar{y} \quad \text{Equation 4.14}$$

Finally the calculated axial force, N , can be determined by multiplying a by the cross sectional area. Figure 4.29 graphically depicts the x_i and y_i geometry to get a better understanding of using the above equations.

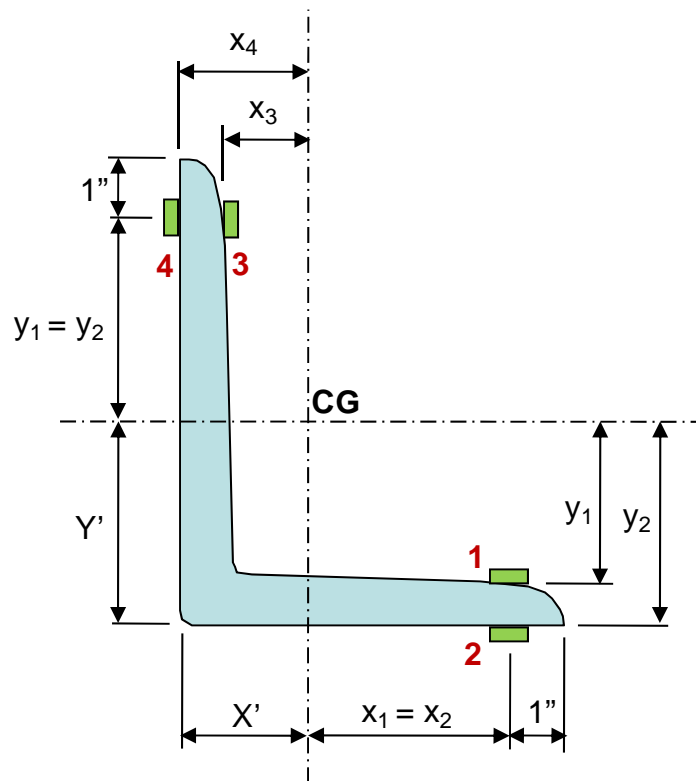


Figure 4.29 Cross Frame with Equation Nomenclature

4.4.2 Cross Frame Results

As mentioned in Chapter 3, two cross frames were instrumented on Span 14 of SH 130/ US 71 Direct Connector. The cross frames were instrumented to monitor their behavior during the critical stage of construction during the concrete deck placement.

Figure 4.30 illustrates how the members were labeled. All of the gages were positioned 1 inch from the edge of the angle. The labeled members correlate with the graphs in this section. Specific events are highlighted on the graphs, to understand the behavior of the cross frame members and relate it to a particular time during the concrete pour.

The results varied for X1, which was the first cross frame instrumented. As shown in Figure 4.32, before the deck in Span 14 was poured, the results were somewhat typical, but during the pour of Span 14 the axial forces differ greatly from the second cross frame (X2). When the strain of each gage is plotted versus time for cross frame X1, it was clear that the inside vertical gage failed on member X1-1 (See Figure 4.30). The strain gages for X1 were reading strain values, but it can be concluded that the results from this cross frame are erroneous and unreliable. Therefore, the results from the second cross frame should be used to compare to future finite element research.

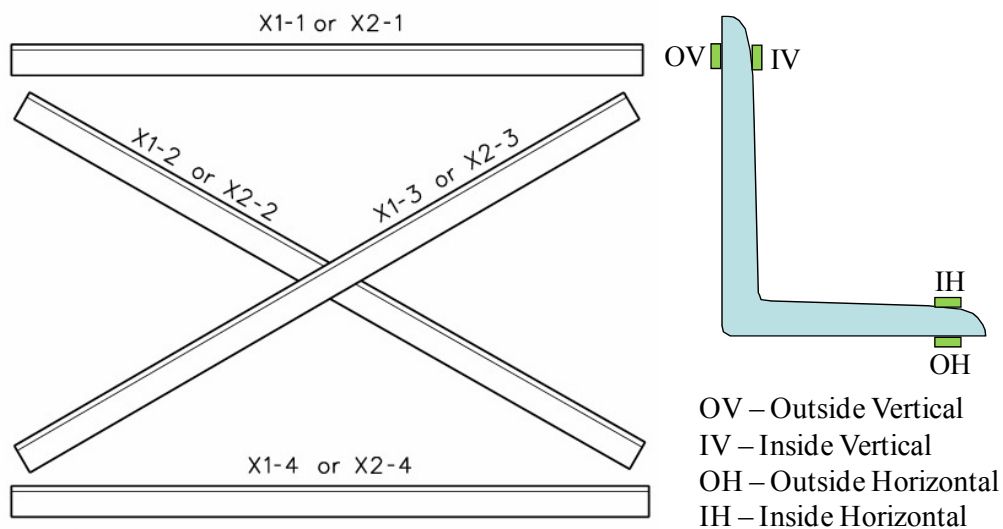


Figure 4.30 Cross Frame X1 and X2 member labels

As stated previously for Girders 3 and 4, in order to find the total strain change due to the construction activity, the researchers must negate the effects of thermal gradients on the bridge. Since the strain gages drift slightly due to thermal changes, the

ambient temperature must be monitored closely. Efforts were made to find nighttime temperatures before and after the construction that are relatively close. The ambient temperature at the beginning of the deck pour was 60.4°F at 1:30am. For Girders 3 and 4, the morning temperature on April 19, 2008 was relatively close to the temperature at the beginning of the deck pour. Therefore, for Girders 3 and 4, the strain values from April 19th at were used to determine the overall change in stress for the construction of the concrete deck. In order to calculate the axial force in the cross frame members, all of the gages have to be working correctly. Unfortunately, two of the X2 cross frame gages malfunctioned after the concrete pour and on the day following the concrete pour (April 17, 2008) at 2pm. The ambient temperature on April 17th averaged to 69°F from midnight to 3:00am, which is roughly 9°F higher than the morning of the concrete pour. In order to get a total change in strain at an appropriate temperature, the strain values for two gages on the bottom horizontal member (X2-4) had to be extrapolated. Figure 4.31 represents the average stress taken from 12:30am to 3:00am on April 17th, 18th, and 19th. The gages that were extrapolated were X2-4-OH and X2-4-IH. The horizontal member of the first cross frame (X1) was used to determine a rough estimate of total stress change in the horizontal member of X2. The following graph represents the outcome of the comparison between cross frame X1 and X2. The spreadsheets used to determine this is located in Appendix A.

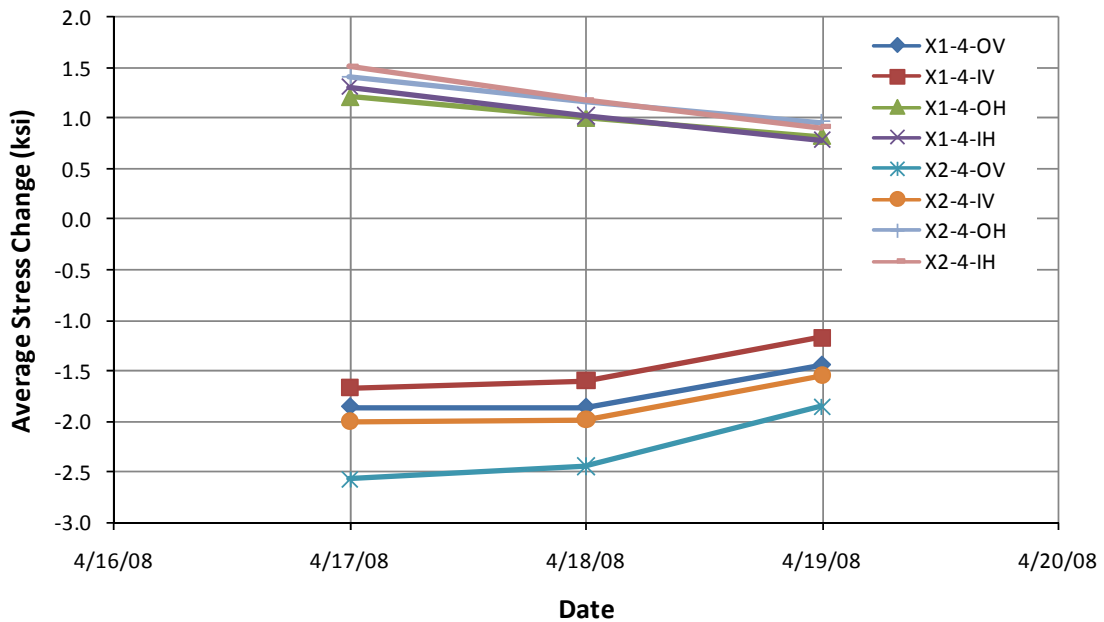


Figure 4.31 Average Stress Change for X2

The axial forces in Cross Frame X2 were minimal at the beginning of the Unit 3 concrete pour. A significant change in the axial forces occurred at 9:00 am, after half of Span 14 was poured. According to Figure 4.33, the axial forces in the members steadily increased until the concrete pour was complete. The higher axial forces were seen in the X2-1 and X2-4 members, which were the horizontal strut members. The following graphs represent the time history relating to axial forces of the four angles in the two cross frames.

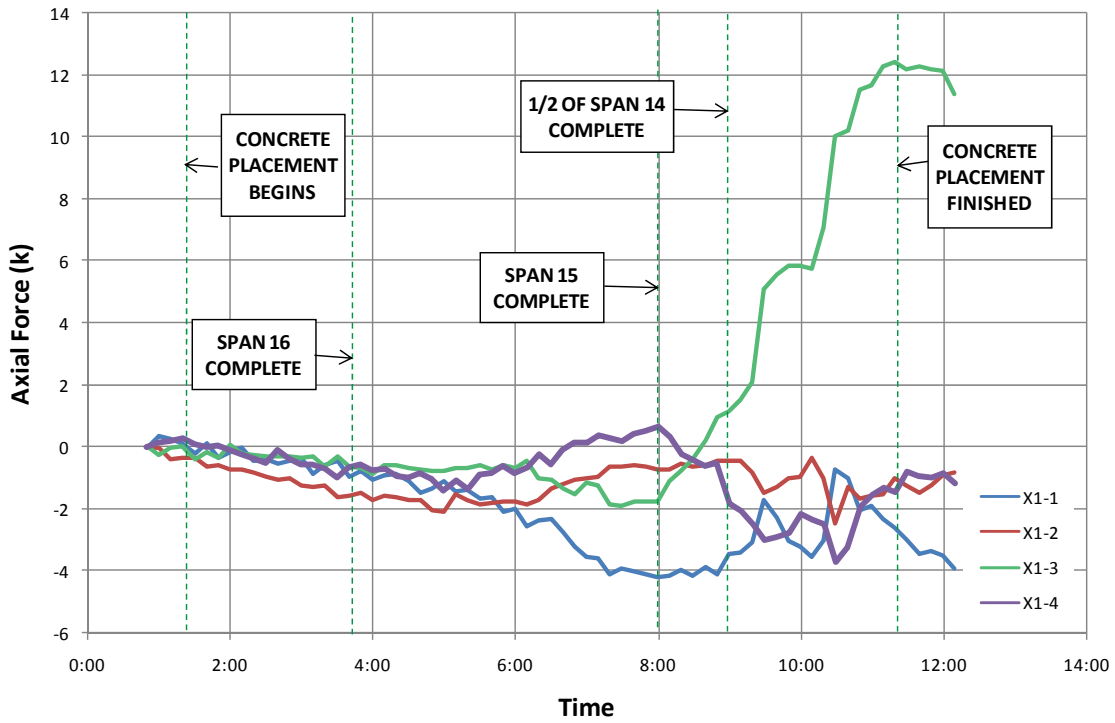


Figure 4.32 Cross Frame X1 Axial Force

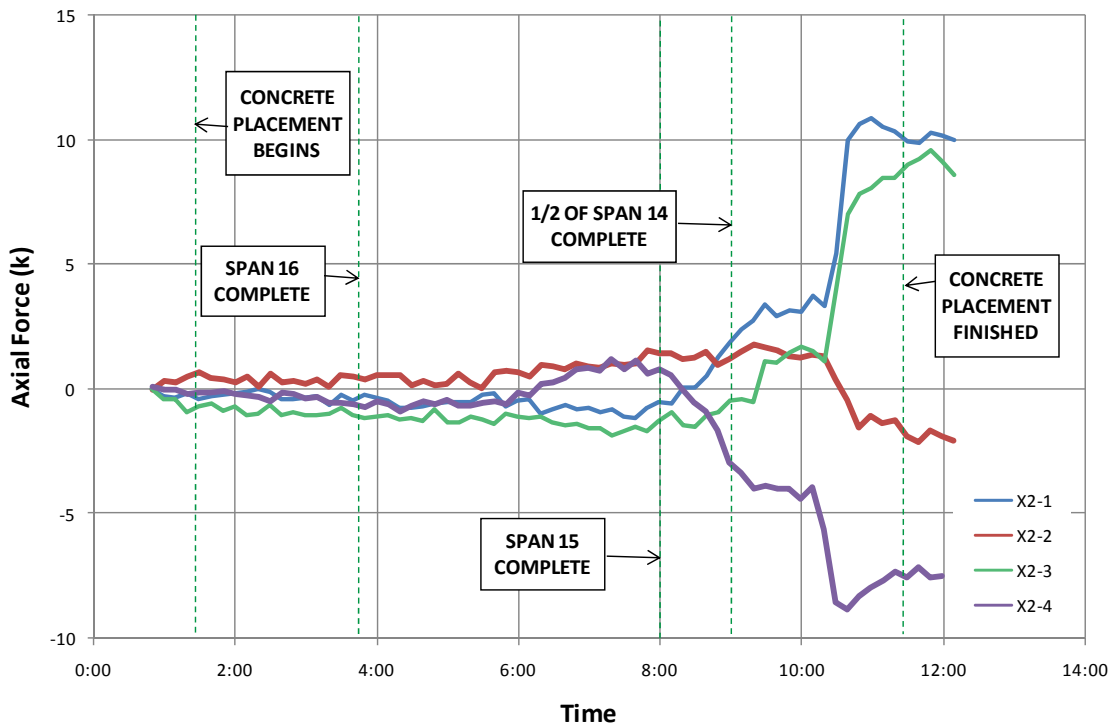


Figure 4.33 Cross Frame X2 Axial Force

4.4.3 Summary of Cross Frame Results

		X2 Axial Force During Concrete Pour (kips)			
Member	Location	½ Span 15 Poured (6:25 am)	Span 15 Pour Complete (8:00 am)	½ Span 14 Poured (9:00 am)	Span 14 Complete *
X2-1	Top horizontal	-0.840	-0.507	1.862	11.98
X2-2	Diagonal	0.954	1.463	1.211	-4.10
X2-3	Diagonal	-1.324	-1.265	-0.432	13.78
X2-4	Bottom horizontal	0.239	0.621	-1.635	-3.60

* Represents total change in axial force for construction activity.

Table 4.5 Cross Frame X2 Axial Force Summary

Table 4.5 summarizes the axial forces in Cross Frame X2. The negative values represent compressive axial forces, whereas the positive values represent tensile axial forces. The results show the gradual increase in axial force of the three of the members (X2-1, X2-3, X2-4) up until half of the concrete is poured on Span 14. The time span between the events of half of Span 14 concrete being poured to the end of the concrete pour, the axial forces increase dramatically. This is because after half of Span 14 is poured, the concrete placement approached Cross Frame X2 and was then directly over the position. The results also show that one of the diagonals (X2-3) is transmitting close to 6 ½ times the amount of axial force than the other diagonal (X2-2). Another point worth noting, is that members X2-1 and X2-3 are loaded in compression (negative axial forces) before Span 14 was poured, but after Span 14 was poured were in tension. This is true for members X2-2 and X2-4, but in the opposite manner (tensile to compressive). The maximum axial force was in member X2-3, which is a diagonal member, with a magnitude of 13.78 kips.

4.5 VERTICAL DEFLECTION RESULTS

Results presented in this section focus on the vertical deflection results from the SH 130/US 71 Direct Connector Unit 3 concrete pour. The techniques used for taking the isolated readings were discussed in Chapter 3. Baseline readings were taken prior to the placement of concrete. During pivotal time periods during the concrete pour, deflection readings were taken. For repeatability, at each location during each recorded event, three readings were taken, and the final reading reported is the average of the three initial readings. The results from this field experimentation will be used to compare to a finite element model in the future.

4.5.1 Mid Span Deflection Readings

Vertical deflection readings were taken at the mid span of Span 14 on all four girders. The mid span was chosen as an isolated location because relatively large deflection and torsional deformations of the four girder system were expected. Figure 4.34 represents the vertical deflection at the mid span for each girder during the concrete pour of Unit 3. A negative vertical deflection value represents a downward deflection and a positive vertical deflection value represents an upward deflection. Significant events were recorded during the concrete pour to correlate the deflection readings to certain times during the pour. At 3:45 am the concrete for Span 16 was finished and all of mid span readings for the girders resulted in negative deflection readings. At this stage during the concrete pour, Girder 3 deflected the most, at -0.50 inches. After a quarter of the second span (Span 15) was placed, Girder 1 recorded a positive deflection of 0.396 inches. According to Figure 4.34, this does not follow the trend of the other three girders. This is also distinctive because Girder 1 is positioned on the inside of the horizontal curve, which means that it would typically deflect the least. Similar to Girder 1, the vertical deflections of Girders 2, 3, and 4 increase in the positive direction, but not by the same magnitude. At the time when half of the second span (Span 15) was poured, the girders seemed to converge to a positive deflection ranging from 0.21 to 0.52 inches. As one could predict, Girder 4 deflected the most at this stage of construction. After three-

quarters of Span 15 was placed, the girders began deflecting upward (positive direction), and continued to deflect upward at mid span until the concrete pour on Span 15 was complete.

As concrete was poured on the last span (Span 14), which is the span containing the instrumentation, the vertical deflection readings began to reflect the weight of the wet concrete on the instrumented span and deflected downward. The change from positive to negative vertical deflection from the time between completing Span 15 and pouring half of Span 14, averaged around 2.25" for the four girders. The last readings, which were taken at the end of the concrete pour, indicated that Girder 4 deflected the most (-2.96") and Girder 1 is deflected the least (-2.41"). Girders 2 and 3 had similar deflection values of -2.69" and -2.67", respectively. One aspect worth noting about the graph shown in Figure 4.34 is that the girders may not have exactly the same deflection readings at the different stages of the concrete pour, but they all follow a similar trend. This reinforces the idea that the girders deflected simultaneously and acted collectively in torsion as one unit, which was expected since they are connected by cross frames. The following figure summarizes the vertical deflection time history for all four girders, at the mid span of Span 14.

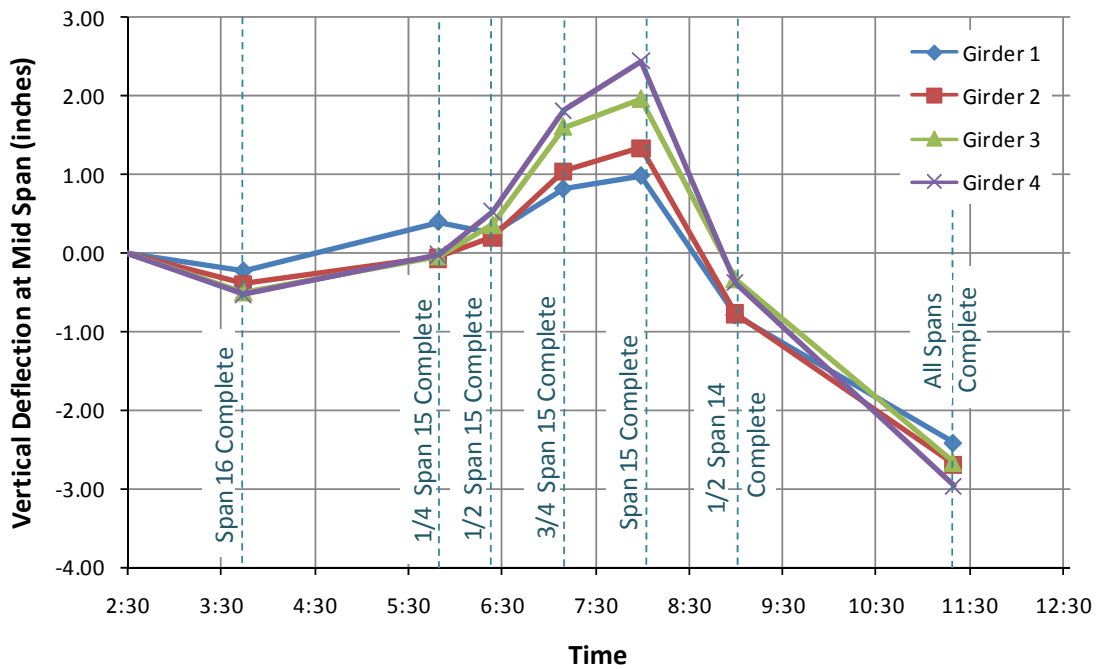


Figure 4.34 Vertical Deflection Readings at Mid Span 14

4.5.2 Girders 3 and 4 Vertical Deflection Results

This section provides a comparison of the vertical deflection results of Girders 3 and 4 of Span 14 of the SH 130/ US 71 Direct Connector. As outlined earlier, deflection readings were taken at five locations: near the pier (Bent 14), at $\frac{1}{8} L$, $\frac{1}{4} L$, $\frac{3}{8} L$, and $\frac{1}{2} L$. Figure 4.35 describes the specific locations along the girders that were monitored. The term, “L,” refers to the total span length of the girder at Span 14. A negative vertical deflection value represents a downward deflection and a positive vertical deflection value represents an upward deflection. The vertical deflection readings were graphed at each stage of the concrete deck construction and can be found in Appendix B. They compare the vertical deflection magnitude along the length of the girder.

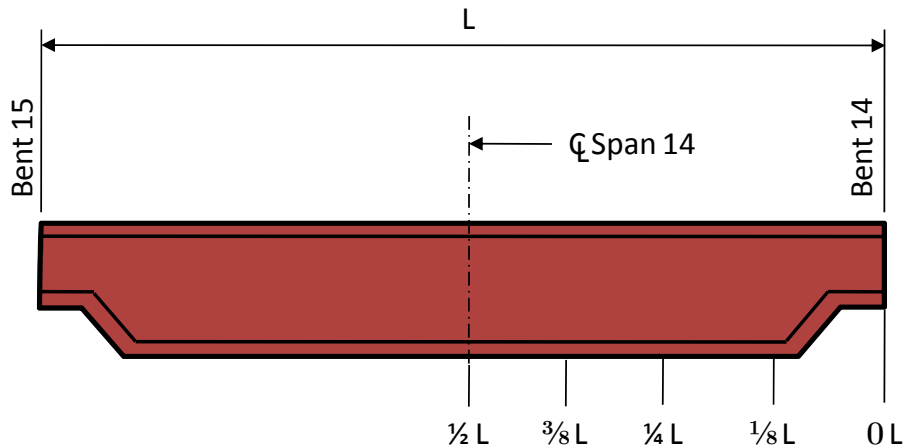


Figure 4.35 Vertical Deflection Reading Locations

After the concrete pour was complete on the first span (Span 16), the data showed negative vertical deflection readings from the mid span of the girders to the pier. The girder deflections then switched to an upward progression in deflection with the next reading after one quarter of the second span (Span 15) was poured at a time of 5:50am. Girders 3 and 4 deflected upward after half of Span 15 was poured. The next vertical deflection readings were taken after three-quarters of the concrete was poured on Span 15. During the time between half of Span 15 being poured and three-quarters of Span 15 being poured, Girder 4 at $\frac{1}{2} L$ (midspan), deflected upward 1.29". Girder 3's significant change in deflection during this same time period also occurred at the $\frac{1}{2} L$ location, with an upward deflection magnitude of 1.25". There was an upward movement on Girders 3 and 4 at all of the locations measured along the girders at this point in time. Furthermore, after Span 15 was complete, another deflection reading was taken, and it indicated a continued positive upward deflection progression. It was not until 9:00 am, when half of the last span (Span 14) was poured, that the girders began to develop a negative vertical deflection magnitude. The change in deflection is noteworthy at this point in time, because the girders began behaving as one would expect for a continuous girder bridge. Figure 4.36 and Figure 4.37, as well as Table 4.6 and Table 4.7 summarize the behavior of the girders relating to vertical deflection during the concrete pour.

Time	Event	Vertical Deflection Along Girder 3 (inches)				
		0 L	1/8 L	1/4 L	3/8 L	1/2 L
3:45	Span 16 Complete	0	-0.021	-0.146	-0.333	-0.500
5:50	1/4 Span 15 Complete	0	0.167	0.083	-0.104	-0.042
6:25	1/2 Span 15 Complete	0	0.417	0.521	0.521	0.354
7:10	3/4 Span 15 Complete	0	0.708	1.167	1.437	1.604
8:00	Span 15 Complete	0	0.792	1.354	1.667	1.958
9:00	1/2 Span 14 Complete	0	-0.229	-0.458	-0.625	-0.333
11:20	All Spans Complete	0	-1.125	-2.229	-2.771	-2.667

Table 4.6 Vertical Deflection Readings Along Girder 3

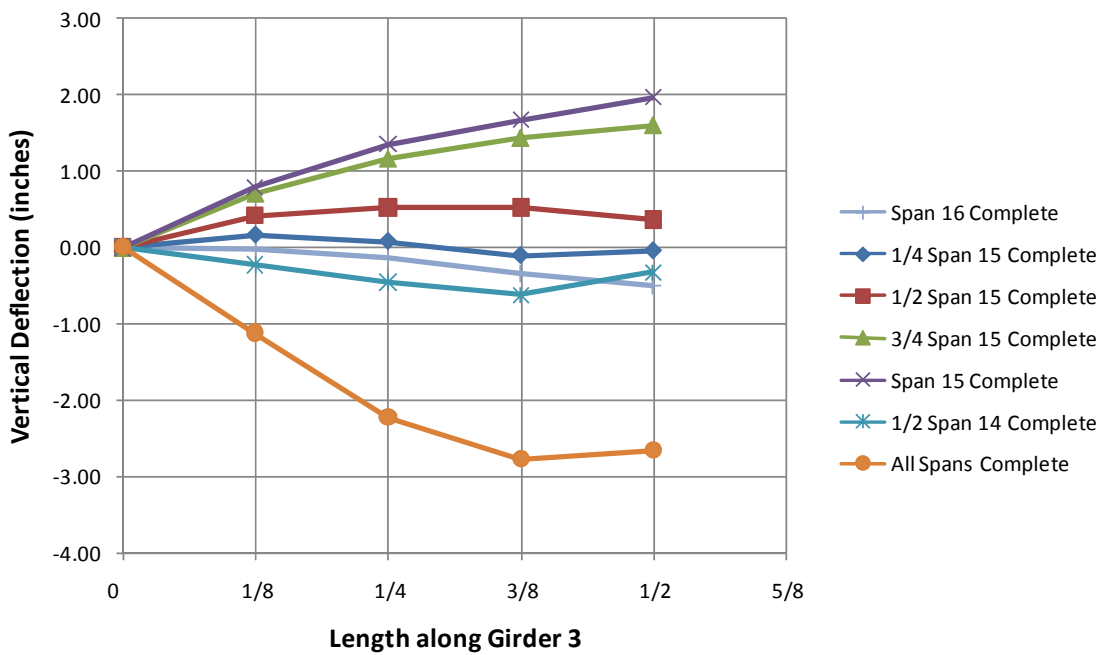


Figure 4.36 Summary of Girder 3 Vertical Deflection Results

		Vertical Deflection Along Girder 4 (inches)				
Time	Event	0 L	1/8 L	1/4 L	3/8 L	1/2 L
3:45	Span 16 Complete	0	-0.312	-0.396	-0.333	-0.521
5:50	1/4 Span 15 Complete	0	-0.125	-0.125	-0.021	-0.021
6:25	1/2 Span 15 Complete	0	0.167	0.458	0.729	0.521
7:10	3/4 Span 15 Complete	0	0.563	1.354	1.938	1.812
8:00	Span 15 Complete	0	0.729	1.583	2.313	2.438
9:00	1/2 Span 14 Complete	0	-0.396	-0.500	-0.312	-0.375
11:20	All Spans Complete	0	-1.646	-2.479	-2.750	-2.958

Table 4.7 Vertical Deflection Readings Along Girder 4

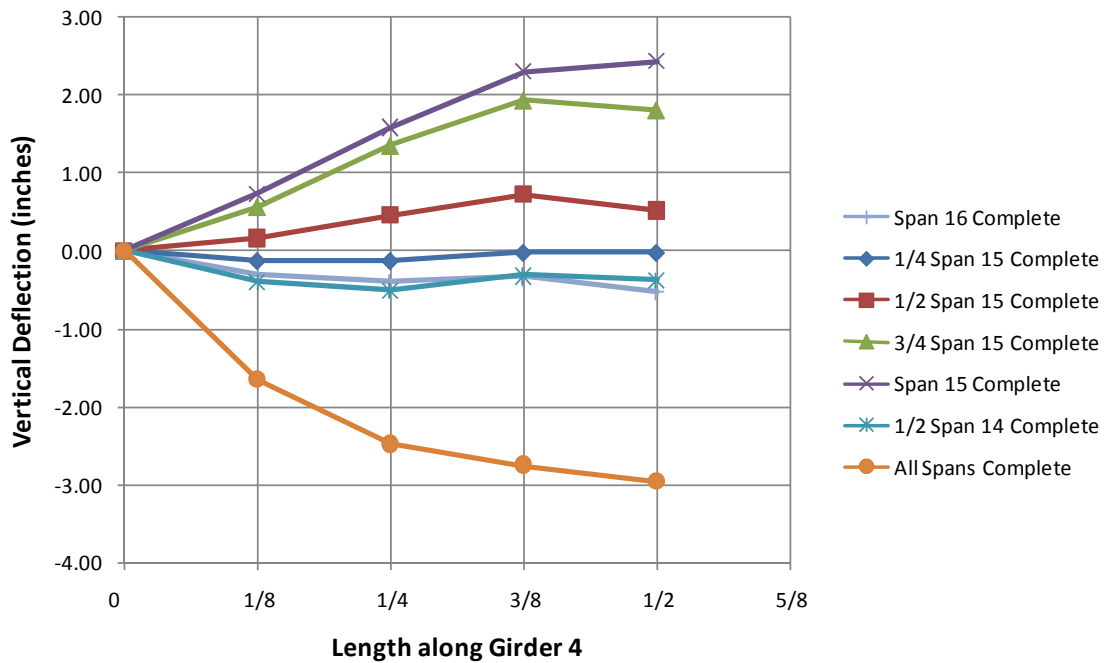


Figure 4.37 Summary of Girder 4 Vertical Deflection Results

4.5.3 Girders 3 and 4 Vertical Deflection Summary

The vertical deflection results for Span 14 are typical of a continuous girder bridge. When the preceding spans were poured, the girders in the last span could be characterized with some uplift, but as the concrete pour progressed onto the last span, the girders started to change from an upward deflection to a downward deflection. The maximum deflection recorded on Girder 4 occurred at $\frac{1}{2} L$, after all spans were complete, with a magnitude of -2.96." Subsequently, the maximum recorded deflection for Girder 3 occurred at $\frac{3}{8} L$, after Unit 3 was completely finished, with a magnitude of -2.77."

4.6 HORIZONTAL THERMAL EXPANSION RESULTS

This section focuses on the results of thermal effects on Span 14 of the SH 130/US 71 Direct Connector (Bridge 88). During daily thermal cycles on most materials, the material expands and contracts as it heats up and cools down, respectively. Continuous steel girder bridges, with their long spans, accumulate large thermal movements as the temperature changes. Although most steel bridges undergo non-uniform temperature gradients in the vertical, transverse, and longitudinal direction, this project will only focus on thermal expansion results in the longitudinal direction (Grisham, 2005). The thermal expansion was measured using a wax horizontal displacement device, as discussed in Chapter 3. As the bridge expands, the stylus, which is attached to the bearing plates of Girders 1 and 4, records the maximum longitudinal movement.



Figure 4.38 Wax Trace Box for Measuring Bearing Movements

The wax trace boxes for measuring thermal bridge movements were placed on Bent 14 of Bridge 88 on April 16, 2008 at 8:15 am and removed on May 8, 2008 at 7:00 pm. The devices recorded the maximum thermal movement that Unit 3 experienced during this time frame. The temperature at the time of placement was 55°F. After Span 14 was poured (11:20 am), which completed the concrete placement for Unit 3, the measured thermal movement for Girder 1 was 0" and for Girder 4, 0.15." The recorded temperature at this time was 70°F.

On May 8, 2008, when the wax device was removed from Bent 14, the measured longitudinal movement was 0.615," as shown in Figure 4.39. The temperature at this time was 86 °F. The maximum temperature that Bridge 88 experienced during the time period of April 16th through May 8th was 90 °F and the minimum temperature was 42 °F (www.weatherbug.com).

The actual measured thermal movements can be compared with theoretical thermal expansion values, which can be calculated according to the AASHTO LRFD Design Bridge Specifications (2007). Theoretical thermal movement is referred to in AASHTO as design thermal movement for uniform temperature change. The following equation, which uses the extreme bridge design temperatures, is used to calculate the design thermal movement range, Δ_T , which is outlined in Section 3.12.3 of AASHTO (2007).

$$\Delta_T = \alpha L (T_{Max} - T_{Min}) \quad \text{Equation 4.15}$$

$\alpha =$ Coefficient of Thermal Expansion
(in/in/F)

$L =$ Expansion Length (in)

$T_{Max} =$ Maximum Design Temperature

$T_{Min} =$ Minimum Design Temperature

To evaluate the maximum and minimum design temperature, AASHTO refers to two figures that are a schematic of temperature contours drawn on a picture of the United States. The design engineer is instructed to use one figure to determine the maximum design temperature and another to determine the minimum design temperature, by locating the bridge site on the map and interpolating between the temperature contours. Since Austin, Texas weather data was available, the AASHTO contour maps were not used to calculate the temperature range for the theoretical thermal expansion; therefore the actual temperatures during the field test were used. Since the temperature at the installation of the wax devices (8:15 am) was 55°F and the temperature increased to 70°F at 11:20 am, the change in temperature used in the first theoretical thermal movement calculation was 15°F. The change in temperature used in the second set of calculations was 48°F, which is equal to the maximum temperature that occurred from April 16 to May 8 (90°F) subtracted by the minimum temperature occurrence (42°F) during the same

time period. The design thermal coefficient for steel was taken as 6.5×10^{-6} in/in/°F. The expansion length was determined by assuming that the thermal neutral point occurs at the mid span of Span 15. This assumption is consistent with the findings of Chen (2008) who found that pier flexure often occurs in bridges even with “fixed” bearings so that the true thermal fixed point is often close to the center of mass of the bridge. Therefore, the total expansion length used to calculate the theoretical thermal movement for Girder 1 was 282.89 ft and 290.28 ft for Girder 4. By adding the length of Span 14 to half of the length of Span 15 for each girder, the total expansion length can be resolved. Table 4.8 references the span lengths for Unit 3 of Bridge 88.

Plan Sheet Girder Lengths (ft)				
	Span 14	Span 15	Span 16	L* (ft)
Girder 1	180.52	204.74	154.05	282.89
Girder 4	185.27	210.01	158.13	290.28

*Expansion Length

Table 4.8 Bridge 88, Unit 3 Girders 1 and 4 Lengths

After calculating the theoretical thermal expansion, it can be compared with the actual movement observed in the field. Table 4.9 compares the calculated theoretical thermal expansion values with the field measured values. The theoretical expansion values are significantly higher than the field measured values. This is an indication that the theoretical expansion calculation is conservative in evaluating this behavior. It is also worth noting that in just the small amount of time between when the wax trace boxes were installed (8:15 am) to when the concrete deck was complete (11:20 am), there was thermal movement, although minor, within the steel unit.

Summary of Thermal Movement		
	After Span 14 Poured (4/16/08 - 11:20 am)	
	Field Measured (in)	Theoretical Expansion (in)
Girder 1	0	0.33
Girder 4	0.15	0.34
	After Thermal Effects (05/08/08 – 7:00 pm)	
Girder 1	0.60	1.06
Girder 4	0.615	1.09

Table 4.9 Summary of Thermal Movement on Unit 3

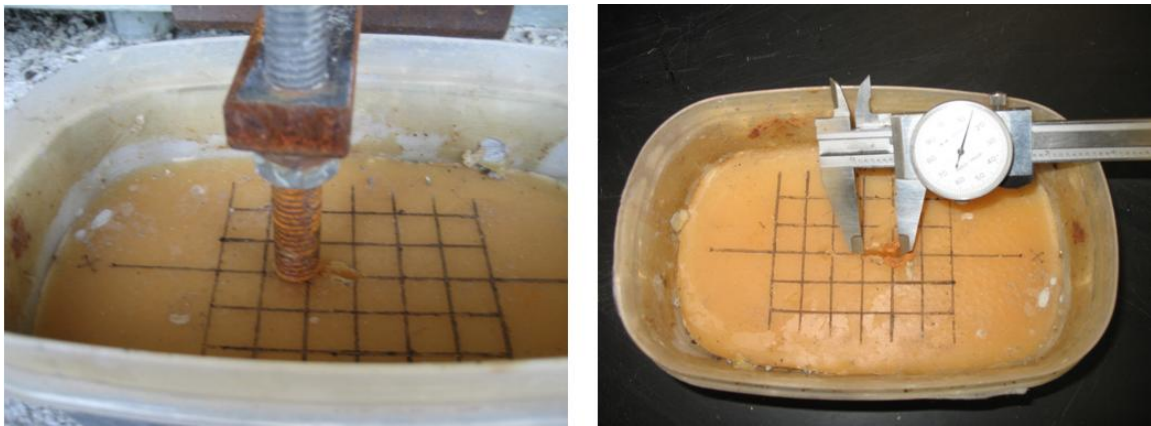


Figure 4.39 Wax Thermal Expansion Device Measurement



Figure 4.40 Wax Device attached to Bent 14

4.7 SUMMARY

Stresses, as well as displacements can have a significant effect on the durability and behavior of a horizontally curved plate girder bridge during the concrete deck placement phase of construction. The details and data from the concrete deck placement of Unit 3 of Bridge 88 were presented in this chapter.

The data showed that significant change in bending stress occurred when concrete placement was completed on the last span (Span 14) on all of the girder sections monitored. There was minimal amount of change in warping stress in the bottom flange region, and less than 1 ksi of change in warping stress in the top flange region on all sections monitored. The web region of Girder 4 produced higher bending and plate bending stresses than Girder 3. The bottom quarter point of the web region in Girders 3 resulted in higher stresses than the web midpoint and bottom quarter points that were instrumented, whereas the top quarter point of the web had higher stresses in Girder 4.

The vertical deflection results were typical of a continuous girder bridge. When the preceding span were poured, the girders in the last span could be characterized with some uplift, but as the concrete pour progressed onto the last span, the girders changed from an upward deflection to a downward deflection.

The actual horizontal displacement results relating to the thermal expansion behavior of Unit 3 were much less to the calculated theoretical values. This is an indication that the theoretical expansion calculation is conservative in evaluating this behavior.

CHAPTER 5

Parametric Study of the Lateral-Torsional Buckling of Non-Prismatic Curved I-Girders During Lifting

5.1 INTRODUCTION

This chapter discusses the background and results for a parametric study for the lateral-torsional buckling of non-prismatic curved I-girders during lifting. The finite element program ANSYS 11.0 (2007) was used to perform an eigenvalue buckling analysis on various non-prismatic girder cross sections to evaluate the impact of several parameters on the buckling behavior. The trends from the analysis results will be evaluated and discussed. The expression for C_b will be formulated which will account for the stability effects on non-prismatic girders. Finally, the method used to evaluate the stability of non-prismatic curved I-girders during lifting will be discussed.

5.2 BACKGROUND

Rules of thumb and experience have often been the foundation for the lifting of curved I-girders. Although many of these rules of thumb have resulted in the successful erection of steel girders, it is important to understand the fundamental behavior to prevent girder instability during the erection process. Improving the understanding of the basic behavior will improve safety during this phase of construction and also save time at a construction stage in which time is a critical parameter to minimize costs for equipment rental as well as the duration of traffic interruption. The work presented in this chapter extends the work presented previously by Schuh (2008).

5.2.1 Lateral -Torsional Buckling

Lateral-torsional buckling is often critical during the early stages of construction when the bracing is not fully installed. Obviously, one of the critical times to evaluate

girder stability occurs during lifting of the unbraced girder. While stability during lifting is a critical period for any steel girder, horizontally curved girders pose particularly difficult systems due to torsion that is naturally present in the curved geometry. The cross sections of the girders are typically based on the structural demand in the finished bridge. When an I-girder is loaded in flexure, the top flange is in compression and the bottom flange in tension. Depending on the positioning of the lifting points, parts of the girder that will be in tension in the finished girder will often be subjected to compression during erection. Although the applied stress during erection is significantly lower during erection compared to the in-service condition, the girders are not braced in the lateral direction with cross frames or the composite concrete slab during this critical stage. As a result, the buckling modes of the girder are highly dependent on the lifting geometry during erection. Figure 5.1 illustrates the failure mode of lateral-torsional buckling of a curved I-girder during lifting.

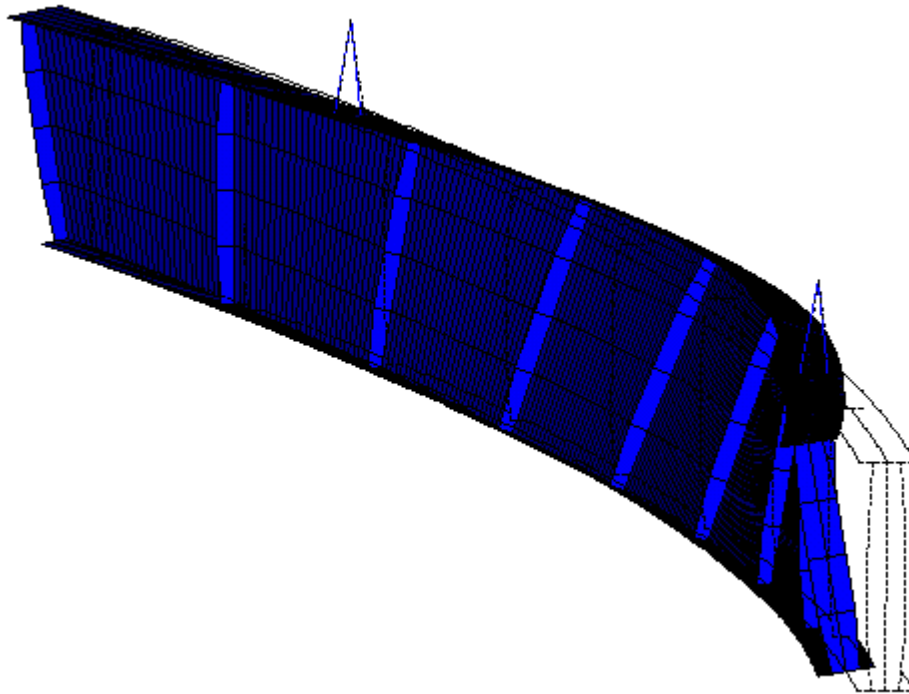


Figure 5.1 Lateral-Torsional Buckling of a Curved I-Girder during Lifting

The lateral torsional buckling capacity of a girder is sensitive to the spacing between brace points as well as the distribution of stress along the unbraced length. The evaluation of the buckling capacity is often based upon solutions that were developed for uniform stress along the unbraced length. The following expression was developed by Timoshenko (Timoshenko, 1961) for evaluating the elastic lateral-torsional buckling capacity of a straight girder with a doubly-symmetric cross-section:

$$M_o = \frac{\pi}{L_b} \sqrt{EI_y GJ + E^2 I_y C_w \left(\frac{\pi^2}{L_b^2} \right)} \quad \text{Equation 5.1}$$

$L_b =$ Unbraced Length of Girder (in)

$E =$ Modulus of Elasticity (ksi)

$I_y =$ Weak Axis Moment of Inertia (in⁴)

$G =$ Shear Modulus (ksi)

$J =$ Torsional Constant (in⁴)

$C_w =$ Warping Constant (in⁶)

The American Association of State Highway and Transportation Officials (AASHTO) *2007 LRFD Bridge Design Specifications* uses a formulation based upon Equation 5.1 in Section 6.10.8.2.3 to limit the compression flange stress. The specification does not cover the stability of the girder during lifting. .

Since Equation 5.1 represents a member with uniform moment, modifications must be instituted for members with a moment gradient. Solutions can be derived for specific moment gradient cases, but this is time consuming and involved for practical design purposes. A moment modification factor, C_b , is often used as a modifier to uniform moment solutions to predict the buckling capacity under variable moment. For common cases, moment gradient factor expressions have been previously formulated in design specifications; however the support conditions of the girder need to match the necessary boundary conditions, which usually requires the beam to be braced at the ends. For the purposes of discussion, the buckling capacity of a girder with uniform moment

loading given by Eq. 5.1 will be referred to as M_o . The C_b factor can be directly applied to the uniform moment solution which yields the following expression:

$$M_{cr} = C_b M_o \quad \text{Equation 5.2}$$

$C_b = \text{Adjustment Factor Derived Computationally}$
 $M_o = \text{Critical Buckling Moment for Uniform Moment}$

Finite element analyses (FEA) can be used to study the lateral torsional buckling behavior; however this usually necessitates evaluating the C_b factor for a variety of load and support conditions. Equation 5.2 can therefore be rearranged to solve for a C_b from the FEA results as shown in Equation 5.3. The critical moment, M_{cr} , is determined from the FEA results as the maximum moment along the girder length at buckling. Since the value of M_{cr} is determined analytically, specific support and loading conditions can be modeled. Although a hand solution such as Equation 5.1 can be used to solve for M_o , in many situations the FEA solution is used for a beam subjected to uniform moment and twist restrained at the ends of the unbraced length.

$$C_b = \frac{M_{cr}}{M_o} \quad \text{Equation 5.3}$$

$M_{cr} = \text{Critical Buckling Moment Determined Analytically}$
 $M_o = \text{Critical Buckling Moment for Uniform Moment}$

Various specifications present different expressions for calculating the C_b factor for accounting for non-uniform moment diagrams when both ends of the unsupported segment are braced. Equation 5.4 is the expression from the American Institute of Steel Construction Specification (AISC 13th 2005). This equation, which is based on absolute values of bending moments, relates the maximum moment to the moment gradient along the unbraced length of the beam. The AASHTO specification expresses the adjustment factor in terms of stresses, which is given in Section 6.10.8.2.3.

$$C_b = \frac{12.5 M_{max}}{2.5M_{max} + 3M_A + 4M_B + 3M_C} \quad \text{Equation 5.4}$$

M_{max} = Maximum Moment Along L_b

M_A = Moment at $0.25L_b$

M_B = Moment at $0.50L_b$

M_C = Moment at $0.75L_b$

L_B = Unbraced Length

The equations presented in AISC and AASHTO specifications are intended moment gradient on straight beams. There is little guidance on the topic of lateral-torsional buckling stability of straight and curved girders during lifting. The following section will discuss previous work related to prismatic curved I-girder stability that will provide background for the non-prismatic curved I-girder parametric study related to this thesis.

5.2.2 Previous Work: Curved I-Girder Rotation During Lifting

Schuh (2008) discussed the challenging issues caused by the potential for excessive prismatic girder rotations during lifting. This topic is important due to the fact that excessive rotations make the girders unmanageable and difficult to fit up in the field. Based on fundamental static principles, Schuh provided a solution for predicting the rigid body rotation of a curved I-girder during lifting. Schuh used results from field measurements on the lifting of curved I-girders to show that the height of axis of rotation of the girder is a crucial parameter in predicting the rotation during lifting. Figure 5.2 illustrates the height of axis of rotation (H) and the ANSYS model graphic for this study along with a picture of the girders used in the field measurements.

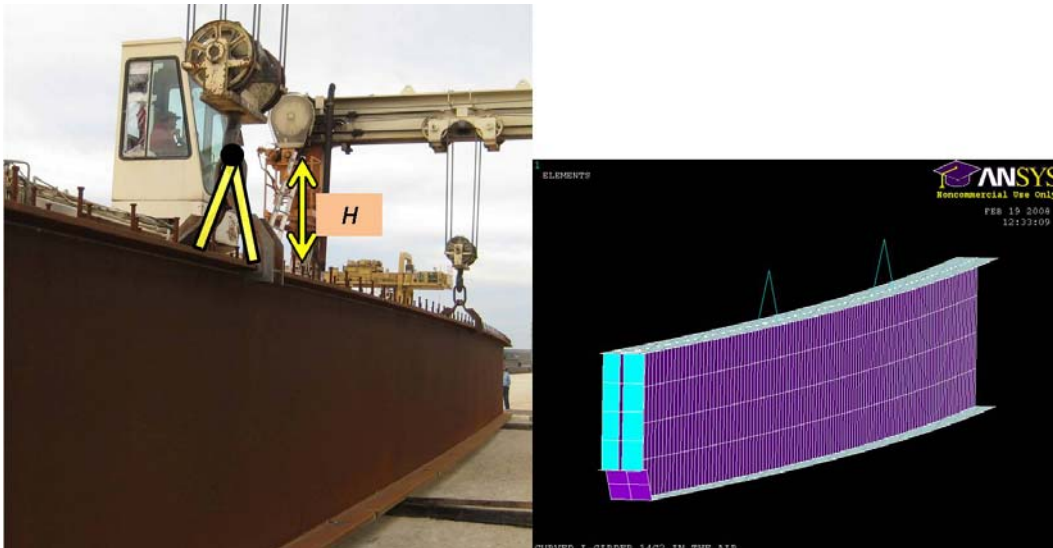
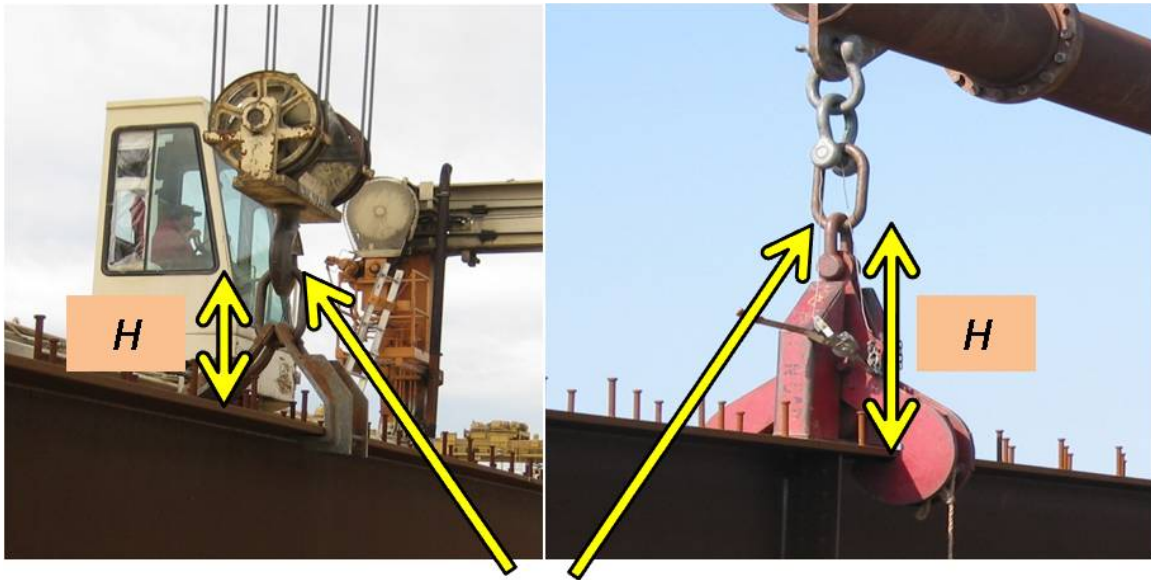


Figure 5.2 Lift Apparatus Axis of Rotation (Schuh 2008)

The validation of a finite element model was described and results were discussed. After further research, the height of the axis of rotation was set at 30" for the remainder of Schuh's study. With the various lifting devices used in construction, the height of the axis of rotation differs for each lifting scenario. The following figure illustrates two examples of different types lifting devices: MIJACK lift apparatus (Figure 5.3 left) and a spreader bar lifting clamp (Figure 5.3 right).



Assumed Axis of Rotation

Figure 5.3 Approximating the Axis of Rotation (Schuh 2008)

The height “H” defines the distance from the top of the girder to the axis of rotation. The axis of rotation should be a location on a lifting apparatus where no moment is transferred and a pivoting motion is relatively uninhibited. The axis of rotation height (H) greatly influenced girder rotation during lifting. As the height increased, the eigenvalue of the lifted girder also increased. The value of H that is used should be representative of the actual lifting apparatus so that the capacity is not over estimated.

The field data from the lifting tests were used to validate the finite element model. Possessing a clear understanding of this behavior is important for the next section related to a parametric study on prismatic curved I-girder stability.

5.2.3 Previous Work: Prismatic Curved I-Girder Stability

Once the FEA model had been validated with the field data, Schuh (2008) conducted parametric studies on the stability of prismatic curved I-girders during lifting. Prismatic girders are homogeneous throughout, meaning that they have the same geometric cross section throughout the length of the girder. Schuh conducted eigenvalue

buckling analyses using the finite element program ANSYS (2007) for various parameters. He developed an expression for C_b , for the girders for evaluating the stability as a function of the lifting location.

For the prismatic curved I-girder study, the eigenvalue is the scale factor that the applied load should be multiplied by to produce the critical buckling load. The applied load is the self weight of the girder. The following expression describes the relationship between the self weight of the girder and the critical buckling load:

$$w_{cr} = \lambda * w_{SW} \quad \text{Equation 5.5}$$

$$w_{cr} = \text{Critical Buckling Load (k/ft)}$$

$$\lambda = \text{Eigenvalue}$$

$$w_{SW} = \text{Girder Self Weight (k/ft)}$$

The critical moment, M_{cr} , can be found by multiplying the maximum moment, which can be determined by static analysis, by the eigenvalue as shown in the following equation:

$$M_{cr} = \lambda M_{max} \quad \text{Equation 5.6}$$

$$\lambda = \text{Eigenvalue from Buckling Analysis}$$

$$M_{max} = \text{From Static Analysis}$$

M_{cr} can be determined from the eigenvalue buckling analysis due to the self weight of the curved I-girder. The maximum moment for a prismatic I-girder is shown in Equation 5.7. This equation is based on symmetric lift points for lifting a single I-girder. Figure 5.4 illustrates the nomenclature used in the following equations.

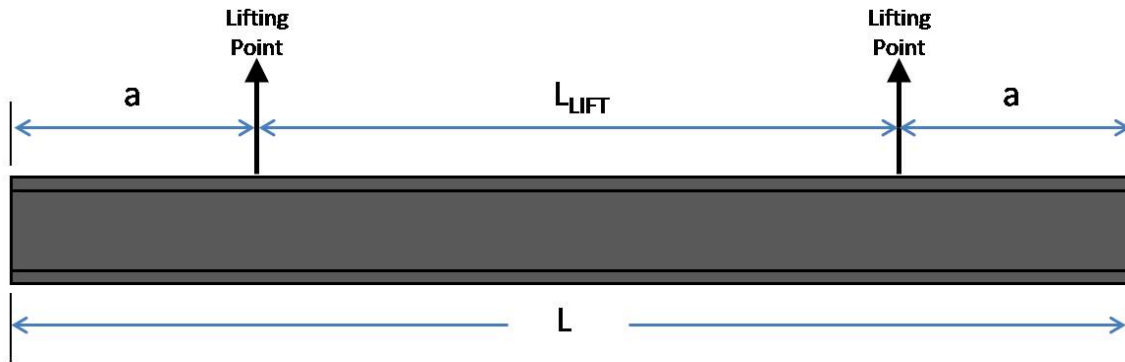


Figure 5.4 Prismatic Girder Lift Point Variable Definition (Schuh 2008)

$$M_{max} = \frac{wa^2}{2} \geq \left| \frac{w(L_{LIFT})^2}{8} - \frac{wa^2}{2} \right| \quad \text{Equation 5.7}$$

$w =$ Factored Girder Self Weight (k/ft)

$a =$ Cantilever Overhang Length (ft)

$L_{LIFT} =$ Span Between Lift Points (ft)

The parameters that were used in Schuh’s study included the radius of curvature (R), the flange width to girder depth ratio (b/d), the span to depth ratio (L/d), and lift point location (a/L). The radius of curvatures used in Schuh’s study ranged from 250’ to Straight. For the parameters of the b/d ratio, Schuh used 1/3, 1/4, and 1/6. Throughout Schuh’s study, the girders analyzed remained doubly symmetric section. The span to depth ratios utilized in this study were 10, 15, 20, and 25. The lift point locations are given as a ratio of the overhang or cantilever length, a , to the total length of the girder, L .

In an effort to isolate the parameters, certain geometric cross sectional properties were kept constant throughout this study. The depth (d) was kept constant at 72” (web height, $h_w = 69$ ”) and the web thickness (t_w) was kept at 0.75”. The thickness of the flange was kept at 1.50”. Along with bearing stiffeners at each end of the girder, the girder web was reinforced with double sided transverse stiffeners that were spaced at 15’

along the length of the girder for all of the analysis cases. The lifting apparatus was modeled as two truss elements pinned together at the top and attached to the top flange a distance of $b/4$ from the flange edges to simulate the actual lifting scenario on a construction site.

The parametric study included a comparison of the eigenvalues from a linear buckling analysis on two geometric configurations; the non-rotated and the rotated girder. Schuh determined that there was not a significant difference between the non-rotated and rotated eigenvalue and that using the non-rotated eigenvalue was more conservative. This resulted in the use of the non-rotated eigenvalue for the remainder of the prismatic I-girder parametric study.

Trends associated with the established parameters are presented from the various finite element analytical models. By relating the trends to the eigenvalue, Schuh formulated an expression for C_b , which is essentially the C_b factor for moment gradient. Although Schuh used the term C_L , the term C_b will be used throughout the remainder of this chapter. Schuh's C_b expression was calculated with the unbraced length (L_b) as the distance between brace points (L_{LIFT}) or the cantilever length (a) if it is greater. The Schuh expression for C_b is as follows in Equation 5.8.

$$\begin{aligned}
 C_b &= 1.0 \quad \text{for} \quad \frac{a}{L} \leq 0.225 && \text{Equation 5.8} \\
 C_b &= 0.5 * \frac{d}{b} \leq 2.5 \quad \text{for} \quad 0.225 < \frac{a}{L} < 0.275 \\
 C_b &= 0.75 \quad \text{for} \quad \frac{a}{L} \geq 0.275
 \end{aligned}$$

Using the C_b factor to adjust the Timoshenko uniform critical buckling moment, M_o , the critical buckling moment for the girder during lifting can be established and a stable system results if $M_{max} < M_{cr}$. The following equation relates the maximum moment to the critical moment.

$$M_{max} < \phi M_{cr} = \phi C_b * \frac{\pi}{L_b} \sqrt{EI_y GJ + E^2 I_y C_w \left(\frac{\pi^2}{L_b^2} \right)} \quad \text{Equation 5.9}$$

M_{max} = Factored Maximum Moment From Static Analysis

M_{cr} = Critical Buckling Moment

ϕ = Reduction Factor = 0.9

C_b = Moment Gradient Factor

L_b = Unbraced Length of Girder (in)

E = Modulus of Elasticity (ksi)

I_y = Weak Axis Moment of Inertia (in⁴)

G = Shear Modulus (ksi)

J = Torsional Constant (in⁴) = $\sum \frac{bt^3}{3}$

C_w = Warping Constant (in⁶) = $\frac{I_y h^2}{4}$

In summary, the largest eigenvalues were observed when the girder was lifted with an a/L of 0.25. The radius of curvature for prismatic curved I-girders was found to have a negligible effect on the eigenvalue. An example calculation using the formulated adjustment factor, C_b , was provided to perform the necessary stability check.

5.3 STUDY DESCRIPTION

The eigenvalue buckling analysis of non-prismatic curved I-girders complements to work from Schuh on prismatic curved I-girders. Based on the eigenvalue, the non-prismatic I-girder study takes similar steps to formulate an adjustment factor, C_b , as the preceding study. Like the previous study, C_b , which accounts for the stability effects on non-prismatic girders, will be formulated using Timoshenko's equation for uniform moment for lateral-torsional buckling acting along the length of a beam.

5.3.1 Non-Prismatic Girders

Most of the curved I-girders used in Texas bridges and around the United States have non-prismatic geometric cross sections. For continuous bridge units, over the negative moment region, the flanges are typically designed with a larger cross sectional area. The buckling behavior of straight or curved non-prismatic girders is not well understood, particularly during erection. This study will encompass doubly symmetric non-prismatic curved I-girders.

Although the work in this thesis is focused on doubly-symmetric sections, in many situations girders with a single plane of symmetry are used in bridge design. The positive moment region the bottom flange is often thicker than the top flange depending on the design bending stresses that the girder experiences and due to the composite nature of steel and concrete action together. In composite girder design, the effective width of the concrete slab in the positive moment region acts as the top flange of the girder, therefore because the top flange plate is relatively close to the neutral axis of the composite girder, a smaller flange plate is often used compared to the bottom flange plate. The author conducted some studies on singly-symmetric sections. This work will be extended on the research project and presented in a later thesis

5.3.2 Eigenvalue Analysis Approach

Results in this chapter will consist of solutions from an eigenvalue buckling analysis using a three-dimensional finite element model developed in ANSYS (2007). The eigenvalue is the scale factor that the applied load should be multiplied by to produce the critical buckling load. The applied load in all cases is the self-weight of the I-girder. Equation 5.5, which is referenced in Schuh's work, is also used in the non-prismatic study to relate the eigenvalue to the critical buckling load.

The critical moment, M_{cr} , can be found by multiplying the maximum moment, which can be determined by static analysis, by the eigenvalue as shown in Equation 5.6. M_{cr} can be determined from the eigenvalue buckling analysis with a reference load

consisting of the self weight of the curved I-girder. The maximum moment for a non-prismatic I-girder will vary with plate transition locations, due to the varying self weight, and un-symmetric lifting locations. This can be determined using a static analysis. Figure 5.5 is an example of a particular lifting scenerio and flange plate transitions.

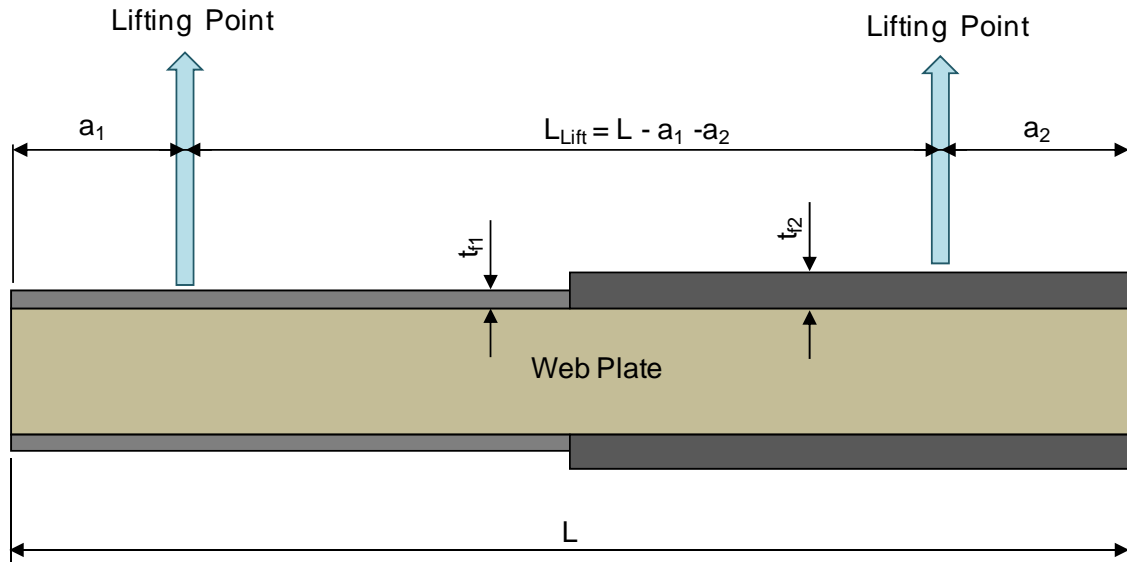


Figure 5.5 Example Non-Prismatic Girder and Lifting Locations

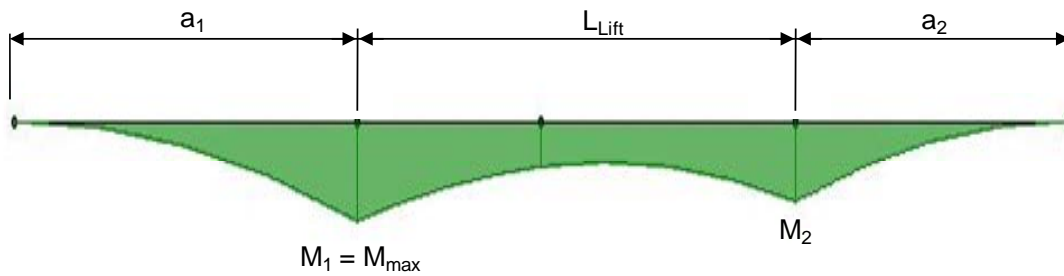


Figure 5.6 Example Non-Prismatic Girder Moment Diagram

Figure 5.6 represents the moment diagram for a particular lifting scenario. Because there is a flange plate transition, the self weight is not uniform throughout the entire length of the girder and therefore the moment at the lifting points is different. The girder may be lifted with either one or two cranes. With two cranes the length of the L_{Lift} can be adjusted by the erector. However in many situations, the girders will be lifted by a single crane with a spreader beam. In this case, the center dimension, L_{Lift} , represents the length of the spreader beam. If a spreader beam is used, the lifting loads must be the same or the girder will rotate end to end. Unsymmetrical lifting arrangements were considered to take this into account. To calculate the static moment, the girder is assumed straight. Schuh found that the difference between the curved and straight Moment Diagrams is negligible (Schuh 2008, Appendix C). Using Equation 5.6, M_{max} would be equal to M_1 in Figure 5.6.

5.3.3 Parameter Descriptions

The parameters chosen for this parametric study were radius of curvature (R), the flange width to girder depth ratio (b/d), the span to girder depth ratio (L/d), and the lift point location. Figure 5.7 depicts the dimensions that were varied in this parametric study.

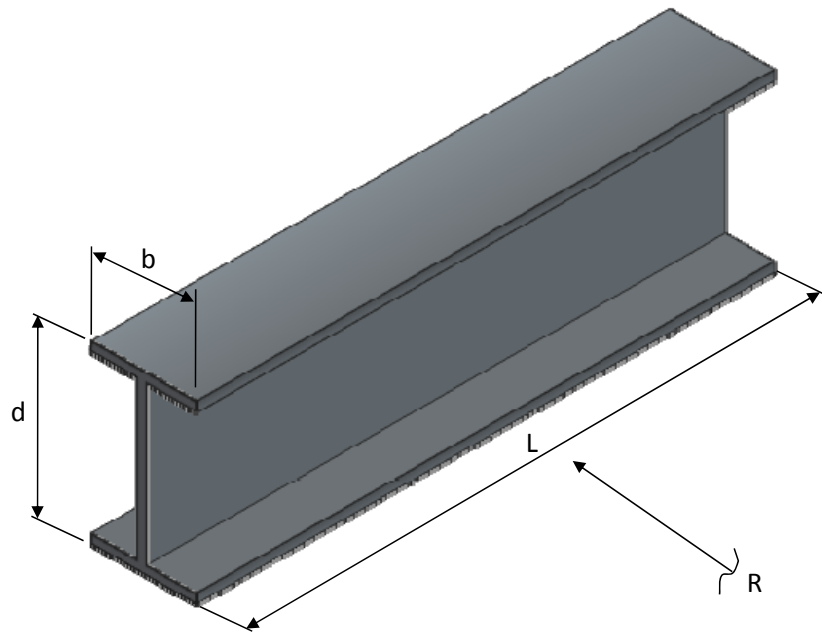


Figure 5.7 Parametric Study Parameter Nomenclature

5.3.3.1 Radius of Curvature

The horizontal radius of curvature is a common term in roadway and bridge design. Roadway alignments are typically designed with tangents and arc lengths. When obstacles such as underlying roadways or established metropolitan areas cannot be avoided, the resulting geometry of the bridge often becomes more complex. Therefore, if the bridge is situated on a curved portion of the roadway alignment, the superstructure must also be “curved.” The radius of curvature of a curved girder refers to the radius of the arc (girder) that comprises a circle. So as to permit reasonable speed limits on curved interchanges, the majority of Texas bridges have a radius of curvature greater than 800 ft. To cover the full spectrum of possible field values, values of the radius of curvature used in this study ranged from 250 ft to straight.

5.3.3.2 Ratio of Flange Width to Girder Depth (b/d)

TxDOT recommends a minimum flange width to depth ratio of $d/3$ in the Preferred Practices for Steel Bridge Design, Fabrication, and Erection (TxDOT 2007).

Smaller flange sizes will satisfy design requirements in the full composite state, but this limit is intended to maintain girder stability before the bridge's concrete deck is poured. A less stringent limit of $d/6$ is the minimum flange width to depth ratio requirement in the AASHTO Equation 6.10.2.2-2 of the AASHTO LRFD Bridge Specification (AASHTO 2007). The b/d ratios used in this study were 1/3, 1/4, 1/4.5, 1/5, and 1/6. To maintain a doubly symmetric section, both the top and bottom flange were adjusted, as this ratio was varied.

5.3.3.3 Ratio of Girder Length to Girder Depth (L/d)

The ratio of span length to girder depth gives a good indication of the slenderness of an element. As this number increases, the expected eigenvalue should decrease, as the girder becomes more slender. Span to depth ratios of 15, 20, and 25 were used in this parametric study.

5.3.3.4 Lifting Locations

For symmetric lift locations, which means the cantilever portion is equal on both ends ($a_1 = a_2$ on Figure 5.5), the lift point location is described as the cantilever dimension (a) over the girder length (L). The cantilever length is the distance from the end of the girder to the lift point. Due to the nature of the non-prismatic girder, the center of gravity in many cases is not symmetrically located in the center. This is the case when the flange sizes are not symmetric about the centerline of the girder. If the girder plates are not symmetric about the centerline, to minimize girder deformations during erection the lifting points will also not be symmetric. Therefore, in these cases $a_1 \neq a_2$ on Figure 5.5. For studies relating to un-symmetric lift locations, the value of L_{Lift} , which is the distance between lifting locations, is varied. The center of the dimension of L_{Lift} is located at the point of the center of gravity of the curved I-girder. The eigenvalue for curved I-girders with un-symmetric lift locations was also compared with the eigenvalue for girders with the same geometric properties, but with symmetric lift locations.

5.3.4 Constant Variables

Certain geometric properties of the girder cross section were kept constant throughout the parametric study. The height of the web plate was kept at 72" (h_w) and the web thickness (t_w) was kept at $\frac{3}{4}$ ". This produced a web slenderness of 96, which was chosen to ensure that local buckling in the web did not occur. The double-sided stiffeners were spaced 15' apart along the length of the girder. Bearing stiffeners were also incorporated at the ends of the girder. As mentioned earlier, the lifting apparatus was modeled in ANSYS as two truss elements pinned together at the top and attached to the top flange of the girder at a distance of $b/4$ from the edge of the flange.

5.4 PARAMETRIC STUDY RESULTS

A number of factors influence the lateral-torsional buckling capacity of steel girders. These factors include the cross-sectional shape, the unbraced length and the support conditions of the beam. For all of the parametric studies that were conducted in this study, the height of the lifting mechanism (H) was kept at 30".

5.4.1 Non-Prismatic I-Girder, Symmetric Lift Locations

The parametric study began with a non-prismatic girder with two flange plate transitions. The flange sizes were varied by changing the thickness of the flange. The first and third cross sections of the girder had top and bottom flange thicknesses of 1.25". The second (middle) cross section has a top and bottom flange thickness of 2.00". The comparison studies within this Section were all analyzed with symmetric lifting points. Figure 5.8 illustrates the plate transition scenario and equal cantilever ends (*a*).

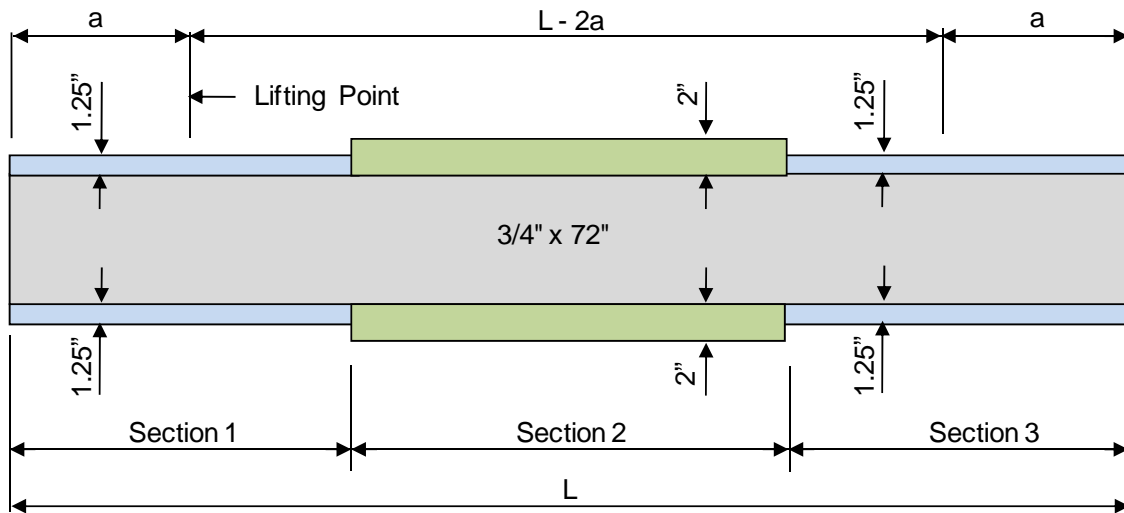


Figure 5.8 Three Cross Section Girder Schematic

5.4.1.1 Eigenvalue (λ) Radius of Curvature Study

The effect that the radius of curvature (R) has on eigenvalue buckling of a non-prismatic curved I-girder is presented in this section. The geometric configuration of Figure 5.8 was used in the study with R values of 250', 300', 500', 750', 1000', 2000', and 20,000' (straight). Figure 5.9 represents the results from one of the many cases within this study. For this case, the total length of the girder remained at 120', and length of Sections 1 through 3 along the girder equaled 40'. A lifting location of a/L of 0.25 is represented in the figure below. The girder has a top and bottom flange width of 18" and web plate of $\frac{3}{4}$ " x 72".

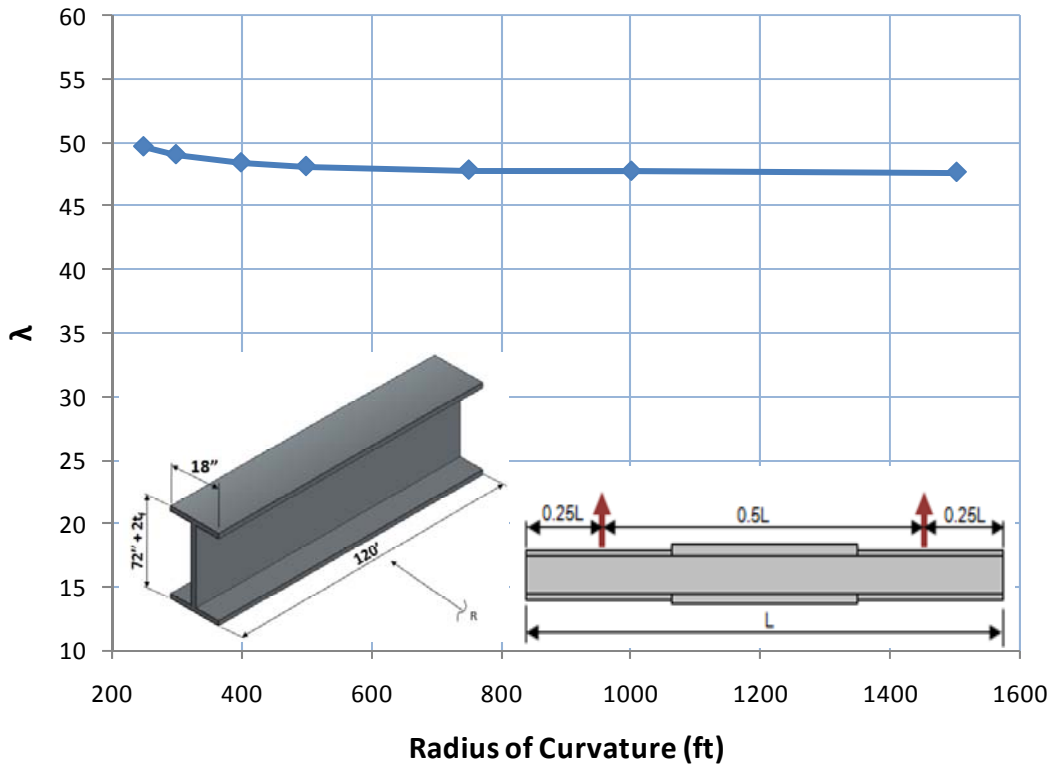


Figure 5.9 Effect of λ on Radius of Curvature

As shown in Figure 5.9, the effect of the radius of curvature has little effect on the eigenvalue. There is minimal change in the eigenvalue when the radius of curvature is small, from 250' to 300'. However, in general the eigenvalue does not change significantly as the radius of curvature is varied. For example, when the radius is 500', the eigenvalue is 48.1, whereas when the radius is 750', the eigenvalue is 47.8. The same trend was seen for girders with other b/d ratios, a/L locations, and L/d ratios. For the following studies, because the change in eigenvalue is minimal, the eigenvalues for the range of radius of curvatures is averaged to compare b/d and L/d .

5.4.1.2 Eigenvalue (λ) L/d Study

The next parameter that was considered in the (Figure 5.8) investigation was the L/d ratio. The top and bottom flange widths were maintained at 18", while the length of

the girder changed. The girder lengths studied were 90', 120', and 150', which produced L/d ratios close to 15, 20, and 25, respectively. For all cases, the lifting point location, a/L , varied from 0.10 to 0.40. The values of the radius of curvature (R) were also varied for each L/d case.

At a girder length of 90' ($L/d = 15$), the lengths of Sections 1 through Section 3 all equal 30'. At a/L of 0.10 for the varying radii, the eigenvalue (λ) averaged to 9. At a/L of 0.25, which would be located at the quarter points, for the varying radii, the eigenvalue (λ) averaged to 115. At a/L of 0.40 for the varying radii, the eigenvalue (λ) averaged to around 30. As outlined in the last section, the variation of the radius of curvature did not have a significant impact on the value of the eigenvalue (λ). The next part of this study analyzed a curved I-girder with an L/d ratio of 20 with a total length of the girder segment of 120', with equal lengths of 40' for Sections 1 through 3. All of the geometric properties remained the same as the 90' girder above. The length of the girder is the only variable that changed. As the girder became more slender, by increasing the length, the eigenvalue decreased significantly. The maximum eigenvalue occurred at a/L of 0.25 with an average value of approximately 48 for the varying radii. This is less than half of the eigenvalue at a/L of 0.25 for the 90' girder. The last case within the L/d study compared curved I-girders with an L/d ratio of around 25 with a total girder length of 150'. Sections 1 and 3 were 55', while Section 2 was 40'. At a/L of 0.25, the average eigenvalue was 26, which is roughly half of the eigenvalue at 0.25 on the 120' girder. For values of the radius of curvature (R) of 250' and 300' the first mode of buckling often produced eigenvalues that were below 1.0 or did not follow the same trend as the other cases at higher R values due with modes that corresponded to either a rigid body deformation or a mode with top flange distortions near the pick-up points. These modes were not generally consistent with the boundary conditions of the actual girders during lifting and were neglected. The second and third modes of buckling were investigated to find the eigenvalue that produced global lateral-torsional buckling for the particular lifting case.

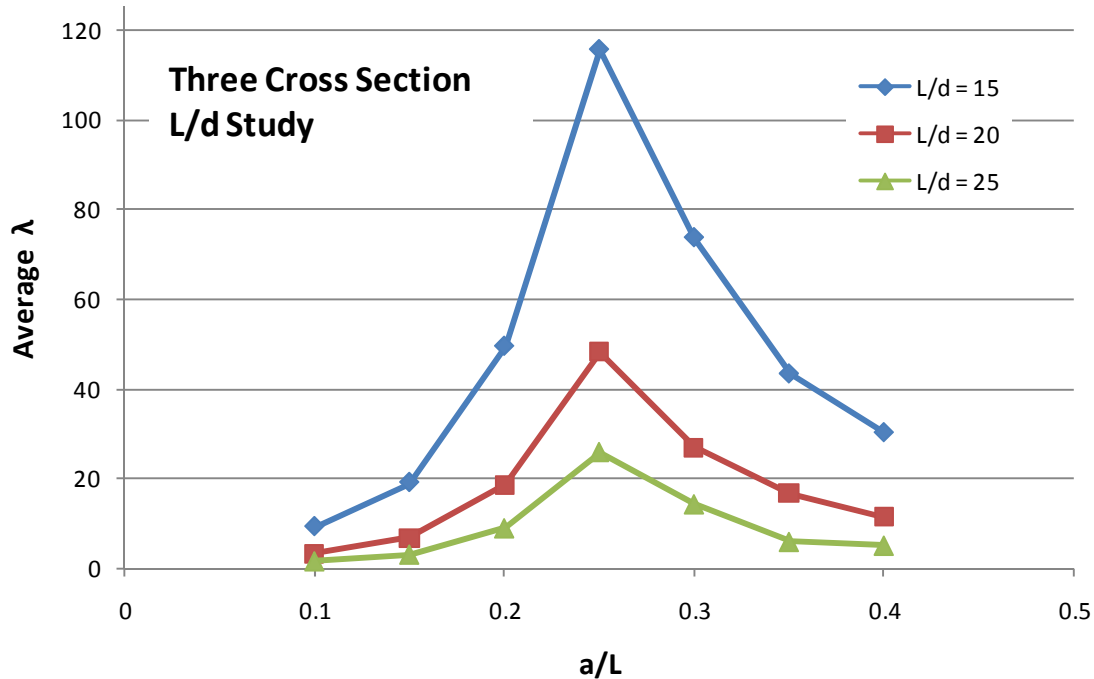


Figure 5.10 Three Cross Section L/d Study (Average λ vs. a/L)

The purpose of explaining the L/d study is to illustrate the behavior of the eigenvalue as a function of girder lifting point. The girder is less stable when the lifting points are very close to the ends of the girder ($a/L = 0.10$) compared to lifting points that are moved closer towards the mid section of the girder ($a/L = 0.4$). The girder is the most stable at an a/L value of 0.25. This will explain the choices made for the Timoshenko M_o equation (Equation 5.1) later within this Chapter.

5.4.1.3 Eigenvalue (λ) b/d Study

The next eigenvalue study investigated the stability of a curved I-girder as the ratio of flange width to girder height changed with the same girder geometry as Figure 5.8. For this comparison study the height of the web plate was maintained at 72" as was the total length of the girder segment at 120'. The length of 120' was chosen because it is close to the maximum hauling length allowed without special permits. The width of the

top and bottom flange (b_f) was changed to produce b/d ratios of 1/3, 1/4, 1/4.5, 1/5, and 1/6. As mentioned earlier, a b/d ratio of 1/3 is the preferred TxDOT limit, whereas a b/d ratio of 1/6 is the outer limit for AASHTO. Similar to the previous L/d study, the values of the radius of curvature analyzed for the b/d cases ranged from 250' to 20,000' (straight). For all cases within this study, the lifting point location, a/L , varied from 0.10 to 0.40.

The maximum eigenvalues were produced with a b/d ratio of 1/3 ($b_f = 24"$), which can be expected, since a wider flange provides added stability due to the larger lateral stiffness of the girders. At a/L of 0.25, the average λ for the different R values was 68. Furthermore, λ reaches its minimum value at this b/d ratio at a/L of 0.10 with a value close to 5. The second case investigated, b/d of 1/4 ($b_f = 18"$), produced lower eigenvalues, with λ equaling 48 (averaged) at a/L of 0.25. The λ drops to 3 at a/L of 0.10, which is close to the same eigenvalue that the b/d ratio of 1/3 produced at this lifting location. The third and fourth cases within this study, b/d of 1/4.5 and 1/5, respectively, followed the same trends as the previously mentioned cases, all with decreasing eigenvalues. The last case within this study investigated a b/d ratio of 1/6 ($b_f = 12"$), which produced the lowest eigenvalues for all lifting locations. At a/L of 0.25, the eigenvalue averaged to 26, which is half the eigenvalue that the b/d ratio of 1/3 produced at this same lifting location. At a radius of curvature of 250' and a lifting location of a/L of 0.10, the lowest λ value in this portion of the study was found to be 1.2, which indicates that the critical buckling load is just slightly larger than the girder self-weight. For the same lifting location, λ increases to 1.5 at a 400' radius of curvature.

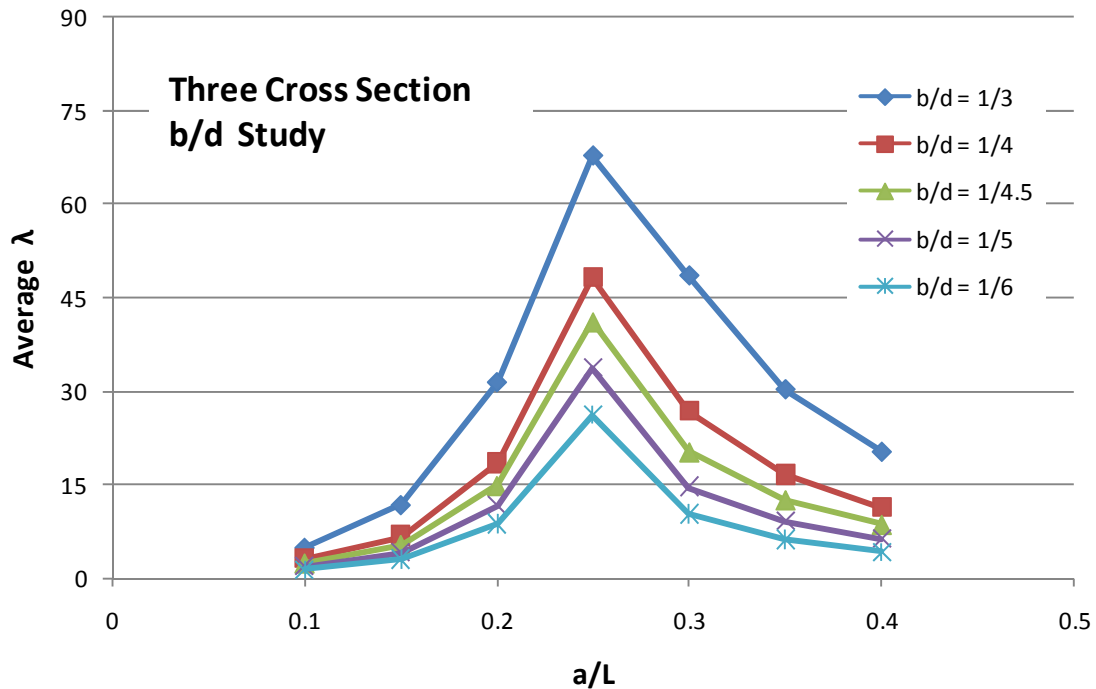


Figure 5.11 Three Cross Section b/d Study (Average λ vs. a/L)

Figure 5.11 shows a graph of the average eigenvalue (λ) versus the lifting location (a/L). As in the previous study, the purpose of explaining the preliminary b/d study is to understand the behavior of the curved I-girder related to eigenvalue buckling as the lifting location changes. The trend that the graph in Figure 5.11 displays will be used to determine the correct method for calculating the C_b factor later in this chapter.

5.4.2 Non-Prismatic I-Girder, Unsymmetric Lift Locations

In order to represent a case with unsymmetrical lift locations, a non-prismatic I-girder with unsymmetrical lifting locations was examined. Figure 5.12 represents the schematic used for the cases discussed in this section. The girder has one plate transition. The first cross section of this girder had top and bottom flange thicknesses of 1.25". The second cross section has a top and bottom flange thickness of 2.00".

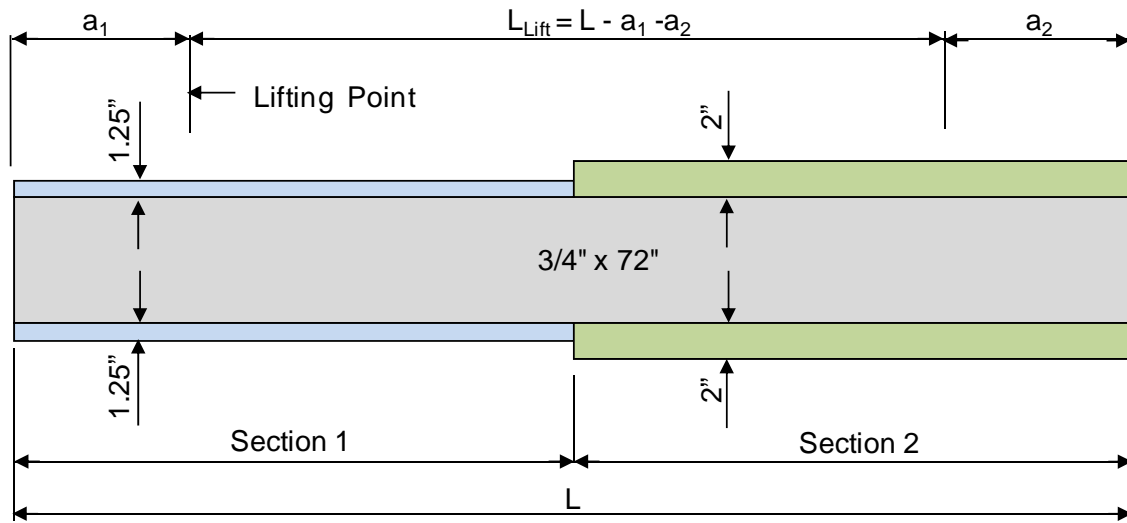


Figure 5.12 Two Cross Section Girder Schematic

The comparison studies within this portion of the investigation were analyzed with unsymmetric lifting points, because the center of gravity (C.G.) does not lie in the center of the girder. The location of the center of gravity along the length of the girder was calculated the center of the spreader beam was centered longitudinally with the C.G. of the girder. Therefore, the two lifting points are located depending on where the center of the spreader beam is located. Figure 5.13 represents the plan view of a curved I-girder and the relationship to the center of gravity and the lifting locations. If the line of support action does not pass through the center of gravity, the girder will rotate once it is lifted so that the center of gravity is in line with the lift points to satisfy moment equilibrium. This rotation will occur about an axis of rotation above the girder at a point on the lifting apparatus that allows rotation. The magnitude and direction of the rotation is determined by the eccentricity (e) between the girder C.G. and the line of support formed by the lift points (Schuh 2008). The girder will also rotate if the longitudinal location of the C.G. is not equal distance between the lifting points.

The distance from the edge of the girder to the center of gravity is referred to as \bar{L} . The distance from the edge of the girder to the first lift point is referred to as a_1 . A spreadsheet was created to calculate the center of gravity location (\bar{L}) by another

graduate student on this research project. The derivation and formulas involved in calculating \bar{L} will be explained in a future dissertation. After \bar{L} is determined, various lengths of spreader beams were analyzed. As the length of the spreader beam changes, a_1 also changes. Because of its insignificant effect on eigenvalue buckling, the radius of curvature was kept at 1000' for this portion of study. The following eigenvalue buckling studies analyze the I-girder depicted in Figure 5.12.

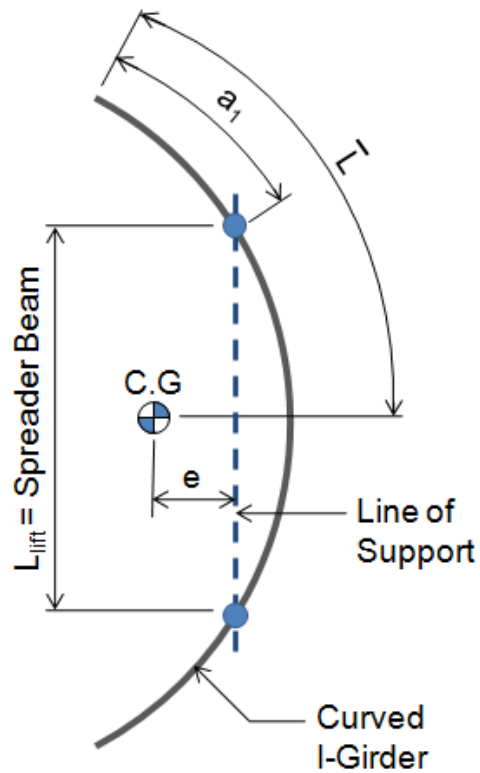


Figure 5.13 Plan View – Center of Gravity, Non-Prismatic Girder

5.4.2.1 Eigenvalue (λ) L_{Lift} Study

To investigate the effects that the length of the spreader beam (L_{Lift}) has on the eigenvalue buckling analysis, various lengths were chosen ranging from 20' to 85'. As L_{Lift} decreases, the length of the cantilever increases (a_1 or a_2). The length of the girder for this study was fixed at 120'. The web plate was 72" x 3/4" which produces a girder

with an L/d ratio close to 20. The location of the top and bottom flange plate transition was varied (Figure 5.12) to investigate the behavior of the I-girder as the sections were modified. Depending on the geometry, different portions of the girders controlled the buckling mode.

Table 5.1 describes the lengths of the sections and the term \bar{L} in Figure 5.13 for each case investigated. Two dimensions of top and bottom flange widths were investigated for each case described in Table 5.1; b_f equaled 12" ($b/d = 1/6$) and 18" ($b/d = 1/4$).

Case	Section 1 Length ($t_f = 1.25''$)	Section 2 Length ($t_f = 2.00''$)	\bar{L} ($b/d = 1/4$)	\bar{L} ($b/d = 1/6$)
1	$L/2 = 60'$	$L/2 = 60'$	63.6'	62.90'
2	$L/3 = 40'$	$2L/3 = 80'$	63.07'	62.5'
3	$2L/3 = 80'$	$L/3 = 40'$	63.33'	62.67'

Table 5.1 Section Definitions

The optimal spreader beam length (L_{Lift}) was calculated with the spreadsheet mentioned earlier. The optimal length is presented as the length of the spreader bar to lift the curved I-girder to produce zero rotation or tilt.

For the first case, Section 1 and Section 2 equaled 60' (Figure 5.12). This means that for the first 60', the top and bottom flanges are 1.25" thick, and then transition to 2" thick for the last 60'. A graph of the eigenvalue (λ) vs. L_{Lift} is presented in Figure 5.14. The location of the center of the spreader beam was positioned at a point 63.6' and 62.9' along the girder for a b/d ratio of 1/4 and 1/6, respectively. This point was held as the length of the spreader beam changed. For zero rotation of the girder while lifting, the optimal spreader beam length was calculated as 69' for both b/d ratios. The maximum λ for both b/d ratios occurred at L_{Lift} equal to 60'. The smallest λ occurred at the extreme lifting points that were selected. The purpose of Figure 5.15 is to relate λ to a/L , similar to the symmetric non-prismatic I-girder study. Since there are two cantilever lengths, a_1

and a_2 , the average of a_1/L and a_2/L was calculated and plotted against λ . Similar to other studies, the highest eigenvalue is seen at an average a/L of 0.25.

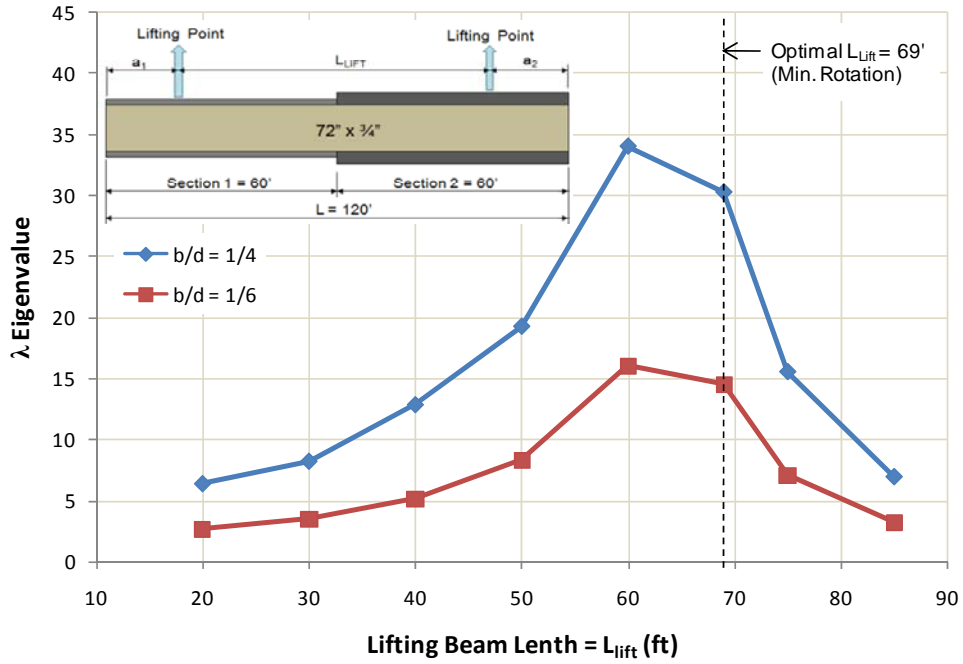


Figure 5.14 λ vs. L_{lift} (Section 1=Section 2 = 60')

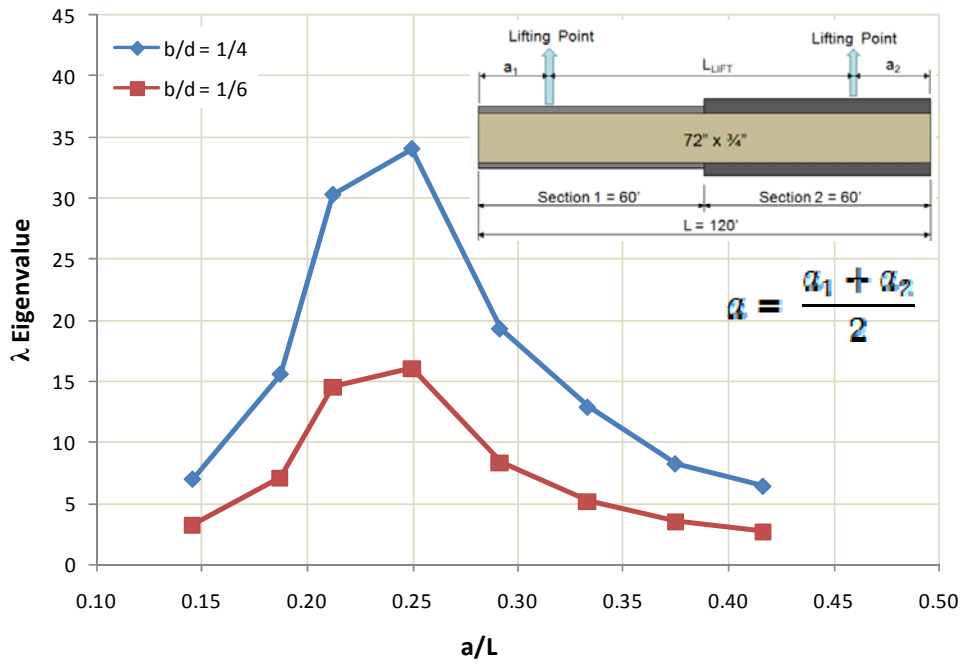


Figure 5.15 λ vs. Average a/L (Section 1=Section 2 = 60')

In the next case, Section 1 and Section 2 were taken as 40' and 80' respectively. The top and bottom flanges were 1.25" thick over the first 40' and then transitioned to 2" thick over the remaining 80'. A graph of the eigenvalue (λ) vs. L_{Lift} for this case is presented in Figure 5.16. The location of the center of the spreader beam was positioned at a point 63.07' and 62.5' along the girder for a b/d ratio of 1/4 and 1/6, respectively. There was not a significant change in \bar{L} between this case and the first case for either b/d ratio. The optimal spreader beam length was calculated as 68' for a b/d ratio of 1/4 and 69' for a b/d ratio of 1/6. The maximum eigenvalue for both b/d ratios occurred at L_{Lift} equal to 60'. The smallest eigenvalues occurred at the extreme lifting points that were selected. Figure 5.17 relates the eigenvalue to a/L , similar to the symmetric non-prismatic I-girder study. Similar to other studies, the highest eigenvalue is seen at an average a/L of 0.25.

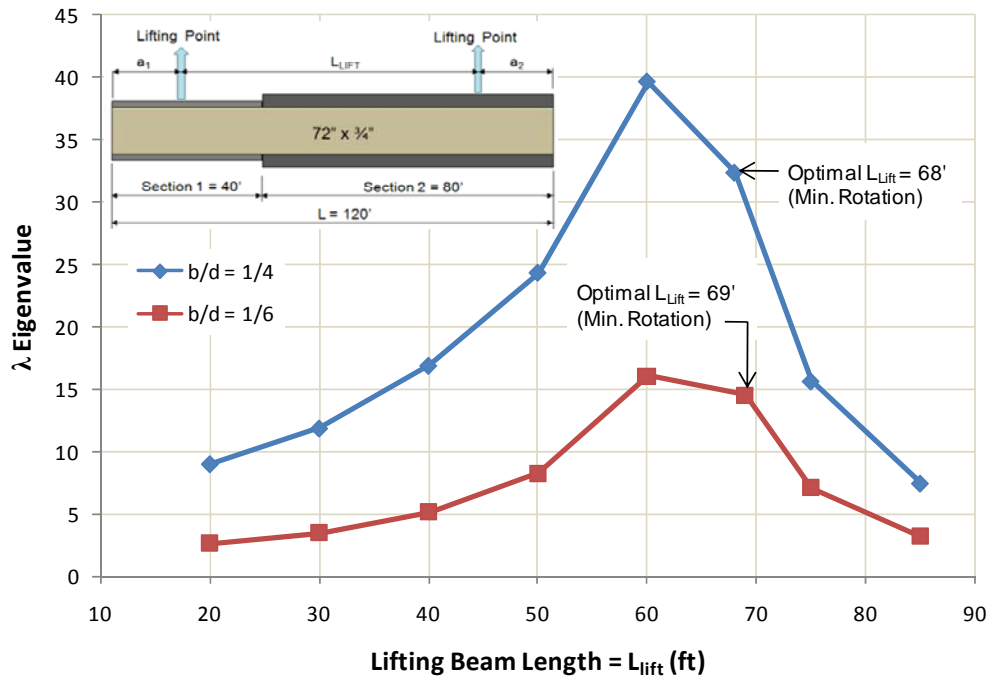


Figure 5.16 λ vs. L_{Lift} (Section 1 = 40', Section 2 = 80')

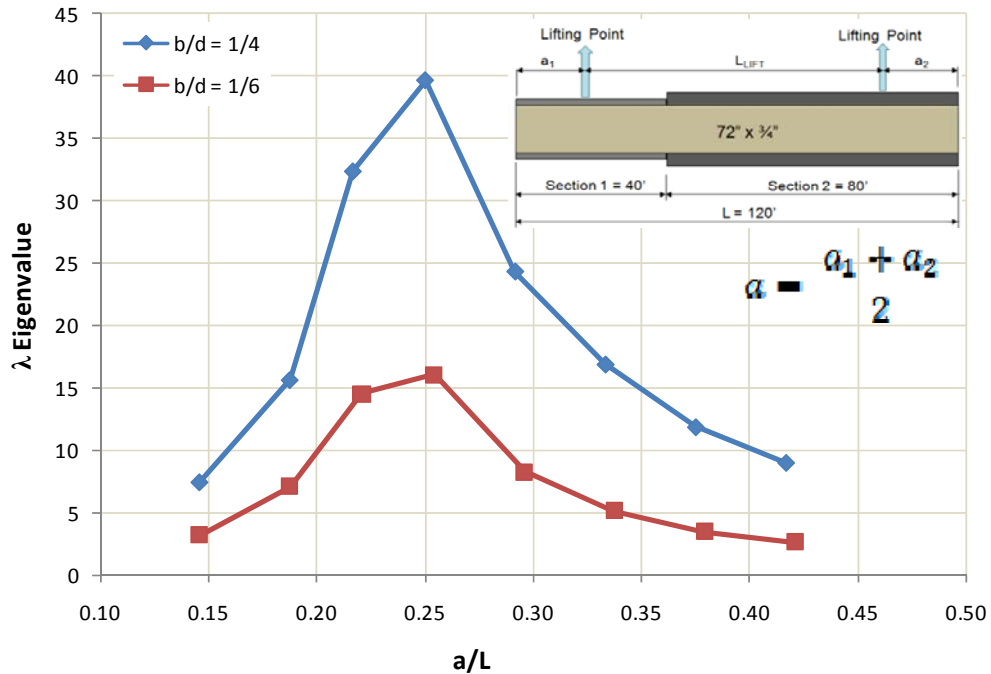


Figure 5.17 λ vs. Average a/L (Section 1 = 40', Section 2 = 80')

Finally, in the last case, Section 1 was set equal to 80' and Section 2 was equal to 40'. For the first 80', the top and bottom flanges are 1.25" thick, and then transition to 2" thick for the last 40'. A graph of the eigenvalue (λ) vs. L_{Lift} is given in Figure 5.18. The location of the center of the spreader beam was positioned at a point 63.33' and 62.67' along the girder for a b/d ratio of 1/4 and 1/6, respectively. The optimal spreader beam length was calculated as 70' for both b/d ratios. Identical to the previous two cases, the maximum eigenvalue for both b/d ratios occurred at L_{Lift} equal to 60' and the smallest eigenvalues occurred at the extreme lifting points that were selected. Figure 5.19 relates λ to a/L . This study also produced the highest eigenvalue at an average a/L of 0.25.

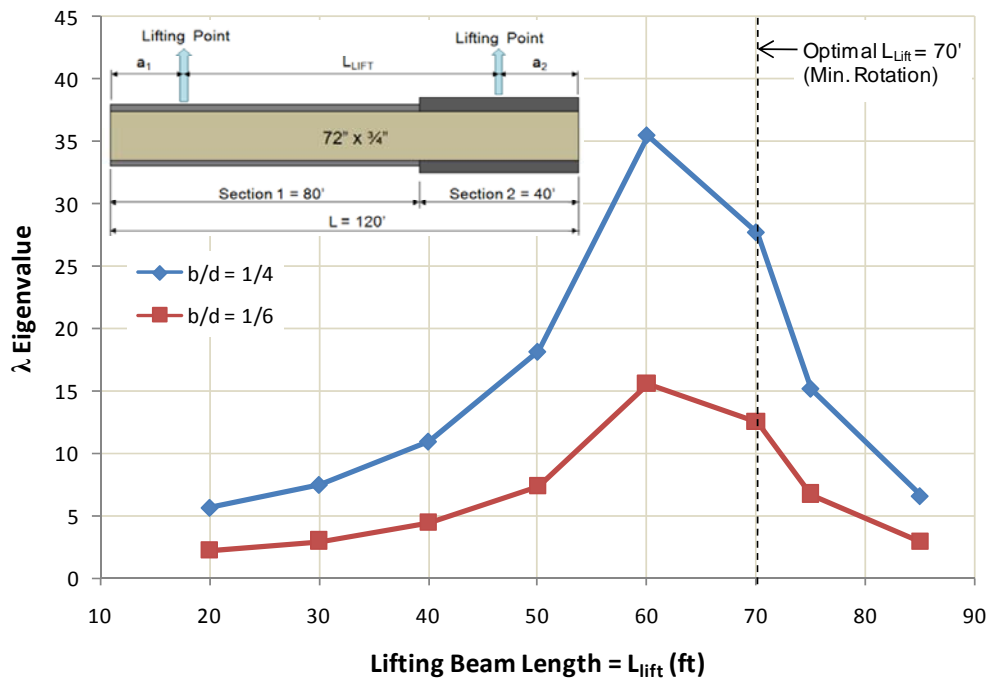


Figure 5.18 λ vs. L_{lift} (Section 1=80', Section 2 = 40')

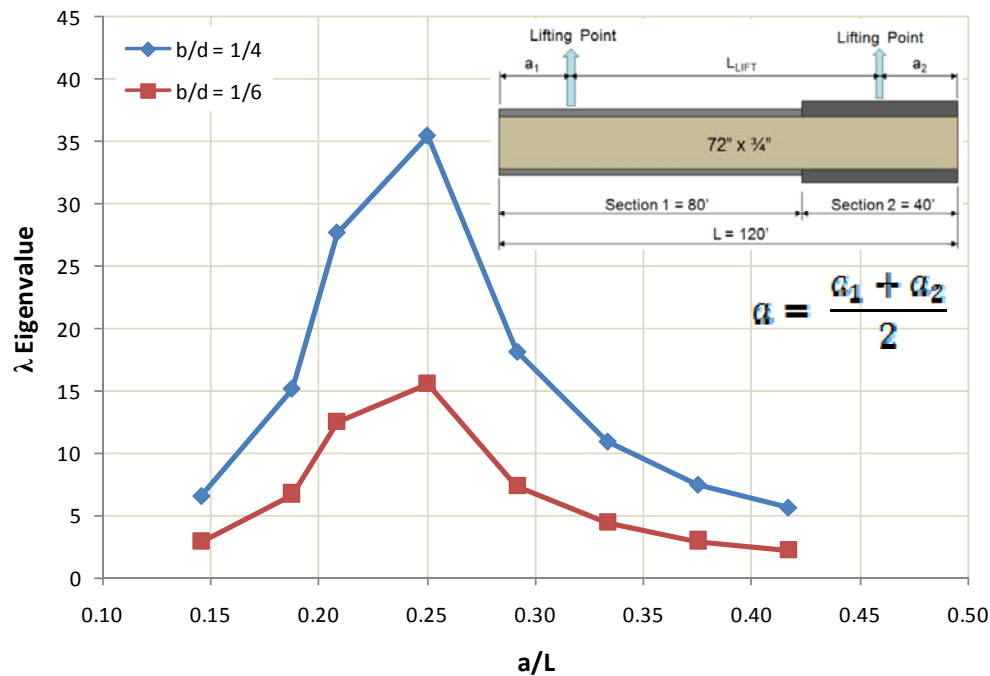


Figure 5.19 λ vs. Average a/L (Section 1=40', Section 2 = 80')

For all three cases, the eigenvalue is greater for a b/d ratio of 1/4, which can be expected because the longer flanges add stability during lifting. The trend for all cases shows that the optimal spreader beam is close to 70' for zero rotation during lifting. The effect of the radius of curvature and the L/d ratio was also investigated for each of the cases (flange plate transitions) presented in this section, but the results from these studies were similar to previous studies presented. Their effects will be discussed in more detail in the next section.

5.5 ACCOUNTING FOR THE EFFECT OF LIFTING OF CURVED I-GIRDERS

Determining the effect of the parameters on the stability of non-prismatic curved I-girders during lifting was the main purpose of the parametric study discussed in this chapter. The case studies involved in determining M_o will be discussed. An expression for the moment gradient factor, C_b , will be formulated within this section as well as its use in checking the stability of non-prismatic I-girder stability during lifting.

5.5.1 Determining M_o for Non-Prismatic Curved I-Girders

A major goal of this study is to develop design methodologies for evaluating the stability of straight and curved girders during erection. As a result, efforts were made to develop a practical approach to the design solution. To gain a clear understanding of the impact of the variables on the behavior, the FEA data needed to be reduced to provide the best insight into the behavior. The eigenvalue needed to be normalized so that the various cases, with varying self weight and moment diagrams, could be compared against each other. A likely expression for evaluating the girder stability necessitates the evaluation of M_o , which is the uniform moment for lateral-torsional buckling along the length of a beam (Equation 5.1). Timoshenko's equation for M_o was used for understanding prismatic girders during lifting, which have the same cross sectional properties throughout the length of the girder (Schuh 2008). The values for the weak axis moment of inertia (I_y), torsional constant (J), and warping constant (C_w) are all related to

the cross sectional properties of the I-girder. If the cross section changes, as in non-prismatic girders, it is unclear as to the correct values to use for the above mentioned geometry related constants. The difficult aspect of working with non-prismatic girders was selecting a suitable solution for the section that has a variable geometry along the length. This section discusses the different cases analyzed to make the proper selection.

$$M_o = \frac{\pi}{L_b} \sqrt{EI_y GJ + E^2 I_y C_w \left(\frac{\pi^2}{L_b^2} \right)} \quad \text{Equation 5.1}$$

$L_b =$ Unbraced Length of Girder (in)

$E =$ Modulus of Elasticity (ksi)

$I_y =$ Weak Axis Moment of Inertia (in⁴)

$G =$ Shear Modulus (ksi)

$J =$ Torsional Constant (in⁴)

$C_w =$ Warping Constant (in⁶)

Another input into the M_o equation which raises many questions is the unbraced length of the member analyzed (L_b). Previous studies (Schuh 2008) calculated M_o using L_b equal to the distance between brace points (L_{LIFT}) or the cantilever length (a) if it is greater. This section will discuss finite element analysis cases used to determine the most effective and efficient value for L_b .

The following cases use Figure 5.20 to investigate the effects that cross sectional geometry and the unbraced length have on the M_o equation and relationship to C_b . The radius of curvature was kept at 1,000' and the length 120'. The girder geometry from Figure 5.20 was used in all of the cases described below.

5.5.1.1 Case 1: I_y, J, C_w

The first case study analyzed the effect that the cross sectional geometry (inputs J, C_w, I_y) has on the uniform moment M_o equation. The lifting location a/L was varied

which effected the location of the critical moment along the girder and changed the buckled shape.

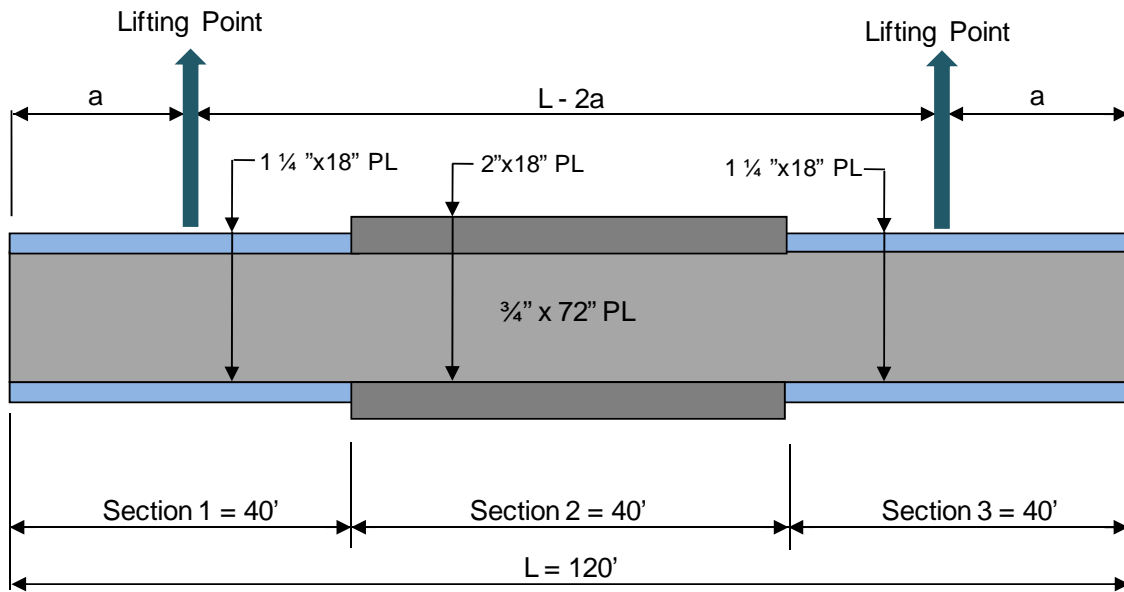


Figure 5.20 Case Study Girder Schematic

The first comparison within Case Study 1 used the cross section geometry inputs into the M_o equation where the maximum moment occurs along the girder. As stated previously, the maximum moment is calculated from static analysis and usually occurs at the lift location point or in the mid region. The second comparison used a “weighted average” of the three cross sections to calculate the variables. This involved adding 2/3 of the cross section properties for Section 1 to 1/3 of the cross section properties from Section 2. The third comparison study used the smallest overall cross section to calculate J , C_w , and I_y for M_o .

For the following graphs, M_o was varied in the calculation for C_b and L_b equaled the full length of the girder. The effect of the unbraced length, L_b , on the M_o equation is discussed in Case 2.

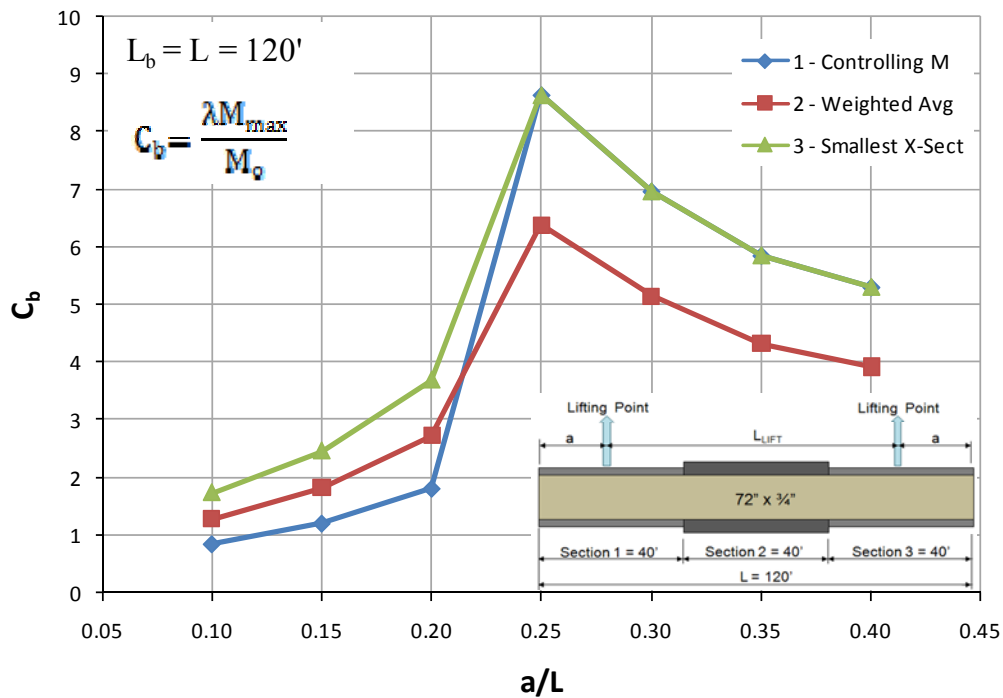


Figure 5.21 Case 1: Cross Sectional Properties for Calculating M_o

Figure 5.21 shows that using the cross section where the controlling maximum moment occurs is similar to using the smallest cross. Using a “weighted average” of the M_o variables produces a lower C_b value for all a/L lifting locations compared to using the smallest cross section values. From this case study, it was determined that the smallest cross section along the non-prismatic girder will be used to calculate M_o to determine C_b .

5.5.1.2 Case 2: Unbraced Length (L_b)

Case 2 investigates the term L_b , which is the unbraced length, in the M_o equation. Section F2 of the *American Institute of Steel Construction Steel Construction Manual* (AISC 13th Edition, 2005) states that the unbraced length is the length between points that are either braced against lateral displacement of the compression flange or braced against twist of the cross section. During the lifting of a curved I-girder, the member has minimal restraint. I-shapes in general are susceptible to lateral-torsional buckling because of their “open cross section” geometry which is composed of slender plates. The

torsional rigidities of I-shaped cross sections are very low so their resistance to torsional instability is limited (Chen and Lui, 1987). It is well known that as the unbraced length gets longer and the less restraint the support can deliver to the beam, the lower the critical lateral buckling load will be.

The first comparison of Case 2 investigates the unbraced length (L_b) as the distance between the lift points ($L-2a$) or the length of the cantilever (a) if it is greater than the distance between the lift points. For the second comparison of Case 2, the unbraced length (L_b) is taken as the full length of the curved I-girder. The smallest cross section is used to determine the geometric properties used to calculate M_o (J , C_w , and I_y). The lifting location (a/L) was varied and the moment due to the self weight of the girder was calculated along the length of the member to find the maximum moment. Figure 5.22 presents a graph of a/L versus C_b lines for the determination of the unbraced length. Two cases are graphed: 1) the case of using the controlling region which is either the overhang or the region between pick points, and 2) the case of using the total length of the girder segment.

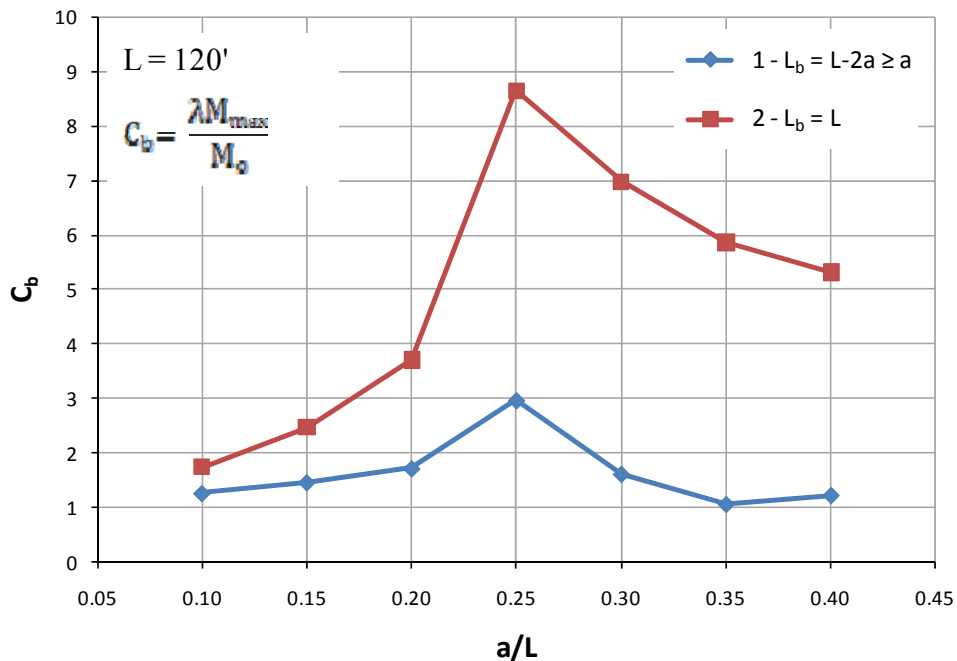


Figure 5.22 Case 2: Unbraced Length (L_b) Comparison (C_b vs. a/L)

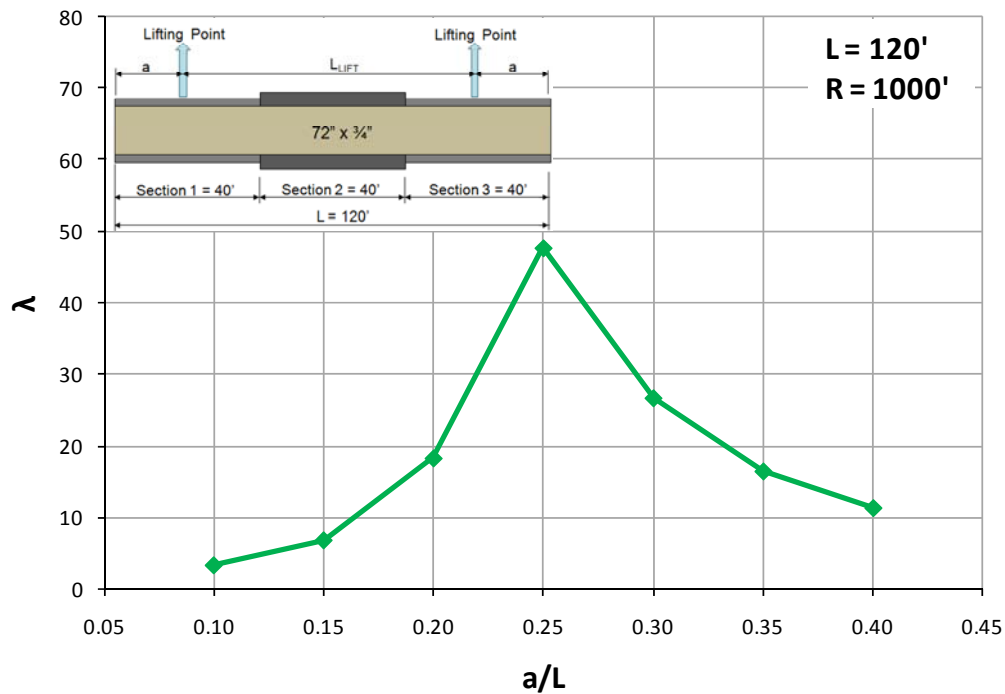


Figure 5.23 Case 2: Unbraced Length (L_b) Comparison (λ vs. a/L)

The value of C_b is greater when L_b is equal to the full length of the girder. This is the effect of M_o decreasing as the unbraced length increases. Since M_o is in the denominator of the C_b equation (Equation 5.3), a smaller M_o increases the value of C_b . In Figure 5.22, when L_b equals L , lifting the girder at an a/L of 0.20 produces a higher C_b than lifting the girder at an a/L of 0.30. In contrast, when L_b equals $L - 2a \geq a$, the graph shows that the girder has the same C_b at an a/L of 0.20 compared to an a/L of 0.30. For the same girder geometry, when the eigenvalue (λ) is plotted against the lifting location (a/L), λ is higher at a/L of 0.30 than at 0.20. The trend of the plot in Figure 5.23 follows the trend of the L_b equals L line in Figure 5.22. For this reason, the unbraced length (L_b) will be taken as the full length of the curved I-girder throughout the remainder of this parametric study. Another advantage of using the full length of the girder segment for evaluating M_o is the reduction in calculations required by an engineer in evaluating girder

stability during erection. The engineer will only have to evaluate M_o once regardless of the lift location that is selected.

5.5.1.3 Case Study Summary

The geometry of the I-girder in Figure 5.20 was used for the case studies presented in this section, but other non-prismatic I-girder geometric configurations were used to investigate the effect of the geometric properties of the M_o equation (J , C_w , and I_y) and unbraced length (L_b). Similar results were produced for cases with L equal to 150', as well as using a girder similar to Figure 5.12 with un-symmetric lift locations.

The purpose of the case studies was to determine the variables of M_o in order to resolve C_b , which accounts for non-uniform moment diagrams when both ends of the unsupported segment are braced. Two decisions were made from this study: The smallest cross section along the non-prismatic girder will be used to calculate M_o to determine C_b and the unbraced length (L_b) will be taken as the full length of the curved I-girder.

5.5.2 C_b Formulation for Non-Prismatic Curved I-Girders

The following section discusses the moment gradient adjustment factor, C_b , during girder lifting as well as its use in checking the stability of a non-prismatic curved I-girder. The value of C_b was found for a given lifting geometry by comparing the eigenvalue buckling capacity for a specific lifting geometry with Timoshenko's equation (Equation 5.1). As shown in Equation 5.3, the C_b factor is the ratio of the maximum moment along the length of the girder to the uniform moment buckling capacity.

Instead of creating a detailed finite element model to determine the stability of a curved I-girder during lifting, Timoshenko's equation (Equation 5.1) can be multiplied by a moment gradient modification factor to determine the critical buckling moment. Similar to Schuh's study on prismatic curved I-girders during lifting, which was discussed earlier in this Chapter, a C_b factor must be formulated to account for the lifting of curved I-girders (Equation 5.3).

The maximum moment occurs at the lift locations or in the region between the lift locations. Depending on the location of the lift points, the girder will buckle in one of the two locations; the cantilever or the mid region. The controlling maximum moment will be taken as the absolute maximum moment wherever it may occur (Equation 5.6).

The following figures summarize the trends related to this parametric study. The figures that are analyzed with symmetric lifting locations represent a curved girder with the same flange plate thicknesses shown in Figure 5.20. Girders represented in the following graphs with un-symmetric lifting locations conform to the same flange plate thicknesses as Figure 5.12. For Figure 5.25, the second mode of buckling was used to determine the eigenvalue at a/L greater than 0.30 and for the radius of curvature of 250'. Since the first mode produced local top flange buckling failure, the second mode was used to capture lateral-torsional buckling (global buckling).

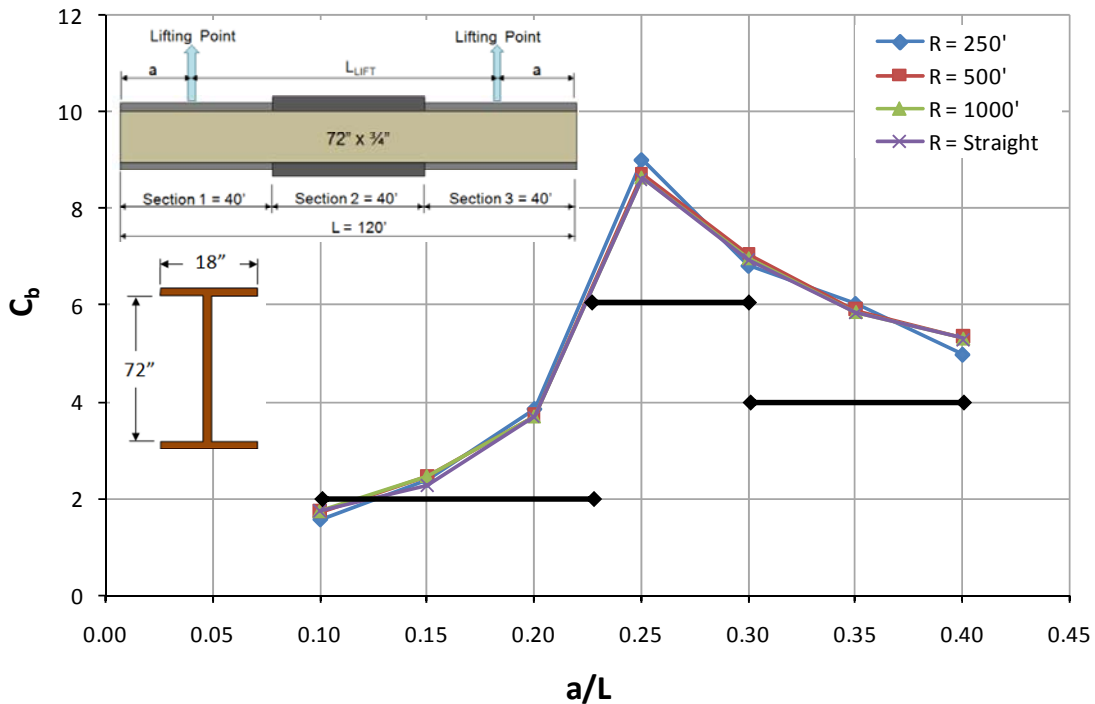


Figure 5.24 C_b vs. a/L for Given Radius of Curvatures (Symmetric Lift)

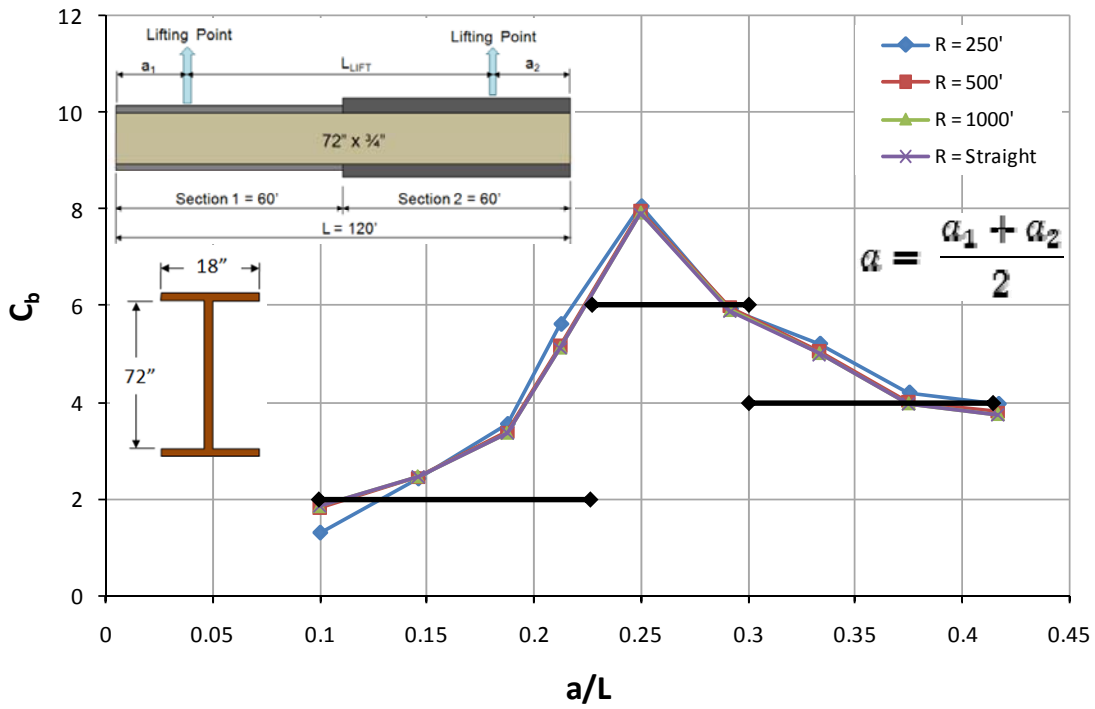


Figure 5.25 C_b vs. a/L for Given Radius of Curvatures (Un-Symmetric Lift)

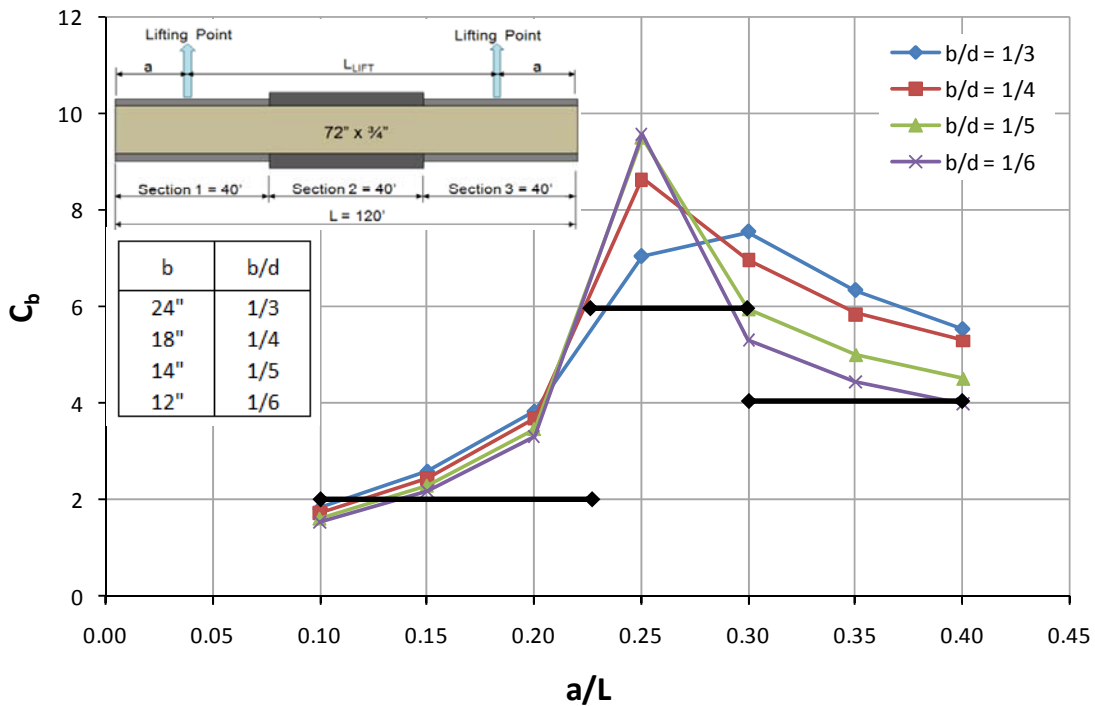


Figure 5.26 C_b vs. a/L for Given Flange Width to Depth Ratios (Symmetric Lift)

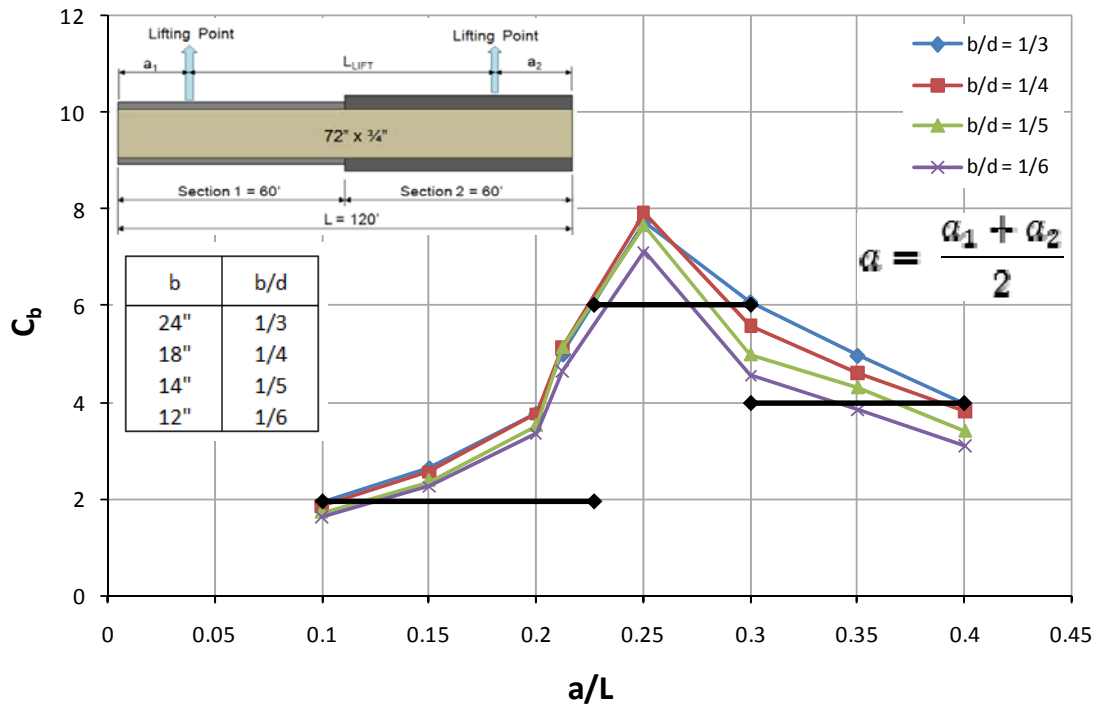


Figure 5.27 C_b vs. a/L for Given Flange Width to Depth Ratios (Un-symmetric Lift)

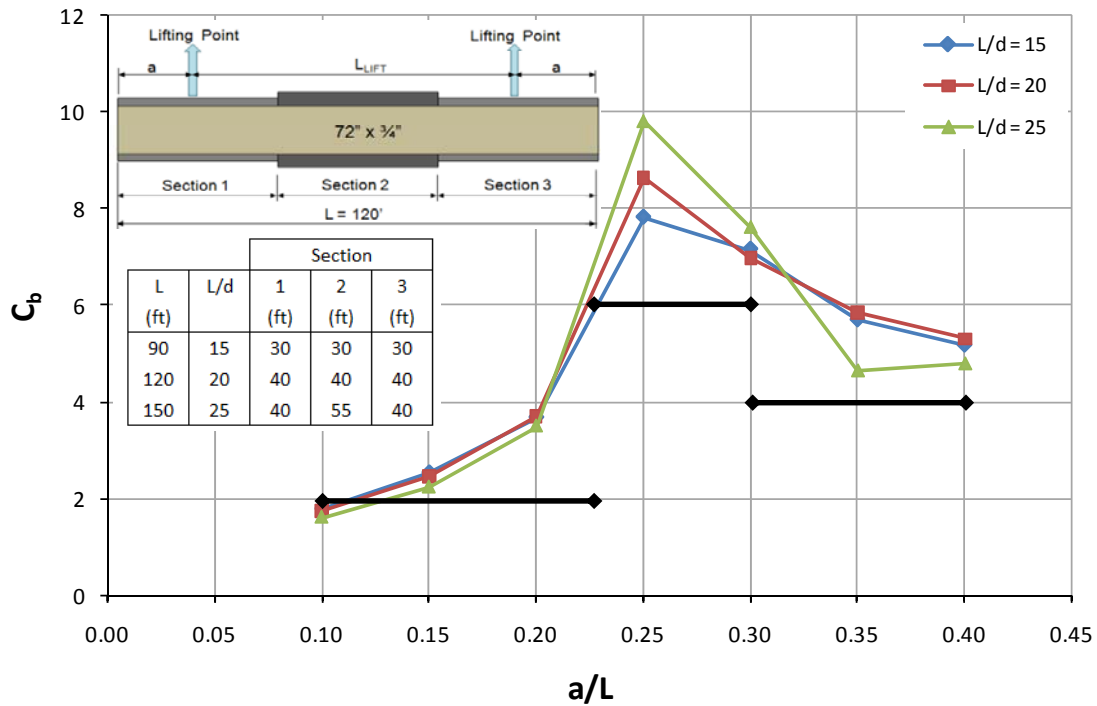


Figure 5.28 C_b vs a/L for Given Span to Depth Ratios (Symmetric Lift)

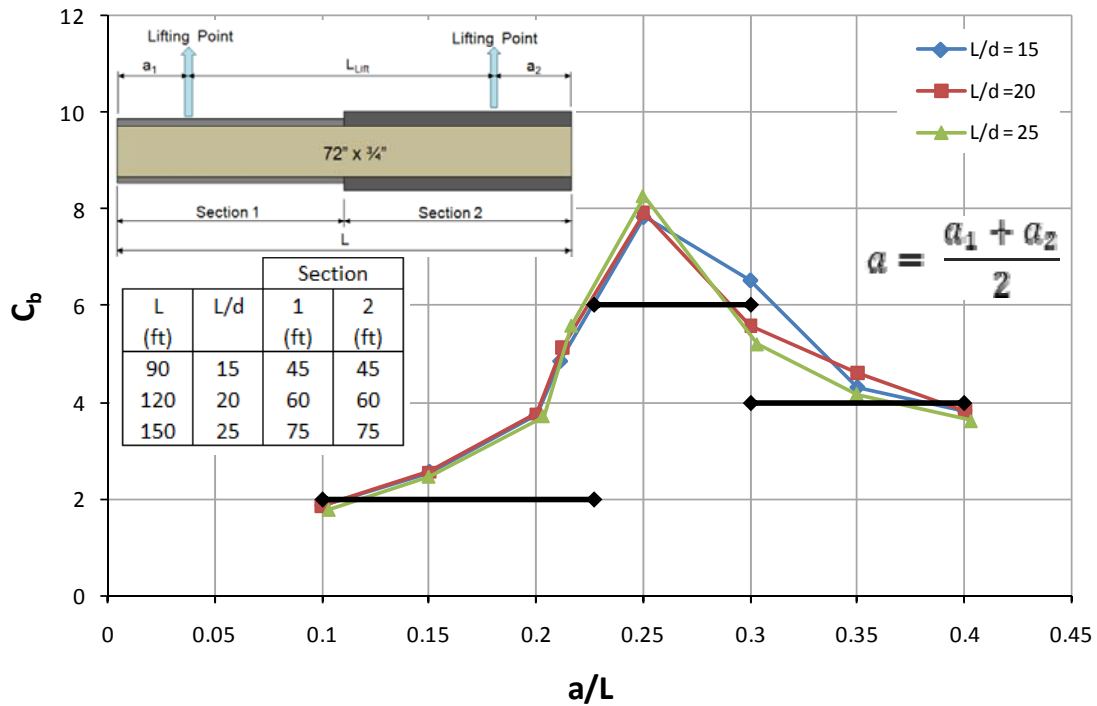


Figure 5.29 C_b vs a/L for Given Span to Depth Ratios (Un-Symmetric Lift)

Equation 5.10 was formulated for the moment gradient factor, C_b , using the trends presented in the previous figures. This expression is represented as the black trend line in the previous figures.

$$C_b = 2.0 \quad \text{for} \quad \frac{a}{L} \leq 0.225$$

$$C_b = 6.0 \quad \text{for} \quad 0.225 < \frac{a}{L} < 0.3$$

$$C_b = 4.0 \quad \text{for} \quad \frac{a}{L} \geq 0.3$$

Equation 5.10

5.5.3 Critical Buckling Moment: Non-Prismatic Curved I-Girder During Lifting

$$M_{max} < \phi M_{cr} = \phi C_b * \frac{\pi}{L_b} \sqrt{EI_y GJ + E^2 I_y C_w \left(\frac{\pi^2}{L_b^2} \right)} \quad \text{Equation 5.11}$$

M_{max} = Factored Maximum Moment From Static Analysis

M_{cr} = Critical Buckling Moment

ϕ = Reduction Factor = 0.9

C_b = Lift Adjustment Factor

L_b = Unbraced Length = L

E = Modulus of Elasticity (ksi)

I_y = Weak Axis Moment of Inertia (in^4)

G = Shear Modulus (ksi)

J = Torsional Constant (in^4) = $\sum \frac{bt^3}{3}$

C_w = Warping Constant (in^6) = $\frac{I_y h^2}{4}$

5.5.4 Checking for Stability

To demonstrate the implementation of the C_b factor in real world curved I-girder lifting stability applications, an example is given below. Figure 5.30 and Table 5.2 show the dimensions and section properties used in the example to check a girder for stability during lifting. The load factor applied to the self weight of the girder, w_{sw} , is taken as 1.25 (AASHTO 2007 Table 3.4.1-2). The reduction factor, ϕ , is taken as 0.9.

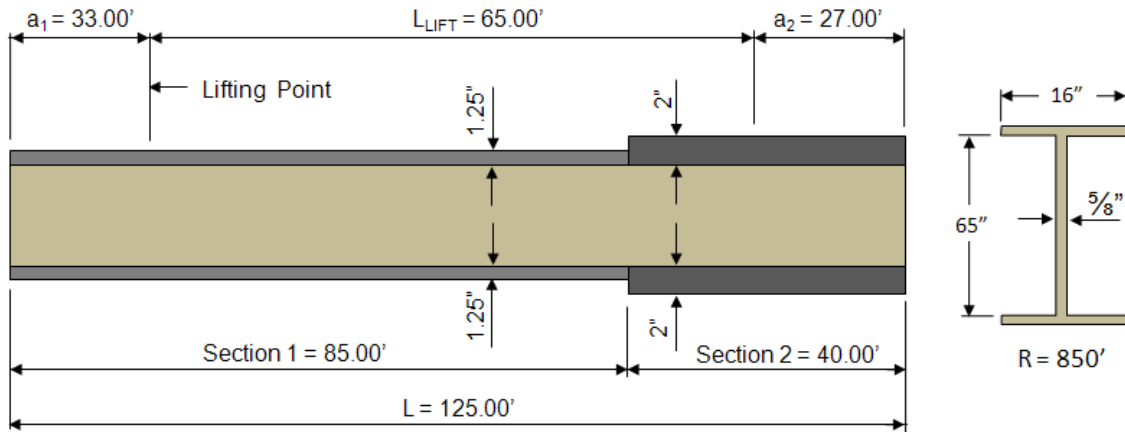


Figure 5.30 Stability Check: Girder Dimensions

Section 1			Section 2		
E =	29,000	ksi	E =	29,000	ksi
C _w =	937,784	in ⁶	C _w =	1,871,147	in ⁶
I _y =	854.66	in ⁴	I _y =	1,367	in ⁴
J =	26.12	in ⁴	J =	91.19	in ⁴
1.25w _{sw} =	0.343	klf	1.25w _{sw} =	0.464	klf

Table 5.2 Stability Check: Girder Cross Section Properties

$$\frac{a_1}{L} = \frac{33 \text{ ft}}{125 \text{ ft}} = 0.264; \quad \frac{a_2}{L} = \frac{27 \text{ ft}}{125 \text{ ft}} = 0.216$$

$$a/L = \frac{a_1/L + a_2/L}{2} = \frac{0.264 + 0.216}{2} = 0.24$$

$$0.225 < \frac{a}{L} < 0.3 \text{ so } C_b = 6.0$$

$$L_b = 125 \text{ ft}$$

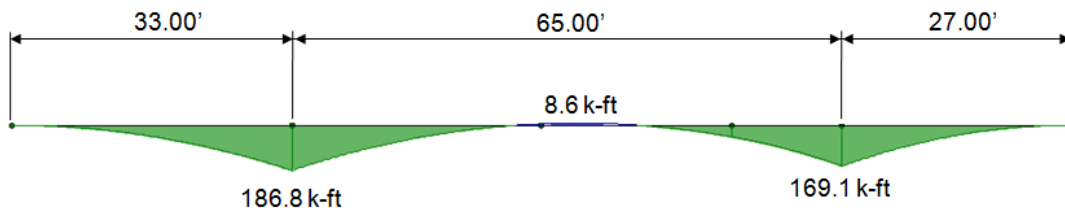
$$M_{cr} = \phi C_b * \frac{\pi}{L_b} \sqrt{EI_y GJ + E^2 I_y C_w \left(\frac{\pi^2}{L_b^2} \right)}$$

$$EI_y GJ = (29,000)(854.7)(11,154)(26.12) = 7.22 * 10^{12}$$

$$E^2 I_y C_w \left(\frac{\pi^2}{L_b^2} \right) = (29,000)^2 (854.7) (937,784) \left(\frac{\pi^2}{(125 * 12)^2} \right) = 2.957 * 10^{12}$$

$$M_{cr} = (0.9)(6.0) * \frac{\pi}{(125 * 12)} \sqrt{(7.22 * 10^{12}) + (2.957 * 10^{12})}$$

$$M_{cr} = 30,081 \text{ kip} * \text{in} = 3,007 \text{ kip} * \text{ft}$$



Moment Diagram

$$M_{max} = 186.8 \text{ k} - \text{ft}$$

$$M_{max} < M_{cr} \text{ STABILITY DURING LIFTING OK}$$

The outcome of the stability check on the girder depicted in Figure 5.30 show that the girder has no risk of lateral-torsional buckling under the lifting conditions shown.

5.5.5 Stability of Curved Girder Systems

The results from the eigenvalue buckling analysis in this chapter showed that the radius of curvature had very little affect on the critical buckling load. In addition, the magnitudes of the eigenvalues showed that the critical load was often significantly higher than the girder self-weight. While the effect of girder curvature does not significantly impact the eigenvalue solution, girder curvature will likely have an impact on the actual girder displacements. Other members of the research team are conducting large-

displacement analysis to investigate the nonlinear behavior of the girders as a function of girder curvature and lifting geometry. The eigenvalue solutions presented in this chapter serve as an important limit to the girder behavior. The results from these additional studies will be presented by another graduate research assistant in a future thesis.

5.6 SUMMARY

Results of a parametric study for the lateral-torsional buckling of non-prismatic curved I-girders during lifting were presented in this chapter. An elastic buckling analysis was performed using the finite element program, ANSYS 11.0 (2007). Background information was introduced to explain the previous work related to the stability of lifting curved I-girders. A section on lateral-torsional buckling was included to explain the behavior that a curved I-girder undergoes during lifting and erection.

The parameters chosen for the parametric study were radius of curvature (R), the flange width to girder depth ratio (b/d), the span to girder depth ratio (L/d), and the lift point location (a/L). The radius of curvature had minimal effects on the eigenvalue, therefore a radius of 1,000' was used for the majority of the studies within this Chapter. Similar to a prismatic I-girder, the eigenvalue increased as the flange width increased. As the span to depth ratio increased, which means the girder becomes more slender, the eigenvalue decreased. These parameters were studied using girder configurations with symmetrical lifting locations as well as un-symmetrical lifting locations. Throughout the parametric study, an a/L value of 0.25 provided the highest eigenvalue.

Finally, the moment gradient adjustment factor for non-prismatic curved I-girder lifting, C_b , was determined through analyzing the trends throughout this parametric study. The definition of the variables for Timoshenko's M_o equation was discussed, which is used to determine the critical buckling moment. An example was provided to explain the procedure used to check a non-prismatic curved I-girder for stability during lifting.

CHAPTER 6

Erection Practices for Lifting of Horizontally Curved I-Girders

6.1 INTRODUCTION

This chapter provides a summary of the results of a questionnaire created to survey various steel curved I-girder erection contractors, inspectors, and engineers. The questionnaire focuses on the common practice for lifting curved I-girders, including spreader beam length, number of cranes, lift points, shore towers, and length of girder segments lifted. The purpose of developing the survey was to verify that the research project solutions incorporate the typical range of parameters that occur in actual practice. A total of 11 people were surveyed with this Questionnaire, representing contractors, construction engineers, inspectors, from 11 companies located in the United States. The responses from the survey are numbered from 1 through 11, representing each person participating in the study. A copy of the Questionnaire can be found in Appendix D.

6.2 QUESTION 1: TYPICAL LIFTING SCENARIO

The objective of Question 1 of the Questionnaire was to determine the typical lifting scenarios that are employed by various contractors. The first part of this question asked what the range of girder segment lengths are, when one girder segment is lifted and then spliced in the air. This situation involves lifting a single girder and placing it on the bent cap at one end and temporarily supporting the girder with a crane or shore tower. This is repeated until a complete span of girder segments is lifted and the cross frames are connected. Then the shored span of girders is spliced in the air, between piers, to the next segment of girders at the field splice location. Figure 6.1 captures the air splice stage of construction for the first connecting girder segment for the instrumented bridge near the Austin airport. Figure 6.2 and Figure 6.3 give an example of the typical temporary shoring used to provide falsework for curved I-girders during construction.



Figure 6.1 Air Splice



Figure 6.2 Shore Tower Supporting Curved Girders



Figure 6.3 Shore Tower Beam Supporting I-Girders

The length of a girder segment is most often controlled by the transportation hauling length. The maximum single girder segment lifted that the surveyed participants reported was 150' and the minimum was 20'. Table 6.1 organizes the minimum and maximum lengths that were reported. Participants 4, 5, and 6 did not give a minimum and maximum length, but gave an explanation of single segment erection and air splicing. The response from Participant 4 stated that the size of the pieces lifted depends on the lengths that can be transported to the site, the size of the crane available and the bending stresses that can be tolerated without buckling. He also said that their company cannot erect girders one at a time in the beginning because the first girder usually has an unbraced length in excess of what is acceptable. They try to erect I-girders with a single crane when possible and avoid using shoring towers. Participant 5 indicated that the segment length depends on the stability of the girder and the capacity of the crane. He also reported that length is not a problem if the girder remains stable for picking and placing. The sixth participant commented on the topic of air splicing. In response to

Question 1, they stated that splicing in the air can be difficult if the girder webs are not on the same grade or exactly plumb. They go on to say that for continuous units, falsework must be used to support one girder as the other is lifted for splicing. This method will work fine if girders are either too long or too heavy to be pre-spliced on the ground, or available cranes are too small to lift heavier loads. Another noteworthy comment from Participant 6 is that falsework must be adequately protected if it is adjacent to a travel way, which means that this method is oftentimes more costly and time consuming especially on multi-level interchanges where the upper levels are high above the ground. Participant 10 responded to this question by first stating that the first lift should always be a pair of girders. He stated that single or double crane lifts requiring cranes over 250 ton cranes will increase the cost of the erection.

Participant	Profession	Min. Length	Max. Length
1	Engineer/Contractor	60'	120'
2	Engineer/Contractor	80'	100'
3	Contractor	--	120'
4	Engineer/Contractor	--	--
5	Construction Engineer	--	--
6	Engineer/Contractor	--	--
7	Inspector	20'	120'
8	Inspector	--	150'
9	Contractor	100'	140'
10	Engineer/Contractor	--	--
11	Construction Engineer	64'	154'

Table 6.1 Single Girder Segment Reported Lengths

The profession of each Participant is also given in the table above. The participants that are labeled “Construction Engineer” work for an engineering firm that is specifically hired by erection contractors to engineer curved I-girder erections. Participants that are labeled “Engineer/Contractor,” are erection engineers that work for construction companies that erect curved I-girders. If a participant’s profession is labeled “Contractor” in Table 6.1, then that person is a superstructure manager or superintendent at an erection construction company.

The second part of Question 1 targeted the range of girder lengths lifted when segments are spliced on the ground and lifted into place. This type of splice is referred to as a ground splice and allows longer girder lengths to be lifted (Figure 6.4). The maximum length reported for a curved girder that was ground spliced and lifted was 300’. The ranges of spliced girder lengths are organized in Table 6.2. Participant 5 commented that if the spliced girder is stable and the crane can pick it, then “you can go to a length that determines the weight and stability.” In reference to Participant 6’s maximum length response of “no limit,” he states that if girders are spliced and paired, the only limitation is the multi-crane setup locations, total lift capacity and reach.



Figure 6.4 Ground Spliced Curved I-Girders

Participant	Min. Length	Max. Length
1	60'	250'
2	80'	150'
3	--	< 200'
4	--	--
5	--	--
6	--	No Limit
7	150'	290'
8	--	300'
9	240'	280'
10	---	160'
11	--	--

Table 6.2 Pre-spliced Girder Segment Reported Lengths

6.3 QUESTION 2: SPREADER BEAMS

The second question focused on the use of spreader beams and what the protocol is for curved I-girder erection. Spreader beams, which are connected to the crane with large cables, attach to the girder lifting clamps on the top flange of the girder, as shown in Figure 6.5, and are used to provide multiple lift points and control the inward force that the top flange is subjected to during lifting. Question 2 queries the use of spreader beams and lengths that are typically used. It also asks if the size of the spreader beam is pre-determined before the girder arrives on the construction site or does the contractor have various sizes of beams on hand to choose from. Figure 6.5 shows an example of a type of spreader beam used in curved I-girder construction. In this case, the spreader beam was a pipe section that could be extended or reduced in length by interchanging segments with the intermediate bolted pipe flange connections.



Figure 6.5 Spreader Beam Connected to I-Girder

All of the curved I-girder erection specialists that were surveyed use spreader beams. It is necessary to use spreader beams in order for the beam clamps to hang vertical. The use of other lifting devices such as slings would not allow the beam clamps to hang vertical, which could cause them to slip, the girder could roll, or cause excessive flange deformation when the girder is lifted (Participant 10). Four out of eleven of the participants mentioned the use of adjustable spreader beams. The consensus of the survey indicated that the size of the spreader beam is pre-determined and engineered before the girder arrives on the construction site. This can be expected due to complex stability issues and the delicate nature of curved steel I-girder erection. Since erection plans are required before the girders can be lifted, the size of the spreader beam is usually included in this set of construction documents. The erection contractor may use the

spreader beam that is in their inventory or a new one can be designed. Participant 5 said that the length of the spreader beam is determined by the radius of the curve. He described the importance of the spreader beam intersecting the center of gravity of the curved I-girder. This is referred to the *line of support* and is also described in Chapter 5 of this report. The parametric study in Chapter 5 concluded that half the segment length was the optimal length for a spreader beam (L_{Lift}) used to lift one girder segment to maximize the buckling strength. Participant 6's company tries to use two cranes to handle individual and spliced curved girders. He goes on to say that a lifting beam can also be used in lieu of multiple spreader beams to make solo lifts. Table 6.3 represents the typical spreader bar lengths that each person surveyed has dealt with during curved I-girder erection. One participant, who is an engineering specialist in this field, said that the erector has multiple spreader beams, including adjustable beams, so there will always be an appropriate size for almost any length of girder.

Participant	Reported Lengths
1	22', 42', 60', 80'
2	25' & 40'
3	10' – 100'
4	20' – 50'
5	All Sizes, 60' Common
6	5' – 150'
7	--
8	40' & 80' Typ.
9	20' – 70'
10	--
11	All Sizes

Table 6.3 Reported Spreader Beam Lengths

6.4 QUESTION 3: CRANES

Cranes are the nucleus of the third question of the Questionnaire. The employment of one or two cranes is surveyed in order to understand the typical lifting scenario that the majority of the construction industry utilizes. The Questionnaire also asked the question: If two cranes are used, is it typical to employ spreader beams for each crane? Figure 6.6 depicts a single crane used to lift a curved I-girder into place.



Figure 6.6 Crane Lifting Curved I-Girder

The majority of the people surveyed reported that it is more desirable to use one crane. Therefore, they typically use one crane and a spreader bar for curved I-girder erection. Contractors typically prefer the use of one crane due to the high cost of renting this type of heavy construction equipment. A common response to whether one or two cranes are employed was that it depended on the segment length, which affects the weight of the member. With this in mind, the capacity of the crane becomes an issue as the girder segment gets longer. Stability of the curved I-girder was also mentioned as a determining factor. Available site access and mobilization of the girder transport truck and crane were also notable answers to this question. Overhead obstructions, such as a power line, that might interfere with a single crane were also given as a reason for using two cranes.

The answers from the second part of Question 3, which asked if spreader beams are used with two cranes, varied, but brought up noteworthy responses. A common thread among many of the responses was that the load magnitude determined the need for spreader beams attached to the two cranes. The effect that the load has on localized top flange bending was also cited as a factor considered on this topic. Participant 4 mentioned that if two cranes are used, it is preferable that they are as nearly identical as possible with respect to boom length and working radius.

6.5 QUESTION 4: GIRDER TILT

A question relating to girder tilt was incorporated into the Questionnaire to evaluate the importance that various contractors, engineers, and inspectors place on this topic. The geometry of curved girders can cause excessive rotations during construction. This is due to the fact that the center of gravity does not lie on the centerline of the girder and therefore there is an eccentricity between the line of support and the center of gravity. Figure 6.7 illustrates the relationship between girder tilt, line of support, and eccentricity. The last part of Question 4 assesses the typical rotation tolerances that various contractors allow.

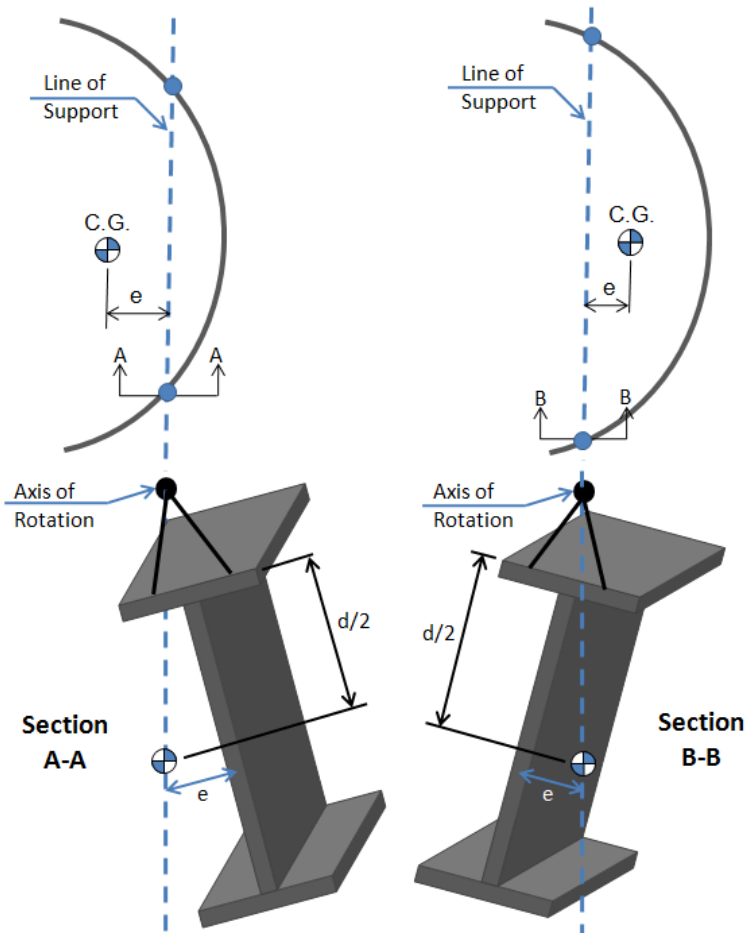


Figure 6.7 Effect of Eccentricity on Curved I-Girder Tilt (Schuh, 2008)

The consensus from the survey participants was that tilting of the girder is a concern when lifting curved I-girders. More than one survey participant indicated that the end rotation of each plate girder at the splice end location is of great concern. This has an impact on how the girder line is connected at the splice location (Figure 6.8). Participant 4 stated that when brought into initial contact, ideally the end rotation of each girder segment should be so that the bottom flanges touch first and the web splice closes as the load is released by the crane. Another typical response from the survey was that if the girder is lifted from the correct location, which is calculated and reported in the

erection plans, girder tilt should not be a problem. A common response to the second part of this question, which asks about rotation tolerances, was that the participant did not have a specific tolerance value, but rotation of the girder was definitely a concern and engineered to minimize this effect. The reported typical rotation tolerance varied among participants, as shown in Table 6.4. One difficulty with three of the responses is that they did not provide a lateral translation limitation based upon the girder depth. Therefore, a 2 inch deformation limit will have a more significant impact on a 60 inch deep girder compared to a 90 inch deep girder. The answer from participant 2 provides a limit that relates to the relative twist of the girder section.

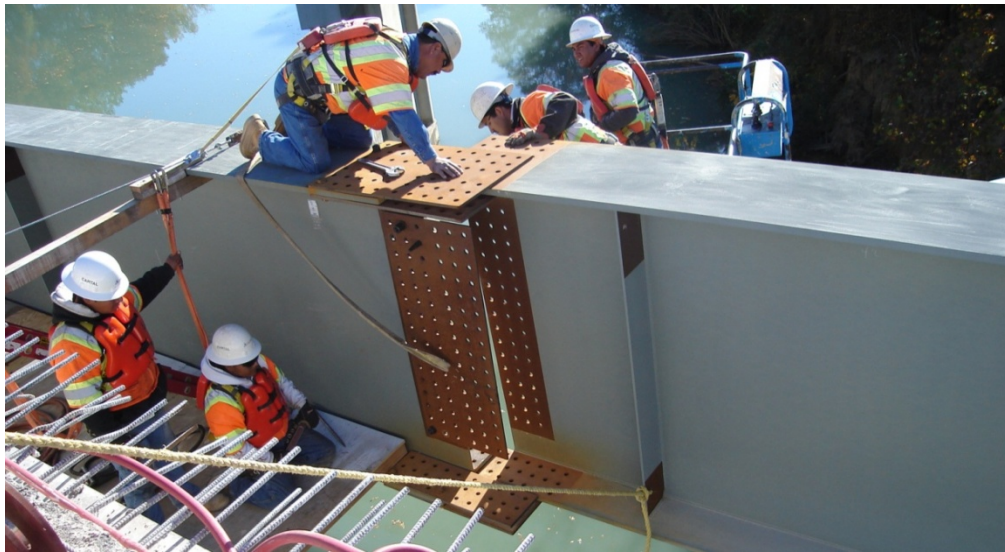


Figure 6.8 Girder Segment Ends Connected at Splice

Participant	Rotation Tolerance
2	2" per 7' depth
3	< 2"
6	1"
11	1"- 2"

Table 6.4 Reported Typical Rotation Tolerances

6.6 QUESTION 5: DETERMINING LIFTING POINTS

Question 5 evaluates the common engineering and construction practice for determining the lifting locations along a curved girder. All of the survey participants indicated that the lifting locations are determined through structural analysis. Unbraced flange length, compression flange stresses, and the ability of the top flange to sustain load transfer to the beam clamps were some of the engineered requirements mentioned. More than one participant stated that a two point lift is preferable to eliminate the “roll.” Typical analysis involves evaluating each girder to determine the center of gravity and then completing a stress analysis to establish the appropriate lift points. Figure 6.9 depicts a girder segment being lifted.



Figure 6.9 Lifting Curved I-Girder Segment

6.7 QUESTION 6: PROBLEMS OR CONCERNS

Finally, the last question surveyed the participants about problems or concerns that they have about lifting horizontally curved I-girder segments and what other aspects of this subject should be considered in this research project or future research projects. This question gives the participants a chance to address their concerns about all aspects of curved I-girder construction and it gives bridge design engineers as well as academia an insight into the real issues that are left unexplored. Table 6.5 organizes the responses for Question 6 into four topics: Shoring, Erection, Tight Radius of Curvature, and Unbraced Length.

Participant	Topic Discussed
1	Shoring
2	Erection
3	Erection
4	Unbraced Length (Lifting)
5	Tight Radius/Erection
6	Stability
7	Shoring
8	Erection/Shoring/Tight Radius
9	Shoring
10	Tight Radius
11	Unbraced Length (Lifting)

Table 6.5 Topics of Question 6 Responses

6.7.1 Shoring

The above table demonstrates the variety of responses received concerning Question 6, yet several focus on similar topics. One of the topics referenced the most

was shoring, which could be due to the high cost of installing and designing falsework to support curved I-girders during erection. Participant 1 indicated the need for the development of criteria for field engineers to determine when shoring is necessary to maintain a certain elevation of erected girders. He noted that on occasion girders could be safely erected without shoring, but this practice may often result in the girder final elevations falling below the required profile grade. Participants 7 and 8's concerns lie with the premature removal of temporary shore towers, improperly locating falsework, and non-existent falsework and the effects that this has on the structural system. The ninth participant mentioned that due to site access issues, girders must be shored, despite the unwelcomed expense. His concern involved the phase of construction when I-girder spans are erected over traffic at elevated heights and when the shoring should be disengaged.

6.7.2 Erection

Issues relating to erection were also the subject matter that was referenced often in the responses to Question 6. Participant 2 expressed the need for simple expressions to evaluate the requirements for single point I-girder lifts. A noteworthy response from Participant 3 centers around the effect of splice locations pertaining to girder erection. He states that many times the first girder that is in a set needs a holding crane or shore tower to temporarily support it until the adjacent girder is erected. When erecting over the top of an existing bridge, it is difficult to support the first girder. His resolution to this scenario is to strategically place the girder splice to ensure that the center of the girder can be supported during these specific situations. Such an idea is ideal for design-build contracts, because the design engineer must know the methods and means that the girders will be erected while designing the superstructure of the bridge. Participant 5 questions the need for erecting curved I-girders in pairs and would like to see this topic examined more closely. Finally, the eighth participant is concerned with the affects that the girder clamp (Figure 6.5), used to lift the girder, has on putting tension on the fillet welds at the top flange to web weld.

6.7.3 Tight Radius of Curvature

The next topic was related to tight radius of curvatures on curved I-girders. Participant 5 speculated on whether the standard calculation methods for stability are affected by extreme curvatures and if they are, what would be the limit of this circumstance. His response also highlighted on the effect that a tight radius has on the erection of a second girder (adjacent girder). Should the girder be blocked at the ends along with installing a central cross-frame before disengaging the lifting crane or should more cross-frames be installed. The eighth participant briefly questioned the length of spreader bar utilized to lift curved I-girders that have tight radius of curvatures. Participant 10 remarked on the problems concerning curved I-girder bridges with tight radius of curvatures and steep cross slopes. In his experience, this scenario sometimes prevents the I-girders in the span or unit from cambering until almost all the dead load of the concrete is placed.

6.7.4 Unbraced Length

As mentioned in Chapter 5, design specifications lack in-depth criteria for horizontally curved I-girder lifting. Therefore, the topic of unbraced length was also given as response for this question by more than one participant. Participant 4 reflected on the equation in the American Association of State Highway and Transportation Officials (AASHTO) *LRFD Bridge Design Specifications* (2007) for allowable bending stress and whether it was applicable for long unbraced lengths (50' to 100'). The subject of unbraced length was also contemplated by Participant 11 who commented that this question was discussed extensively in their office. Their questions initiated with respect to the top flange of the girder and whether this lifting point constitutes as a brace point against lateral-torsional buckling.

6.8 SUMMARY

This chapter focused on the common practice for curved I-girder erection procedures. A questionnaire was created to engage various curved I-girder construction

specialists around the United States on their experience with certain lifting scenarios, spreader beams, cranes, and girder tilt.

The first part of Question 1 asked what the range of segment lengths are, when one girder segment is lifted and then spliced in the air. The maximum single girder segment lifted that the surveyed participants reported was 150' and the minimum was 20'. The second part of Question 1 targeted the range of girder lengths lifted when segments are spliced on the ground, which is referred to as a ground splice, and lifted into place. The maximum length reported for a curved girder that was ground spliced and lifted is 300'.

Question 2 centered around the use of spreader beams and sizes that are typically used as well as whether the size is pre-determined before the girder arrives on the construction site. All of the curved I-girder erection specialists that were surveyed use spreader beams. The results of the survey indicated that the size of the spreader beam is pre-determined and engineered before the girder arrives on the construction site. There is a wide range of spreader beam sizes reported due to the unique nature of each specific curved I-girder lifting situation. The conclusion from Chapter 5 was discussed, which stated that half the segment length was the optimal length for a spreader beam (L_{Lift}) used to lift one girder segment to maximize the buckling strength. However, additional work from this research group is finding that the optimum location for strength is often different from the optimum location to minimize twist of the girder during lifting. As stated in Question 1, having the webs plumb to facilitate assembling the connection is an important aspect of girder stability. The results of a study on girder twist during lifting will be presented in a future thesis by another member of the research team.

The third question surveyed the employment of one or two cranes in order to understand the typical lifting scenario that the majority of the construction industry utilizes. The majority of the people surveyed reported that it is more desirable to use one crane. Therefore, contractors typically use one crane and a spreader bar for curved I-girder erection.

Question 4 evaluated the importance that various contractors and construction engineers place on girder tilt as well as assesses the typical rotation tolerances that they allow. Tilting of the girder is a concern when lifting curved I-girders, according to the overall responses from the survey participants. More than one surveyed participant indicated that the end rotation of each plate girder at the splice end location is of great concern. Few specific rotation tolerance values were given by the participants and this was because they did not have a specific tolerance value established.

Question 5 evaluated the common practice for determining the lifting locations along a curved girder. All of the survey participants indicated that the lifting locations are determined through structural analysis.

Finally, Question 6 examined the problems or concerns that the participating erection contractors and engineers have about lifting horizontally curved I-girder segments. The outcome of this question generated a variety of responses, yet several focus on similar topics. The concerns or problems centered around four topics: shoring, erection, tight radius of curvature, and unbraced length.

CHAPTER 7

Conclusions

7.1 OVERVIEW

Expanding urban environments as well as deterioration in the aging infrastructure is resulting in the need for many new highway bridges. Elevated direct connector bridges have become a frequent solution to moving traffic from intersecting highways at efficient operating levels. An increasingly complicated aspect to these structures is the need to avoid disturbing the underlying roadways and businesses. Horizontally curved I-girders provide a means to build longer spans with complex roadway geometry. With the increasing use of curved I-girders, their behavior is of paramount concern during the critical construction stages of erection and concrete deck placement.

This thesis is part of the TxDOT funded project 0-5574, which was initiated in 2006. TxDOT has guidelines and requirements for designing and proportioning curved I-girders that are based on past experience, with no research justification. While these past guidelines have generally resulted in safe structures during erection and construction, questions have evolved about the level of conservatism relative to the guidelines given in AASHTO. There is also a lack of research on field monitoring of curved I-girders during critical construction stages. This project was implemented in order to bridge the gap that exists in curved I-girder construction investigation. The primary intent of this thesis was to report the behavior of curved I-girders during concrete deck construction, extend the work for analyzing curved I-girders during lifting, and discuss common practices for curved I-girder erection.

7.2 SUMMARY OF RESULTS

Based upon the results presented in this thesis, several conclusions can be reached on the behavior of curved I-girders during construction. Most of curved I-girder design

focuses on the strength and stability of the girder in the completed bridge state. The extreme importance of the construction aspects of curved I-girder design is the driving force behind this research project. The summary of the results has been divided into the areas of field instrumentation, parametric finite element analyses, and feedback from erectors on practices during girder erection. Results from each of these respective areas are given in the following three subsections.

7.2.1 Field Instrumentation

A continuous three-span horizontally curved I-girder bridge unit was investigated in this field study. The bridge was comprised of four girders with a baseline horizontal radius of curvature of 1206'. Strain gages were placed on two girders and two cross-frames in order to monitor their behavior during early construction stages. Stresses, vertical deflections, and horizontal displacements were determined during the concrete deck pour on April 16, 2008. A summary of the results are as follows:

- There was a significant change in bending stress that occurred when concrete placement was completed on the last span in the bridge unit on all of the girder sections that were monitored.
- There was a minimal amount of change in warping stress in the top and bottom flange region on all sections that were monitored.
- The instrumented webs on Girders 3 and 4 resulted in significant plate bending stresses.
- The vertical deflection results were typical of a continuous girder bridge. When the preceding spans were poured, the girders in the last span could be characterized with some uplift, but as the concrete pour progressed onto the last span, the girders changed from an upward deflection to a downward deflection.
- The measured translational displacements at the bearings relating to the thermal expansion behavior of Unit 3 on the instrumented bridge were much less than the calculated theoretical values.

7.2.2 Parametric Study

The effect that different parameters have on an elastic buckling analysis for non-prismatic curved I-girders during lifting was presented in Chapter 5. The parameters that were studied used girder configurations with symmetrical and un-symmetrical lifting locations. This study was an extension of a previous study on prismatic curved I-girders during lifting (Schuh 2008). The buckling modes of the girder are highly dependent on the lifting geometry during erection. The limit state of lateral-torsional buckling was discussed to explain the behavior that a curved I-girder undergoes during lifting and erection. This study also analyzed the trends that resulted from the eigenvalue buckling analysis in order to determine an expression for the C_b factor, which is the moment gradient adjustment factor for lateral torsional buckling. The C_b factor can then be applied to the Timoshenko critical buckling moment to calculate the lateral-torsional buckling capacity of the curved I-girder during lifting. For calculating the buckling capacity of the girder, the unbraced length (L_b) was taken as the full length of the curved I-girder. For non-prismatic girders, the smallest cross section was used to calculate M_o to determine the C_b factor. The following conclusions were made regarding the eigenvalue of a non-prismatic curved I-girder section when specific parameters were varied:

- The radius of curvature had minimal effects on the eigenvalue.
- The eigenvalue increased as the flange width increased.
- As the span to depth ratio increased the eigenvalue decreased.
- Both symmetrical and unsymmetrical lifting locations were considered in the study with the distance from the end of the girder to the lifting location represented by the variable, a . Refer to Figure 7.1 for variable definitions. Throughout the parametric study, an a/L value of 0.25 provided the highest eigenvalue for symmetrical lift locations, where L is the total length of the girder segment. The lowest eigenvalues were produced with either small or large a/L values such as 0.10 or 0.40, respectively. This

was also the case for unsymmetrical lift locations when the value of a was taken as the average of the two cantilevered ends ($a_1 + a_2 / 2$).

- For non-prismatic girders with unsymmetrical lifting locations, the optimal distance between lifting points resulted in roughly 70 feet for minimum girder rotation.

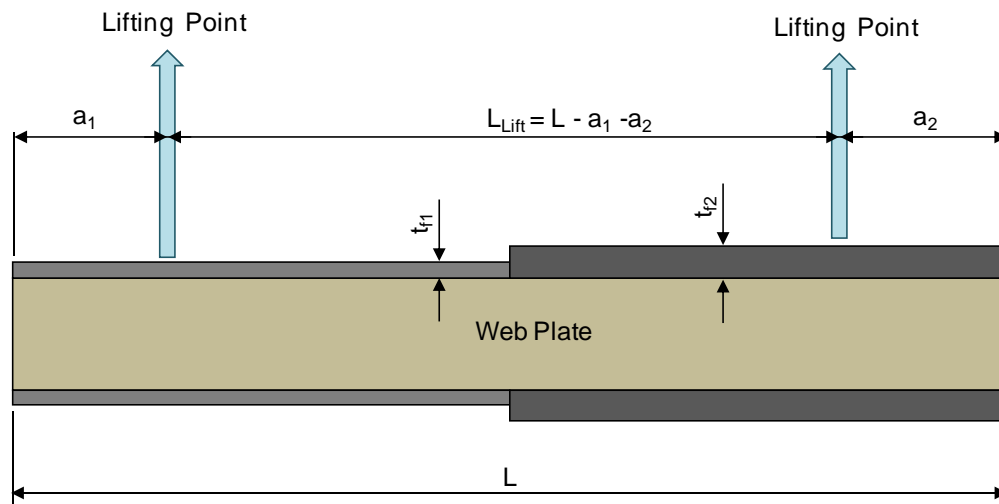


Figure 7.1 Lift Point Location Variable Definition

Finally, an expression for the moment gradient adjustment factor, C_b , for non-prismatic curved I-girders during lifting, was developed by analyzing the trends from the parametric study. An example was provided to explain the procedure used to check a non-prismatic curved I-girder for stability during lifting.

7.2.3 Questionnaire

In order to capture actual curved I-girder erection situations, a questionnaire was developed and sent to erection construction contractors, inspectors, and engineers in Texas and around the United States. The questionnaire focused on the common practices for lifting curved I-girders, including spreader beam length, number of cranes, lift points,

shore towers, and length of girder segments lifted. A copy of the Questionnaire can be found in Appendix C. A summary of the results from the questionnaire are as follows:

- The maximum single girder segment lifted reported was 150' and the minimum was 20'. The maximum length reported for a curved girder that was ground spliced and lifted is 300'.
- All of the survey participants reported that they use spreader beams. The size of the spreader beam is pre-determined and engineered before the girder arrives on the construction site.
- Whenever possible, contractors generally use one crane and a spreader beam for curved I-girder erection.
- Tilting of the girder is of great concern when lifting curved I-girders. Few specific rotation tolerance values were given by the participants and this was because they did not have a specific tolerance value established.
- All of the survey participants indicated that the lifting locations are determined through structural analysis.
- The concerns or problems that the participating erection contractors and engineers have about lifting horizontally curved I-girder segments focused on four topics: shoring, erection, tight radius of curvature, and unbraced length.

7.3 FUTURE WORK

This results presented in this thesis were part of a research project on steel curved I-girder construction. The results from the concrete deck placement monitoring are significant to the future work on this study because they will be used to compare to a finite element analysis program, which is currently being developed.

The parametric study in this thesis provides the continued framework on which to build subsequent studies on curved I-girder lifting. A large displacement analysis parametric study is currently being performed for curved I-girders during lifting. While the results of this study provide guidance on the application of buckling solutions on

curved girder systems, the additional analysis will consider the application of these buckling solutions versus deformational limits and secondary stresses that may also control the girder erection. These follow up studies will consider a variety of sections and geometries including non-prismatic, doubly symmetric curved I-girders during lifting as well as non-prismatic, singly symmetric curved I-girders. Furthermore, ground spliced girders, with longer lifting lengths will also be evaluated during lifting. With this in mind, the effect that two cranes and two spreader beams will be examined.

Temporary supports, which are commonly referred to as shore towers, are expensive to construct because of their varying design from project to project and consumption of a large amount of man hours. Instead of constructing a shore tower, many contractors chose to use a second “holding” crane. This type of temporary support is also expensive to rent and operate. Furthermore, the contractor must hire an engineer to design the temporary supports and there is not a uniform guideline for which a shore tower should be analyzed. TxDOT currently has requirements in place that have no research justification for the placement and removal of temporary supports. Future work on this project must analyze curved I-girder bridge construction scenarios to develop safe and effective criteria for shore tower requirements.

APPENDIX A

Cross Frame X2 Extrapolation

This appendix provides the stress information used to extrapolate the stress values for two strain gages that malfunctioned after the concrete deck placement, which is described in Chapter 4. The first table (A.1) compares the bottom horizontal member (X1-4) in the first cross frame (X1) with the bottom horizontal member in cross frame X2 (X2-4). Using the relative percent difference between the gages for each cross frame, an estimate can be made to determine the missing data. The second spreadsheet uses the estimated values from the first spreadsheet to determine a rough estimate for the stress on April 19, 2008 between the time of 12:30am and 3:00am. This date was chosen because the ambient temperature is relatively close to the temperature at the time that the concrete deck pour began. The purpose for extrapolating the stress values was to roughly estimate the total stress change due to the construction of the concrete slab, while minimizing the effects of thermal gradients.

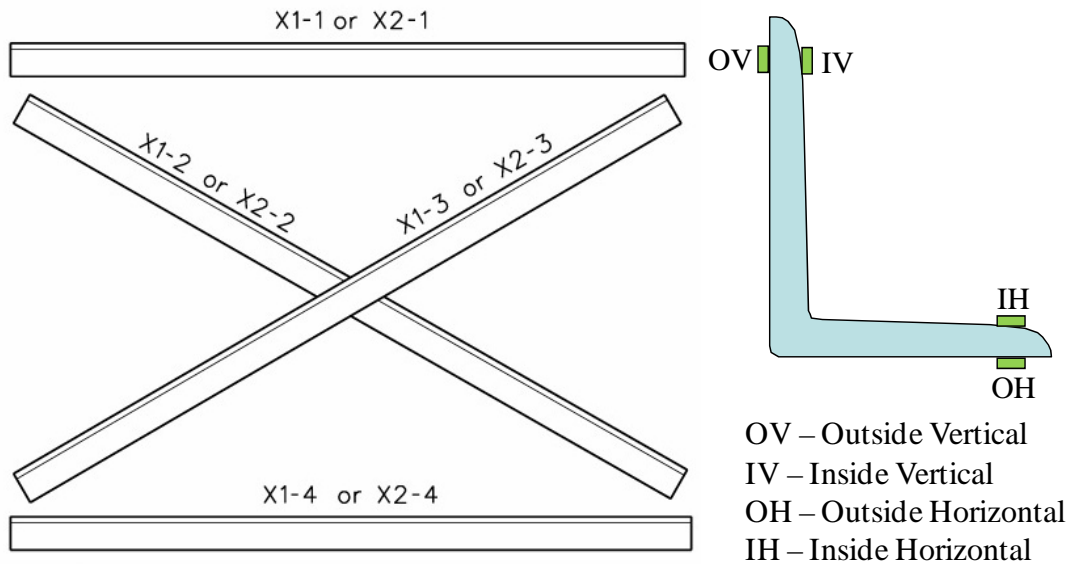


Figure A.1 Cross Frame Member Labels

Date and Time	Temp (°F)	X1-4-OV	X2-4-OV	% Diff	X1-4-IV	X2-4-IV	% Diff	X1-4-OH	X2-4-OH	% Diff	X1-4-IH	X2-4-IH	% Diff
4/17/2008 0:30	69.931	-1.823	-2.505	31.513	-1.672	-1.940	14.827	1.242	1.453	15.668	1.347	1.563	14.851
4/17/2008 1:00	69.327	-1.862	-2.552	31.286	-1.674	-1.989	17.211	1.213	1.420	15.668	1.346	1.524	12.446
4/17/2008 1:30	68.834	-1.862	-2.562	31.641	-1.655	-1.980	17.861	1.204	1.409	15.668	1.299	1.506	14.746
4/17/2008 2:00	68.392	-1.853	-2.609	33.874	-1.674	-2.017	18.570	1.204	1.408	15.668	1.280	1.506	16.227
4/17/2008 2:30	68.203	-1.862	-2.590	32.685	-1.655	-2.027	20.185	1.204	1.408	15.668	1.270	1.515	17.543
4/17/2008 3:00	68.026	-1.882	-2.627	33.082	-1.694	-2.055	19.297	1.203	1.408	15.668	1.270	1.496	16.346
AVERAGES	68.786	-1.857	-2.574	32.347	-1.671	-2.001	17.992	1.212	1.418	15.668	1.302	1.518	15.360
4/18/2008 0:30	69.308	-1.655	-2.308	32.973	-1.495	-1.828	20.084	1.054	1.223	14.815	1.121	1.328	16.879
4/18/2008 1:00	67.053	-1.797	-2.449	30.708	-1.544	-1.953	23.420	1.063	1.233	14.815	1.073	1.261	16.116
4/18/2008 1:30	65.513	-1.798	-2.421	29.534	-1.563	-1.973	23.177	1.015	1.177	14.815	1.034	1.204	15.131
4/18/2008 2:00	63.758	-1.931	-2.487	25.203	-1.640	-2.031	21.333	0.967	1.122	14.815	1.014	1.146	12.202
4/18/2008 2:30	62.642	-1.941	-2.497	25.051	-1.641	-2.042	21.797	0.976	1.132	14.815	0.948	1.117	16.407
4/18/2008 3:00	61.568	-2.045	-2.507	20.287	-1.745	-2.071	17.119	0.938	1.088	14.815	0.928	1.060	13.261
AVERAGES	64.974	-1.861	-2.445	27.293	-1.604	-1.983	21.155	1.002	1.163	14.815	1.020	1.186	14.999
4/19/2008 0:30	63.658	-1.434	-1.93364	29.681	-1.190	-1.591	28.858	0.883	1.033	15.668	0.883	1.024	14.815
4/19/2008 1:00	62.534	-1.463	-1.95266	28.664	-1.210	-1.640	30.174	0.854	0.999	15.668	0.844	0.979	14.815
4/19/2008 1:30	62.026	-1.398	-1.80247	25.308	-1.135	-1.490	27.048	0.826	0.966	15.668	0.797	0.925	14.815
4/19/2008 2:00	61.714	-1.323	-1.70868	25.445	-1.070	-1.415	27.830	0.816	0.955	15.668	0.750	0.870	14.815
4/19/2008 2:30	60.929	-1.427	-1.7933	22.772	-1.136	-1.491	27.056	0.778	0.910	15.668	0.731	0.847	14.815
4/19/2008 3:00	59.779	-1.587	-1.95298	20.704	-1.277	-1.642	25.001	0.759	0.888	15.668	0.702	0.814	14.815
AVERAGES	61.77347	-1.438	-1.857	25.429	-1.169	-1.545	27.661	0.819	0.959	15.668	0.784	0.910	14.815

Table A.1 Stress Change Comparison of X1-4 and X2-4

Date and Time	Temp (°F)	X1 Stress - Member X1-4 (ksi)				X2 Stress - Member X2-4 (ksi)			
		X1-4-OV	X1-4-IV	X1-4-OH	X1-4-IH	X2-4-OV	X2-4-IV	X2-4-OH	X2-4-IH
4/17/2008 0:30	69.931	-1.823	-1.672	1.242	1.347	-2.505	-1.940	1.453	1.563
4/17/2008 1:00	69.327	-1.862	-1.674	1.213	1.346	-2.552	-1.989	1.420	1.524
4/17/2008 1:30	68.834	-1.862	-1.655	1.204	1.299	-2.562	-1.980	1.409	1.506
4/17/2008 2:00	68.392	-1.853	-1.674	1.204	1.280	-2.609	-2.017	1.408	1.506
4/17/2008 2:30	68.203	-1.862	-1.655	1.204	1.270	-2.590	-2.027	1.408	1.515
4/17/2008 3:00	68.026	-1.882	-1.694	1.203	1.270	-2.627	-2.055	1.408	1.496
AVERAGES	68.786	-1.857	-1.671	1.212	1.302	-2.574	-2.001	1.418	1.518
4/18/2008 0:30	69.308	-1.655	-1.495	1.054	1.121	-2.308	-1.828	1.223	1.328
4/18/2008 1:00	67.053	-1.797	-1.544	1.063	1.073	-2.449	-1.953	1.233	1.261
4/18/2008 1:30	65.513	-1.798	-1.563	1.015	1.034	-2.421	-1.973	1.177	1.204
4/18/2008 2:00	63.758	-1.931	-1.640	0.967	1.014	-2.487	-2.031	1.122	1.146
4/18/2008 2:30	62.642	-1.941	-1.641	0.976	0.948	-2.497	-2.042	1.132	1.117
4/18/2008 3:00	61.568	-2.045	-1.745	0.938	0.928	-2.507	-2.071	1.088	1.060
AVERAGES	64.974	-1.861	-1.604	1.002	1.020	-2.445	-1.983	1.163	1.186
4/19/2008 0:30	63.658	-1.434	-1.190	0.883	0.883	-1.93364	-1.591	1.033	1.024
4/19/2008 1:00	62.534	-1.463	-1.210	0.854	0.844	-1.95266	-1.640	0.999	0.979
4/19/2008 1:30	62.026	-1.398	-1.135	0.826	0.797	-1.80247	-1.490	0.966	0.925
4/19/2008 2:00	61.714	-1.323	-1.070	0.816	0.750	-1.70868	-1.415	0.955	0.870
4/19/2008 2:30	60.929	-1.427	-1.136	0.778	0.731	-1.7933	-1.491	0.910	0.847
4/19/2008 3:00	59.779	-1.587	-1.277	0.759	0.702	-1.95298	-1.642	0.888	0.814
AVERAGES	61.773	-1.438	-1.169	0.819	0.784	-1.857	-1.545	0.959	0.910

Table A.2 Stress Change Extrapolation of X2-4 Member

APPENDIX B

SH 130/US 71 Span 14 Vertical Deflection Figures

This appendix provides the vertical deflection readings of Girders 3 and 4 of Span 14 of the SH 130/ US 71 Direct Connector at each stage of the concrete deck construction. As outlined earlier in Chapter 4, deflection readings were taken at five locations: near the pier (Bent 14), at $\frac{1}{8} L$, $\frac{1}{4} L$, $\frac{3}{8} L$, and $\frac{1}{2} L$. The term, “L,” refers to the total span length of the girder at Span 14. A negative vertical deflection value represents a downward deflection and a positive vertical deflection value represents an upward deflection. The graphs below compare the vertical deflection magnitude along the length of the girder.

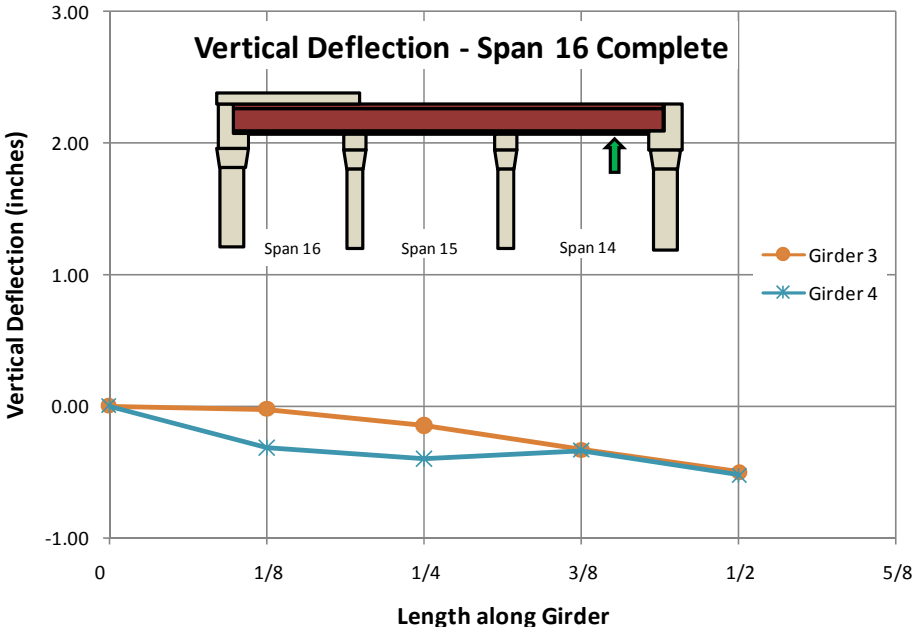


Figure B.1 Vertical Deflection – Span 16 Complete (3:45am)

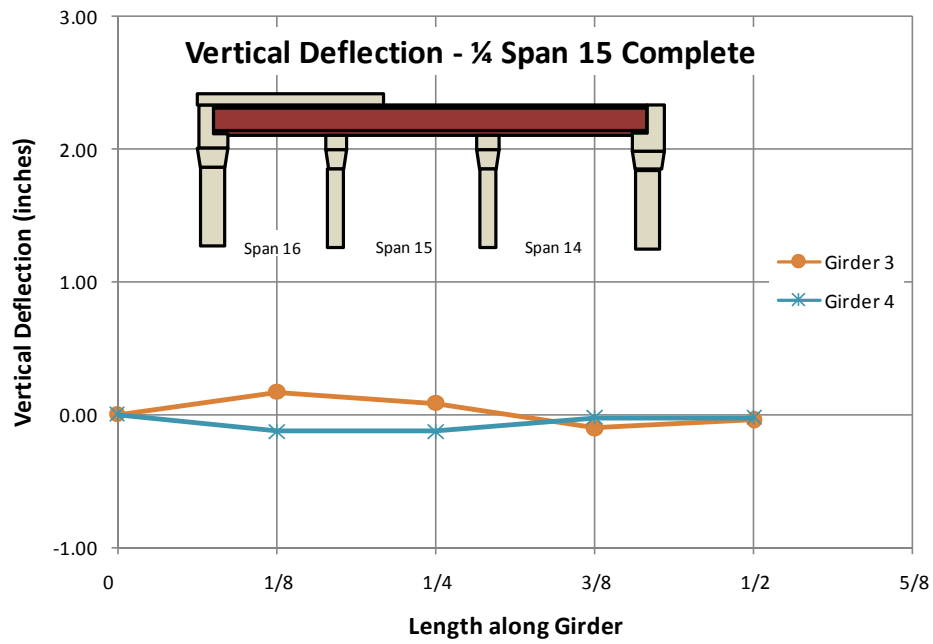


Figure B.2 Vertical Deflection – 1/4 Span 15 Complete (5:50am)

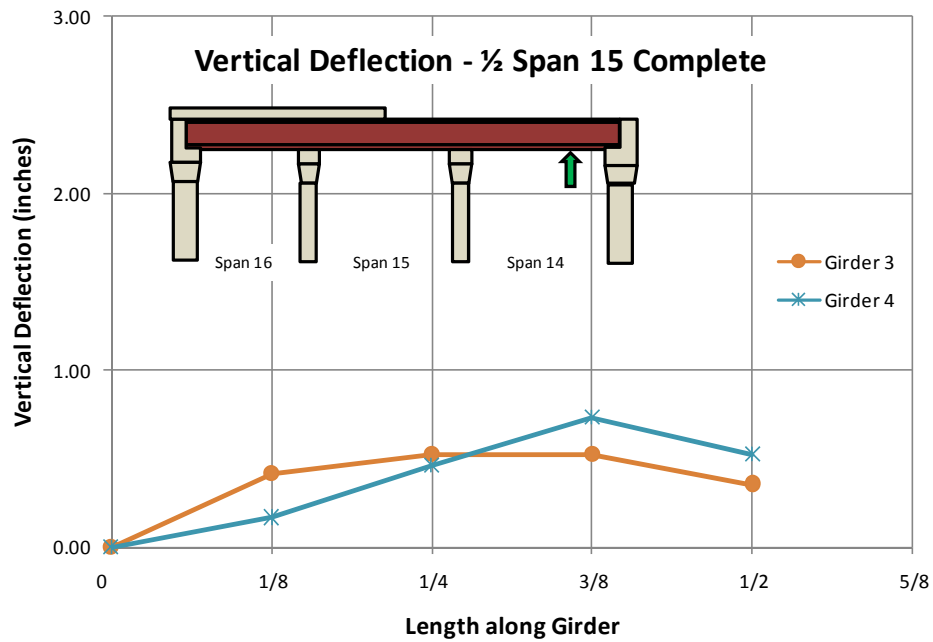


Figure B.3 Vertical Deflection – 1/2 Span 15 Complete (6:25am)

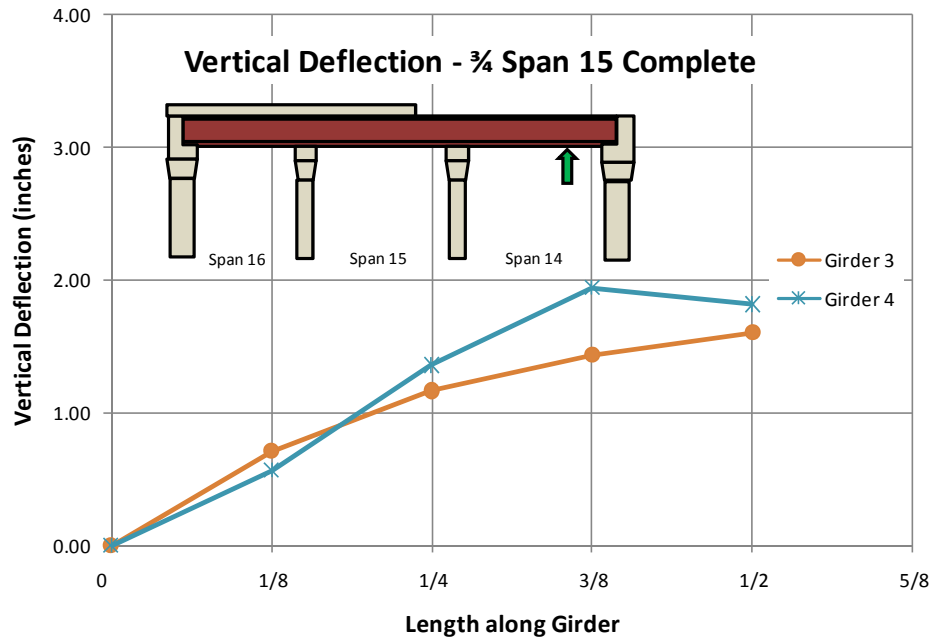


Figure B.4 Vertical Deflection – $\frac{3}{4}$ Span 15 Complete (7:10am)

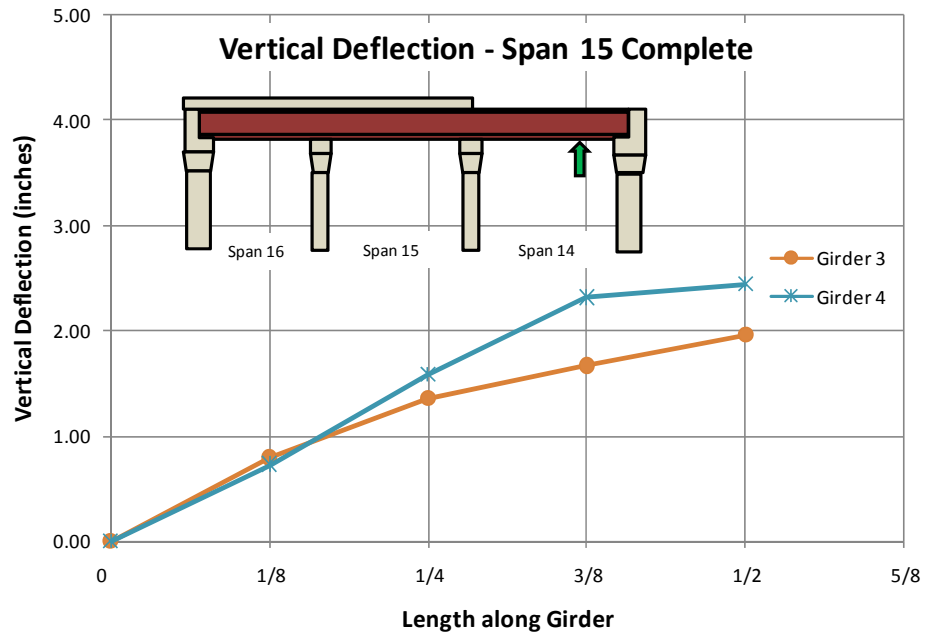


Figure B.5 Vertical Deflection – Span 15 Complete (8:00am)

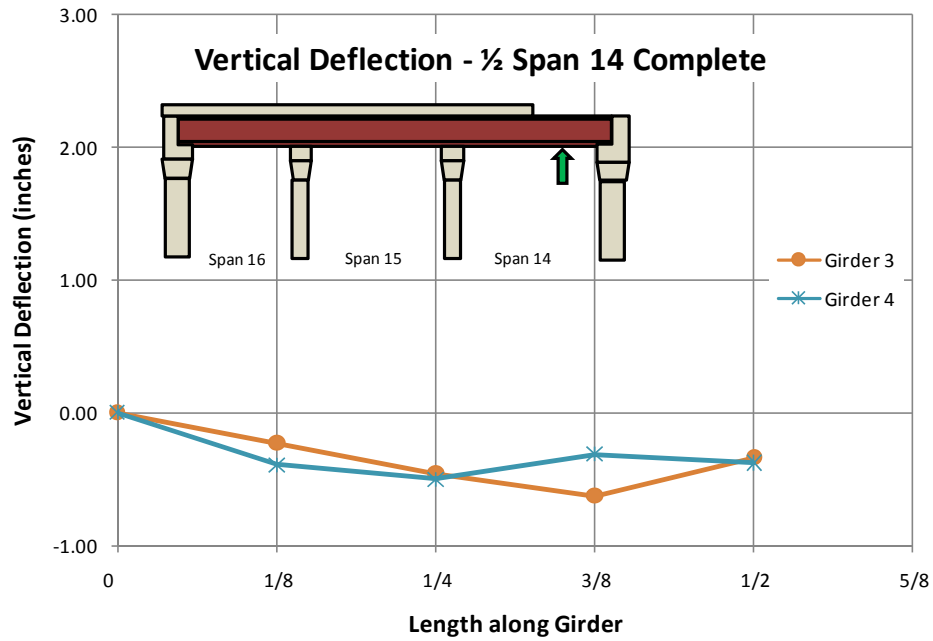


Figure B.6 Vertical Deflection – 1/2 Span 14 Complete (9:00am)

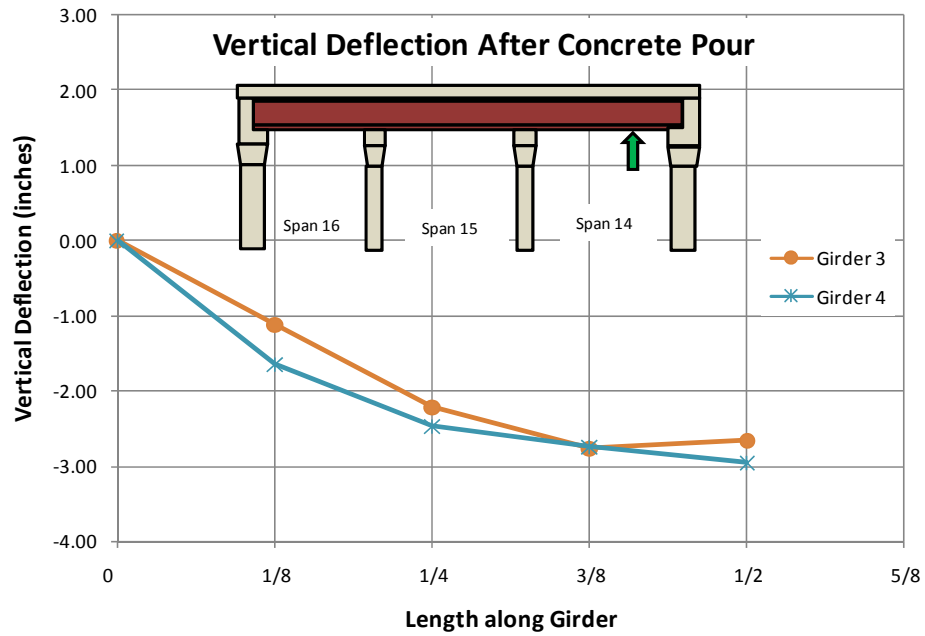


Figure B.7 Vertical Deflection – Span 14 Complete (11:20am)

APPENDIX C

Parametric Study Summary and Example Calculations

As mentioned in Chapter 5, numerous finite element models were run for a parametric study for the lateral-torsional buckling of non-prismatic curved I-girders during lifting. The finite element program ANSYS 11.0 (2007) was used to perform an eigenvalue (λ) buckling analysis on various non-prismatic girder cross sections to evaluate the impact of several parameters on the buckling behavior. This appendix serves as a supplement to Chapter 5 and provides a summary of the various lifting scenarios and girder geometry used to determine the results of the parametric study. Example spread sheets, showing the calculation of C_b , follow the parametric study summary.

C.1 PARAMETRIC STUDY SUMMARY

The following summary is organized by time frame that the study began. Each “Study” has certain common aspects, which are described below the Study sections. Within the various studies are “Comparisons,” which are used to compare different changing parameters. The parameters that were varied are outlined under each Comparison.

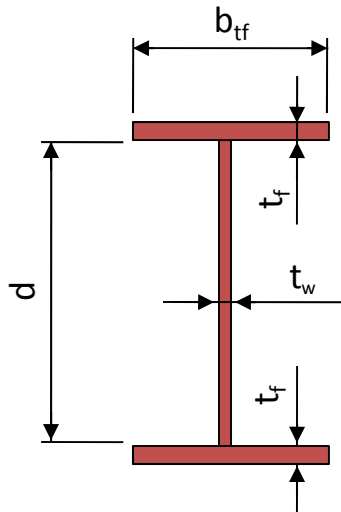


Figure C.1 Girder Cross Section Nomenclature

C.1.1 Study 1

- Symmetric Lift Locations
- Comparing L/d Ratios
- Comparing b/d Ratios

C.1.1.1 Comparison No. 1.1

- L (90', 120', 150'), same d = 72"
- a (0.1L, 0.15L, 0.2L, 0.25L, 0.3L, 0.35L, 0.4L)
- R (300', 400', 500', 750', 1000', 2000', Straight)
- Cross sections: 2 cross-section (Figure C.1) and 3 cross-section (Figure C.2)
- flange thickness varies ($t_f = 1.25''$, $t_f = 2''$)
- Graphed λ vs. a/L

C.1.1.2 Comparison No. 1.2

- b_f (24", 18", 16", 14", 12"), same d = 72", same L = 120'
- a (0.1L, 0.15L, 0.2L, 0.25L, 0.3L, 0.35L, 0.4L)
- R (300', 400', 500', 750', 1000', 2000', Straight)
- Cross sections: 2 cross-section (Figure C.1) and 3 cross-section (Figure C.2)
- flange thickness varies ($t_f = 1.25''$, $t_f = 2''$)
- Graphed λ vs. a/L

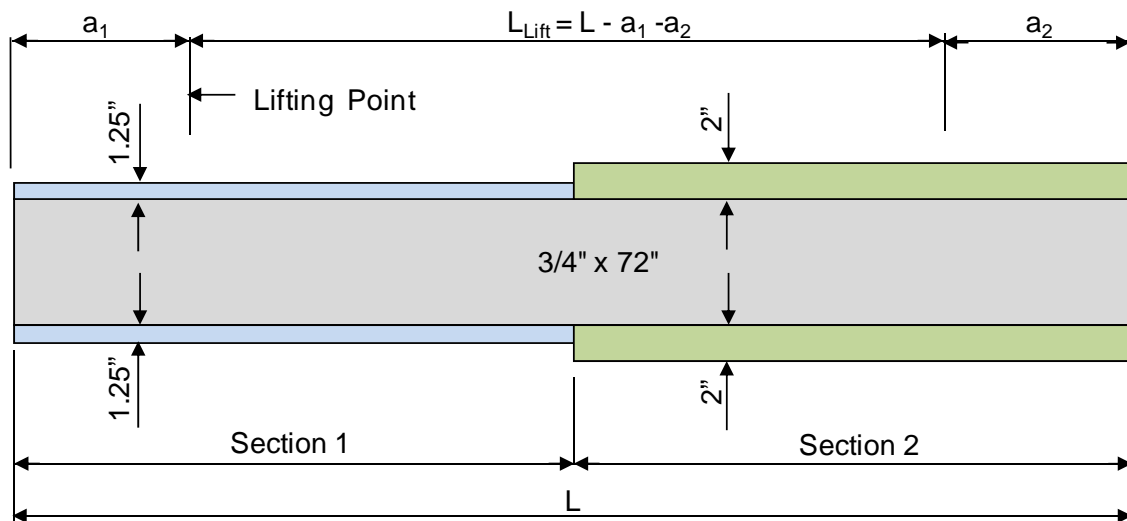


Figure C.2 Two Cross Section Girder Schematic

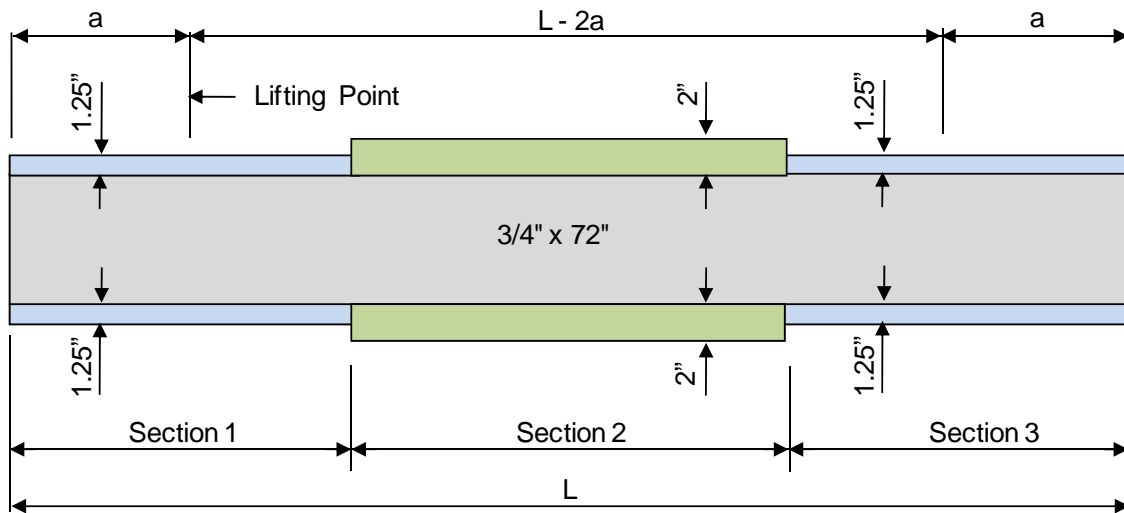


Figure C.3 Three Cross Section Girder Schematic

C.1.1.3 Comparison No. 1.3

- L (90', 120', 150'), same $d = 72''$
- a (0.1L, 0.15L, 0.2L, 0.25L, 0.3L, 0.35L, 0.4L)
- R (250', 300', 400', 500', 750', 1000', 2000', Straight)
- Cross sections: flange thickness does not vary ($t_f = 1.25''$) (Figure C.4)
- Graphed λ vs. a/L

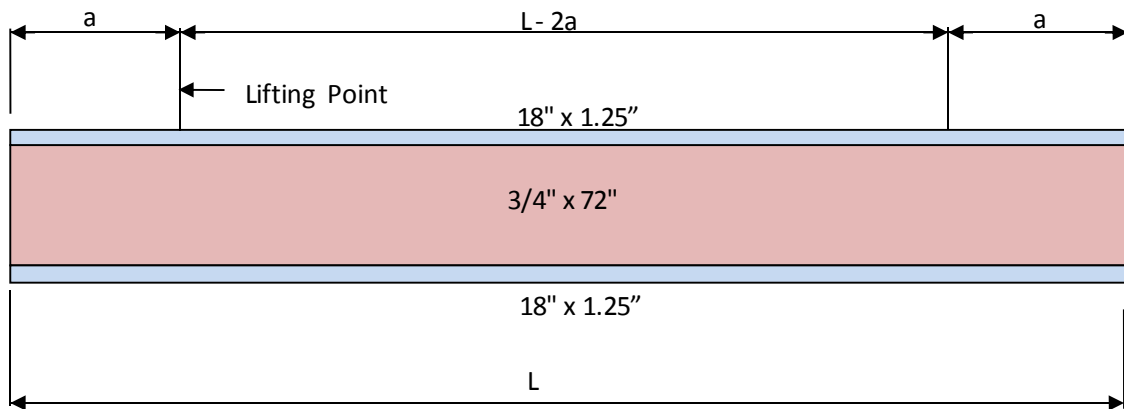


Figure C.4 Prismatic Girder Schematic ($t_f = 1.25''$)

C.1.1.4 Comparison No. 1.4

- L (90', 120', 150'), same $d = 72''$
- a (0.1L, 0.15L, 0.2L, 0.25L, 0.3L, 0.35L, 0.4L)
- R (250', 300', 400', 500', 750', 1000', 2000', Straight)
- Cross sections flange thickness does not vary ($t_f = 2.00''$) (Figure C.5)
- Graphed λ vs. a/L

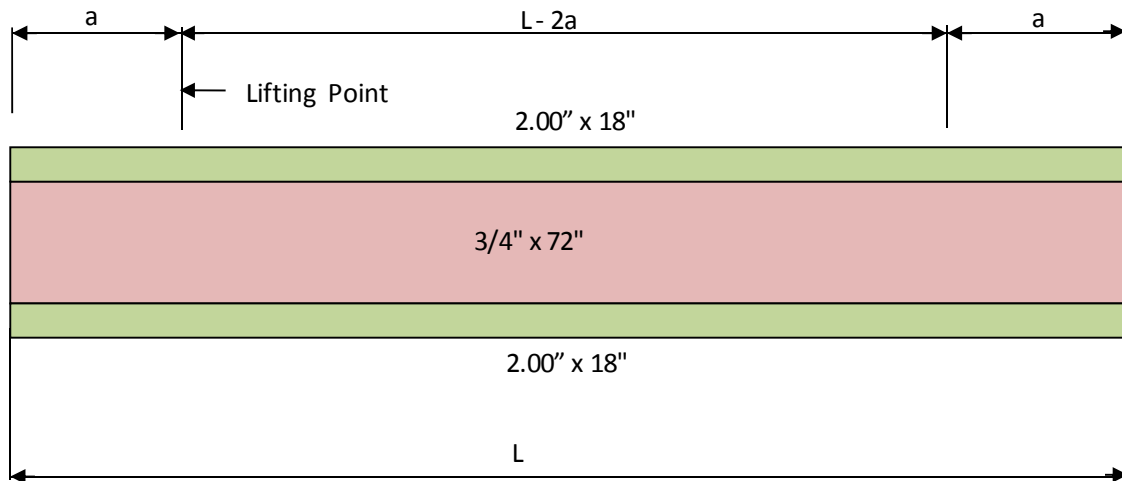


Figure C.5 Prismatic Girder Schematic ($t_f = 2.00''$)

C.1.1.5 Comparison No. 1.5

- L (120', 150'), same $d = 72''$
- a (0.1L, 0.15L, 0.2L, 0.25L, 0.3L, 0.35L, 0.4L)
- R (250', 500', 1000', Straight)
- Cross sections: Top Flg $t_f = 1.25''$ entire length; Bottom Flg $t_f = 1.25'' L/2$, $t_f = 2.00'' L/2$
- Graphed results of λ vs. a/L

C.1.1.6 Comparison No. 1.6

- b_f (24", 18", 16", 14", 12"), same $d = 72"$, same $L = 120'$
- a (0.1L, 0.15L, 0.2L, 0.25L, 0.3L, 0.35L, 0.4L)
- R (250', 500', 1000', Straight)
- Cross sections: Top Flg $t_f = 1.25"$ entire length; Bottom Flg $t_f = 1.25" L/2$, $t_f = 2.00" L/2$ (Figure C.6)
- Graphed results of λ vs. a/L

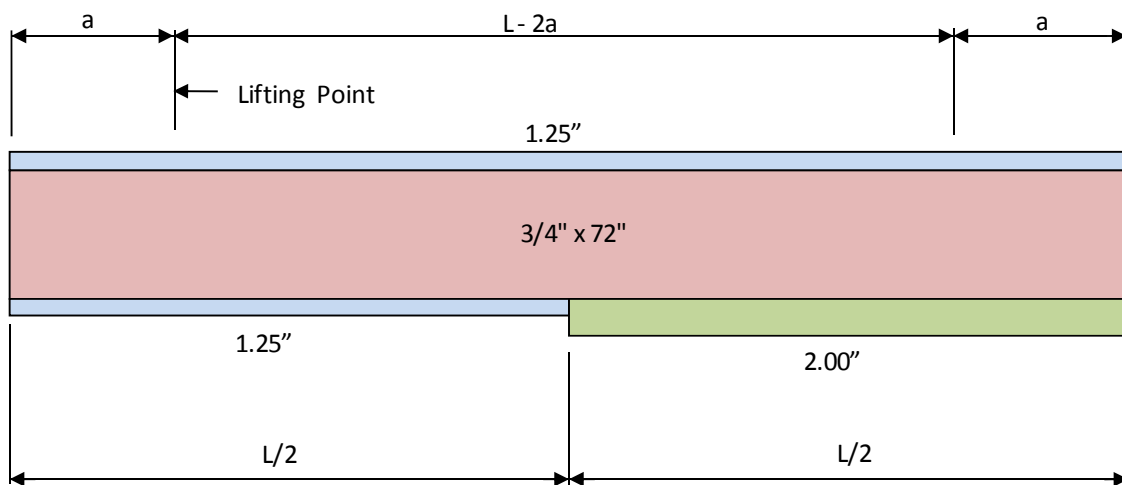


Figure C.6 Singly Symmetric Girder Schematic

C.1.1.7 Comparison No. 1.7

- $L = 120', 150'$; $d = 72"$
- $a = 0.25$
- R (250', 500', 1000', Straight)
- Cross- sections: vary transition of bottom flange plate thicknesses ($x = 0.2L$ to $0.5L$) (Figure C.7)
- Graphed results of λ vs. a/L

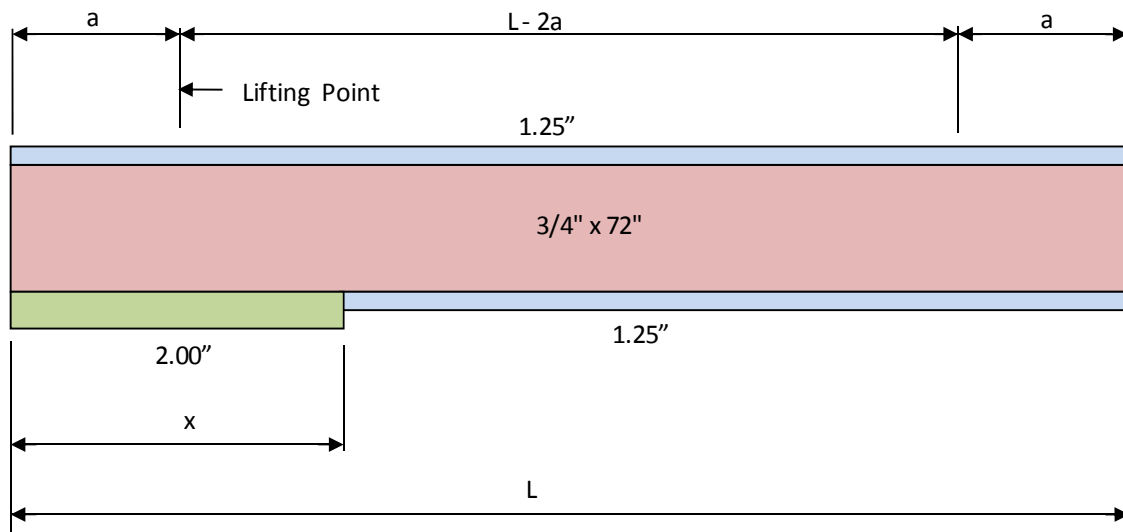


Figure C.7 Singly Symmetric Girder Schematic, Varying Flange Transition

C.1.2 Study 2

- Symmetric Lift Points
- Comparing L_b scenarios ($L_b = L$ or $L_b = L_{Lift}$)
- Web = 72" x 3/4"
- Length = 120.00'
- Radius = 1000.00'

C.1.2.1 Comparison No. 2.1

- $L_b =$ Entire girder length
- Geometry: 3 Cross sections (Figure C.3)
 - Section 1 = Section 2 = Section 3 = 40.00'
 - Flanges: $b_f = 18"$, Section 1 & 3: $t_f = 1.25"$ and Section 2: $t_f = 2"$
- Determined buckling location with ANSYS graphics
- Varied lift location (a/L)
- Calculated Moment due to self weight at lift location and mid span
- Calculated M_o using the I_y at the critical Moment (controlling cross section)
- Compared values with 2 different symmetric, prismatic girders (top and bottom $t_f = 1.25"$; top and bottom $t_f = 2.00"$)
- Graphed results of C_b vs. a/L

C.1.2.2 Comparison No. 2.2

- L_b = Entire girder length
- Geometry: 3 Cross sections (Figure C.3)
 - Section 1 = Section 2 = Section 3 = 40.00'
 - Flanges: $b_f = 18''$, Section 1 & 3: $t_f = 1.25''$ and Section 2: $t_f = 2''$
- Determined buckling location with ANSYS graphics
- Varied lift location (a/L)
- Calculated Moment due to self weight at lift location and mid span
- Calculated M_o using the weighted average of the girder properties (C_w, J, I_y)
- Compared values with 2 different symmetric, prismatic girders (top and bottom $t_f = 1.25''$; top and bottom $t_f = 2.00''$)
- Graphed results of C_b vs. a/L

C.1.2.3 Comparison No. 2.3

- L_b = Entire girder length
- Geometry: 2 Cross sections (Figure C.2)
 - Section 1 = Section 2 = 60.00'
 - Flanges: $b_f = 18''$, Section 1: $t_f = 1.25''$ and Section 2: $t_f = 2''$
- Determined buckling location with ANSYS graphics
- Varied lift location (a/L)
- Calculated Moment due to self weight at lift location and mid span
- Calculated C_b using the I_y at the critical Moment
- Compared values with 2 different symmetric, prismatic girders (top and bottom $t_f = 1.25''$; top and bottom $t_f = 2.00''$)
- Graphed results of C_b vs. a/L

C.1.2.4 Comparison No. 2.4

- L_b = Controlling length ($L-2a$ or a)
- Geometry: 3 Cross sections (Figure C.3)
 - Section 1 = Section 2 = Section 3 = 40.00'
 - Flanges: $b_f = 18''$, Section 1 & 3: $t_f = 1.25''$ and Section 2: $t_f = 2''$
- Determined buckling location with ANSYS graphics
- Varied lift location (a/L)
- For M_{cr} calculation - Used the Moment due to self weight that was located at the determined buckling location

- Calculated C_b using the I_y at the critical Moment
- Compared values with 2 different symmetric, prismatic girders (top and bottom $t_f = 1.25''$; top and bottom $t_f = 2.00''$)
- Graphed results of C_b vs. a/L

C.1.2.5 Comparison No. 2.5

- $L_b =$ Controlling length (L-2a or a)
- Geometry: 2 Cross sections (Figure C.2)
 - Section 1 = Section 2 = 60.00'
 - Flanges: $b_f = 18''$, Section 1: $t_f = 1.25''$ and Section 2: $t_f = 2''$
- Determined buckling location with ANSYS graphics
- Varied lift location (a/L)
- For M_{cr} calculation - Used the Moment due to self weight that was located at the determined buckling location
- Calculated C_b using the I_y at the critical Moment
- Compared values with 2 different symmetric, prismatic girders (top and bottom $t_f = 1.25''$; top and bottom $t_f = 2.00''$)
- Graphed results of C_b vs. a/L

C.1.3 Study 3

- Symmetric Lift Points
- Comparing L_b scenarios ($L_b = a$, $L_b = L$ or $L_b = L_{Lift}$)
- Comparing M_{cr} possibilities ($M_{cr} = \lambda M_{max}$, $M_{cr} = \lambda M_{Lift}$, or $M_{cr} = \lambda M_{mid}$)
- Comparing M_o calculation section properties
- Web = 72"x 3/4 "
- Length = 120.00'
- Radius = 1000.00'
- Geometry: 3 Cross sections (Figure C.3)
 - Section 1 = Section 2 = Section 3 = 40.00'
 - Flanges: $b_f = 18''$, Section 1 & 3: $t_f = 1.25''$ and Section 2: $t_f = 2''$

C.1.3.1 Comparison No. 3.1

- $C_b = \frac{\lambda M_{Lift}}{M_o}$; M_o properties using $L_b = a$, Cantilever Section Properties

- Varied lift location (a/L)
- Calculated Moment due to self weight at lift location
- Compared values with 2 different symmetric, prismatic girders (top and bottom $t_f = 1.25''$; top and bottom $t_f = 2.00''$)
- Graphed C_b vs. a/L

C.1.3.2 Comparison No. 3.2

- $C_b = \frac{\lambda M_{mid}}{M_o}$; M_o properties using $L_b = L - 2a$, Center Section Properties
- Varied lift location (a/L)
- Calculated Moment due to self weight at mid span
- Compared values with 2 different symmetric, prismatic girders (top and bottom $t_f = 1.25''$; top and bottom $t_f = 2.00''$)
- Graphed C_b vs. a/L

C.1.3.3 Comparison No. 3.3

- $C_b = \frac{\lambda M_{max}}{M_o}$; M_o properties using $L_b = L - 2a \geq a$, Smaller Section Properties
- Varied lift location (a/L)
- Calculated Moment due to self weight at lift location and mid span – Used Max Moment for C_b calculation
- Compared values with 2 different symmetric, prismatic girders (top and bottom $t_f = 1.25''$; top and bottom $t_f = 2.00''$)
- Graphed C_b vs. a/L

C.1.3.4 Comparison No. 3.4

- $C_b = \frac{\lambda M_{max}}{M_o}$; M_o properties using $L_b = L$, Smaller Section Properties
- Varied lift location (a/L)
- Calculated Moment at lift location and mid span – Used Max Moment for C_b calculation
- Compared values with 2 different symmetric, prismatic girders (top and bottom $t_f = 1.25''$; top and bottom $t_f = 2.00''$)
- Graphed C_b vs. a/L

C.1.4 Study 4

- Symmetric Lift Points

- Comparing L_b scenarios ($L_b = L - 2a \geq a$, $L_b = L$)
- M_o calculation – smallest section properties
- Web = 72" x 3/4"
- Length = 150.00'
- Radius = 1000.00'
- Geometry: 3 Cross sections (Figure C.8)
 - Section 1 = 55.00' Section 2 = 40.00' Section 3 = 55.00'
 - Flanges: $b_f = 18"$, Section 1 & 3: $t_f = 1.25"$ and Section 2: $t_f = 2"$

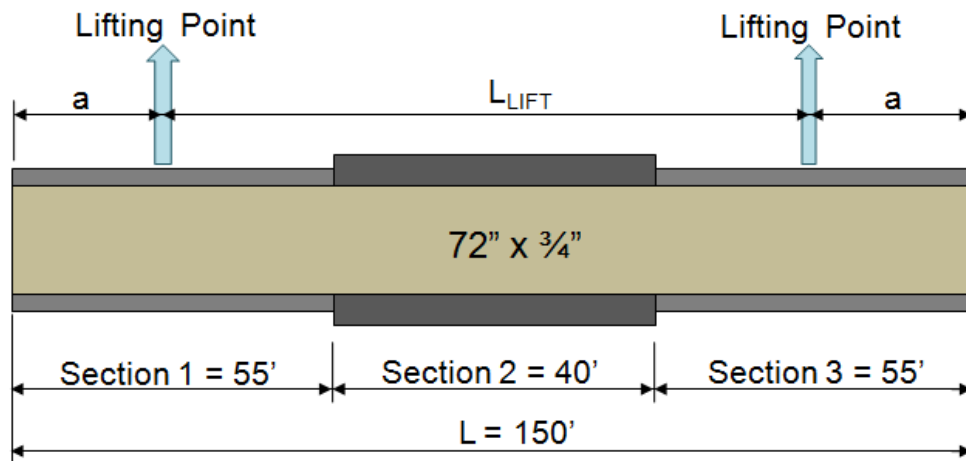


Figure C.8 Study 4 Girder Schematic

C.1.4.1 Comparison No. 4.1

- $C_b = \frac{\lambda M_{\max}}{M_o}$; M_o properties using $L_b = L - 2a \geq a$, Smallest Cross Section Properties
- Varied lift location (a/L)
- Calculated Moment due to self weight at lift location and mid span
- Compared values with 2 different symmetric, prismatic girders (top and bottom $t_f = 1.25"$; top and bottom $t_f = 2.00"$)
- Graphed results

C.1.4.2 Comparison No. 4.2

- $C_b = \frac{\lambda M_{\max}}{M_o}$; M_o properties using $L_b = L$, Smallest Cross Section Properties

- Varied lift location (a/L)
- Calculated Moment due to self weight at lift location and mid span
- Compared values with 2 different symmetric, prismatic girders (top and bottom $t_f = 1.25''$; top and bottom $t_f = 2.00''$)
- Graphed results

C.1.5 Study 5

- Symmetric Lift Points
- Comparing b/d Ratio
- $C_b = \frac{\lambda M_{max}}{M_o}$; M_o properties using $L_b = L$, Smallest Cross Section Properties
- Symmetric Lift points
- Geometry: 3 Cross sections (Figure C.3)
 - Section 1 = Section 2 = Section 3 = 40.00'
 - Flanges: $b_f = 18''$, Section 1 & 3: $t_f = 1.25''$ and Section 2: $t_f = 2''$
 - Web = 72" x $\frac{3}{4}$ "
 - Length = 120.00'
 - Radius = 1000.00'
- Varied lift location (a/L)
- Calculated Moment due to self weight at lift location and mid span
- b/d ranges: 1/3, 1/5, 1/6
- Graphed results – compared all b/d ratios (C_b vs a/L)

C.1.6 Study 6

- Symmetric Lift Points
- Comparing Radius of Curvature
- Comparing L_b scenarios ($L_b = L - 2a \geq a$, $L_b = L$)

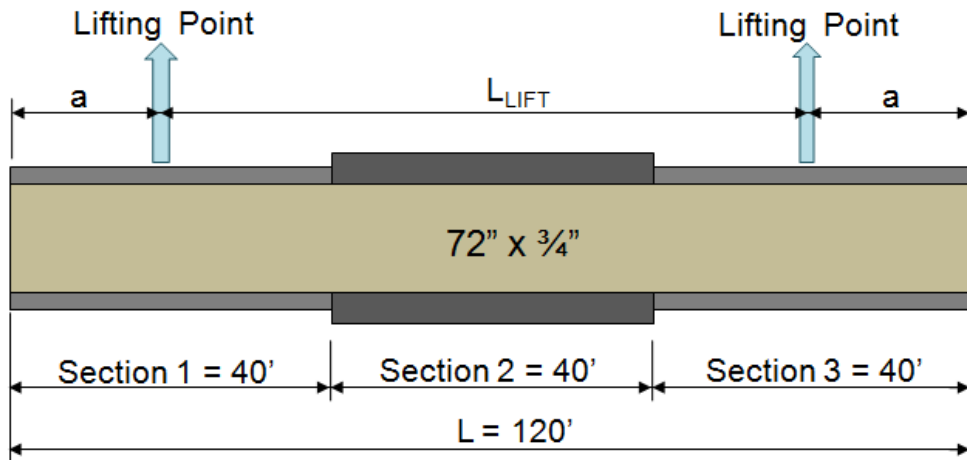


Figure C.9 Study 6 Girder Schematic

C.1.6.1 Comparison No. 6.1

- $C_b = \frac{\lambda M_{max}}{M_o}$; M_o properties using $L_b = L$, Smallest Cross Section Properties
- Symmetric Lift points ($a_1 = a_2$)
- Geometry: 3 Cross sections
 - Section 1 = Section 2 = Section 3 = 40.00'
 - Flanges: $b_f = 18''$, Section 1 & 3: $t_f = 1.25''$ and Section 2: $t_f = 2''$
 - Web = $72'' \times \frac{3}{4}''$
 - Length = 120.00'
- Varied lift location (a/L)
- Calculated Moment due to self weight at lift location and mid span
- Radius values compared: 250', 500', 1000', Straight
- Graphed C_b vs. a/L for given Radius of Curvature

C.1.6.2 Comparison No. 6.2

- $C_b = \frac{\lambda M_{max}}{M_o}$; M_o properties using $L_b = L - 2a \geq a$, Smallest Cross Section Properties
- Symmetric Lift points ($a_1 = a_2$)
- Geometry: 3 Cross sections
 - Section 1 = Section 2 = Section 3 = 40.00'
 - Flanges: $b_f = 18''$, Section 1 & 3: $t_f = 1.25''$ and Section 2: $t_f = 2''$

- Web = 72"x 3/4"
- Length = 120.00'
- Varied lift location (a/L)
- Calculated Moment due to self weight at lift location and mid span
- Radius values compared: 250', 500', 1000', Straight
- Graphed C_b vs. a/L for given Radius of Curvature

C.1.7 Study 7

- 2 Cross Sections
- Comparing flange thickness transition locations (60'-60', 40'-80', 80'-40')
- Comparing Un-Symmetric and Symmetric Lift Locations
- b/d ratio $\approx 1/4$
- Web = 72"x 3/4"
- Length = 120.00'
- Radius = 1000.00'

C.1.7.1 Comparison No. 7.1

- L_b = Entire girder length
- Un-symmetric Lift points ($a_1 \neq a_2$)
- Geometry: 2 Cross sections
 - Section 1 = Section 2 = 60.00'
 - Flanges: $b_f = 18"$, Section 1: $t_f = 1.25"$ and Section 2: $t_f = 2"$
- Used spreadsheet to calculate the length along girder to the center of mass
- Kept the CL of lifting beam location at the C.G. of girder, changed lifting beam length
- Calculated Moment due to self weight at lift locations and mid span ($M_{cr} = M_{max}$)
- Calculated C_b using the smallest section
- Graphed L_{Lift} vs. λ and L_{Lift} vs. C_b

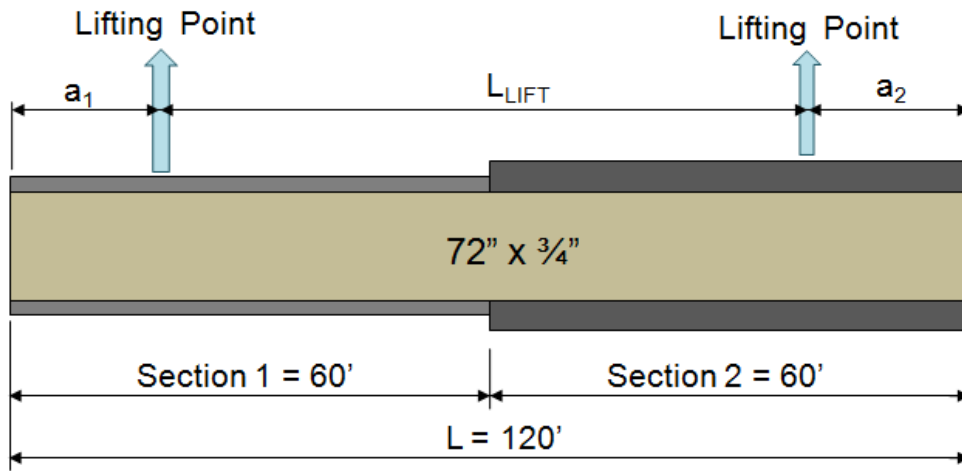


Figure C.10 Two Cross Section Girder Schematic (60' - 60')

C.1.7.2 Comparison No. 7.2

- L_b = Entire girder length
- Un-symmetric Lift points ($a_1 \neq a_2$)
- Geometry: 2 Cross sections
 - Section 1 = 40.00' Section 2 = 80.00'
 - Flanges: $b_f = 18''$, Section 1: $t_f = 1.25''$ and Section 2: $t_f = 2''$
- Used spreadsheet to calculate the length along girder to the center of mass
- Kept the CL of lifting beam location at the C.G. of girder, changed lifting beam length
- Calculated Moment due to self weight at lift locations and mid span ($M_{cr} = M_{max}$)
- Calculated C_b using the smallest section
- Graphed L_{Lift} vs. λ and L_{Lift} vs. C_b

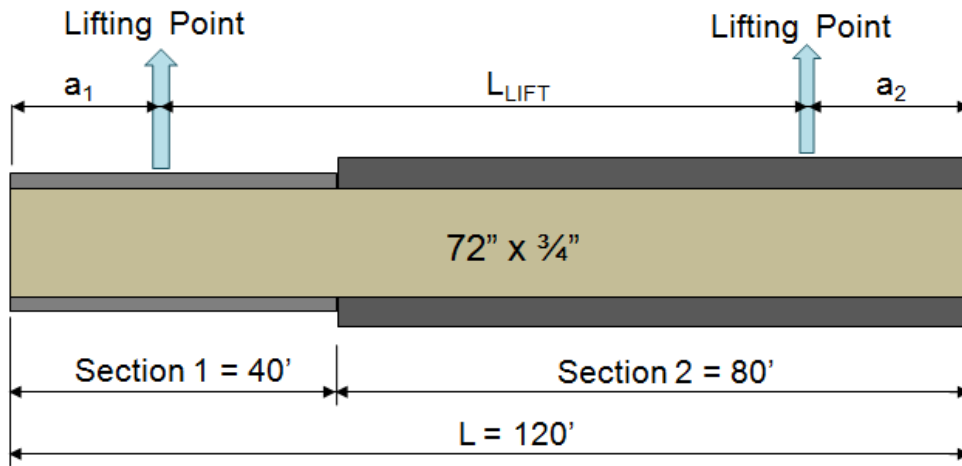


Figure C.11 Two Cross Section Girder Schematic (40' - 80')

C.1.7.3 Comparison No. 7.3

- L_b = Entire girder length
- Un-symmetric Lift points ($a_1 \neq a_2$)
- Geometry: 2 Cross sections
 - Section 1 = 80.00' Section 2 = 40.00'
 - Flanges: $b_f = 18''$, Section 1: $t_f = 1.25''$ and Section 2: $t_f = 2''$
- Used spreadsheet to calculate the length along girder to the center of mass
- Kept the CL of lifting beam location at the C.G. of girder, changed lifting beam length
- Calculated Moment due to self weight at lift locations and mid span ($M_{cr} = M_{max}$)
- Calculated C_b using the smallest section
- Graphed L_{Lift} vs. λ and L_{Lift} vs. C_b

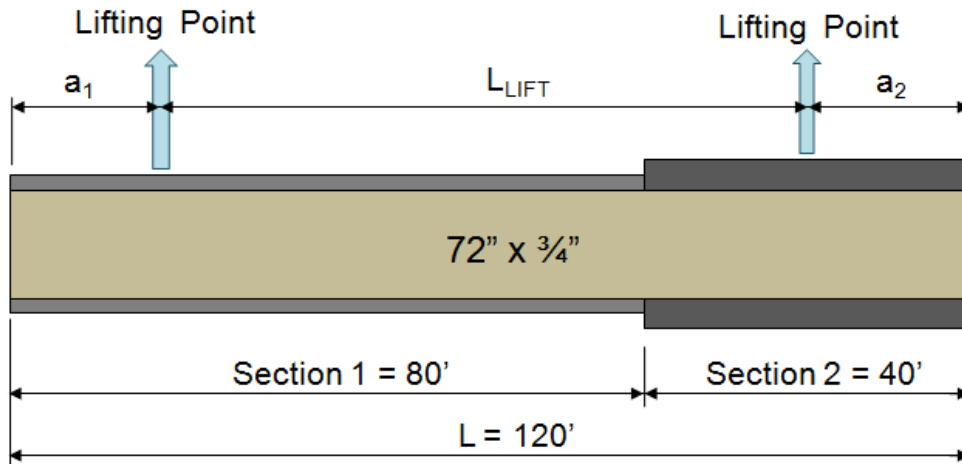


Figure C.12 Two Cross Section Girder Schematic (80' - 40')

C.1.7.4 Comparison No. 7.4

- L_b = Entire girder length
- Symmetric Lift points ($a_1 = a_2$)
- Geometry: 2 Cross sections
 - Section 1 = Section 2 = 60.00'
 - Flanges: $b_f = 18''$, Section 1: $t_f = 1.25''$ and Section 2: $t_f = 2''$
- Used the same a/L locations of (0.10, 0.15, 0.20, 0.25, 0.30, 0.35, 0.40)
- Calculated Moment due to self weight at lift locations and mid span ($M_{cr} = M_{max}$)
- Calculated M_o , C_b using the smallest section
- Graphed L_{Lift} vs. λ and L_{Lift} vs. C_b

C.1.7.5 Comparison No. 7.5

- L_b = Entire girder length
- Symmetric Lift points ($a_1 = a_2$)
- Geometry: 2 Cross sections
 - Section 1 = 40.00' Section 2 = 80.00'
 - Flanges: $b_f = 18''$, Section 1: $t_f = 1.25''$ and Section 2: $t_f = 2''$
- Used the same a/L locations of (0.10, 0.15, 0.20, 0.25, 0.30, 0.35, 0.40)
- Calculated Moment due to self weight at lift locations and mid span ($M_{cr} = M_{max}$)
- Calculated M_o , C_b using the smallest section
- Graphed L_{Lift} vs. λ and L_{Lift} vs. C_b

C.1.8 Study 8

- 2 Cross Sections
- Comparing flange thickness transition locations (60'-60', 40'-80', 80'-40')
- Comparing Un-Symmetric and Symmetric Lift Locations
- b/d ratio $\approx 1/6$
- Web = 72" x $\frac{3}{4}$ "
- Length = 120.00'
- Radius = 1000.00'

C.1.8.1 Comparison No. 8.1

- L_b = Entire girder length
- Un-symmetric Lift points ($a_1 \neq a_2$)
- Geometry: 2 Cross sections
 - Section 1 = Section 2 = 60.00'
 - Flanges: $b_f = 12''$, Section 1: $t_f = 1.25''$ and Section 2: $t_f = 2''$
- Used spreadsheet to calculate the length along girder to the center of mass
- Kept the CL of lifting beam location at the C.G. of girder, changed lifting beam length
- Calculated Moment due to self weight at lift locations and mid span ($M_{cr} = M_{max}$)
- Calculated C_b using the smallest section
- Graphed L_{Lift} vs. λ and L_{Lift} vs. C_b

C.1.8.2 Comparison No. 8.2

- L_b = Entire girder length
- Un-symmetric Lift points ($a_1 \neq a_2$)
- Geometry: 2 Cross sections
 - Section 1 = 40.00' Section 2 = 80.00'
 - Flanges: $b_f = 12''$, Section 1: $t_f = 1.25''$ and Section 2: $t_f = 2''$
- Used spreadsheet to calculate the length along girder to the center of mass
- Kept the CL of lifting beam location at the C.G. of girder, changed lifting beam length
- Calculated Moment due to self weight at lift locations and mid span ($M_{cr} = M_{max}$)
- Calculated C_b using the smallest section
- Graphed L_{Lift} vs. λ and L_{Lift} vs. C_b

C.1.8.3 Comparison No. 8.3

- L_b = Entire girder length
- Un-symmetric Lift points ($a_1 \neq a_2$)
- Geometry: 2 Cross sections
 - Section 1 = 80.00' Section 2 = 40.00'
 - Flanges: $b_f = 12''$, Section 1: $t_f = 1.25''$ and Section 2: $t_f = 2''$
- Used spreadsheet to calculate the length along girder to the center of mass
- Kept the CL of lifting beam location at the C.G. of girder, changed lifting beam length
- Calculated Moment due to self weight at lift locations and mid span ($M_{cr} = M_{max}$)
- Calculated C_b using the smallest section
- Graphed L_{Lift} vs. λ and L_{Lift} vs. C_b

C.1.8.4 Comparison No. 8.4

- L_b = Entire girder length
- Symmetric Lift points ($a_1 = a_2$)
- Geometry: 2 Cross sections
 - Section 1 = Section 2 = 60.00'
 - Flanges: $b_f = 12''$, Section 1: $t_f = 1.25''$ and Section 2: $t_f = 2''$
- Used the same a/L locations of (0.10, 0.15, 0.20, 0.25, 0.30, 0.35, 0.40)
- Calculated Moment due to self weight at lift locations and mid span ($M_{cr} = M_{max}$)
- Calculated M_o , C_b using the smallest cross section
- Graphed L_{Lift} vs. λ and L_{Lift} vs. C_b

C.1.8.5 Comparison No. 8.5

- L_b = Entire girder length
- Symmetric Lift points ($a_1 = a_2$)
- Geometry: 2 Cross sections
 - Section 1 = 40.00' Section 2 = 80.00'
 - Flanges: $b_f = 12''$, Section 1: $t_f = 1.25''$ and Section 2: $t_f = 2''$
- Used the same a/L locations of (0.10, 0.15, 0.20, 0.25, 0.30, 0.35, 0.40)
- Calculated Moment due to self weight at lift locations and mid span ($M_{cr} = M_{max}$)
- Calculated M_o , C_b using the smallest cross section
- Graphed L_{Lift} vs. λ and L_{Lift} vs. C_b

C.2 EXAMPLE CALCULATIONS

Comparison 1 - L=120'

Unsymmetric Lift Locations

$$C_b = \frac{\lambda M_{max}}{M_o}$$

$$R = 1000 \text{ ft}$$

$$L = 120 \text{ ft}$$

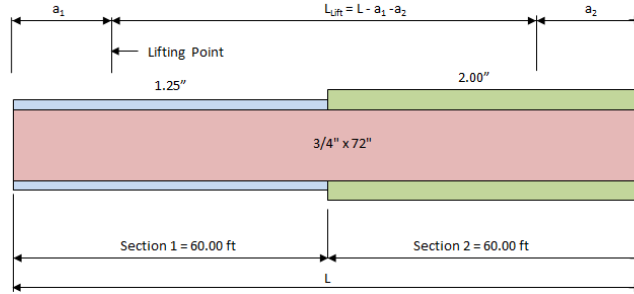
$$L_b = L$$

$$M_o = \frac{\pi}{L_b} \sqrt{EI_y GJ + E^2 I_y C_w \left(\frac{\pi^2}{L_b^2}\right)}$$

M_o calculated using smallest cross section

$$\bar{Z} = 63.6 \text{ ft}$$

= Length along girder to center of mass



Section 1 60.00 ft

Section 2 60.00 ft

Kept the CL of lifting beam location at the center of mass.

λM_{MID} is calculated at M_{max} (Shear = 0)

Section 1 Properties	
b_{ft}	18 in
t_{ft}	1.25 in
b_{fb}	18 in
t_{fb}	1.25 in
h_w	72 in
t_w	0.75 in
A_{ft}	22.5 in ²
A_{web}	54 in ²
A_{fb}	22.5 in ²
A_{total}	99 in ²
SW	336.88 lb/ft
I_y	1217.53 in ⁴
C_w	1633185.00 in ⁶
I_x	83696.44 in ⁴
S_x	2246.88 in ³
J	33.56 in ⁴
E	29000.00 ksi
G	11153.85 ksi
Parameters	
L/d	20
b/d	0.242

Section 2 Properties	
b_{ft}	18 in
t_{ft}	2 in
b_{fb}	18 in
t_{fb}	2 in
h_w	72 in
t_w	0.75 in
A_{ft}	36 in ²
A_{web}	54 in ²
A_{fb}	36 in ²
A_{total}	126 in ²
SW	428.75 lb/ft
I_y	1946.53 in ⁴
C_w	2664801.28 in ⁶
I_x	121920.00 in ⁴
S_x	3208.42 in ³
J	106.13 in ⁴
E	29000.00 ksi
G	11153.85 ksi
Parameters	
L/d	20
b/d	0.237
L	120 ft

a_1 (ft)	a_2 (ft)	a_1/L	a_2/L	avg a/L	λ	L_{lift} (ft)	L_b (ft)	$\lambda M_{LIFT 1}$ (k-ft)	$\lambda M_{LIFT 2}$ (k-ft)	λM_{MID} (k-ft)	M_o (k-ft)	M_{cr} (k-ft)	C_B
54.000	46.000	0.450	0.383	0.417	6.39	20.000	120.0	-3140.78	-2900.69	-2860.29	836.64	3140.78	3.75
49.000	41.000	0.408	0.342	0.375	8.23	30.000	120.00	-3328.57	-2965.98	-2746.91	836.64	3328.57	3.98
44.000	36.000	0.367	0.300	0.333	12.87	40.000	120.0	-4195.54	-3574.56	-2823.65	836.64	4195.54	5.01
39.000	31.000	0.325	0.258	0.292	19.29	50.000	120.0	-4941.46	-3973.61	-2023.97	836.64	4941.46	5.91
34.000	26.000	0.283	0.217	0.250	34.04	60.000	120.0	-6628.25	-4933.14	330.62	836.64	6628.25	7.92
29.000	22.000	0.242	0.183	0.213	30.29	69.000	120.0	-4290.76	-3142.81	3393.36	836.64	4290.76	5.13
26.000	19.000	0.217	0.158	0.188	15.58	75.000	120.0	-1773.66	-1205.49	2818.66	836.64	2818.66	3.37
21.000	14.000	0.175	0.117	0.146	6.976	85.000	120.000	-518.206	-293.126	2063.684	836.644	2063.684	2.467

Comparison 2 - L=120'

Unsymmetric Lift Locations

$$C_b = \frac{\lambda M_{max}}{M_o}$$

$$R = 1000 \text{ ft}$$

$$L = 120 \text{ ft}$$

$$L_b = L$$

$$M_o = \frac{\pi}{L_b} \sqrt{EI_y GJ + E^2 I_y C_w \left(\frac{\pi^2}{L_b^2} \right)}$$

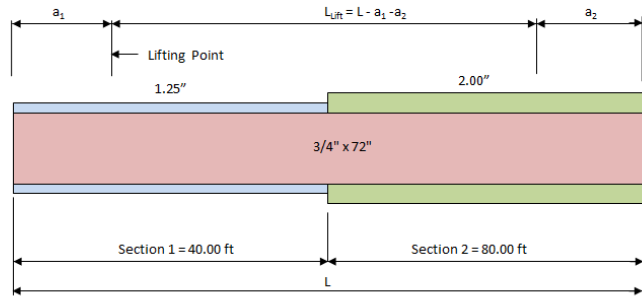
M_o calculated using smallest cross section

$$\bar{L} = 63.07 \text{ ft}$$

= Length along girder to center of mass

Kept the CL of lifting beam location at the center of mass.

λ_{MMD} is calculated at M_{max} (Shear = 0)



Section 1 40.00 ft

Section 2 80.00 ft

Section 1 Properties	
b _{fl,t}	18 in
t _{fl,t}	1.25 in
b _{fl,b}	18 in
t _{fl,b}	1.25 in
h _w	72 in
t _w	0.75 in
A _{fl,t}	22.5 in ²
A _{web}	54 in ²
A _{fl,b}	22.5 in ²
A _{total}	99 in ²
SW	336.88 lb/ft
I _y	1217.53 in ⁴
C _w	1633185.00 in ⁶
I _x	83696.44 in ⁴
S _x	2246.88 in ³
J	33.56 in ⁴
E	29000.00 ksi
G	11153.85 ksi
Parameters	
L/d	20
b/d	0.242

Section 2 Properties	
b _{fl,t}	18 in
t _{fl,t}	2 in
b _{fl,b}	18 in
t _{fl,b}	2 in
h _w	72 in
t _w	0.75 in
A _{fl,t}	36 in ²
A _{web}	54 in ²
A _{fl,b}	36 in ²
A _{total}	126 in ²
SW	428.75 lb/ft
I _y	1946.53 in ⁴
C _w	2664801.28 in ⁶
I _x	121920.00 in ⁴
S _x	3208.42 in ³
J	106.13 in ⁴
E	29000.00 ksi
G	11153.85 ksi
Parameters	
L/d	20
b/d	0.237
L	120 ft

a ₁ (ft)	a ₂ (ft)	a2/L	a1/L	avg a/L	λ	L _{lift} (ft)	L _b (ft)	λ M _{LIFT 1} (k-ft)	λ M _{LIFT 2} (k-ft)	λ M _{MMD} (k-ft)	M _o (k-ft)	M _{cr} (k-ft)	C _B
53.000	47.000	0.392	0.442	0.417	9.006	20.000	120.0	4262.44	4266.94	4071.72	836.64	4266.94	5.10
48.000	42.000	0.350	0.400	0.375	11.862	30.000	120.0	4605.001	4488.749	3972.733	836.644	4605.001	5.504
43.000	37.000	0.308	0.358	0.333	16.89	40.000	120.0	-5268.42	-4955.68	3660.30	836.64	5268.42	6.30
38.000	32.000	0.267	0.317	0.292	24.34	50.000	120.0	-5922.81	-5347.03	-2367.30	836.64	5922.81	7.08
33.000	27.000	0.225	0.275	0.250	39.67	60.000	120.0	-7279.22	-6204.19	883.38	836.64	7279.22	8.70
29.000	23.000	0.192	0.242	0.217	32.36	68.000	120.0	-4585.70	-3673.09	3815.48	836.64	4585.70	5.48
26.000	19.000	0.158	0.217	0.188	15.63	75.000	120.0	-1780.40	-1209.86	3155.95	836.64	3155.95	3.77
21.000	14.000	0.117	0.175	0.146	7.45	85.000	120.000	-553.311	-312.984	2393.682	836.644	2393.682	2.861

Comparison 3 - L=120'

Unsymmetric Lift Locations

$$C_b = \frac{\lambda M_{max}}{M_o}$$

$$R = 1000 \text{ ft}$$

$$L = 120 \text{ ft}$$

$$L_b = L$$

$$M_o = \frac{\pi}{L_b} \sqrt{EI_y GJ + E^2 I_y C_w \left(\frac{\pi^2}{L_b^2} \right)}$$

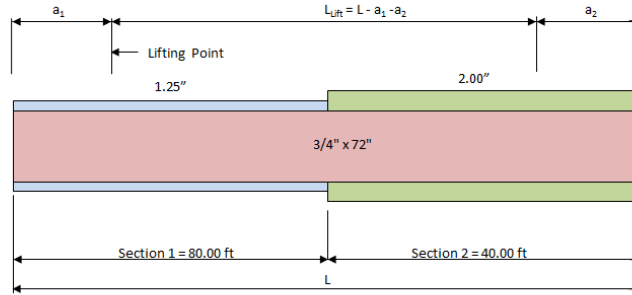
M_o calculated using smallest cross section

$$\bar{L} = 63.33 \text{ ft}$$

= Length along girder to center of mass

Kept the CL of lifting beam location at the center of mass.

λM_{MID} is calculated at M_{max} (Shear = 0)



Section 1 80.00 ft

Section 2 40.00 ft

Section 1 Properties	
$b_{f,t}$	18 in
$t_{f,t}$	1.25 in
$b_{f,b}$	18 in
$t_{f,b}$	1.25 in
h_w	72 in
t_w	0.75 in
$A_{f,t}$	22.5 in ²
A_{web}	54 in ²
$A_{f,b}$	22.5 in ²
A_{total}	99 in ²
SW	336.88 lb/ft
I_y	1217.53 in ⁴
C_w	1633185.00 in ⁶
I_x	83696.44 in ⁴
S_x	2246.88 in ³
J	33.56 in ⁴
E	29000.00 ksi
G	11153.85 ksi
Parameters	
L/d	20
b/d	0.242

Section 2 Properties	
$b_{f,t}$	18 in
$t_{f,t}$	2 in
$b_{f,b}$	18 in
$t_{f,b}$	2 in
h_w	72 in
t_w	0.75 in
$A_{f,t}$	36 in ²
A_{web}	54 in ²
$A_{f,b}$	36 in ²
A_{total}	126 in ²
SW	428.75 lb/ft
I_y	1946.53 in ⁴
C_w	2664801.28 in ⁶
I_x	121920.00 in ⁴
S_x	3208.42 in ³
J	106.13 in ⁴
E	29000.00 ksi
G	11153.85 ksi
Parameters	
L/d	20
b/d	0.237
L	120 ft

a_1 (ft)	a_2 (ft)	$a1/L$	$a2/L$	avg a/L	λ	L_{lift} (ft)	L_b (ft)	$\lambda M_{LIFT 1}$ (k-ft)	$\lambda M_{LIFT 2}$ (k-ft)	λM_{MID} (k-ft)	M_o (k-ft)	M_{cr} (k-ft)	C_B
53.000	47.000	0.442	0.392	0.417	5.650	20.000	120.0	2673.93	2676.76	2580.38	836.64	2676.76	3.20
48.000	42.000	0.400	0.350	0.375	7.491	30.000	120.000	2906.563	2834.648	2586.160	836.644	2906.563	3.474
43.000	37.000	0.358	0.308	0.333	10.96	40.000	120.0	-3413.66	-3217.56	-2570.65	836.64	3413.66	4.08
38.000	32.000	0.317	0.267	0.292	18.15	50.000	120.0	-4414.66	-3984.12	-2255.72	836.64	4414.66	5.28
33.000	27.000	0.275	0.225	0.250	35.49	60.000	120.0	-6511.51	-5549.86	493.17	836.64	6511.51	7.78
28.000	22.000	0.233	0.183	0.208	27.71	70.000	120.0	-3660.77	-2876.52	2674.22	836.64	3660.77	4.38
26.000	19.000	0.217	0.158	0.188	15.19	75.000	120.0	-1730.08	-1175.66	2313.35	836.64	2313.35	2.77
21.000	14.000	0.175	0.117	0.146	6.58	85.000	120.000	-489.023	-276.619	1728.150	836.644	1728.150	2.066

Comparison 4 - L=120'

$$C_b = \frac{\lambda M_{max}}{M_o}$$

Symmetric Lift Locations

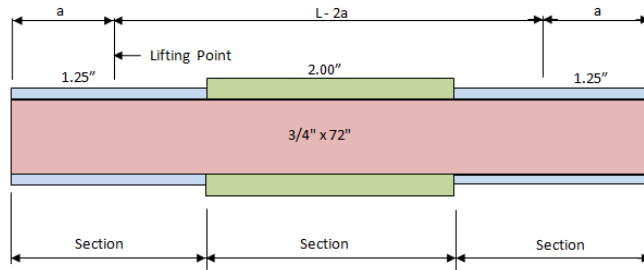
$$R = 1000 \text{ ft}$$

$$L = 120 \text{ ft}$$

$$L_b = L$$

$$M_o = \frac{\pi}{L_b} \sqrt{EI_y GJ + E^2 I_y C_w \left(\frac{\pi^2}{L_b^2}\right)}$$

M_o calculated using smallest cross section



Section 1 40.00 ft

Section 2 40.00 ft

Section 3 40.00 ft

Section 1 Properties		Section 2 Properties		Section 3 Properties	
$b_{f,t}$	18 in	$b_{f,t}$	18 in	$b_{f,t}$	18 in
$t_{f,t}$	1.25 in	$t_{f,t}$	2 in	$t_{f,t}$	1.25 in
$b_{f,b}$	18 in	$b_{f,b}$	18 in	$b_{f,b}$	18 in
$t_{f,b}$	1.25 in	$t_{f,b}$	2 in	$t_{f,b}$	1.25 in
h_w	72 in	h_w	72 in	h_w	72 in
t_w	0.75 in	t_w	0.75 in	t_w	0.75 in
$A_{fl,t}$	22.5 in ²	$A_{fl,t}$	36 in ²	$A_{fl,t}$	22.5 in ²
A_{web}	54 in ²	A_{web}	54 in ²	A_{web}	54 in ²
$A_{fl,b}$	22.5 in ²	$A_{fl,b}$	36 in ²	$A_{fl,b}$	22.5 in ²
A_{total}	99 in ²	A_{total}	126 in ²	A_{total}	99 in ²
SW	336.88 lb/ft	SW	428.75 lb/ft	SW	336.88 lb/ft
I_y	1217.53 in ⁴	I_y	1946.53 in ⁴	I_y	1217.53 in ⁴
C_w	1633185.00 in ⁶	C_w	2664801.28 in ⁶	C_w	1633185.00 in ⁶
I_x	83696.44 in ⁴	I_x	121920.00 in ⁴	I_x	83696.44 in ⁴
S_x	2246.88 in ³	S_x	3208.42 in ³	S_x	2246.88 in ³
J	33.56 in ⁴	J	106.13 in ⁴	J	33.56 in ⁴
E	29000.00 ksi	E	29000.00 ksi	E	29000.00 ksi
G	11153.85 ksi	G	11153.85 ksi	G	11153.85 ksi
		Parameters			
		L/d = 20			
		b/d = 0.237			
		L = 120 ft			

a/L	a (ft)	λ	L_b (ft)	λM_{LIFT} (k-ft)	λM_{MID} (k-ft)	M_o (k-ft)	M_{cr} (k-ft)	C_B
0.10	12	3.36	120.0	-81.47	1456.63	836.64	1456.63	1.74
0.15	18	6.85	120.0	-373.99	2065.15	836.64	2065.15	2.47
0.20	24	18.31	120.0	-1776.34	3095.14	836.64	3095.14	3.70
0.25	30	47.72	120.0	-7233.30	1753.53	836.64	7233.30	8.65
0.30	36	26.73	120.0	-5835.46	-2554.24	836.64	5835.46	6.97
0.35	42	16.49	120.0	-4903.20	-3757.70	836.64	4903.20	5.86
0.40	48	11.37	120.0	-4443.94	-4093.10	836.64	4443.94	5.31

Comparison5 - L=150'

$$C_b = \frac{\lambda M_{max}}{M_o}$$

Symmetric Lift Locations

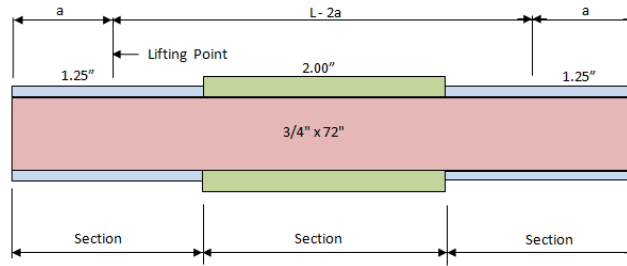
R = 1000 ft

L = 150 ft

L_b = L

$$M_o = \frac{\pi}{L_b} \sqrt{EI_y GJ + E^2 I_y C_w \left(\frac{\pi^2}{L_b^2} \right)}$$

M_o calculated using smallest cross section



Section 1 55.00 ft

Section 2 40.00 ft

Section 3 55.00 ft

Section 1 Properties		Section 2 Properties		Section 3 Properties	
b_{ft}	18 in	b_{ft}	18 in	b_{ft}	18 in
t_{ft}	1.25 in	t_{ft}	2 in	t_{ft}	1.25 in
b_{fb}	18 in	b_{fb}	18 in	b_{fb}	18 in
t_{fb}	1.25 in	t_{fb}	2 in	t_{fb}	1.25 in
h_w	72 in	h_w	72 in	h_w	72 in
t_w	0.75 in	t_w	0.75 in	t_w	0.75 in
A_{ft}	22.5 in ²	A_{ft}	36 in ²	A_{ft}	22.5 in ²
A_{web}	54 in ²	A_{web}	54 in ²	A_{web}	54 in ²
A_{fb}	22.5 in ²	A_{fb}	36 in ²	A_{fb}	22.5 in ²
A_{total}	99 in ²	A_{total}	126 in ²	A_{total}	99 in ²
SW	336.88 lb/ft	SW	428.75 lb/ft	SW	336.88 lb/ft
I_y	1217.53 in ⁴	I_y	1946.53 in ⁴	I_y	1217.53 in ⁴
C_w	1633185.00 in ⁶	C_w	2664801.28 in ⁶	C_w	1633185.00 in ⁶
I_x	83696.44 in ⁴	I_x	121920.00 in ⁴	I_x	83696.44 in ⁴
S_x	2246.88 in ³	S_x	3208.42 in ³	S_x	2246.88 in ³
J	33.56 in ⁴	J	106.13 in ⁴	J	33.56 in ⁴
E	29000.00 ksi	E	29000.00 ksi	E	29000.00 ksi
G	11153.85 ksi	G	11153.85 ksi	G	11153.85 ksi
		Parameters			
		L/d = 20			
		b/d = 0.237			
		L = 150 ft			

a/L	a (ft)	λ	L _b (ft)	λM_{LIFT} (k-ft)	λM_{MID} (k-ft)	M _o (k-ft)	M _{cr} (k-ft)	C _B
0.10	15.0	1.52	150.0	-57.42	1000.43	622.39	1000.43	1.61
0.15	22.5	3.04	150.0	-258.97	1388.15	622.39	1388.15	2.23
0.20	30.0	8.58	150.0	-1300.37	2177.14	622.39	2177.14	3.50
0.25	37.5	25.76	150.0	-6100.94	1301.53	622.39	6100.94	9.80
0.30	45.0	13.89	150.0	-4737.00	-2121.28	622.39	4737.00	7.61
0.35	52.5	6.22	150.0	-2885.35	-2212.64	622.39	2885.35	4.64
0.40	60.0	4.90	150.0	-2977.47	-2741.08	622.39	2977.47	4.78

Radius Comparison 1

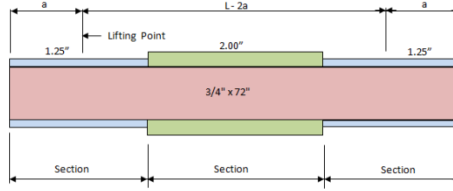
$$C_b = \frac{\lambda M_{max}}{M_o}$$

Symmetric Lift Locations

$$\frac{L}{L_b} = \frac{120 \text{ ft}}{L}$$

$$M_o = \frac{\pi}{L_b} \sqrt{EI_y GJ + E^2 I_y C_w \left(\frac{\pi^2}{L_b^2}\right)}$$

M_o calculated using smallest cross section



Section 1 40.00 ft Section 2 40.00 ft Section 3 40.00 ft

Section 1 Properties		Section 2 Properties		Section 3 Properties	
b_{t1}	18 in	b_{t1}	18 in	b_{t1}	18 in
t_{t1}	1.25 in	t_{t1}	2 in	t_{t1}	1.25 in
b_{tb}	18 in	b_{tb}	18 in	b_{tb}	18 in
t_{tb}	1.25 in	t_{tb}	2 in	t_{tb}	1.25 in
h_w	72 in	h_w	72 in	h_w	72 in
t_w	0.75 in	t_w	0.75 in	t_w	0.75 in
A_{t1}	22.5 in ²	A_{t1}	36 in ²	A_{t1}	22.5 in ²
A_{web}	54 in ²	A_{web}	54 in ²	A_{web}	54 in ²
A_{fb}	22.5 in ²	A_{fb}	36 in ²	A_{fb}	22.5 in ²
A_{total}	99 in ²	A_{total}	126 in ²	A_{total}	99 in ²
SW	336.88 lb/ft	SW	428.75 lb/ft	SW	336.88 lb/ft
I_y	1217.53 in ⁴	I_y	1946.53 in ⁴	I_y	1217.53 in ⁴
C_w	1633185.00 in ⁶	C_w	2664801.28 in ⁶	C_w	1633185.00 in ⁶
I_x	83696.44 in ⁴	I_x	121920.00 in ⁴	I_x	83696.44 in ⁴
S_x	2246.88 in ³	S_x	3208.42 in ³	S_x	2246.88 in ³
J	33.56 in ⁴	J	106.13 in ⁴	J	33.56 in ⁴
E	29000.00 ksi	E	29000.00 ksi	E	29000.00 ksi
G	11153.85 ksi	G	11153.85 ksi	G	11153.85 ksi
		Parameters			
		L/d = 20			
		b/d = 0.237			
		L = 120 ft			

	a/L	a (ft)	λ	L_b (ft)	λM_{IFT} (k-ft)	λM_{MD} (k-ft)	M_o (k-ft)	M_{cr} (k-ft)	C_B
R = 250'	0.10	12	3.02	120.0	-73.17	1308.19	836.64	1308.19	1.56
	0.15	18	6.63	120.0	-361.71	1997.35	836.64	1997.35	2.39
	0.20	24	19.07	120.0	-1850.37	3224.12	836.64	3224.12	3.85
	0.25	30	49.67	120.0	-7530.12	1825.48	836.64	7530.12	9.00
	0.30	36	26.12	120.0	-5701.21	-2495.48	836.64	5701.21	6.81
	0.35	42	16.96	120.0	-5042.63	-3864.56	836.64	5042.63	6.03
R = 500'	0.10	12	3.32	120.0	-80.48	1438.85	836.64	1438.85	1.72
	0.15	18	6.83	120.0	-372.52	2057.02	836.64	2057.02	2.46
	0.20	24	18.39	120.0	-1784.39	3109.17	836.64	3109.17	3.72
	0.25	30	48.09	120.0	-7290.60	1767.42	836.64	7290.60	8.71
	0.30	36	27.08	120.0	-5911.43	-2587.49	836.64	5911.43	7.07
	0.35	42	16.62	120.0	-4940.95	-3786.64	836.64	4940.95	5.91
R = 1000'	0.10	12	3.36	120.0	-81.47	1456.63	836.64	1456.63	1.74
	0.15	18	6.85	120.0	-373.99	2065.15	836.64	2065.15	2.47
	0.20	24	18.31	120.0	-1776.34	3095.14	836.64	3095.14	3.70
	0.25	30	47.72	120.0	-7233.30	1753.53	836.64	7233.30	8.65
	0.30	36	26.73	120.0	-5835.46	-2554.24	836.64	5835.46	6.97
	0.35	42	16.49	120.0	-4903.20	-3757.70	836.64	4903.20	5.86
R = Straight	0.10	12	3.37	120.0	-81.74	1461.40	836.64	1461.40	1.75
	0.15	18	6.35	120.0	-346.33	1912.37	836.64	1912.37	2.29
	0.20	24	18.31	120.0	-1776.15	3094.80	836.64	3094.80	3.70
	0.25	30	47.60	120.0	-7216.47	1749.45	836.64	7216.47	8.63
	0.30	36	26.63	120.0	-5812.76	-2544.31	836.64	5812.76	6.95
	0.35	42	16.46	120.0	-4893.68	-3750.41	836.64	4893.68	5.85
0.40	48	11.35	120.0	-4436.51	-4086.26	836.64	4436.51	5.30	

Radius Comparison 2

$$C_B = \frac{\lambda M_{max}}{M_o}$$

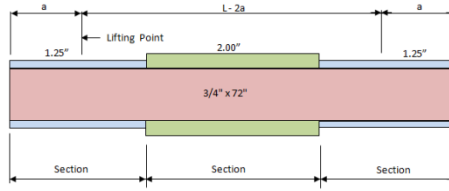
Symmetric Lift Locations

$$L = 120 \text{ ft}$$

$$L_b = L - 2a \geq a$$

$$M_o = \frac{\pi}{L_b} \sqrt{EI_y GJ + E^2 I_y C_w \left(\frac{\pi^2}{L_b^2}\right)}$$

M_o calculated using smallest cross section



Section 1 40.00 ft Section 2 40.00 ft Section 3 40.00 ft

Section 1 Properties		Section 2 Properties		Section 3 Properties	
b_{T1}	18 in	b_{T1}	18 in	b_{T1}	18 in
t_{T1}	1.25 in	t_{T1}	2 in	t_{T1}	1.25 in
b_{TB}	18 in	b_{TB}	18 in	b_{TB}	18 in
t_{TB}	1.25 in	t_{TB}	2 in	t_{TB}	1.25 in
h_w	72 in	h_w	72 in	h_w	72 in
t_w	0.75 in	t_w	0.75 in	t_w	0.75 in
A_{fl}	22.5 in ²	A_{fl}	36 in ²	A_{fl}	22.5 in ²
A_{web}	54 in ²	A_{web}	54 in ²	A_{web}	54 in ²
A_{fb}	22.5 in ²	A_{fb}	36 in ²	A_{fb}	22.5 in ²
A_{total}	99 in ²	A_{total}	126 in ²	A_{total}	99 in ²
SW	336.88 lb/ft	SW	428.75 lb/ft	SW	336.88 lb/ft
I_y	1217.53 in ⁴	I_y	1946.53 in ⁴	I_y	1217.53 in ⁴
C_w	1633185.00 in ⁶	C_w	2664801.28 in ⁶	C_w	1633185.00 in ⁶
I_x	83696.44 in ⁴	I_x	121920.00 in ⁴	I_x	83696.44 in ⁴
S_x	2246.88 in ³	S_x	3208.42 in ³	S_x	2246.88 in ³
J	33.56 in ⁴	J	106.13 in ⁴	J	33.56 in ⁴
E	29000.00 ksi	E	29000.00 ksi	E	29000.00 ksi
G	11153.85 ksi	G	11153.85 ksi	G	11153.85 ksi
		Parameters			
		L/d = 20			
		b/d = 0.237			
		L = 120 ft			

	a/L	a (ft)	λ	L_b (ft)	λM_{LIFT} (k-ft)	λM_{MID} (k-ft)	M_o (k-ft)	M_{cr} (k-ft)	C_B
R = 250'	0.10	12	3.02	96.0	-73.17	1308.19	1151.06	1308.19	1.14
	0.15	18	6.63	84.0	-361.71	1997.35	1409.73	1997.35	1.42
	0.20	24	19.07	72.0	-1850.37	3224.12	1800.99	3224.12	1.79
	0.25	30	49.67	60.0	-7530.12	1825.48	2440.68	7530.12	3.09
	0.30	36	26.12	48.0	-5701.21	-2495.48	3606.57	5701.21	1.58
	0.35	42	16.96	42.0	-5042.63	-3864.56	4593.28	5042.63	1.10
R = 500'	0.10	12	3.32	96.0	-80.48	1438.85	1151.06	1438.85	1.25
	0.15	18	6.83	84.0	-372.52	2057.02	1409.73	2057.02	1.46
	0.20	24	18.39	72.0	-1784.39	3109.17	1800.99	3109.17	1.73
	0.25	30	48.09	60.0	-7290.60	1767.42	2440.68	7290.60	2.99
	0.30	36	27.08	48.0	-5911.43	-2587.49	3606.57	5911.43	1.64
	0.35	42	16.62	42.0	-4940.95	-3786.64	4593.28	4940.95	1.08
R = 1000'	0.10	12	3.36	96.0	-81.47	1456.63	1151.06	1456.63	1.27
	0.15	18	6.85	84.0	-373.99	2065.15	1409.73	2065.15	1.46
	0.20	24	18.31	72.0	-1776.34	3095.14	1800.99	3095.14	1.72
	0.25	30	47.72	60.0	-7233.30	1753.53	2440.68	7233.30	2.96
	0.30	36	26.73	48.0	-5835.46	-2554.24	3606.57	5835.46	1.62
	0.35	42	16.49	42.0	-4903.20	-3757.70	4593.28	4903.20	1.07
R = Straight	0.10	12	3.37	96.0	-81.74	1461.40	1151.06	1461.40	1.27
	0.15	18	6.35	84.0	-346.33	1912.37	1409.73	1912.37	1.36
	0.20	24	18.31	72.0	-1776.15	3094.80	1800.99	3094.80	1.72
	0.25	30	47.60	60.0	-7216.47	1749.45	2440.68	7216.47	2.96
	0.30	36	26.63	48.0	-5812.76	-2544.31	3606.57	5812.76	1.61
	0.35	42	16.46	42.0	-4893.68	-3750.41	4593.28	4893.68	1.07
0.40	48	11.35	48.0	-4436.51	-4086.26	3606.57	4436.51	1.23	

APPENDIX D

Curved I-Girder Erection Questionnaire

This appendix provides a copy of the questionnaire used to survey various steel curved I-girder erection contractors, inspectors, and engineers. The questionnaire focuses on the common practice for lifting curved I-girders, including spreader beam length, number of cranes, lift points, shore towers, and length of girder segments lifted. Refer to Chapter 6 for the discussion of the responses to the questions.

Questionnaire

Erecting Curved Plate I-Girders

Company: _____

Name: _____

Phone: _____

Date: _____

1. What is the typical lifting scenario?

- a. 1 girder segment lifted, then spliced in the air. What is the range of the segment lengths lifted?

- b. Multiple girder segments spliced on the ground, then lifted. What is the range of the lengths lifted?

- 2. Are spreader beams used? Before a girder is delivered to the site, do you know the size of spreader beam(s) that will be used? Or do you wait until the girder arrives and then choose from various spreader beams that you have on hand? What are the typical spreader beam lengths that you use?**

- 3. When lifting a girder, is it typical to use one crane or two cranes? If you use two cranes do you employ spreader beams for each crane?**

- 4. Is tilting of the girder a concern when lifting curved girders? When lifting a curved girder, what is your typical rotation tolerance?**

- 5. How do you determine where to lift the girder and the number of lifting points?**

- 6. What problems or concerns do you have about lifting curved plate girder segments that you would like to be considered in this research?**

References

1. American Association of State Highway and Transportation Officials (AASHTO). (1980). *Guide specifications for horizontally curved bridges*, Washington, D.C.
2. American Association of State Highway and Transportation Officials (AASHTO). (1993). *Guide specifications for horizontally curved bridges*, Washington, D.C.
3. American Association of State Highway and Transportation Officials (AASHTO). (2003). *Guide specifications for horizontally curved bridges*, Washington, D.C.
4. American Association of State Highway and Transportation Officials (AASHTO). (2007). *AASHTO LRFD Bridge Design Specifications*, Washington, D.C.
5. American Institute of Steel Construction Inc.(AISC). (2005). *Steel construction manual, 13th edition*, The United States of America.
6. ANSYS, Finite element program users' manual, Version 11.0. (2007). ANSYS, Inc.
7. Beal, D. B., and Kissane, R. J. (1971). *First Interim Report on Research Project 42-1*, New York State Department of Transportation, Engineering Research and Development Bureau, Albany, New York.
8. Beal, D. B., and Kissane, R. J. (1971). *Second Interim Report on Research Project 42-1*, New York State Department of Transportation, Engineering Research and Development Bureau, Albany, New York.
9. Beal, D. B., and Kissane, R. J. (1972). *Third Interim Report on Research Project 42-1*, New York State Department of Transportation, Engineering Research and Development Bureau, Albany, New York.
10. Brennan, P.J. (1970). "Horizontally curved bridges first annual report: Analysis of horizontally curved bridges through three-dimensional mathematical model and small scale structural testing." *Syracuse Univ., First Annual Rep., Research Project HPR-2(111)*, Syracuse, N.Y.
11. Brennan, P.J. (1971). "Horizontally curved bridges second annual report: Analysis of Seekonk River Bridge small scale structure through three-dimensional mathematical model and small scale structural testing." *Syracuse Univ., Second Annual Rep., Research Project HPR-2(111)*, Syracuse, N.Y.

12. Brennan, P.J. (1974). "Analysis and structural testing of a multiple configuration small scale horizontally curved highway bridge." *Syracuse Univ., Research Project HPR-2(111)*, Syracuse, N.Y.
13. Campbell Scientific, Inc. (1996). *AM416 Relay Multiplexer Instruction Manual* (Revision 2/96). Retrieved August 28, 2008, from <http://www.campbellsci.com/documents/manuals/am416.pdf>
14. Campbell Scientific, Inc. (2001). *CR5000 Measurement and Control system Operator's Manual* (Revision 2/96). Logan, UT.
15. Campbell Scientific, Inc. (2006). *CR5000 Measurement and Control System Operator's Manual* (Revision 11/06). Logan, UT.
16. Campbell Scientific, Inc. (2007). *4WFB120, 4WFB350, 4WFB1K 4 Wire Full Bridge Terminal Input Modules Instruction Manual* (Revision 5/07). Logan, UT.
17. Chen, Q. (2008). *Effects of Thermal Loads on Texas Steel Bridges*. PhD dissertation, University of Texas.
18. Chen, W. F. and Lui, E. M. (1987). *Structural Stability Theory and Implementation*, Prentice-Hall, Inc., New Jersey
19. Espinoza, O. (2007). *Measurements of Deformations and Stresses Due to Plate Out-of-Flatness in a Steel Twin Box Girder Bridge System*. Thesis, University of Texas.
20. Fan, Z. (1999). *Field and Computational Studies of Steel Trapezoidal Box Girder Bridges*. PhD dissertation, University of Houston.
21. Fasl, J. D. (2008). *The Influence of Overhang Construction on Girder Design*. Thesis, University of Texas.
22. Galambos, T. V., Hajjar, J. F., Huang, W., Pulver, B. E., Leon, R. T., and Rudie, B. J. (2000). "Comparison of measured and computed stresses in a steel curved girder bridge." *J. Bridge Eng.*, 5(3), 191-199.
23. Grisham, G. P. (2005). *Field Measurements of Bearing Displacements in Steel Girder Bridges*. Thesis, University of Houston.
24. *Guide to Stability Design Criteria for Metal Structures*, 5th Ed. (1998) T. V. Galambos, ed., John Wiley & Sons, Inc., New York, N.Y.
25. Helwig, T., & Fan, Z. (2000). *Field and Computational Studies of Steel Trapezoidal Box Girder Bridges*. TxDOT Research Report 1395-3, University of Houston.

26. Helwig, Todd A., Frank, Karl H., Yura, Joseph A. (1997). "Lateral-torsional buckling of singly symmetric I-beams." *J. of Struct. Eng.*, 123(9), 1172-1179.
27. Linzell, D., Hall, D., White, D. (2004). "Historical perspective on horizontally curved I-girder bridge design in the United States." *J. of Bridge Eng.*, 9(3), 218-229.
28. Linzell, D., Leon, R. T., and Zureick, A. (2004). "Experimental and analytical studies of horizontally curved steel I-girder bridge during erection." *J. Bridge Eng.*, 9(6), 521-530.
29. Omega Engineering. (2008). The Strain Gage. Retrieved August 28, 2008, from <http://www.omega.com/Literature/Transactions/volume3/strain.html>
30. Schuh, A. C. (2008). *Behavior of Horizontally Curved Steel I-Girders During Lifting*. Thesis, University of Texas.
31. Texas Department of Transportation (TXDOT). (2007). *Preferred Practices for Steel Bridge Design, Fabrication, and Erection*. Texas Steel Quality Council.
32. Timoshenko, S. P. and Gere, J. M. (1961). *Theory of Elastic Stability*. 2nd Ed., McGraw-Hill Book Company, Inc., New York
33. Zureick, A., Naquib, R., and Yadlosky, J. M. (1994). "Curved steel bridge research project. Interim report I: Synthesis." *Rep. No. FHWA-RD-93-129*, HDR Engineering, Inc., Omaha, Neb.

Vita

Jamie Fiedelia Farris, son of Don and Sandy Hybner, was born in Austin, Texas on May 21, 1977. She enrolled at The University of Texas at Austin in 1997 and graduated with a Bachelor of Science in Architectural Engineering in December of 1999. After working in bridge design for two engineering consulting companies, Jamie accepted a job with the Texas Department of Transportation (TxDOT) Bridge Division in February 2003. In December of 2004, Jamie became a registered Professional Engineer in the state of Texas. For over four years Jamie designed concrete and steel bridges as well as restored and rehabilitated historic truss bridges at TxDOT. In May of 2007, she was awarded an academic grant through the TxDOT Master's Program, which allowed her to advance her education and work on a TxDOT funded research project. Jamie enrolled in graduate school at The University of Texas at Austin in August of 2007, where she worked as a research assistant at the Phil M. Ferguson Structural Engineering Laboratory. After graduating with a Master of Science degree, Jamie plans to return to TxDOT Bridge Division as a bridge design engineer.

Permanent Address: 8611 Verona Trail
Austin, TX 78749

This thesis was typed by the author.